University of Alberta

The origin and evolution of eclogite xenoliths and associated diamonds from the Jericho kimberlite, northern Slave craton, Canada: an integrated petrological, geochemical and isotopic study

by

Kathleen Alexandra Smart

A thesis submitted to the Faculty of Graduate Studies and Research
in partial fulfillment of the requirements for the degree of

Doctor of Philosophy

Department of Earth and Atmospheric Sciences

Fall 2011
Edmonton, Alberta

Abstract

Diamond-bearing eclogite xenoliths are relatively rare but provide insight into the composition and evolution of the cratonic lithospheric mantle and also insight into the diamond formation process. The major-, trace-element and Sr-Pb-O-isotope compositions of both high- and low-MgO diamond eclogites from the Jericho kimberlite, Nunavut, Canada, indicate that each group had different geneses. Both eclogite groups formed as parts of ancient oceanic lithosphere; positive Sr anomalies and $\delta^{18}O$ values of 6.5-6.6‰ of the low MgO eclogites indicate seawater-altered gabbroic protoliths, while the high Mg and Cr, fractionated HREEs, and $\delta^{18}O$ values of 5.3-5.5‰ of the high-MgO eclogites indicate a mantle origin. High-MgO eclogite crystallization probably occurred at 2-3 GPa where mantle-derived melts are generally basaltic, as melts in the diamond stability field are far too Mg-rich. As such, eclogite crystallization likely occurred as pyroxenite veins at the underside of thick Archean oceanic lithosphere. Although there are no age constraints for the diamond eclogites, both groups could have been imbricated into the cratonic mantle by subduction stacking of lithosphere during putative Neoarchean or Paleoproterozoic subduction events in the Slave craton. The petrogenesis of the high-MgO eclogites is further complicated by diamond inclusions with lower Cr_2O_3 and Mg-numbers but higher CaO, Na_2O and Al_2O_3; element exchange with surrounding peridotite after diamond formation altered the eclogite composition.

Diamonds from each eclogite group have widely different carbon isotope compositions and nitrogen contents and thus the diamond forming fluids/melts were derived from disparate sources. Diamonds from the high-MgO eclogites have extremely low $\delta^{13}C$ values of -40‰ which require derivation from subducted organic carbon; diamonds from the low-MgO eclogites have $\delta^{13}C$ values from -4.75 to -3.5 and could have been sourced from either fractionated mantle-derived carbon or subducted carbonate sediments. The reducing nature of the deep CLM favors the latter carbon source. Detailed SIMS investigations of both diamond groups revealed coupled increases in $\delta^{13}C$ and decreases in N in growth zones

towards diamond rims. The coupled δ^{13}C-N changes indicate diamond growth occurred from oxidized fluids or melts, where nitrogen behaved compatibly in diamond compared to the source fluid/melt.

Acknowledgement

First and foremost I would like to recognize my supervisor, Tom Chacko, for his exceptional guidance and patience. Tom has been instrumental in developing my knowledge, cultivating my drive to excel and for demonstrating the value of discussion and collaboration. I especially wish to thank Tom for patiently instilling his high standard of excellence and the value of a cool head - despite my (often vocal) protests, I sincerely appreciate all you have taught me.

I would also like to acknowledge my committee for their dedication. My sincere gratitude to Thomas Stachel for his guidance, extremely helpful discussions, excellent library and all the coffees! In particular I appreciate the encouragement to keep my 'ears up' during the final trying months. Many thanks to Karlis Muehlenbachs for his contributions and straightforward insight into the world of stable isotopes. I am very grateful for the experience Karlis provided in the stable isotope lab, especially for letting me 'play' with BrF_5. Special thanks to Graham Pearson for the beneficial discussions, thoughtful input and for being a part of my supervisory committee.

Thanks to Sergei Matveev for his knowledge, assistance and considerable patience with the microprobe, and also for his friendly conversations. Thanks to Antonio Simonetti and GuangCheng Chen for their help with LA-ICP-MS analyses and Gayle Hatchard for assistance with the "green machine".

I would like to recognize the CGS M and PGS D scholarships I received from NSERC, and also the scholarships I received from the U of A and Dept. of EAS. This project would not have been possible without the kind invitation from Dale Mah and Tahera Diamond Corp. to visit the Jericho mine and for provision of samples. Thanks to Delene Daniels for sending additional material that was the backbone for Chapter 4.

Thanks to Josh Davies for listening to countless versions of the contents of Chapter 3. To my fellow Girl Partiers Aleksandra Mloszewski, Karen Smit and Lucy Hunt: Karen - for explaining highways in Africa and being a wonderful office roommate - I am very glad we never, ever got distracted by conversation. Aleks - for your calm and collected presence, perceptive advice, and for exploring

the mysteries of Asian cuisine with me. Lucy, my British sister – for being there every day and for knowing what I mean before I even say it. You are the best.

I would like to sincerely thank my family, Mom, Dad, Lauren and Robyn, for supporting me throughout my thesis: for assistance with my countless moves, for the unfailing and active interest in my work, and for the counsel and care during all the difficult moments. I truly have the best family in the world.

Finally, I would like to acknowledge Sebastian Tappe for his essential advise and invaluable knowledgeable that he very willingly bestowed throughout my project – your dedication, curiosity and talent inspires me to be a better researcher. I cannot even begin to express how happy I am Toronto did not work out for you.

Table of Contents

List of Tables

List of Figures

Symbols, Nomenclature, Abbreviations

‰	Parts per thousand (per mil)
%B	Proportion of nitrogen aggregated to B centers in diamond
α	Isotopic fractionation factor
Archean	Geologic eon from 3.8 to 2.5 Ga
ca.	Circa
c.f.	Confer with
CLM	Cratonic Lithospheric Mantle
cm	Centimetre
cps	Counts per second
D	Partition coefficient between mineral and melt
°C	Degrees Celsius
Δ	'Big delta' approximation of 1000 ln α
$\delta^{13}C$	Carbon isotope composition relative to a standard
e.g.	For example
f	Fraction of fluid or melt remaining during fractionation
fO_2	Oxygen fugacity
FTIR	Fourier transform infrared spectroscopy
Ga	Billions of years ago
GPa	Gigapascal
HFSE	High Field Strength Element
HREE	Heavy Rare Earth Element
ICP-MS	Inductively Coupled Plasma Mass Spectrometry
i.e.	that is
J/cm^3	Joules per cubic centimeter, energy fluence
kbar	Kilobars
km	Kilometre
kV	Kilovolt
LILE	Large Ion Lithophile Element
ln	Natural logarithm
LREE	Light Rare Earth Element
Ma	Millions of years ago
Mesoproterozoic	Geologic era within the Proterozoic from 1600 to 1000 Ma
Mg-Number	Molar ratio of Mg/(Mg+Fe)
μm	Micrometer
MREE	Middle Rare Earth Element
$_N$	Subscript to indicate normalized values
N	Normality; molar concentration
nA	Nanoampere
Neoarchean	Geological era within the Archean from 2.8 to 2.5 Ga
nm	Nanometer
Paleoarchean	Geologic era within the Archean from 3.6 to 3.2 Ga
Paleoproterozoic	Geologic era within the Proterozoic from 2.5 to 1.6 Ga
PDB	Pee Dee Belemite carbon isotope standard
ppm	Parts per million, concentration

Proterozoic	Geologic eon from 2500 to 542 Ma
REE	Rare Earth Element
σ	One standard deviation from the mean
s	second
SE	Standard error of the mean
SIMS	Secondary Ion Mass Spectrometry
SMOW	Standard Mean Ocean Water oxygen isotope standard
Type IaA	Diamond with nitrogen aggregated in A centers
Type IaAB	Diamond with nitrogen aggregated in A and B centers
Type IaB	Diamond with nitrogen aggregated in B centers
wt. %	Weight percent, concentration

1 Chapter 1: Introduction

Vestiges of the early Earth are observed in rare occurrences of ancient, ca. 3.8-4.2 billion year old rocks and minerals that are found in the ancient cores of continental crust. These ancient cores, termed 'cratons', are >2.5 Ga pieces of continental crust that have been tectonically stable and quiescent for billion-year timescales (Hoffman, 1988), thus providing the best insight into the evolution of the Earth. The survival of cratons for such long timescales has been attributed to the coupling of cratons to thick, cold and buoyant mantle roots (Jordan, 1978). These roots, which are referred to as cratonic lithospheric mantle (CLM), are generally 150-250 km thick (Rudnick et al., 1998; Pearson and Nowell, 2002), much thicker than the mantle lithosphere below oceanic basins (Jordan, 1978). CLM is composed of peridotite that has undergone high degrees of melt-depletion (e.g., Jordan, 1978; Boyd, 1989), where incompatible elements (elements that preferentially enter the melt phase over the solid residue) such as Al and Ca have been removed via melting processes. This process produces olivine-rich harzburgitic to dunitic residua with high-Mg numbers (e.g., Walter, 1998) that are relatively buoyant due to elimination of more dense mineral phases such as garnet (Boyd and McCallister, 1976). This melt depletion also removes H_2O and heat-producing incompatible elements (such as Th, U, K), thus creating a strong and cold residual root that has resisted erosion by the convecting asthenosphere for billions of years (e.g., Carlson et al., 2005).

Small mantle fragments of the CLM, termed xenoliths, are brought to the Earth's surface by deep-seated volcanism and allowing researchers to directly study the CLM. Studies of xenoliths yield chronological and geochemical information that is necessary to determine the age and the processes by which the CLM formed and evolved. From radiometric dating, CLM-derived xenoliths have been found to be as old as 3.5 Ga, but most have Neoarchean to Paleoproterozoic ages (e.g., Walker et al., 1989; Pearson et al., 1995a,b; Griffin et al., 2004) where the ages of xenoliths generally overlap with the ages of the overlying crust (Pearson et al., 2003; Carlson et al., 2005). Additionally, these common crust-

mantle ages often coincide with major crustal growth and tectonic events observed in cratons, indicating that the cratonic crust and mantle root have had a shared history (Pearson 1999). The formation and evolution of CLM is controversial (e.g., Griffin et al., 2003; Pearson and Wittig, 2008), and debate continues on whether the CLM formed by subduction-driven oceanic lithosphere stacking (e.g., Helmsteadt and Schulze, 1989; Pearson and Wittig, 2008) or from vertical subcretion of mantle plumes (e.g., Griffin et al. 2003; Aulbach et al., 2007). While much of the information on the antiquity and origin of the CLM is derived from peridotite xenoliths, mantle eclogites xenoliths also provide important information on the formation and evolution of the CLM (e.g., Shirey et al., 2001; Jacob 2004).

Eclogites, *sensu lato*, are the high-pressure equivalent of broadly basaltic composition rocks and are, by definition, plagioclase-free rocks where garnet and omphacitic clinopyroxene comprise >75 vol. % of the rock but neither mineral makes up more than 75 vol. % of the rock alone (Desmons and Smulkowski, 2007). Eclogites can also contain minor and accessory minerals such as kyanite, rutile, coesite or quartz, diamond or graphite, orthopyroxene, olivine, apatite, zircon and phlogopite, but not plagioclase (e.g., Carswell, 1990; Jacob 2004). In contrast to eclogites found as bands/lenses in orogenic massifs, eclogite xenoliths in kimberlites rarely contain a free-SiO_2 phase, are more MgO-rich, more SiO_2-, TiO_2-, and Na_2O-poor and are more 'picritic' than 'basaltic' (Liou et al., 1998; Jacob et al., 2003; Pearson et al., 2003; Jacob 2004). The abundance of eclogite in CLM is thought to be quite small (<1%) based on mineral concentrate studies (Schulze 1989), even though some kimberlites have a significant eclogite xenolith population (Pearson et al., 2003; Jacob 2004). Despite this, eclogites are very important due to their involvement in subduction processes (e.g., Ringwood and Green, 1966), formation of mantle heterogeneities (Hirschmann and Stolper, 1996) and contribution to mantle melt generation (e.g., Kogiso et al., 2004; Sobolev et al., 2007). Eclogite xenoliths were originally interpreted to represent cumulates that crystallized within the mantle at high pressures (e.g., O'Hara and Yoder, 1967), but now are generally interpreted to be remnants of subducted

oceanic crust due to their geochemical and isotopic signatures (e.g., Helmsteadt and Doig, 1975; MacGregor and Manton, 1986; Jacob et al., 1994) and therefore are effective links between crustal processes and evolution of the CLM (Pearson 1999; Jacob 2004). However, a recycled oceanic crust origin for eclogite xenoliths is not universally accepted and some researchers still advocate eclogite crystallization at high pressures from mantle-derived melts (e.g., Smyth et al., 1989; Griffin and O'Reilly, 2007). Some eclogite xenoliths are Archean in age (e.g., Jagoutz et al., 1984; Pearson et al., 1995c; Jacob and Foley, 1999; Shirey et al., 2001; Barth et al., 2002) and thus have implications for the formation of Archean crust (e.g., Rapp et al., 1991; Ireland et al., 1994; Rollinson, 1997) and constraints on geodynamic processes operating on early Earth (e.g., Foley et al., 2003; Shirey et al., 2008). Although eclogite (and peridotite) xenoliths are imperative for the investigation of CLM formation and geodynamic processes, many are overprinted by transient melts or fluids during their residence in the CLM that may partially obscure original composition and age information (e.g., Harte 1987). This secondary modification ('metasomatism') of the CLM by migrating fluids or melts may also crystallize diamond (e.g., Cartigny et al., 2004), which, along with any encapsulated minerals ('diamond inclusions') provide additional ways to study the CLM.

Diamonds are economically and scientifically valuable minerals that are largely derived from kimberlites in cratonic settings. They are robust, chemically inert minerals that dominantly sample the lower reaches of the CLM, but some 'super-deep' diamonds are known from the lower mantle (Stachel et al., 2005). Diamonds commonly contain mineral inclusions that, due to their encapsulation, are shielded from metasomatism by passing melts and fluids and thus can provide pristine composition and age information of their source mantle (Richardson et al., 1984; Ireland et al., 1994; Taylor et al., 1996). The mineralogy and composition of diamond inclusions (DIs) from worldwide sources have shown that approximately two thirds are peridotitic and one third are eclogitic, and DI mineral compositions broadly overlap with mineral compositions from peridotite and eclogite xenoliths (Stachel and Harris, 2008). Diamonds are xenocrysts in

kimberlites based on DIs with ages much older than the host kimberlite (Richardson et al., 1984) and the chemical systematics of nitrogen impurities in diamond that can only be generated by million to billion year mantle residence times (Leahy and Taylor, 1997). DI ages range from Paleoarchean to Proterozoic, overlapping with those determined from xenoliths, although some diamonds have relatively young ages, revealing that diamond formation has episodically occurred throughout the history of the CLM (Pearson et al., 2003). Thus, in the same manner as xenoliths, the composition and ages derived from diamond-hosted inclusions are useful for further constraining the development of the CLM.

Whereas diamond mineral inclusions are invaluable for their insight into the petrogenesis of CLM, mantle-derived diamonds also constrain the carbon reservoirs and mechanisms involved in diamond growth, and in turn elucidate the oxidation state of the CLM (e.g., Cartigny 2005; Creighton et al., 2008; Stachel and Harris, 2009). Xenocrystic diamonds sampled from a kimberlite can contain multiple diamond populations of different formation ages and different source rocks (e.g., Richardson et al., 1993); in contrast, xenolith-hosted diamonds are more likely to represent a single diamond population formed during one growth event (e.g., Thomassot et al., 2007). Therefore, diamond-bearing xenoliths are extremely useful as 'natural laboratories' where the mechanism of diamond growth can be studied in great detail. This includes determining the type(s) of fluids or melts involved in diamond growth, and, as the xenoliths themselves serve as passive recorders of this process, the chemical effects of diamond formation on the CLM are revealed from comparison of DIs to host xenoliths. In conclusion, the integrated study of diamonds, diamond inclusions, and the host xenolith are invaluable in order to better understand the processes that encompass diamond formation and its effect on the evolution of the CLM.

Numerous studies of diamond-bearing eclogites have been conducted on samples from kimberlites in the Kaapvaal and Siberian cratons and have greatly improved the understanding of the origin and age of eclogite xenoliths and their hosted diamonds (e.g., MacGregor and Manton, 1986; Jerde et al., 1993; Ireland

et al., 1994; Jacob et al., 1994; Taylor et al., 2000; Menzies et al., 2004; Viljoen et al., 2005; Thomassot et al., 2007; Palot et al., 2009; Spetsius et al., 2009). However, very few studies exist on diamond-bearing samples from other cratons. The Slave craton in northwestern Canada has some several hundred kimberlite occurrences (Bleeker and Hall, 2007) and hosts three operating diamond mines. There have been numerous studies of mantle material from kimberlites in the Slave craton (see Chapter 2 for a detailed review) but studies of diamondiferous eclogites are comparatively rare and thus far diamondiferous eclogites are only known from the Diavik (e.g., Aulbach et al., 2007; Schmidberger et al., 2007) and Jericho kimberlites (e.g., Cookenboo et al., 1998; Heaman et al., 2006). Diamondiferous eclogites from Diavik cover a range of compositions (Aulbach et al., 2007; Schmidberger et al., 2007), whereas those from Jericho have constant high-MgO and Cr_2O_3 compositions. Previous studies of diamond bearing Jericho eclogite xenoliths revealed unusual major-element compositions, but a better understanding of the petrogenesis of these high-MgO and Cr_2O_3 eclogites can be accomplished through further and more in-depth geochemical and isotopic studies. Additionally, the diamond-rich nature of the Jericho eclogites provides an excellent opportunity to study the diamond-formation process in eclogites and also provide insight into processes operating in the Slave CLM.

This study investigates two suites of diamond-rich eclogite xenoliths from the Jericho kimberlite, located in the northern Slave craton of northwestern Canada. The goal of this study is to conduct a geochemical and isotopic investigation of the eclogites, diamonds and diamond inclusions such that the petrogenesis of the diamond-bearing portion of the northern Slave CLM can be elucidated. As well, due to the unique nature of the samples, inferences can be made into the process of diamond formation in the eclogitic portions of the CLM. This thesis begins in Chapter 2 with an overview of the geology of the Slave Craton and underlying CLM, and a summary of previous work done on Jericho eclogites. The main findings of my research are then presented in Chapters 3-5:

(1) Chapter 3: The petrogenesis of the host eclogite xenoliths. A modified version of this chapter was published as *Smart, K.A., Heaman, L.M., Chacko, T.,*

Simonetti, A., Kopylova, M., Mah, D. and Daniels, D. (2009) The origin of high-MgO eclogites from the Jericho kimberlite, Canada. Earth and Planetary Science Letters ***284****, 527-537*. K.A. Smart's contribution to this publication included: data acquisition (with assistance from A. Simonetti with the ICP-MS operation), data processing and manuscript preparation. Contributions from other authors included providing samples and scientific and editorial reviews of the manuscript.

(2) Chapter 4: Formation of the diamonds in the host eclogite xenoliths. A modified version of this chapter is accepted for publication as *Smart, K.A., Chacko, T., Stachel, T., Muehlenbachs, K., Stern, R.A. and Heaman, L.M. (2011) Diamond growth from oxidized carbon sources beneath the northern Slave craton, Canada: A* δ^{13}*C-N study of eclogite-hosted diamonds from the Jericho kimberlite. Geochimica et Cosmochimica Acta In Press*. K.A. Smart's contribution included data acquisition and processing (excluding ion probe analyses of δ^{13}C and N in diamond which was facilitated by R.A. Stern) and manuscript preparation. R.A. Stern contributed Table 4.2. Contributions from other authors included scientific and editorial reviews of the manuscript.

(3) Chapter 5: Eclogite formation beneath the Slave craton revealed by diamond inclusions: an ocecanic origin without a crustal signature? A modified version of this Chapter is submitted to *Earth and Planetary Science Letters*. Co-authors will include T. Chacko, T. Stachel, S. Tappe, R.A. Stern, R.B. Ickert, and Edinburgh Ion Microprobe Facility (EIMF). K.A. Smart completed all data acquisition and processing (excluding δ^{18}O analyses at the University of Alberta) and manuscript preparation. Contributions from other authors included scientific and editorial reviews of the manuscript.

1 References

Aulbach S., Griffin W.L., Pearson N.J., O'Reilly S.Y. and Doyle B.J. (2007) Lithosphere formation in the central Slave Craton (Canada): plume subcretion of lithosphere accretion? Contributions to Mineralogy and Petrology **154**, 409-427.

Barth M.G., Rudnick R.L., Carlson R.W., Horn I. and McDonough W.F. (2002) Re-Os and U-Pb geochronological constraints on the eclogite-tonalite connection in the Archean Man Shield, West Africa. Precambrian Research **118**, 267-283.

Boyd F.R. (1989) Compositional distinction between oceanic and cratonic lithosphere. Earth and Planetary Science Letters **96**, 15-26.

Boyd F.R. and McCallister R.H. (1976) Densities of fertile and sterile garnet peridotites, Geophysical Research Letters **3**: 503-512.

Carlson R.W., Pearson D.G. and James D.E. (2005) Physical, chemical and chronological characteristics of continental mantle. Reviews of Geophysics **43**, RG1001.

Carswell D.A. (1990) Eclogites and the eclogite facies: definitions and classification. Carswell D.A. (ed.) In, Eclogite Facies Rocks, Chapman & Hall, New York, 1-13.Cartigny P. (2005). Stable isotopes and the origin of diamond. Elements **1**, 79-84.

Creighton S., Stachel T., McLean H., Muehlenbachs K., Simonetti A., Eichenberg D., and Luth R. (2008). Diamondiferous peridotitic microxenoliths from the Diavik Diamond Mine, NT. Contributions to Mineralogy and Petrology **155**, 541-554.

Desmons J. and Smulkowski W. (2007) High P/T metamorphic rocks. *In Metamorphic Rocks: A Classification and Glossary of Terms. Recommendations of the International Union of Geological Sciences* (eds. D. Fettes and J. Desmons). Cambridge University Press, Cambridge.

Foley S.F., Buhre S. and Jacob D. (2003) Evolution of the Archean crust by delamination and shallow subduction. Nature **421**, 249-252.

Griffin W.L. and O'Reilly S.Y. (2007). Cratonic lithospheric mantle: Is anything subducted? Episodes **30**, 43-53.

Griffin W.L., O'Reilly S.Y., Abe N., Aulbach S., Davies R.M., Pearson N.J., Doyle B.J. and Kivi K. (2003) The origin and evolution of Archean lithospheric mantle. Precambrian Research **127**, 19-41.

Griffin W.L., Graham S., O'Reilly S.Y., and Pearson N.J. (2004) Lithosphere evolution beneath the Kaapvaal Craton: Re–Os systematics of sulfides in mantle-derived peridotites. Chemical Geology **208**, 89-118.

Harte B. (1987) Metasomatic events recorded in mantle xenoliths: An overview. In: Nixon, P. H. (Ed.), Mantle Xenoliths. John Wiley and Sons, UK, pp. 625-640.

Helmstaedt H. and Doig R. (1975) Eclogite nodules from kimberlite pipes in the Colorado Plateau-samples of subducted Franciscan type oceanic lithosphere. Physics and Chemistry of the Earth **9**, 95-111.

Hirschmann M.M., and Stolper E.M. (1996) A possible role for garnet pyroxenite in the origin of the "garnet signature" in MORB. Contributions to Mineralogy and Petrology **124**, 185-208.

Hoffman P.F. (1988) United Plates of America: the birth of a craton. Annual Reviews in Earth and Planetary Sciences **16**, 543-603.

Ireland T.R., Rudnick R.L. and Spetsius Z. (1994) Trace elements in diamond inclusions from eclogites reveal link to Archean granites. Earth and Planetary Science Letters **128**, 199-213.

Jacob D.E. (2004) Nature and origin of eclogite xenoliths from kimberlites. Lithos **77**, 295-316.

Jacob D.E. and Foley S.F. (1999) Evidence for Archean ocean crust with low high field strength element signature from diamondiferous eclogite xenoliths. Lithos **48**, 317-336

Jacob D., Jagoutz E., Lowry D., Mattey D. and Kudrjavtseva G. (1994) Diamondiferous Eclogites from Siberia - Remnants of Archean Oceanic-Crust. Geochimica et Cosmochimica Acta **58**, 5191-5207.

Jacob D.E., Schmickler B. and Schulze D.J. (2003) Trace element geochemistry of coesite-bearing eclogites from the Roberts Victor kimberlite, Kaapvaal craton. Lithos **71**, 337-351.

Jagoutz E., Dawson J.B., Hoernes S., Spettel B. and Wänke H. (1984) Anorthositic oceanic crust in the Archean Earth. 15th Lunar Planetary Science Conference, pp. 395-396.

Jerde E.A., Taylor L.A., Crozaz G., Sobolev N.V. and Sobolev V.N. (1993) Diamondiferous eclogites from Yakutia, Siberia: evidence for a diversity of protoliths. Contributions to Mineralogy and Petrology **114**, 189-202.

Jordan T.H. (1978) Composition and development of the continental lithosphere. Nature **274**, 544-548.

Kogiso T., Hirschmann M.M. and Pertermann M. (2004) High-pressure partial melting of mafic lithologies in the mantle. Journal of Petrology **45**, 2407-2422.

Leahy K. and Taylor W.R. (1997) The influence of the Glennie domain deep structure on the diamonds in Saskatchewan kimberlites. *Russian Geology and Geophysics* **38**, 481–491.

Liou J.G., Zhang R.Y., Ernst W.G., Rumble D and Maruyama S. (1998) High-pressure minerals from deeply subducted metamorphic rocks. In: R.J. Hemley (ed) *Ultrahigh-Pressure Mineralogy*, Reviews in Mineralogy and Geochemistry **37**, 33-96.

MacGregor I.D. and Manton W.I. (1986) Roberts Victor eclogites: ancient oceanic crust. Journal of Geophysical Research **91 (B14)**, 14063-14079.

Menzies A.H., Carlson R.W., Shirey S.B. and Gurney J.J. (2003) Re–Os systematics of diamond-bearing eclogites from the Newlands kimberlite. Lithos **71**, 323-336.

Palot M., Cartigny P. and Viljoen F. (2009) Diamond origin and genesis: A C and N stable isotope study on diamonds from a single eclogitic xenolith (Kaalvallei, South Africa). *Lithos* **112S**, 758-766.

Pearson D.G. (1999) The age of continental roots. Lithos **48**, 171-194.

Pearson D.G. and Nowell G.M. (2002). The continental lithospheric mantle: characteristics and significance as a mantle reservoir. Philosophical Transactions of the Royal Society of London **360**, 2383-2410.

Pearson D.G. and Wittig N. (2008) Formation of Archaean continental lithosphere and its diamonds: the root of the problem. Journal of the Geological Society of London **165**, 895-914.

Pearson D.G., Shirey S.B., Carlson R.W., Boyd F.R., Pokhilenko N.P. and Shimizu N. (1995a) Re-Os, Sm-Nd, and Rb-Sr isotope evidence for thick Archean lithospheric mantle beneath the Siberian Craton modified by multistage metasomatism. Geochimica et Cosmochimica Acta **59**, 959-977.

Pearson D.G., Carlson R.W., Shirey S.B., Boyd F.R., and Nixon P.H. (1995b) The stabilization of Archean lithospheric mantle: a Re-Os isotope study of

peridotite xenoliths from the Kaapvaal craton. Earth and Planetary Science Letters **134**, 341-357.

Pearson D.G., Snyder G.A., Shirey S.B., Taylor L.A., Carlson R.W. and Sobolev N.V. (1995c) Archean Re–Os age for Siberian eclogites and constraints on Archaean tectonics. Nature **374**, 711-713.

Pearson D.G., Canil D. and Shirey S.B. (2003) Mantle Samples Included in Volcanic Rocks: Xenoliths and Diamonds. 171-275. In *The Mantle and Core* (ed. R.W. Carlson) Vol 2 *Treatise on Geochemistry* (eds. H.D. Holland and K.K. Turekian), Elsevier-Pergamon, Oxford.

Rapp R.P., Watson E.B. and Miller C.F. (1991) Partial melting of amphibolite/eclogite and the origin of Archean trondhjemites and tonalites. Precambrian Research **51**, 1-25.

Richardson S.H., Gurney J.J., Erlank A.J. and Harris J.W. (1984) Origin of diamonds in old enriched mantle. Nature **310**, 198-202.

Richardson S.H., Harris J.W. and Gurney J.J. (1993) Three generations of diamonds from old continental mantle. Nature **366**, 256-258.

Ringwood A.E. and Green D.H. (1966) An experimental investigation of the gabbro-eclogite transformation and some geophysical implications. Tectonophysics **3**, 383-427.

Rollinson H. (1997) Eclogite xenoliths in west African kimberlites as residues from Archean granitoid crust formation. Nature **389**, 173-176.

Rudnick R.L., McDonough W.F. and O'Connell R.J. (1998) Thermal structure, thickness and composition of continental lithosphere, Chemical Geology, Special issue: Geochemical Earth Reference Model, **145**: 399-416.

Schulze D.J. (1989) Constraints on the abundance of eclogite in the upper mantle, Journal of Geophysical Research **94**, 4205-4212.

Shirey S.B., Carlson R.W., Richardson S.H., Menzies A., Gurney J.J., Pearson D.G., Harris J.W. and Wiechert U. (2001) Archean emplacement of eclogitic components into the lithospheric mantle during formation of the Kaapvaal Craton. Geophysical Research Letters **28**, 2509-2512.

Shirey S.B., Kamber B.S., Whitehouse M.J., Meuller P.A. and Basu A.R. (2008) A review of the isotopic and trace element evidence for mantle and crustal processes in the Hadean and Archean: Implications for the onset of plate tectonic subduction. The Geological Society of America Special Paper **440**, 1-29.

Smyth J.R., Caporuscio F.A. and McCormick T. (1989) Mantle eclogites: evidence of igneous fractionation in the mantle. Earth and Planetary Science Letters **93**, 133-141.

Sobolev A.V., Hofmann A.W., Kuzmin D.V., Yaxley G.M., Arndt N.T., Chung S.L., Danyushevsky L.V., Elliott T., Frey F.A., Garcia M.O., Gurenko A.A., Kamenetsky V.S., Kerr A.C., Krivolutskaya N.A., Matvienkov V.V., Nikogosian I.K., Rocholl A., Sigurdsson I.A., Sushchevskaya N.M., Teklay M., 2007. The amount of recycled crust in sources of mantle-derived melts. Science **316**, 412–417.

Spetsius Z.V., Wiggers de Vries D.F. and Davies G.R. (2009) Combined C isotope and geochemical evidence for a recycled origin for diamondiferous eclogite xenoliths from kimberlites of Yakutia. Lithos **112S**, 1032-1042.

Stachel T. and Harris J.W. (2008) The origin of cratonic diamonds - Constraints from mineral inclusions. Ore Geology Reviews **34**, 5-32.

Stachel T. and Harris J.W. (2009) Formation of diamond in the Earth's mantle. Journal of Physics: Condensed Matter **21**, 364206.

Stachel T., Brey G.P., and Harris J.W. (2005) Inclusions in sublithospheric diamonds: Glimpses of deep Earth. Elements **1**, 73-78.

Taylor L.A., Keller R., Snyder G., Wang W., Carlson W., Hauri E., McCandless T., Kim, K-R., Sobolev N. and Bezborodov S. (2000) Diamonds and their Mineral Inclusions, and What They Tell Us: A Detailed "Pull-Apart" of a Diamondiferous Eclogite. International Geology Review **42**, 959-983.

Taylor L.A., Snyder G.A., Crozaz G., Sobolev V.N., Yefimova E.S. and Sobolev N.V. (1996) Eclogitic inclusions in diamonds: Evidence of complex mantle processes over time. Earth and Planetary Science Letters **142**, 535-551.

Thomassot E., Cartigny P., Harris J.W. and Viljoen K.L. (2007) Methane-related diamond crystallization in the Earth's mantle: Stable isotope evidence from a single diamond-bearing xenolith. Earth and Planetary Science Letters **257**, 362-371.

Viljoen K.S., Schulze D.J. and Quadling A.G. (2005) Contrasting Group I and Group II Eclogite Xenolith Petrogenesis: Petrological, Trace Element and Isotopic Evidence from Eclogite, Garnet-Websterite and Alkremite Xenoliths in the Kaalvallei Kimberlite, South Africa. Journal of Petrology **46**, 2059-2090.

Walker R.J., Carlson R.W., Shirey S.B. and Boyd F.R. (1989) Os, Sr, Nd, and Pb isotope systematics of southern African peridotite xenoliths: Implications for the chemical evolution of subcontinental mantle. Geochimica et Cosmochimica Acta **53**, 1583-1595.

Walter M.J. (1998). Melting of garnet peridotite and the origin of komatiite and depleted lithosphere. Journal of Petrology **39**, 29-60.

2 Chapter 2: Slave Craton Background

Cratonic crust and lithospheric mantle have been proposed to have a shared history (e.g., Pearson 1999), such that the interpretation of CLM-derived material benefits by a good understanding of the overlying craton history. As discussed above in Chapter 1, this is especially true for mantle eclogite xenoliths, which may be linked to subduction or melting events that undoubtedly impacted the formation and modification of cratonic crust. The following sections will review the current state of knowledge of composition, age and evolution of the Slave Craton and its lithospheric mantle.

2.1 Slave Craton geology and evolution

The Archean Slave craton of northwest Canada (Figure 2.1) is characterized by an ancient (4.03-2.85 Ga) basement complex that occupies the central and western parts of the craton and a juvenile, 2.72-2.55 Ga volcanic and granitoid terrain in the east (Bleeker and Hall, 2007). The central and western parts of the craton are underlain by ca. 4.0-2.9 Ga tonalitic to gabbroic gneisses, which have been termed the Central Slave Basement Complex (Bleeker et al., 1999a). The Central Slave Basement Complex includes the Acasta gneisses, which have crystallization ages as old as 4.03 Ga (Bowring and Williams, 1999), and a xenocrystic zircon core hosted in granitic gneiss with a still older age of 4.2 Ga (Iizuka et al., 2006). Overlying the basement complex is the 2.9-2.8 Ga Central Slave Cover Group, consisting of fuchsitic quartzites, banded iron formations, semi-pelitic schists and mafic igneous rocks (Bleeker et al., 1999b). Between 2.73-2.70 Ga, large volumes of tholeiitic basalt and subordinate rhyolites of the Kam Group were extruded over the cover group (Bleeker et al., 1999b). Calc-alkaline volcanism from 2.80-2.66 Ga occurred in both the western and eastern portions of the craton and was followed by deposition of turbidite sediments between 2.68-2.66 Ga (Bleeker and Hall, 2007). Major NE-SW shortening and a high temperature-low pressure metamorphic event affected the craton concomitant with the intrusion of voluminous tonalites at 2.63 Ga (Davis and Bleeker, 1999). This was followed by further deformation of the craton and the

2.60-2.58 Ga 'granite-bloom', which consisted of voluminous intrusions of one- and two-mica granites (Davis and Bleeker, 1999; Davis et al., 2003a). The ca. 2.6 Ga deformation, volcanism and granitoid intrusion affecting the craton has been interpreted to result from lithospheric delamination following tectonic thickening by amalgamation of the ancient west and juvenile east cratonic terranes (Davis et al., 1994; Davis et al., 2003a). Later intrusions of mafic dykes from 2.2 to 1.8 Ga cut across the craton (Le Cheminant and van Breemen, 1994). The margins of the craton were modified by Paleoproterozoic orogens to the south and east (Taltson-Thelon; Hoffman, 1988), and west (Wopmay Orogen; Hildebrand et al., 1987) from ca. 2.0-1.8 Ga. The Mackenzie igneous event occurred at 1.27 Ga in the northwest of the craton, and included the giant radiating Mackenzie dyke swarm, Muskox layered ultramafic intrusion, and Coppermine River flood basalts (Le Cheminant and Heaman, 1989). Phanerozoic kimberlites occur throughout the Slave and are particularly concentrated in the Lac de Gras area in the center of the craton (Creaser et al., 2004; Figure 2.1).

2.2 Cratonic lithospheric mantle petrology

The architecture of the lithospheric mantle underlying the Slave craton is vertically and horizontally stratified with respect to its chemical composition (e.g., Griffin et al., 1999; Grütter et al., 1999). Based on the CaO-Cr_2O_3 compositions of garnet xenocrysts from Slave kimberlites, Grütter et al. (1999) divided the Slave CLM into NE-trending northern, central and southern domains. The central domain, sampled by the Lac de Gras kimberlites, has a distinctive shallow ultra-depleted peridotitic layer containing subcalcic garnets thought to represent depleted harzburgites or dunites and extends to depths of ~140 km (Griffin et al., 1999; 2004; Grütter et al., 1999). This ultra-depleted layer is underlain by less depleted lherzolites to the base of the CLM at ~ 200km (Griffin et al., 1999; 2004; Grütter et al., 1999). The ultra-depleted layer is thought to extend beyond the Lac de Gras area in an E-NE trending swath through the central Slave CLM (Grütter et al., 1999). The southern domain, in contrast, is dominated by lherzolitic and eclogitic compositions, with a minor population of ultra-depleted harzburgitic

garnets (Grütter et al., 1999). In the northern domain, the upper CLM (to a depth of ~130 km) is dominated by fertile lherzolitic compositions and below by metasomatized lherzolites, with depleted harzburgitic garnets being very rare (Griffin et al., 2004). The Jericho kimberlite lies in the northern domain and contains a significant eclogitic and pyroxenitic component based on both garnet xenocryst and xenolith populations (Grütter et al., 1999; Kopylova et al., 1999a,b). Kopylova and Russell (2000) found a strong chemical layering in peridotite xenoliths, observed as increases in total FeO with depth and an overall metasomatic enrichment of the Jericho lithospheric mantle.

Geophysical evidence from teleseismic (Bostock, 1998) and deep seismic reflection (Cook et al., 1999) data also indicates the Slave CLM is structurally layered. Shallow, near horizontal reflectors at ~70-80 and 120-150 km (M2 of Cook et al., 1999) are interpreted to represent remnant Archean shallow subduction relating to accretion of the Slave craton (Bostock, 1998). Deeper, east-dipping reflectors found at 170 km under the western Slave and at 230 km under the central Slave (M1 of Cook et al., 1999) are interpreted to be associated with Paleoproterozoic subduction attributed to the accretion of ca. 1.9 Ga arc terranes during the ca. 1.8-2.0 Ga Wopmay orogen (Bostock, 1998; Cook et al., 1999).

2.2.1 Age of the CLM from mantle-derived xenoliths

Ages derived from Slave CLM broadly overlap with those observed in the Slave cratonic crust. A probability density plot of Re-Os model ages for whole-rock peridotites from kimberlites in the central and northern domains show major peaks at 2.7-2.8, 1.8 and 1.3 Ga (Pearson and Wittig, 2008). The peak at ca. 2.7 Ga is similar to 2.8-2.9 Ga model ages from sulfide inclusions in olivine xenocrysts (Aulbach et al., 2004). Peridotitic sulfide inclusions in diamond from the central domain appear to record older ages of 3.3-3.5 Ga (e.g., Westerlund et al., 2006; Aulbach et al., 2009a, 2011). These Paleoarchean ages include (1) initial radiogenic $^{187}Os/^{188}Os$ compositions of pertidotitic sulfide diamond inclusions (Aulbach et al., 2009a; 2011), (2) Re-Os isochron age of 3.27 ± 0.34 Ga from sulfide inclusions in olivine xenocrysts from Diavik kimberlite (Aulbach

et al., 2004), and (3) Re-Os isochron age of 3.52 ± 0.17 Ga from peridotitic sulfide diamond inclusions (Westerlund et al., 2006). These ages imply the existence of an ancient CLM component in the Slave craton where melt extraction and diamond formation occurred in the Paleoarchean, and the diamonds survived later Neoarchean heating events (e.g., Davis et al., 2003a). The 3.52 ± 0.17 Ga age from Westerlund et al. (2006) has been disputed by Pearson and Wittig (2008) who interpret this as a mixing age and alternatively postulate the diamonds may have formed at ca. 2.7 Ga, coinciding with the abundant approximately 2.7 Ga Re-Os model ages derived from the same inclusions and the 2.6-3.1 Ga model ages from harzburgite xenoliths from the same kimberlite. Younger Paleoproterozoic Re-Os model ages are found throughout the central and northern Slave domains. However, 1.8 Ga ages are more abundant from the Jericho kimberlite in the northern domain, and Mesoproterozoic ages of ca. 1.3 Ga are almost exclusively found from Jericho as well (Irvine et al., 1999; Pearson and Wittig, 2008).

In contrast to the Archean ages derived from Slave peridotites and P-type sulfide inclusions, eclogite xenoliths and E-type diamond inclusions dominantly record ca. 2.1-1.8 Ga ages, derived from Lu-Hf, U-Pb, and Pb-Pb isotopic systems (Heaman et al., 2002; 2006; Schmidberger et al., 2005; 2007; Aulbach et al., 2009 a,b). A probability density plot of Slave eclogite ages from Heaman and Pearson (2010) clearly shows the dominance of younger Paleo- and Mesoproterozoic ages in eclogitic material. Recalculations of Lu-Hf and Sm-Nd isotopic data from Diavik eclogites appear to show Neoarchean isochron and model ages of ca. 2.4-2.6 Ga (Heaman and Pearson, 2010), however, the errors associated with some of the re-calculated ages are very large with high MSWDs (> 1 Ga and > 90, respectively), such that Archean ages for eclogites should be treated with caution. Paleoproterozoic ages are found in eclogite xenoliths from both the Jericho and Diavik kimberlites. In detail, eclogite xenoliths from the Diavik kimberlite in the central domain display a Lu-Hf "errorchron" age of 2.1±0.3 Ga, which is complemented by a Pb-Pb model age of 2.1 Ga (Schmidberger et al., 2007). Zircon-bearing eclogite xenoliths from the Jericho kimberlite in the northern

domain have U-Pb ages from 2.0-0.8 Ga and model Lu-Hf ages of 2.1 and 2.3 Ga, but importantly, a minimum age of eclogite growth is constrained by a zircon with upper intercept ages of ca. 1.9 ± 0.07 Ga (Schmidberger et al., 2005). Paleoproterozoic ages are also observed in eclogitic and pyroxenitic sulfide diamond inclusions from the Diavik kimberlite, which have Re-Os isochron ages of 1.86 ± 0.19 and 1.84 ± 0.14 Ga, respectively (Aulbach et al., 2009a,b).

Some of the ages derived from Slave CLM peridotites and eclogites overlap with ages observed in the overriding cratonic crust, and potentially may be linked to craton formation and evolution (e.g., Pearson, 1999). In particular, the significant peak of CLM peridotite ages at ~2.7 Ga correspond to concurrent voluminous Neoarchean basaltic volcanism (Bleeker et al., 1999b) and younger granitic magmatism at ca. 2.6 Ga (Davis et al., 2003a). Thus, peridotitic material with these Neoarchean ages may represent CLM formation associated with amalgamation and cratonization of the Slave craton (e.g., Davis et al., 2003a; Heaman and Pearson, 2010). Diamonds with Paleoarchean inclusion ages are in apparent conflict with the major ca. 2.6 Ga cratonic thermal heating event, as diamonds were predicted to be younger than the widespread heating event (Davis et al., 2003a, b). Thus, assuming the Paleoarchean diamond ages are accurate and do not represent an artifact of isotopic mixing, these diamonds could have formed in an exotic piece of old lithospheric mantle, perhaps coupled to the ancient western half of the Slave craton, which was thrust under the Slave craton after ca. 2.6 Ga (e.g., Aulbach et al, 2009a; Heaman and Pearson, 2010). Paleoproterozoic ages observed in peridotitic and eclogitic xenoliths and diamond inclusions have been related to subduction associated with the ca. 1.8-1.9 Wopmay orogen, as oceanic lithosphere was brought into the Slave CLM at this time (e.g., Bostock, 1999; Cook et al., 1999; Schimidberger et al., 2005, 2007). Paleoproterozoic eclogite formation is supported by Diavik eclogite xenoliths that contain geochemical and Sr-isotopic evidence for a seawater-altered gabbroic protolith (Schmidberger et al., 2007). Alternatively, eclogites from the Slave CLM have been interpreted as ponded basalts at depth, related to intrusion of mafic dikes into the crust at 2.2, 2.0 and 1.8 Ga (Heaman and Pearson, 2010). The ~1.3 Ga ages

observed in some eclogites and peridotites are interpreted to reflect metasomatic overprinting associated with the 1.27 Ga Mackenzie igneous event (Le Cheminant and Heaman, 1989; Heaman et al., 2006).

2.3 Previous investigations of the CLM beneath the Jericho kimberlite

2.3.1 Eclogite xenoliths

The Jericho kimberlite has a precise age of 173.3±1.3 Ma from Rb-Sr dating of phlogopite from eclogite xenoliths (Heaman et al., 2006). Early studies of the xenolith population from the Jericho kimberlite revealed a high proportion of eclogite xenoliths (25%) and these were divided into textural 'massive' and 'anisotropic' groups (Cookenboo et al., 1998; Kopylova et al., 1999b). These studies also revealed a high number (8%) of megacrystalline pyroxenitic and ilmenite-garnet wehrlite-clinopyroxenite xenoliths (Kopylova et al., 1999a). Detailed petrographic and geochemical descriptions of eclogite xenoliths at Jericho can be found in Cookenboo et al. (1998), Kopylova et al. (1999b) and Heaman et al. (2006). Massive eclogites are composed of coarse, subhedral garnet and clinopyroxene with 1-3% rutile and occasional zircon, olivine and diamond. The anisotropic eclogites exhibit a preferred orientation of minerals, and, in places, compositional banding. Some of these xenoliths have appreciable amounts of kyanite (up to 20%), rutile (1-7%) and rare zircon and apatite. Geochemically, all Jericho eclogites contain low-Cr, pyrope-almandine garnet and omphacitic clinopyroxene; massive eclogites comprise garnet with higher MgO and lower CaO and clinopyroxene with lower Al_2O_3 and Na_2O contents than their anisotropic eclogite counterparts. According to the geochemical classification of Coleman et al. (1965) and Taylor and Neal (1990), the massive eclogites belong to Group A and B, and anisotropic eclogites to Group C. All eclogites record final equilibration temperatures (calculated at 5 GPa) from 600-1150ºC. In contrast, the pyroxenitic xenoliths were found to have higher Cr_2O_3 contents and contain jadeite-poor clinopyroxene and pyrope-rich garnet. These xenoliths also record higher temperatures of 1050-1250ºC (calculated at 5 GPa).

Investigation of unusual zircon-bearing Jericho eclogite xenoliths (Heaman et al., 2002; 2006; Schmidberger et al., 2005) revealed extreme whole-rock HFSE-enrichments, a consequence of the presence of zircon and rutile. The zircons yield U-Pb ages ranging from 2.0-0.8 Ga and Lu-Hf ages of 2.1 and 2.3±0.1 Ga. On the basis of their Paleoproterozoic ages, the Jericho zircon-bearing eclogites were interpreted to represent remnants of subducted oceanic crust associated with accretion of ca. 1.9 Ga magmatic arcs (e.g., Hottah or Great Bear) to the western margin of the Slave craton occurring during the Wopmay Orogen (Heaman et al., 2002; 2006; Schmidberger et al., 2005). Diamond-bearing eclogites from Jericho dominantly were found to have 'massive' textures with uniformly high-MgO contents that resulted in a fairly restricted range of calculated temperatures (1010±30ºC) at 5 GPa (Cookenboo et al., 1998; Heaman et al., 2006). Based on these observations, Cookenboo et al. (1998) and Heaman et al. (2006) hypothesized that these eclogites formed from melts derived from peridotite at depths >180 km.

2.3.2 Peridotite xenoliths

Peridotite xenoliths from the Jericho kimberlite, as discussed in 2.2, are dominantly lherzolites that have variably experienced an alkali-, LREE-rich metasomatic event (Kopylova et al., 1999a; Kopylova and Russel, 2000; Griffin et al., 2004). The peridotitic mantle at Jericho is vertically layered as indicated by a decrease in Mg-number and oxygen fugacity (fO_2), and an increase in FeO_T, Y, Zr, and Ti and clinopyroxene abundance in garnet peridotites with increasing depth (Kopylova and Russel, 2000; Griffin et al., 2004; McCammon and Kopylova 2004). Combined, these vertical geochemical and mineralogical changes have been interpreted as an increase in fertility with depth, either resulting from melt-metasomatism or downward-younging of the peridotitic CLM (Kopylova and Russel, 2000; Griffin et al., 2004). Re-Os model ages derived from Jericho peridotites (Irvine et al., 1999; 2003) range from 0.5-3.1 Ga, where shallow spinel peridotites have model ages of 2.6-3.1 Ga (excluding one model age of ca. 1.3 Ga) and deeper garnet peridotites have dominantly younger ages

<2.7 Ga with concentrations of model ages at ca. 1.8 and 1.3 Ga (Irvine et al., 1999). Pyroxenites and megacrysts with magmatic textures record the highest P-T conditions and form a relatively thin layer (20-40 km in thickness) and are overlain by the most fertile peridotite (Kopylova et al. 1999a). This thin layer of pyroxenitic material was interpreted to represent relatively young magmatic activity at the petrological base of the CLM (Kopylova and Russel, 2000).

2.3.3 Diamonds

De Stefano et al. (2009) investigated xenocrystic diamonds from the Jericho kimberlite and discovered the diamonds dominantly contain eclogitic inclusions (90%) and had a wide range of carbon isotope compositions ($\delta^{13}C$ = -5 to -41‰). Garnet diamond inclusions (DIs) from De Stefano et al. (2009) have variable compositions with Mg-numbers ranging from 53 to 81 and only garnets with Mg-numbers > 80 have elevated Cr_2O_3 contents up to 0.8 wt.%. These latter garnets overlap with those from the diamond-bearing Jericho eclogites described previously and led De Stefano et al. to classify these high-MgO garnets as 'websteritic', which was supported by the occurrence of orthopyroxene with high-MgO garnet in one diamond. Clinopyroxene DIs are less abundant than garnet and have Mg-numbers from 77-90 and Na_2O contents between 1.4-3.4 wt. %. Based on studies of other Jericho eclogites with enrichments in incompatible elements and MgO-enriched secondary minerals, De Stefano et al. postulated that the Jericho eclogites formed via multiple melt extraction and metasomatism events. Formation of diamond with very low $\delta^{13}C$ values was thought to have occurred from hydrous, K-rich fluids that contained an "exotic", isotopically light mantle carbon source.

References

Aulbach S., Griffin W.L., Pearson N.J., O'Reilly S.Y., Kivi K., Doyle B.J. (2004) Mantle formation and evolution, Slave Craton: constraints from HSE abundances and Re-Os isotope systematics of sulfide inclusions in mantle xenocrysts. Chemical Geology **208**, 61-88.

Aulbach S., Stachel T., Creaser R.A., Heaman L.M., Shirey S.S., Muehlenbachs K., Eichenberg D. and Harris J.W. (2009a) Sulphide survival and diamond genesis during formation and evolution of Archaean subcontinental lithosphere: A comparison between the Slave and Kaapvaal cratons. Lithos **112S**, 747-757.

Aulbach S., Creaser R.A., Pearson N.J., Simonetti S.S., Heaman L.M., Griffin W.L. and Stachel T. (2009b) Sulfide and whole-rock Re-Os systematics of eclogite and pyroxenite xenoliths from the Slave craton, Canada. Earth and Planetary Science Letters **283**, 48-58.

Aulbach S., Stachel T., Heaman L.M., Creaser R.A. and Shirey S.B. (2011) Formation of cratonic subcontinental lithospheric mantle and complementary komatiite from hybrid plume sources. Contributions to Mineralogy and Petrology **161**, 947-960.

Bleeker W. and Hall B. (2007) The Slave Craton: Geology and metalligenic evolution, In: Goodfellow, W.D., ed., *Mineral Deposits of Canada: A Synthesis of Major Deposit-Types, District Metallogeny, the Evolution of Geological Provinces, and Exploration Methods:* GAC Mineral Deposits Division Specical Publication **5**, pp 849-879.

Bleeker W., Ketchum J., and Davis W. (1999a) The Central Slave Basement Complex, Part II: age and tectonic significance of high-strain zones along the basement-cover contact. Canadian Journal of Earth Sciences **36**, 1111-1130.

Bleeker W., Ketchum J., Jackson V., and Villeneuve M. (1999b) The Central Slave Basement Complex, Part I: its structural topology and autochthonous cover. *Canadian Journal of Earth Sciences* **36**, 1083-1109.Boyd F.R. (1989) Compositional distinction between oceanic and cratonic lithosphere. Earth and Planetary Science Letters **96**, 15-26.

Bostock M.G. (1998) Mantle stratigraphy and evolution of the Slave province. Journal of Geophysical Research **103**, 21183-21200.

Bowring S.A. and Williams I.S. (1999) Priscoan (4.00-4.03 Ga) orthogneisses from northwestern Canada. Contributions to Mineralogy and Petrology **134**, 3-16.

Coleman R.G., Lee E.D., Beatty L.B. and Brannock W.W. (1965) Eclogites and eclogites: their differences and similarities. Geologic Society of America Bulletin **76**, 483-508.

Cook F.A., van der Velden A.J. and Hall K.W. (1999) Frozen subduction in Canada's Northwest Territories: Lithoprobe deep lithospheric reflection profiling of the western Canadian Shield. Tectonics **18**, 1-24.

Cookenboo H.O., Kopylova M.G., Daoud D.K. (1998) A chemically and texturally distinct layer of diamondiferous eclogite beneath the Slave craton, Northern Canada 7th International Kimberlite Conference, Cape Town.

Creaser R.A., Grutter H., Carlson, J. and Crawford B. (2004) Macrocrystal phlogopite Rb-Sr dates for the Ekati property kimberlites, Slave Province, Canada: evidence for multiple intrusive episodes in the Paleocene and Eocene. Lithos, **76**, 399-414.

Davis W.J. and Bleeker W. (1999) Timing of plutonism, deformation and metamorphism in the Yellowknife Domain, Slave Province, Canada. Canadian Journal of Earth Sciences **36**, 1169-1187.

Davis W.J., Fryer B.J. and King J.E. (1994) Geochemistry and evolution of Late Archean plutonism and its significance to tectonic development of the Slave Craton. Precambrian Research **67**, 207-241.

Davis W.J., Jones A.G., Bleeker W. and Grütter H. (2003a) Lithosphere development in the Slave craton: a linked crustal and mantle perspective. Lithos, **71,** 575-589.

Davis W.J., Canil D., MacKenzie J.M. and Carbno G.B. (2003b). Petrology and U-Pb geochronology of lower crustal xenoliths and the development of a craton, Slave Province, Canada. Lithos **71**, 541-573.

De Stefano A., Kopylova M.G., Cartigny P. and Afanasiev V. (2009) Diamonds and eclogites of the Jericho kimberlite (Northern Canada). Contributions to Mineralogy and Petrology **158**, 295-315.

Griffin W.L., Doyle B.J., Ryan C.G., Pearson N.J., O'Reilly S.Y., Natapov L., Kivi K., Kretschmar U. and Ward J. (1999) Lithospheric Structure and Mantle Terranes: Slave Craton, Canada. *In* Proceedings of the 7th international Kimberlite Conference. J.B. Dawson Vol. *Edited* by J.J. Gurney, J.L. Gurney, M.D. Pascoe and S.H. Richardson. Red Roof Design, Cape Town, South Africa, pp 299-306.

Griffin W.L., O'Reilly S.Y., Doyle B.J., Pearson N.J., Coopersmith H., Kivi K., Malkovets V. and Pokhilenko N. (2004) Lithosphere mapping beneath the north American plate. Lithos **77**, 873-922.

Grütter H.S., Apter D.B. and Kong J. 1999. Crust–mantle coupling: Evidence from mantle-derived xenocrystic garnets. *In* Proceedings of the 7th international Kimberlite Conference. J.B. Dawson Vol. *Edited* by J.J. Gurney, J.L. Gurney, M.D. Pascoe and S.H. Richardson. Red Roof Design, Cape Town, South Africa, pp 307-313.

Heaman L.M. and Pearson D.G. (2010) Nature and evolution of the Slave Province subcontinental lithospheric mantle. Canadian Journal of Earth Science **47**, 369-388.

Heaman L.M., Creaser R.A., and Cookenboo H.O. (2002). Extreme enrichment of high field strength elements in Jericho eclogite xenoliths: A cryptic record of Paleoproterozoic subduction, partial melting, and metasomatism beneath the Slave craton, Canada. Geology **30**, 507-510.

Heaman L.M., Creaser R.A., Cookenboo H.O., and Chacko T. (2006). Multi-stage modification of the northern Slave mantle lithosphere: Evidence from zircon- and diamond-bearing eclogite xenoliths entrained in Jericho kimberlite, Canada. Journal of Petrology **47**, 821-858.

Hildebrand R.S., Hoffman P.F., and Bowring S. (1987) Tectono-magmatic evolution of the 1.9 Ga Great Bear magmatic zone, Wopmay orogen, northwestern Canada. Journal of Volcanology and Geothermal Research **32**, 99–118.

Hoffman P.F. (1989) Precambrian geology and tectonic history of North America. *In* Bally A.W. and Palmer A.R., eds. The geology of North America: an overview, The Geology of North America, Geological Society of America, Boulder CO v.A, pp 447-512.

Iizuka T., Horie K., Komiya T., Mauruyama S., Hirata T., Hidaka H. and Windley B.F. (2006) 4.2 Ga zircon xenocryst in an Acasta gneiss from northwestern Canada: Evidence for early continental crust. Geology **34**. 245-248.

Irvine G., Kopylova M.G., Carlson R.W., Pearson D.G., Shirey S.B. and Kjarsgaard B.A. (1999) Age of the lithospheric mantle beneath and around the Slave craton: A Re–Os isotope study of peridotite xenoliths from the Jericho and Somerset Island kimberlites. Abstract, 9th Annual Goldschmidt Conference.

Irvine G., Pearson D.G., Kjarsgaard B.A., Carlson R.W., Kopylova M.G. and Dreibus G. (2003) A Re-Os isotope and PGE study of kimberlite-derived peridotite xenoliths from Somerset Island and a comparison to the Slave and Kaapvaal cratons. Lithos **71**, 461-488.

Kopylova M.G. and Russell J.K. (2000) Chemical stratification of the cratonic lithosphere: Constraints from the northern Slave craton, Canada. Earth and Planetary Science Letters **181**, 71-87.

Kopylova M.G., Russell J.K., and Cookenboo H. (1999a). Petrology of peridotite and pyroxenite xenoliths from the Jericho kimberlite: Implications for the thermal state of the mantle beneath the Slave craton, Northern Canada. Journal of Petrology **40**, 79-104.

Kopylova M.G., Russell J.K. and Cookenboo H. (1999b). Mapping the lithosphere beneath the north central Slave Craton. In: Gurney, J. J., Gurney, J. L., Pascoe, M. D. & Richardson, S. H. (eds) Proceedings of the 7th International Kimberlite Conference. Cape Town: Red Roof Design pp. 468-479.

Le Cheminant A.N. and van Breemen O. (1994) U-Pb ages of Proterozoic dyke swarms, Lac de Gras area, N.W.T.: Evidence for progressive break-up of an Archean supercontinent: GAC Programs with Abstracts **19**, 62.

Le Cheminant A.N. and Heaman L.M. (1989). Mackenzie igneous events, Canada: Middle Proterozoic hotspot magmatism associated with ocean opening. Earth and Planetary Science Letters **96**, 38-48.

McCammon C. and Kopylova M.G. (2004) A redox profile of the Slave mantle and oxygen fugacity control in the cratonic mantle. Contributions to Mineralogy and Petrology **148**, 55-68.

Pearson D.G. (1999) The age of continental roots. Lithos **48**, 171-194.

Pearson D.G. and Wittig N. (2008) Formation of Archaean continental lithosphere and its diamonds: the root of the problem. Journal of the Geological Society of London **165**, 895-914.

Schmidberger S.S., Heaman L.M., Simonetti A., Creaser R.A. and Cookenboo H.O. (2005) Formation of Paleoproterozoic eclogitic mantle, Slave Province (Canada): Insights from in-situ Hf and U-Pb isotopic analyses of mantle zircons. Earth and Planetary Science Letters **240**, 621-633.

Schmidberger S.S., Simonetti A., Heaman L.M., Creaser R.A. and Whiteford S. (2007) Lu-Hf, in-situ Sr and Pb isotope and trace element systematics for mantle eclogites from the Diavik diamond mine: Evidence for

Paleoproterozoic subduction beneath the Slave craton, Canada. Earth and Planetary Science Letters **254**, 55-68.

Taylor L.A. and Neal C.R. (1990) Eclogites with oceanic crustal and mantle signatures from the Bellsbank kimberlite, South Africa, Part 1: Mineralogy, petrology, and whole-rock chemistry. Journal of Geology **97**, 551-567.

Westerlund K. J., Shirey S. B., Richardson S. H., Carlson R. W., Gurney J. J. and Harris, J. W. (2006). A subduction wedge origin for Paleoarchean peridotitic diamonds and harzburgites from the Panda kimberlite, Slave craton, evidence from Re-Os isotope systematics. Contributions to Mineralogy and Petrology **152**, 275-294.

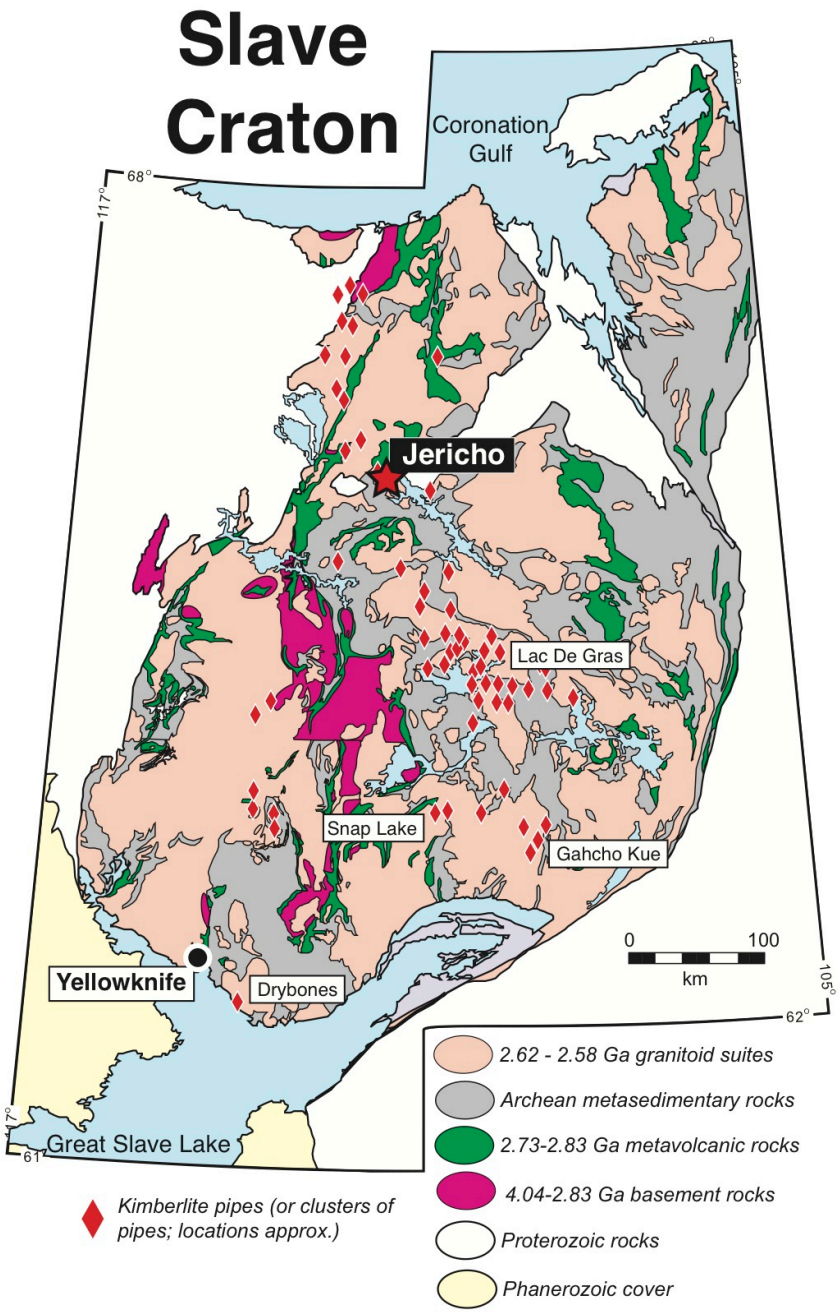

Figure 2.1 Geological map of the Slave craton.

Geological map of the Slave craton, located in northwestern Canada. Modified from Davis et al. (2003a).

3 Chapter 3: The Origin of High-MgO Diamond Eclogites from the Jericho Kimberlite, Canada[1]

3.1 Introduction

Although the proportion of eclogite within the cratonic lithospheric mantle is inferred to be small (<1%, Schulze, 1989), the proportion of eclogite xenoliths and eclogitic diamonds recovered from some kimberlites, including the Jericho kimberlite, is surprisingly large (e.g., Stachel and Harris, 2008). Despite the worldwide abundance of eclogitic diamonds, there are comparatively fewer diamondiferous eclogite xenoliths available for study, limiting our understanding of the origin of eclogitic diamonds and their host rocks. Additionally, mantle eclogites can provide insight on the composition and evolution of the cratonic lithospheric mantle. Two main hypotheses have been proposed for the origin of eclogite xenoliths: 1) remnants of subducted and metamorphosed oceanic crust (e.g., Helmstaedt and Doig, 1975; Jagoutz et al., 1984; MacGregor and Manton, 1986; Jacob et al., 1994; Jacob 2004) and 2) cumulates of basaltic magmas crystallized at high pressure (e.g., O'Hara and Yoder, 1967; Shervais et al., 1988; Smyth et al., 1989). In this study, we evaluate these hypotheses in light of the major-, trace-element and Sr and Pb isotope compositions of minerals in a suite of high-MgO eclogite xenoliths recently recovered from the Jericho kimberlite, including thirteen spectacularly fresh, diamond-rich eclogites.

3.1.1 Background

The 173 Ma Jericho kimberlite (Heaman et al., 2006) is located in the northern Slave craton in Nunavut, Canada approximately 400 km NNE of Yellowknife (see Figure 2.1). Our new data and previous studies on Jericho eclogites (Cookenboo et al., 1998; Kopylova et al., 1999a; Heaman et al., 2002, 2006; Schmidberger et al., 2005) reveal that in addition to garnet and clinopyroxene, Jericho eclogites may also contain diamond, kyanite, corundum,

[1] A version of this chapter is published as Smart K.A., Heaman L.M., Chacko T., Simonetti A., Kopylova M., Mah D. and Daniels D. (2009) The Origin of high-MgO Diamond Eclogites from the Jericho Kimberlite, Canada. Earth and Planet Science Letters 284: 527-537.

rutile, phlogopite, apatite or zircon. The Jericho eclogites can be subdivided into three broad geochemical groups based on garnet composition; 1) Mg-rich (19.6-21.2 wt.% MgO), 2) Ca-rich (up to 17.5 wt.% CaO), including kyanite-bearing eclogites, and 3) Fe-rich (up to 26.5 wt.% FeO), including zircon-bearing xenoliths. This grouping broadly correlates geochemically with the Group A-B-C eclogite classification originally proposed by Coleman et al. (1965), and will be used to describe the three groups hereafter. The diamond-bearing eclogites at Jericho are predominantly Mg-rich Group A eclogites and have homogeneous mineral compositions (Cookenboo et al., 1998; Heaman et al., 2006). A few intermediate-MgO, Group B (~14.0 wt.% MgO) diamond eclogite xenoliths have recently been reported from Jericho by De Stefano et al. (2009). Garnet-clinopyroxene thermometry of the high-MgO diamond eclogites using the calibrations of Ellis and Green (1979) and Krogh Ravna (2000) indicates a restricted temperature range of about 30ºC at 1000°C (calculated at 5.0 GPa) for last equilibration (Cookenboo et al., 1998; Heaman et al., 2006). This differs from diamond-bearing eclogites from the Diavik kimberlites, just 100 km south of Jericho, which have Group B and C compositions and record much higher temperatures (1127-1299°C, Schmidberger et al., 2007). The uniform mineral compositions and limited range of equilibration temperatures of the Jericho diamond eclogites led Cookenboo et al. (1998) and Heaman et al. (2006) to propose that these rocks represent high-pressure cumulates from primary mantle melts. This origin is distinct from all other Group B and C eclogites at Jericho, which have been interpreted to be remnants of Paleoproterozoic subducted oceanic crust (Heaman et al., 2002, 2006; Schmidberger et al., 2005). Although Paleoproterozoic to Mesoproterozoic formation and modification ages have been reported for other suites of Jericho eclogites (Heaman et al., 2002; 2006; Schmidberger et al., 2005), there is no age information available for the high-MgO, Jericho diamond eclogites.

3.1.2 Petrography of the Jericho Diamond Eclogites

The Jericho diamond eclogites (abbreviated JDE hereafter) investigated in

this study are dominantly garnet-clinopyroxene-diamond±phlogopite rocks, where diamond and phlogopite can comprise up to 20% and 2% of the mode, respectively (Figure 3.1a). Reddish-orange garnet and vibrant green clinopyroxene occur as 1-3 mm, generally fresh inclusion-free crystals with a granoblastic texture. These rocks are not layered or deformed and garnet and clinopyroxene are fresh. Diamonds are 0.5-2 mm colorless and transparent octahedra, twinned-octahedra and irregularly shaped aggregates that occur at the grain boundaries of garnet and clinopyroxene, where commonly diamond shape is controlled by the presence of garnet and clinopyroxene. The diamonds are variably surrounded by a fine-grained black material, consisting of fine phlogopite, apatite, carbonate and a Mg- and Al-rich silicate phase. This assemblage also occurs as thin vein networks throughout the eclogites, locally transecting both garnet and clinopyroxene crystals. Diamonds in the Jericho eclogites are also commonly mantled by phlogopite and these diamonds invariably have resorbed grain boundaries (Figure 3.1b). However, a small population of diamond is in direct contact with neighboring garnet and clinopyroxene and a few sharp-edged, <0.5 mm diamonds occur as inclusions in garnet (Figure 3.1c). Inter-connected networks of Ni-rich (NiO ~ 71 wt. %, Table 3.1) sulfide globules rimmed by phlogopite and carbonate are also present in the JDE (Figure 3.1d). An additional discovery of this study is the occurrence of a tiny (~20 μm) garnet inclusion in diamond in eclogite JDE 03 (Figure 3.1b), which is compositionally different from garnet in the host eclogite.

3.2 Analytical Methods

We report results on thirteen previously unstudied JDE from the Jericho kimberlite, and present new data on a suite of Group B and C eclogites, of which six (of fifteen total) were studied by Kopylova et al. (1999a). All JDE reported here are between 2-4 cm in diameter and were recovered during ore processing at the Jericho mine. Eclogite xenoliths were wrapped in multiple layers of plastic and coarsely crushed. Inclusion-free garnet and clinopyroxene grains were handpicked in ethanol under a binocular microscope, mounted in epoxy, and

analyzed for major-elements using a JEOL 8900 electron microprobe at the University of Alberta. Analyses were performed using a 20nA beam current and 20kV accelerating voltage. Ten spots per mineral grain were analyzed in tracks across grains from rim to rim and a minimum of five garnet and five clinopyroxene were analyzed per xenolith. Major-element compositional data were also obtained for garnet, clinopyroxene and phlogopite in polished "thick" sections of the same xenoliths using the electron microprobe.

Trace-element compositions were obtained in both grain mounts (garnet and clinopyroxene) and thick sections (phlogopite) by laser ablation Quadrupole ICP-MS, using a New Wave Research Nd:YAG UP213 laser system coupled to a Perkin Elmer Elan 6000 Quadrupole ICP-MS. Laser spot size for all minerals was 160 μm and each ablation was 50s in duration after 20s of background counting times with a fluence of ~15 J/cm^2. Because of the small grain size, only one spot per mineral grain was analyzed, with a minimum of five grains of each mineral analyzed per xenolith. The NIST 612 standard was analyzed at the start and finish of each ablation session, and the CaO content of each mineral, as determined by electron microprobe analysis, was used as an internal standard for calibration. Data was reduced using the GLITTER® software (van Achterbergh et al., 2001). The analytical precision for most elements at the 2σ level is between 7 and 40%, and is generally better than 10% with the higher uncertainties typical for elements present in low abundances (e.g., U, Th in garnet and HREEs in clinopyroxene). Further details on the techniques employed here can be found in Schmidberger et al. (2007).

Sr and Pb isotope compositions of clinopyroxene were obtained in-situ using the same laser system noted above coupled to a NuPlasma multicollector-ICP-MS. For clinopyroxene Sr isotope analyses, 160 μm diameter spots were ablated in clinopyroxene and data were collected using five Faraday detectors, following the procedure described in Schmidberger et al. (2003). Repeated analysis of a modern coral standard (Bizzarro et al., 2003) for Sr isotope investigations were completed during each analytical session and the $^{87}Sr/^{86}Sr$ ratios determined in this study (0.709115±0.000071 and 0.709011±0.000074) and

from previously determined thermal ionization mass spectrometry analyses (0.709098±0.000019, Bizzarro et al., 2003) are indistinguishable. Thus, a normalization factor was not required for the Sr isotope analyses of clinopyroxene. For Pb isotope analyses, clinopyroxene was ablated using a 320 μm by 320 μm raster pattern and a 160 μm diameter spot size. The Pb data were collected using three ion counters plus two Faraday detectors for Tl collection. The NIST 614 standard glass was analyzed for its Pb isotope composition at each session where measured $^{206}Pb/^{204}Pb$ deviated from the accepted values by less than 0.7%. The procedure employed here for Pb isotope data collection is similar to that described in Simonetti et al. (2005).

3.3 Results

3.3.1 Mineral chemistry

Tables 3.1 and 3.2 list the average garnet and clinopyroxene major- and trace-element compositions of the JDE, one diamond-absent Group A eclogite (44-9) and an average Jericho Group B eclogites for comparison. All mineral grains analyzed have homogeneous major-element compositions that lack chemical zonation. Compared to Group B and C Jericho eclogites, garnets from the JDE investigated in this study have higher MgO (20.3 vs. 11.6 wt.%), and Cr_2O_3 (0.57 vs. 0.06 wt.%) contents (Figure 3.2). The JDE also have higher TiO_2 (0.16 vs. 0.07 wt.%), Sc (102 vs. 48 ppm) and Zr (32 vs. 6.4 ppm) contents, and lower FeO (8.62 vs. 16.7 wt.%) and CaO (4.14 vs. 8.31 wt.%) contents than Group B eclogites. Garnets from high-MgO, diamond-absent eclogite 44-9 have a similar major-element composition to garnets from the JDE, but have slightly higher TiO_2 (0.50 wt.%). Interestingly, the composition of the garnet inclusion in diamond in JDE 03 is similar to the Jericho Group B eclogites with much lower MgO (13.2 wt.%) and higher FeO (17.4 wt.%) and CaO (7.4 wt.%) than the garnet of the host eclogite.

Compared to the average composition of Group B eclogites, clinopyroxene from the JDE and eclogite 44-9 have significantly lower Al_2O_3 (2.5 vs. 9.2 wt.%) and Na_2O (1.7 vs. 5.0 wt.%) contents and higher MgO (16.6 vs. 10.6

wt.%), CaO (20.4 vs. 15.8 wt.%), Zr (21.6 vs. 9.1 ppm), Nb (1.23 vs. 0.07 ppm), V (546 vs. 201 ppm) and Cr_2O_3 (0.32 vs. 0.08 wt.%). Clinopyroxene from eclogite 44-9 has a major-element composition that is similar to the JDE clinopyroxene, but Group B-like Zr (8.3 ppm), Nb (0.22 ppm) and V (258 ppm). The major-element compositions obtained here for garnet and clinopyroxene are similar to those previously reported for JDE (Cookenboo et al., 1998; Heaman et al., 2006).

Whole-rock compositions of the JDE were calculated using a visually estimated mode of 50% clinopyroxene and 50% garnet. Due to the small xenolith size (< 4 cm in diameter) and coarse grain size in some cases (mineral grains up to 5 mm), modes are very difficult to determine. Variation of the mode by ±10% (e.g., 60% garnet, 40% clinopyroxene) can markedly change calculated whole-rock compositions, especially in terms of Al_2O_3, CaO, Na_2O and SiO_2 contents. For example, the Al_2O_3 content of eclogite JDE 01 increases from 12.7 to 14.8 wt. % when the garnet:clinopyroxene ratio is increased from 50:50 to 60:40. However, calculated whole-rock MgO and FeO contents are relatively independent of the mode estimate due to the MgO-rich nature of both garnet and clinopyroxene, and distinctly different from Group B or C eclogites.

3.3.2 Rare earth elements

Chondrite-normalized REE plots for both garnet and clinopyroxene in the JDE are shown in Figure 3.3 and are compared to Jericho Group B eclogites. Garnets in the JDE have enriched and fractionated chondrite-normalized HREE patterns (Lu_N~30-54, $[Lu/Gd]_N$~5.8; N indicates chondrite normalization using values from McDonough and Sun, 1995), contrasting with the relatively flat HREE patterns of garnets from Group B and C eclogites ($[Lu/Gd]_N$~0.34-1.3) and 44-9 ($[Lu/Gd]_N$=1.4), a diamond-absent, Group A eclogite (Figure 3.3a). Although less apparent, garnets from the JDE also have slight enrichments in Ce (Ce_N 0.38-1.23) and Pr (Pr_N 1.14-1.78) compared to garnets from the Group B eclogites (Ce_N 0.11-0.51, Pr_N 0.47-1.38). On a primitive mantle-normalized multi-element diagram (Figure 3.4), the garnets from the JDE are distinguished from the

Group B garnets by lack of a negative Zr-Hf anomaly and only a slight negative Ti anomaly.

Clinopyroxene from JDE (Figure 3.3b) is markedly enriched in LREE (e.g., La_N=78-103, La/Sm_N=2.03-3.48) compared to Group B and C clinopyroxene (e.g., La_N=0.2-17.6, La/Sm_N=0.19-0.75). Calculated whole-rock chondrite-normalized REE plots, assuming a mode of 50% garnet and 50% clinopyroxene as described above, have sinusoidal shapes with enrichments in LREE and HREE, and relative depletions from Gd to Dy (Figure 3.3c). Unlike the major-elements, the REEs are not as sensitive to modes (Jerde et al., 1993, Aulbach et al., 2007) such that the overall sinusoidal-like pattern remains constant, but the degree of LREE or HREE enrichment varies with varying proportion of clinopyroxene or garnet, respectively. Although diamond makes up a significant portion of the mode, diamond is a secondary mineral in these eclogites and is thus excluded from the whole-rock calculation.

3.3.3 Sr and Pb isotopes

The average Sr and Pb isotopic compositions of fresh clinopyroxene are listed in Table 3.2 and represent the average of four to nine grain analyses per xenolith. Clinopyroxene grains from the JDE are compositionally homogeneous and have average Sr contents of 499 ppm. Excluding sample JDE 03, $^{87}Sr/^{86}Sr$ values (0.7057-0.7061, 2σ errors range from 0.00008-0.00012) of JDE clinopyroxene are more radiogenic than the Jericho Group B and C eclogites (0.7032-0.7053, errors from individual eclogites range from ±0.00008-0.0003, 2σ). Clinopyroxene from the JDE also have more radiogenic $^{87}Sr/^{86}Sr$ values than the least radiogenic values reported for Jericho kimberlite whole-rock samples (present day~0.7045; Kopylova et al., 2008) and an initial value from a Jericho phlogopite megacryst Rb-Sr isochron (0.7053±0.0003, 2σ; Heaman et al., 2006). Of note, clinopyroxene grains from one diamond eclogite (JDE 03) record a range of $^{87}Sr/^{86}Sr$ values from 0.7039 to 0.7052±0.0001 (2σ); the variation in isotopic composition occurs both on an inter- and an intra-grain scale, and this range overlaps with the more radiogenic $^{87}Sr/^{86}Sr$ of the Group B and C clinopyroxene.

Clinopyroxenes contain on average 1.42 ppm Pb and have homogeneous Pb isotopic compositions ($^{206}Pb/^{204}Pb$ of 18.54-18.68 and $^{207}Pb/^{204}Pb$ of 15.46-15.73). Clinopyroxene from eclogite 44-9 has lower Sr (131 ppm) and Pb (0.27 ppm) contents and a range of less radiogenic $^{87}Sr/^{86}Sr$ values (0.7028-0.7036) than the JDE, but identical $^{206}Pb/^{204}Pb$ and $^{207}Pb/^{204}Pb$ values. The generally uniform Pb isotopic composition of the JDE clinopyroxene contrasts with the variable isotopic composition of the Jericho group B and C eclogites ($^{206}Pb/^{204}Pb$=14.67-18.03).

3.4 Discussion

Any model invoked to explain the formation of the Jericho high-MgO diamond eclogites must explain the following observations: 1) the high whole-rock MgO content in otherwise normal composition eclogites; 2) the sinusoidal whole-rock REE pattern, 3) the high Mg and Cr content and distinctive fractionated HREE pattern of eclogitic garnet; 4) the high LREE content and elevated $^{87}Sr/^{86}Sr$ of clinopyroxene; 5) the diamond-rich nature of the eclogite; and 6) the presence of a garnet inclusion in diamond that is markedly more Fe-rich than host garnet. However, before evaluating the origin of the high-MgO eclogites, it is important to assess the role of metasomatism in the formation of these eclogites.

3.4.1 Relative order of crystallization

The morphology of diamond appears in some cases to be controlled by the adjacent garnet or clinopyroxene grains, and thus likely formed after or during recrystallization of the host eclogite. However, the presence of small diamond inclusions in garnet suggests that some diamond formation predated or was synchronous with the growth of garnet. Coarse-grained (up to 2 cm), low-Ba (0.42 wt.% BaO) phlogopite corrodes and fragments garnet and diamond (Figure 3.1b) and therefore must have formed after diamond and garnet. Phlogopite formation in the JDE may also be related to the fine-grained veins that transect the host mineralogy of the xenoliths (Figure 3.1b). Sulfide-bearing veins also formed

late and may be linked to the phlogopite-carbonate-apatite veins suggested by similar vein assemblages.

3.4.2 Evaluating the effects of metasomatism

3.4.2.1 Cryptic Metasomatism

There are numerous studies of mantle xenoliths that have identified mineralogical, geochemical, and isotopic evidence of metasomatism (e.g., Erlank et al., 1987; Harte 1987). The JDE show evidence of at least two metasomatic events: a largely-cryptic event evidenced by the unique trace-element and isotopic composition of clinopyroxene, and a later modal event, indicated by the growth of large phlogopite grains and calcite-apatite-phlogopite vein assemblages at the expense of other minerals.

Evidence for an early, cryptic metasomatic event includes the unique trace-element and Sr isotope composition of clinopyroxene, the slight Ce and Pr enrichment in garnet, and the occurrence of diamond inclusions in garnet (Figure 3.1c). JDE clinopyroxene is strongly LREE-enriched and interestingly has a trace-element pattern that is nearly identical to those reported for clinopyroxene from MARID and metasomatized garnet lherzolite xenoliths (Gregoire et al., 2002; 2003). These patterns are consistent with the interpretation that the clinopyroxene crystals either grew from or equilibrated with a LREE-enriched fluid or melt. In addition, the radiogenic Sr composition of JDE clinopyroxene is similar to high $^{87}Sr/^{86}Sr$ values reported from metasomatized lherzolites and the MARID xenolith suite from South Africa (0.7039-0.7078, Kramers et al., 1983). The slightly higher Sr, Ba and Pb contents of the JDE clinopyroxene (Table 3.2) can also be explained by this metasomatic event. Well-formed diamond inclusions in garnet (Figure 3.1c) provide additional evidence of an early carbon-bearing metasomatic event that enabled diamond growth when conditions were favorable. It is plausible that this carbon addition to the eclogites occurred during the same metasomatic event recorded by clinopyroxene, but regardless of exact timing, the event must have occurred relatively early in eclogite formation. These geochemical and isotopic features of the JDE clinopyroxene are best explained by

the involvement of a highly radiogenic $^{87}Sr/^{86}Sr$, LREE-enriched and carbon-bearing metasomatic agent. It is important to note that these features are absent in Jericho Group B and C eclogites and also in sample 44-9, the only Group A eclogite of this study that lacks diamond.

3.4.2.2 Modal Metasomatism

Later episodes of modal metasomatism are indicated in the JDE xenoliths by the growth of large phlogopite crystals at the expense of garnet and diamond (Figure 3.1b). In addition, all JDE contain veins with secondary growth of apatite, phlogopite, carbonate and Ni-sulfide (Figure 3.1b, d), potentially linked to the infiltration of a carbonatite-like metasomatic agent. The timing of this metasomatism is currently poorly constrained but is considered to pre-date kimberlite magmatism and post-date eclogite formation, as the composition of the low-BaO (~0.42 wt.% BaO) phlogopite in the JDE is distinct from higher-BaO (up to 5.86 wt.% BaO) phlogopite in the Jericho kimberlite (Heaman et al., 2006). The fragmentation of eclogite and growth of large phlogopite crystals, corrosion of diamond at diamond-phlogopite contacts (Figure 3.1b), and crystallization of fine grained phlogopite, apatite and carbonate along fractures all indicate a metasomatic overprint, subsequent to eclogite formation.

Unlike the carbonatite modal metasomatism discussed above, we consider the metasomatic overprint recorded by clinopyroxene to have occurred early in the history of these xenoliths, as clinopyroxene is also fragmented and locally transected by phlogopite-carbonate-apatite veins. As well, the lack of compositional zoning in both garnet and clinopyroxene argues against more recent (i.e. Jericho kimberlite related) metasomatic overprints. This early metasomatism was pervasive and produced Sr isotope compositions that are too radiogenic to permit direct derivation of these eclogites from pre-2.0 Ga oceanic crust or seawater-altered oceanic crust, which have $^{87}Sr/^{86}Sr$ of ~0.7013 and ~0.7040, respectively (Veizer and Compston, 1976; Workman and Hart, 2005). It is noteworthy that the carbonatitic, high-density fluids (HDF) that occur as inclusions in fibrous diamonds from the Diavik kimberlite in the central Slave craton (Klein BenDavid et al. 2007; 2008) are also LREE-enriched and have

radiogenic $^{87}Sr/^{86}Sr$ (up to 0.718). Therefore, similar fluids may have been widespread in the Slave lithospheric mantle and also may be responsible for the observed cryptic metasomatism coupled with diamond growth.

It should be noted that the radiogenic $^{87}Sr/^{86}Sr$ values of the JDE are difficult to reconcile with carbonatite metasomatism as known 2.7 to 0.1 Ga North American carbonatites generally have lower initial $^{87}Sr/^{86}Sr$ (0.701-0.703; Bell and Blenkinsop, 1989) than the JDE. As well, JDE lack the Zr-Hf relative depletion commonly ascribed to carbonatite-like metasomatism (e.g., Yaxley et al., 1991) although such depletion may not be characteristic of primary mantle carbonatite melts (Foley et al., 2008).

The $^{206}Pb/^{204}Pb$ values of clinopyroxene in the JDE are very similar to the initial $^{206}Pb/^{204}Pb$ values reported for Jericho eclogite rutile and garnet (Heaman et al., 2006) and within the range of values reported for South African Group I kimberlites (Smith, 1983). Thus, it is plausible that the agent responsible for cryptic metasomatism was a kimberlite-like fluid or melt. In summary, we propose that there are two metasomatic overprints that affected the JDE: an older, LREE-enriched metasomatic event and younger carbonatite-like modal metasomatic event.

Although metasomatism has played a significant role in the history of the Jericho high-MgO diamond eclogites, the metasomatic agents discussed above cannot produce all the geochemical features of these xenoliths. Specifically, these agents alone cannot explain several of the compositional characteristics of garnet, including the fractionated HREE patterns, relatively high Cr_2O_3 and the absence of a Zr-Hf anomaly. For example, the effect of metasomatism on altered garnet from a Koidu high-MgO eclogite was investigated by Barth et al. (2002a) and although they report slight LREE-enrichment coupled with growth of ilmenite, phlogopite, amphibole, carbonate, sulfides and spinel in veins and along grain boundaries in these eclogites, they convincingly demonstrated that the HREE content of the metasomatized garnet was not perturbed. As discussed below, we propose that these features require a process not directly related to the

metasomatism that profoundly changed the REE pattern and Sr isotope composition of clinopyroxene in these xenoliths.

3.4.3 Applicability of existing eclogite models to the JDE

Results from previous studies on Jericho eclogites (Schmidberger et al., 2005; Heaman et al., 2006) indicate that the Group B and C eclogite xenoliths are most likely remnants of subducted oceanic crust – a finding that agrees with the widely invoked theory for mantle eclogite genesis (Jacob, 2004). However, it is difficult to reconcile the high Mg and Cr contents and other geochemical and isotopic characteristics of the JDE with an ocean-floor basalt protolith. Picritic or komatiitic protoliths can account for the high Mg contents but have much higher Fe and lower Al and Ca contents (e.g., Arndt, 1986; Barnes, 1985; Parman et al., 2004) than the JDE.

Mantle eclogites have also been interpreted to represent cumulates of basaltic melts generated and crystallized at high pressure (e.g., O'Hara and Yoder, 1967; Smyth, 1989) and such an origin has been suggested for the JDE (Cookenboo et al., 1998). Although the uniform high-Mg and -Cr composition of most JDE garnets is broadly consistent with this hypothesis, there are several difficulties the model. Firstly, experiments (Herzberg and Zhang, 1997; Kawamoto and Holloway, 1997; Walter, 1998) indicate that high-pressure (> 4 GPa) melts of peridotite are too low in Al and generally too high in Mg to match JDE compositions (Figure 3.5). Secondly, the same experimental data indicate that olivine is an ubiquitous liquidus phase, yet all JDE and other high-Mg eclogites lack olivine (Kopylova et al., 1999a; Barth et al., 2002a; Heaman et al., 2006). Partial melting of an olivine-free mantle lithology such as garnet pyroxenite can perhaps explain the absence of olivine in the JDE, but the JDE calculated whole-rock compositions (Table 3.1) also do not coincide with melt compositions of high-pressure partial melts of garnet pyroxenite (e.g., Tuff and Gibson, 2007) or those produced by mixing of partial melts of peridotite, pyroxenite and eclogite (Figure 3.5). Thirdly, residual garnets in high-pressure peridotite or garnet pyroxenite melting experiments (Walter 1998; Kogiso et al.,

2003; Tuff and Gibson, 2007) do not match JDE garnet compositions. Specifically, garnet produced from peridotite melting (e.g., Walter, 1998; Brey et al., 2008) has higher MgO (up to 27 wt.%) and Cr_2O_3 (0.9-2.3 wt.%) than JDE garnets. Garnets formed during partial melting of garnet pyroxenite have major-element compositions that are more akin to JDE garnets, but in general have lower MgO and Cr_2O_3 contents (Kogiso et al., 2003; Tuff and Gibson, 2007). Furthermore these garnets have flat to slightly fractionated $HREE_N$ ($[Lu/Gd]_N$~1.4; Tuff and Gibson, 2007) compared to the strongly fractionated HREE patterns ($[Lu/Gd]_N$~5.8) of the JDE garnets. We conclude therefore that a high-pressure cumulate origin is unlikely for this suite and an alternative model is required.

One possibility is that the high MgO and Cr_2O_3 contents of the JDE were generated by infiltration of normal basaltic melt into peridotite and formation of a rock compositionally intermediate between basalt and peridotite. This type of basaltic metasomatism has been observed in peridotite xenoliths that have complexly zoned garnets (Burgess and Harte, 1999) and elevated garnet and clinopyroxene modes (Simon et al., 2003). However, such rocks contain significant olivine (e.g., Burgess and Harte, 1999) in contrast to the olivine-free nature of JDE. Moreover, chemical modeling of basalt-peridotite mixtures indicates the mixtures are too high in FeO (>8.5 wt.%) and low in CaO (<10.5 wt.%) and Mg-numbers (~70) at a MgO content of 19 wt.% (the whole-rock JDE composition) to be compatible with JDE whole-rock compositions (cf. Table 3.1).

3.5 Origin of Jericho High-MgO Diamond Eclogites

High-MgO diamond eclogites are rare worldwide but have been reported from South Africa, Russia and Finland (Jacob and Foley, 1999; Peltonen et al., 2002; Jacob et al., 2005). The JDE also share some compositional similarities with non-diamondiferous, high-MgO eclogites recovered at Koidu and Diavik eclogites (Figure 3.2). We evaluate two possible explanations for the high-MgO content of the JDE: 1) metasomatic modification of Group B eclogites, and 2) derivation of Group A eclogites from a high MgO protolith, such as picrites or olivine gabbros (c.f. Barth et al., 2002a; De Stefano et al., in press). Given the

inability of these models to explain all the JDE features, we propose an alternative model that involves melt-facilitated equilibration of basaltic, Group B eclogite with surrounding peridotite.

3.5.1 Nature of the garnet diamond inclusion

The garnet diamond inclusion (DI) is of crucial import to the petrogenesis of the JDE as the DI is compositionally similar to Jericho Group B garnets, albeit with elevated Ti and Na. We interpret that the garnet DI represents the composition of the JDE *before* the process that created the high-Mg composition and attribute the higher Ti and Na to interaction with the diamond-forming agent during encapsulation. Although it is possible that the garnet diamond inclusion was formed by extensive metasomatism of a high MgO, Group A garnet by a HDF, modeling of known HDF compositions suggests that this type of interaction produces Ca-rich and Fe-poor compositions unlike the Fe-rich garnet DI. Interaction of Group A eclogites with basaltic liquids can produce the appropriate Group B Fe-Mg composition, but this produces Al and Ca contents in the resulting modeled eclogite that are incompatible with Group B eclogite compositions. However, on the basis of the available data, we cannot discount the transformation of a JDE garnet to the Fe-rich garnet by complete equilibration with a Fe-rich melt/fluid, but it is important to note that there is no other record of such an interaction in the Jericho eclogites.

3.5.2 Metasomatic modification of basaltic eclogites

One explanation for the origin of the JDE could be that a high-Mg and trace-element enriched metasomatic agent modified Group B eclogites (compositionally similar to the garnet diamond inclusion described above) to the JDE composition. Two lines of evidence documented in other Jericho eclogites and diamond inclusions by De Stefano et al. (2009) support such model: 1) the range of compositions of diamond-inclusion garnets between Group A and B compositions; and 2) the recognition of secondary, high-Mg garnet and clinopyroxene in some Group B eclogites. There are, however, several difficulties with such a metasomatic conversion. The high MgO, secondary garnet in Group

B eclogites form smaller polycrystalline aggregates around primary garnet cores (De Stefano et al., 2009), which is in marked contrast to the relatively coarse and compositionally homogeneous mineral grains present in the JDE. Note that although the secondary garnet compositions reported by De Stefano et al. (2009) have higher MgO than the primary garnets, these secondary garnets are still not as MgO-rich as the JDE garnet compositions (Figure 3.2).

Another difficulty with this metasomatic conversion is that it not only requires addition of Mg but also of relatively fluid immobile Ti, HREE and HFSE (e.g., Nb, Zr, Hf). As well, if an Mg-rich fluid is responsible for the Group B to A conversion then other elements concentrated in the agent would become enriched in the JDE. For example, the Mg-rich, high-density fluids involved in the growth of fibrous diamonds at Diavik (Klein BenDavid et al., 2007; 2008) are variably enriched in K (15-20 wt.%), Na (2-20 wt.%) and Ba (7.7 wt.%) but none of these elements are overly enriched in the JDE (see Table 3.1). Therefore, Mg-rich HDF, like those documented at Diavik, were probably not responsible for the distinctive composition of the JDE. Interaction of Group B eclogites with a Mg-rich carbonatite magma could potentially explain some of the features of the JDE, including the phlogopite-apatite-carbonate vein assemblage and the LREE-enrichment of clinopyroxene. However, carbonatite metasomatism by itself cannot produce sufficient enrichment in Mg to account for the JDE compositions as most experimentally generated and mantle-derived primitive carbonatites (e.g., Wallace and Green, 1988; Tappe et al., 2006, respectively) have lower MgO contents than these eclogites. As well, carbonatite metasomatism cannot explain the HREE and HFSE enrichments present in the JDE.

Neither of the metasomatic agents discussed above can account for the REE patterns of the JDE. JDE garnets have fractionated, steeply sloping HREE (Figure 3.3a) and to our knowledge, there is no mantle metasomatic process that can fractionate the HREE in garnet. Thus, it is difficult to envision how an Mg-rich metasomatic fluid/melt could have produced the fractionated HREE patterns of the JDE garnets. In this regard, garnet from Group A eclogite 44-9 has HREE patterns like those of Group B garnets rather than the fractionated HREE patterns

of garnets in the JDE. If a single metasomatic process was responsible for modifying both the Mg contents and HREE patterns of the Group B garnets, then all Group A garnets, including 44-9, would be expected to display similar REE patterns.

3.5.3 Remnants of mafic lower oceanic crust

A second model for the origin of high MgO eclogites invokes an oceanic lower crustal protolith. Barth et al. (2002a) proposed this model for high-MgO Koidu eclogites, noting their normative compositions (40% plagioclase, 14% clinopyroxene, 12% orthopyroxene, and 29% olivine) are similar to some olivine gabbros and troctolites recovered from oceanic drill core (Aumento et al., 1977). They interpreted their eclogites as lower oceanic crust cumulates, which had originally crystallized at shallow levels, but had subsequently been subducted to great depth. The CIPW normative compositions of the Jericho Group A eclogites are very similar to the Koidu high-MgO eclogites, and Jericho eclogite 44-9 is almost identical to the Koidu high-Mg eclogites in terms of its REE composition (Figure 3.6). As such, oceanic gabbro may be a viable protolith for the Jericho Group A eclogites.

There are, however, two problems with this hypothesis. Firstly, with the exception of two gabbro-norites (referred to as "eucrites" by Aumento et al., 1977), all other gabbros and troctolites reported from the DSDP and ODP studies (e.g., Hart et al., 1999; Bach et al., 2001) have Al_2O_3 contents that are too high (gabbros and olivine gabbros, 13.7-21.4 wt.%), MgO contents that are either too high (troctolites, >24 wt.%) or too low (gabbros and olivine gabbros, 7.1-13.1 wt.%), compared to the Jericho Group A eclogites. Secondly, due to their elevated plagioclase contents, almost all the aforementioned samples, including the two eucrites, have positive Eu anomalies on chondrite-normalized REE plots (Figure 3.6a), and positive Sr anomalies on a primitive-mantle-normalized multi-element plot (Figure 3.6b). Thus, if the protoliths of the Jericho Group A eclogites were in fact relatively plagioclase rich, as suggested by their normative compositions, their trace-element patterns should display clear positive Eu and Sr anomalies.

However, Eu and Sr anomalies are conspicuously absent from all Jericho Group A eclogites (Figure 3.3, 3.6b), conflicting with the low-pressure cumulate model.

3.5.4 Preferred model for the origin of high-MgO eclogites at Jericho

From the discussion of the two models above, it should be clear that finding a compositional match to the JDE has proven difficult. We therefore suggest a third model that focuses on the compositional similarity of garnet and clinopyroxene from JDE and those from Jericho mantle peridotites (e.g., Figure 3.2), listed in Table 3.3. This new model proposes a melt-facilitated exchange of elements between neighboring eclogite bodies and mantle peridotite, envisioning a process similar to the mixed eclogite-peridotite melting experiments of Yaxley and Green (1998). In these experiments, equal amounts of peridotite and basaltic-composition eclogite were mixed and layered in the experimental charges and heated to temperatures of 1300-1500°C at 3.5 GPa. Melts generated from the eclogite facilitated elemental exchange between eclogite and peridotite, producing a residual eclogite with Mg- and Cr-enriched garnet and clinopyroxene. The similarity between the major-element compositions of residual garnet produced in the Yaxley and Green (1998) experiments and JDE garnet is striking (Table 3.3).

3.5.4.1 Eclogite-peridotite elemental equilibration

It is possible that a similar hybridization process occurred in the Slave cratonic lithospheric mantle, whereby enclaves of basaltic, Group B-type eclogite (similar in composition to the garnet diamond inclusion), surrounded by peridotite underwent partial melting followed by equilibration with the surrounding mantle. Melt extraction alone from basaltic-composition eclogites cannot produce both the high MgO and low FeO observed in the JDE (e.g., Yaxley and Green, 1998; Yaxley and Sobolev, 2007) and therefore, the secondary, peridotite-equilibration step is required. Eclogite and pyroxenites have a lower solidus temperature than peridotite (Hirschmann and Stolper, 1996) and will therefore start to melt before surrounding peridotite during adiabatic ascent or thermal disturbance. During such an event, partial melting of carbon-bearing eclogite (carbon added during the

precursor metasomatic event discussed in Section 3.4.2.2.) generates a melt that facilitates relatively rapid diffusional Fe-Mg and Al-Cr exchange between restitic eclogite and surrounding peridotite. This exchange process may also be responsible for elevating the Sc, Zr and Ni contents of garnets in the JDE relative to their Group B eclogite precursors.

If we consider eclogite 44-9 to be the most pristine Group A eclogite at Jericho, then the HREE patterns of garnet in the diamond eclogites require an additional process subsequent to emplacement at high pressure. One of the most enigmatic geochemical features of the JDE is the fractionated HREE in garnet. Previous element partitioning and experimental studies of peridotite and garnet pyroxenite compositions have yielded garnets with flat HREE patterns (e.g., Johnson, 1998; Hauri et al., 1994; Harte and Kirkley, 1997; Tuff and Gibson, 2007), similar to the patterns found in the garnets of 44-9, Group B eclogites and most other mantle eclogites worldwide (e.g., Jacob 2004). However, melting experiments of basaltic and gabbroic compositions at 3.0 to 4.5 GPa have residual garnets with variably fractionated HREE (e.g., Green et al., 2000; Pertermann et al., 2004; Yaxley and Sobolev, 2007), comparable to the HREE patterns of the JDE. Interestingly, a recent experimental study of high-pressure (ca. 6 GPa) partial melting of carbonated peridotite (Brey et al., 2008) also produced residual garnets with strongly fractionated HREE patterns ($[Lu/Gd]_N$=5.0-7.2), nearly identical to those of the JDE garnets ($[Lu/Gd]_N$=4.0-6.6).

Figure 3.7 plots D_{Yb}/D_{Gd} in the experimental garnets versus the SiO_2 content of the coexisting melt. It appears that garnets equilibrated with lower SiO_2 and less-polymerized melts, such as carbonatites, tend to have higher D_{Yb}/D_{Gd} than garnets coexisting with more silica-rich melts. This observation suggests that restitic garnets associated with carbonatitic or other low-silica melts are more likely to have strongly fractionated HREE patterns. Based on this experimental association, we speculate that the melts generated from the eclogite were silica-poor and responsible for the fractionated HREE patterns in the restitic garnets. These same melts may have facilitated elemental exchange between the eclogite enclaves and host peridotite.

3.5.5 Length-scale elemental equilibration in the mantle

The applicability of the eclogite-peridotite equilibration hypothesis to the formation of the JDE is critically dependent on the length-scales of elemental equilibration that might be expected in the mantle. Specifically, a small equilibration length-scale of only a few centimeters or decimeters would imply that this process, though possible, is volumetrically insignificant. Conversely, a larger equilibration length-scale would suggest a more extensive process that might well be reflected in the xenolith population. Length-scales can be estimated using bulk diffusion coefficients (D_{bulk} = weighted average of volume diffusion through mineral lattices and grain boundary diffusion) for relevant elements and an approximate time frame for mantle melting events (Brady, 1983; Joesten, 1983). In our calculations, we have used the experimentally measured diffusion rate of Mg in haplobasaltic melt (LaTourrette et al., 1996) to approximate the diffusion rate of Mg and Fe along melt-filled grain boundaries and the diffusion rate of Fe and Mg in garnet (Carlson, 2006) to approximate volume diffusion rates in eclogite minerals. The calculations indicate that, even at low melt fractions (1% melt), Mg-Fe equilibration length-scales (length $=\sqrt{D_{bulk}t}$) would be on the order of 0.7 to 5 meters for melting events lasting 10^5 to 10^6 years at temperatures between 1200 and 1400°C. Thus, provided that a grain boundary melt was present, minerals in Group B eclogite bodies located within a few meters of eclogite-peridotite interfaces would be expected to undergo significant amounts of Fe-Mg exchange with Mg-rich minerals in the adjacent peridotite. An appealing feature of this model is that it can account for the presence of the Fe-rich, Group B-like garnet inclusion in diamond in eclogite JDE03. The inclusion would reflect the primary garnet composition in the eclogite prior to the onset of partial melting and consequent Fe-Mg exchange with peridotite. Elements such as Al and Cr may also reflect exchange between eclogite and peridotite but the length-scale of this exchange is likely smaller because of the slower diffusion rate of trivalent relative to divalent cations in melts (LaTourrette et al., 1996).

3.6 Conclusions

Existing models that invoke a high-pressure cumulate or subducted oceanic crust origin cannot easily explain the unusual high-MgO diamond eclogites at Jericho. Furthermore, we believe that previous models invoked to explain the generation of other high-MgO eclogites do not apply to the Jericho high-MgO suite. Rather, we propose a multi-stage, hybrid model to account for the mineralogical, geochemical, and isotopic features of these mantle eclogites, schematically represented in Figure 3.8. The first stage involves emplacement of a Group B eclogite into the diamond stability field, producing a mixed low- to intermediate-MgO eclogite and peridotite mantle parcel. The second stage involves heterogeneous metasomatism of these mixed mantle lithologies by a carbon-bearing, LREE-enriched fluid. This metasomatic event was responsible for some diamond growth and the unusual geochemical (high LREE, Sr, Ba) and radiogenic Sr and possibly Pb isotope composition recorded by clinopyroxene. After metasomatism, the basaltic composition eclogites experienced a partial melting event, which facilitated Fe-Mg exchange between the eclogite and the surrounding peridotite and produced the strongly fractionated HREE patterns in the restitic garnets. The final stage involved carbonatite-like metasomatism, and produced phlogopite, apatite, carbonate and facilitated more diamond growth.

References

Arndt N.T. (1986) Differentiation of komatiite flows. Journal of Petrology **27**, 279-301.

Aulbach S., Pearson N.J., O'Reilly S.Y. and Doyle B.J. (2007) Origins of xenolithic eclogites and pyroxenites from the central Slave Craton, Canada. Journal of Petrology **48**, 1843-1873.

Aumento F. Melson, W. G. Hall, J. M. et al. (1977) Site 334, in: Aumento, F., Melson, W.G., Hall, J.M., et al. (Eds.), Initial Reports of the Deep Sea Drilling Project, U.S. Government Printing Office, Washington, DC. Vol. **37**, pp. 239–287.

Bach W., Alt J.C., Niu Y., Humphris S.E. Erzinger J. and Dick H.J.B. (2001) The geochemical consequences of late-stage low-grade alteration of lower ocean crust at the SW Indian Ridge: Results form ODP Hole 735B (Leg 176). Geochimica et Cosmochimica Acta **65**, 3267-3287.

Barnes S. J. (1985) The petrography and geochemistry of komatiite flows in the Abitibi Greenstone Belt and a model for their formation. Lithos **18**, 241-270.

Barth M.G., Rudnick R.L., Horn I., McDonough W.F., Spicuzza M.J., Valley J.W. and Haggerty S.E. (2002a) Geochemistry of xenolithic eclogites from West Africa. Part 2: Origins of high MgO eclogites. Geochimica et Cosmochimica Acta **66**, 4325-4434.

Barth M.G., Foley S.F., and Horn I. (2002b) Partial melting in Archean subduction zones: constrains from experimentally determined trace element partition coefficients between eclogitic minerals and tonalitic melts under upper mantle conditions. Precambrian Research **113**, 323-340.

Bell K., and Blenkinsop J. (1989) Archean depleted mantle: Evidence from Nd and Sr initial isotopic ratios of carbonatite. Geochimica et Cosmochimica Acta **51**, 291-298.

Bizzarro M., Simonetti A., Stevenson R.K. and Kursziaukis S. (2003) In situ $^{87}Sr/^{86}Sr$ investigation of igneous apatites and carbonates using laser ablation MC-ICP-MS. Geochimica et Cosmochimica Acta **67**, 289-302.

Brady J.B. (1983) Intergranular diffusion in metamorphic rocks. American Journal of Science **283**-A, 181-200.

Brey G.P., Bulatov V.K., Girnis A.V. and Lahaye Y. (2008) Experimental melting of carbonated peridotite at 6-10 GPa. Journal of Petrology **49**, 797-821.

Burgess S.R., and Harte B. (1999) Tracing lithosphere evolution through the analysis of heterogeneous G9/G10 garnets in peridotite xenoliths I: major-element chemistry. In: Proceeding of the 7th International Kimberlite Conference, Cape Town. 1, 66-80.

Carlson W.D. (2006) Rates of Fe, Mg, Mn and Ca diffusion in garnet. American Mineralogist **91**, 1-11.

Coleman R.G., Lee E.D., Beatty L.B. and Brannock W.W. (1965) Eclogites and eclogites: their differences and similarities. Geological Society of America Bulletin **76**, 483-508.

Cookenboo H.O., Kopylova M.G., Daoud D.K. (1998) A chemically and texturally distinct layer of diamondiferous eclogite beneath the Slave craton, Northern Canada. Extended Abstracts, 7th International Kimberlite Conference, Cape Town. 164-166.

Dawson J.B. (1984) Contrasting types of upper-mantle metasomatism, in: Kornprobst, J. (Ed.), Kimberlites II - The Mantle and Crust-Mantle Relationships, Elsevier Sci. Publ., Amsterdam, Netherlands, pp. 289-294.

De Stefano A., Kopylova M.G., Cartigny P., and Afanasiev V. (2009) Diamonds and eclogites of the Jericho kimberlite (Northern Canada). Contributions to Mineralogy and Petrology **158**, 295-315.

Ellis D.J. and Green D.H., (1979) An experimental study of the effect of Ca upon garnet-clinopyroxene Fe–Mg exchange equilibria. Contributions to Mineralogy and Petrology **71**, 13–22.

Erlank A.J., Waters F.G., Hawkesworth C.J., Haggerty S.E., Allsopp H.L., Rickard R.S., and Menzies M.A. (1987) Evidence for mantle metasomatism in peridotite nodules from the Kimberley pipes, South Africa, in: Menzies, M.A. and Hawkesworth, C.J. (Eds.), Mantle Metasomatism. Academic Press, London, pp: 221-311,

Foley S.F., Yaxley G.M., Rosenthal A., Rapp R.P., and Jacob D.E. (2008) Experimental melting of peridotite in the presence of CO_2 and H_2O at 40 – 60 kbar. 9th International Kimberlite Conference Extended Abstracts no. 156.

Green T.H., Blundy J.D., Adam J., and Yaxley G.M. (2000) SIMS determination of trace element partitioning coefficients between garnet, clinopyroxene and hydrous basaltic liquids at 2-7.5 GPa and 1080-1200ºC. Lithos **53**, 165-187.

Gregoire M., Bell D.R., and Le Roex A.P. (2002) Trace element geochemistry of phlogopite-rich mafic mantle xenoliths: their classification and their relationship to phlogopite-bearing peridotites and kimberlites revisited. Contributions to Mineralogy and Petrology **142**, 603-625.

Gregoire M., Bell D.R. and Le Roex A.P. (2003) Garnet lherzolites from the Kaapvaal Craton (South Africa): trace element evidence for a metasomatic history. Journal of Petrology **44**, 629-657.

Hart S.R., Blusztain J., Dick H.J.B., Meyer P.S. and Muehlenbachs K. (1999) The fingerprint of seawater circulation in a 500-meter section of ocean crust gabbros. Geochimica et Cosmochimica Acta **63**, 4059-4080.

Harte B. (1987) Metasomatic events recorded in mantle xenoliths: An overview, in: Nixon, P.H. (Ed.), Mantle Xenoliths, John Wiley and Sons, United Kingdom, pp.625-640.

Harte B. and Kirkley M.B. (1997) Partitioning of trace elements between clinopyroxene and garnet: data from mantle eclogites. Chemical Geology **136**, 1-24.

Hauri E.H., Wagner T.P., and Grove T.L. (1994) Experimental and natural partitioning of Th, U, Pb and other trace elements between garnets, clinopyroxene and basaltic melts. Chemical Geology **117**, 149-166.

Heaman L.M., Creaser R.A., Cookenboo H.O. (2002) Extreme enrichment of HFSE in Jericho eclogite xenoliths: A cryptic record of Paleoproterozoic subduction, partial melting, and metasomatism beneath the Slave Craton, Canada. Geology **30**, 507-510.

Heaman L.M., Creaser R.A., Cookenboo H.O., Chacko T. (2006 Multi-stage modification of the Northern slave mantle lithosphere: evidence from zircon-and diamond-bearing eclogite xenoliths entrained in Jericho kimberlite, Canada. Journal of Petrology **47**, 821-858.

Helmstaedt H. and Doig R. (1975) Eclogite nodules from kimberlite pipes in the Colorado Plateau-samples of subducted Franciscan type oceanic lithosphere. Physics and Chemistry of the Earth **9**, 95-111.

Herzberg C. and Zhang J. (1997) Melting experiments on komatiite analog composition at 5 GPa. American Mineralogist **82**, 354-367.

Hills D.V. and Haggerty S.E. (1989) Petrochemistry of eclogites from the Koidu Kimberlite Complex, Sierra Leone. Contributions to Mineralogy and Petrology **103**, 397-422.

Hirschmann M.M. and Stolper E.M. (1996) A possible role for garnet pyroxenite in the origin of the "garnet signature" in MORB Contributions to Mineralogy and Petrology **124**, 185-208.

Jacob D. E. (2004) Nature and origin of eclogite xenoliths from kimberlites. Lithos **77**, 295–316.

Jacob D.E., Jagoutz E., Lowry D., Mattey D. and Kudrjavtseva G. (1994) Diamondiferous eclogites from Siberia: Remnants of Archean oceanic crust. Geochimica et Cosmochimica Acta **58**, 5191-5207.

Jacob D.E. and Foley S.F. (1999) Evidence for Archean ocean crust with low high field strength element signature from diamondiferous eclogite xenoliths. Lithos **48**, 317-336

Jacob D.E., Bizimis M. and Salters V.J.M. (2005) Lu–Hf and geochemical systematics of recycled ancient oceanic crust: evidence from Roberts Victor eclogites. Contributions to Mineralogy and Petrology **148**, 707-720.

Jagoutz E., Dawson J.B., Hoernes S., Spettle B. and Wanke H. (1984) Anorthositic oceanic crust in the Archean Earth. 15th Lunar Planet Sci. Conf. pp 395-396. Abs.

Jerde E.A., Taylor L.A., Crozaz G., Sobolev N.V. and Sobolev V.N. (1993) Diamondiferous eclogites from Yakutia, Siberia: evidence for a diversity of protoliths. Contributions to Mineralogy and Petrology **114**, 189-202.

Joesten R. (1983) Grain growth and grain-boundary diffusion in quartz from the Christmas Mountains (Texas) contact aureole. American Journal of Science 283-A, 233-254.

Johnson K.T.M. (1998) Experimental determination of partition coefficients for rare earth and high-field-strength elements between clinopyroxene, garnet, and basaltic melt at high pressures. Contributions to Mineralogy and Petrology **133**, 60-68.

Kawamoto T., and Holloway J.R. (1997) Melting temperature and partial melt chemistry of H_2O-saturated mantle peridotite to 11 GPa. Science **276**, 240-243.

Klein-BenDavid O., Pearson D.G., Nowell G.M., and Cartigny P. (2008) Origins of diamond forming fluids – constraints from a coupled Sr-Nd isotope and trace element approach. 9th International Kimberlite Conference Extended Abstracts no. 118.

Klein-BenDavid O., Izraeli E.S., Hauri E., and Navon O. (2007) Fluid inclusions in diamonds from the Diavik mine, Canada and the evolution of diamond-forming fluids. Geochimica et Cosmochimica Acta **70**, 723-744.

Kopylova M., Nowell G.M., Pearson D.G., and Markovic G. (2008) Crystallization of megacrysts from kimberlites: Geochemical evidence from high-Cr megacrysts in the Jericho kimberlite. 9th International Kimberlite Conference Extended Abstracts no. 192.

Kopylova M.G., Russell J.K. and Cookenboo H. (1999a) Mapping the Lithosphere beneath the North Central Slave Craton, in: Proceeding of the 7th International Kimberlite Conference, Cape Town. **1**, 468-479.

Kopylova M.G., Russell J.K. and Cookenboo H. (1999b) Petrology of peridotite and
pyroxenite xenoliths from the Jericho kimberlite: implications for the thermal state of the mantle beneath the Slave craton, Northern Canada. Journal of Petrology **40**, 79-104

Kogiso T., Hirschmann M.M. and Frost D.J. (2003) High-pressure partial melting of garnet pyroxenite: possible mafic lithologies in the source of ocean island basalts. Earth and Planetary Science Letters Earth and Planetary Science Letters **216**, 603-617.

Kramers J.D., Roddick J.C.M., and Dawson J.B. (1983) Trace element and isotope studies on veined, metasomatic and "MARID" xenoliths from Bultfontein, South Africa. Earth and Planetary Science Letters **65**, 90-106.

Krogh Ravna E. (2000) The garnet-clinopyroxene Fe^{2+}-Mg geothermometer: an updated calibration. Journal of Metamorphic Geology **18**, 211-219.

LaTourrette T., Wasserburg G.J. and Fahey A.J. (1996) Self diffusion of Mg, Ca, Ba, Nd, Yb, Ti, Zr, and U in haplobasaltic melt. Geochimica et Cosmochimica Acta **60**, 1329-1340.

McDonough W.F. and Sun S.S. (1995) The composition of the Earth. Chemical Geology **120**, 223-253.

MacGregor I.D. and Manton W.I. (1986) Roberts Victor eclogites: ancient oceanic crust. Journal of Geophysical Research **91** (B14), 14063-14079.

O'Hara M.J. and Yoder H.S. (1967) Formation and fractionation of basic magmas at high pressures, Scottish Journal of Geology **3**, 67–117.

Parman S. W., Grove T. L., Dann J. C. and De Wit M. J. (2004) A subduction origin for komatiites and cratonic lithospheric mantle. South African Journal of Geology **107**, 107-118.

Peltonen P., Kinnunen K.A., and Huhma H. (2002). Petrology of two diamondiferous eclogite xenoliths from the Lahtojoki kimberlite pipe, eastern Finland. Lithos **63**, 151-164.

Pertermann M., Hirschmann M.M., Hametner K., Gunther D. and Schmidt M.W. (2004) Experimental determination of trace element partitioning between garnet and silica-rich liquid during anhydrous partial melting of MORB-like eclogite. Gechem. Geophys. Geosys. **5**, 1-23.

Price S.E., Russell J.K., and Kopylova M.G. (2000) Primitive magma from the Jericho

pipe, N.W.T., Canada: constraints on primary kimberlite Melt chemistry. Journal of Petrology **41**, 789-808.

Schmidberger S.S., Simonetti A., and Francis D. (2003) Small-scale Sr isotope investigation of clinopyroxenes from peridotite xenoliths by laser ablation MC-ICP-MS – implications for mantle metasomatism. Chemical Geology **199**, 317-329.

Schmidberger S.S., Heaman L.M., Simonetti A., Creaser R.A. and Cookenboo H.O. (2005) Formation of Paleoproterozoic eclogitic mantle, Slave Province (Canada): Insights from in-situ Hf and U-Pb isotopic analyses of mantle zircons. Earth and Planetary Science Letters **240**, 621-633.

Schmidberger S.S., Simonetti A., Heaman L.M., Creaser R.A. and Whiteford S. (2007) Lu-Hf, in-situ Sr and Pb isotope and trace element systematics for mantle eclogites from the Diavik diamond mine: Evidence for Paleoproterozoic subduction beneath the Slave craton, Canada. Earth and Planetary Science Letters **254**, 55-68.

Schulze D.J. (1989) Constraints on the abundance of eclogite in the upper mantle, Journal of Geophysical Research **94**, 4205-4212.

Simon N.S.C., Irvine G.J., Davies G.R., Pearson D.G. and Carlson R.W. (2003) The origin of garnet and clinopyroxene in "depleted" Kaapvaal peridotites. Lithos **71**, 289-322.

Simonetti A., Heaman L.M., Hartlaub R.P., Creaser R.A., MacHattie T.G. and Bohm C., (2005) U-Pb zircon dating by laser ablation-MC-ICP-MS using a new multiple ion counting Faraday collector array. Journal Anal. At. Spectrom. **20**, 677-686.

Smith C.B. (1983) Pb, Sr and Nd isotopic evidence for sources of southern Africa Cretaceous kimberlites. Nature **304**, 51-54.

Smyth J.R., Caporuscio F.A. and McCormick T. (1989) Mantle eclogites: evidence of igneous fractionation in the mantle. Earth and Planetary Science Letters **93**, 133-141.

Spandler C., Yaxley G., Green D.H. and Rosenthal A. (2008) Phase relations and melting of anhydrous K-bearing eclogite from 1200-1600^{O}C and 3 to 5 GPa. Journal of Petrology **49**, 771-795.

Stachel T. and Harris J.W. (2008) The origin of cratonic diamonds – Constraints from mineral inclusions. Ore Geology Reviews **34**, 5-32.

Stachel T., Aulbach S., Brey G.P., Harris J.W., Leost I. and Viljoen K.S. (2004) The trace element composition of silicate inclusions in diamonds: a review. Lithos **77**, 1-19.

Tappe S., Foley S.F., Jenner G.A., Heaman L.M., Kjarsgaard B.A., Romer R.L., Stracke A., Joyce N. and Hoefs J. (2006) Genesis of ultramafic lamprophyres and carbonatites at Aillik Bay, Labrador: a consequence of incipient lithospheric thinning beneath the North Atlantic Craton. Journal of Petrology **47**, 1261-1315.

Tuff J., and Gibson S.A. (2007) Trace-element partitioning between garnet, clinopyroxene and Fe-rich picritic melts at 3 to 7 GPa. Contributions to Mineralogy and Petrology **153**, 369-387.

van Achterbergh E., Ryan C., Jackson S. and Griffin W.L. (2001) Laser-Ablation-ICPMS in the Earth Sciences - Appendix 3 data reduction software for LA-ICP-MS, In, Sylvester, P. (ed.), Mineralogical Association of Canada Short Course **29**, 239-243.

Veizer J. and Compston W. (1976) $^{87}Sr/^{86}Sr$ in Precambrian carbonates as an index of crustal evolution. Geochimica et Cosmochimica Acta **40**, 905-914.

Wallace M.E. and Green D.H. (1988) An experimental determination of primary carbonatite magma composition. Nature **335**, 343-346.

Walter M.J. (1998). Melting of garnet peridotite and the origin of komatiite and depleted lithosphere. Journal of Petrology **39**, 29-60.

Workmann R.K., and Hart S.R. (2005) Major and trace element composition of the depleted MORB mantle (DMM). Earth and Planetary Science Letters **231**, 53-72.

Yaxley G.M. and Green D.H. (1998) Reactions between eclogite and peridotite: mantle refertilization by subduction of oceanic crust. Schweiz. Mineral. Petrogr. Mitt, **78**, 243-255.

Yaxley G.M., Crawford A.J., and Green D.H. (1991) Evidence for carbonatite metasomatism in spinel peridotite xenoliths from western Victoria, Australia. Earth and Planetary Science Letters **107**, 305-317.

Yaxley G.M. and Brey G.P. (2004) Phase relations of carbonate-bearing eclogite assemblages from 2.5 to 5.5 GPa: implications for petrogenesis of carbonatites. Contributions to Mineralogy and Petrology **146**, 606-619.

Yaxley G.M. and Sobolev A.V. (2007) High-pressure partial melting of gabbro and its role in the Hawaiian magma source. Contributions to Mineralogy and Petrology **154**, 371-383.

Table 3.1 Major-element composition of garnet, clinopyroxene, phlogopite and calculated whole-rock from the Jericho eclogites

Major element composition of garnet, clinopyroxene, phlogopite and calculated whole-rock from the Jericho eclogites

	JDE 01	**JDE 02**	**JDE 03**	**JDE 07**	**JDE 16**	**JDE 17**	**JDE 18**	**JDE 19**	**JDE 20**	**JDE 21**	**JDE 22**	**JDE 23**	**JDE 24**	**44-9**	**Group B**	**JDE 03**
	Grt	*Grt*	*Grt*	*Grt*	*Grt*	*Grt*	*Grt*	*Grt*	*Grt*	*Grt*	*Grt*	*Grt*	*Grt*	*Grt*	*Grt*	*Grt D.I.*
SiO_2	42.28	42.22	42.63	42.45	41.43	41.91	41.70	42.49	42.33	42.23	42.28	41.87	42.04	41.46	39.87	38.99
TiO_2	0.16	0.16	0.16	0.14	0.16	0.18	0.15	0.15	0.14	0.15	0.20	0.15	0.15	0.49	0.07	0.55
Al_2O_3	23.03	22.96	23.73	23.78	23.65	23.68	23.52	23.60	23.71	23.77	23.71	23.33	23.53	22.63	23.09	21.45
Cr_2O_3	0.58	0.59	0.58	0.60	0.34	0.46	0.62	0.72	0.52	0.70	0.30	0.72	0.61	0.54	0.06	0.10
FeO	8.29	8.27	8.25	8.32	9.38	9.29	8.33	8.32	8.50	8.31	10.44	8.33	8.34	9.19	16.73	17.36
MnO	0.38	0.38	0.42	0.43	0.38	0.40	0.40	0.39	0.39	0.38	0.38	0.39	0.39	0.37	0.30	0.39
MgO	21.17	20.98	20.95	20.65	19.45	19.53	20.18	20.38	19.92	20.07	19.02	20.39	19.99	20.07	11.64	13.16
CaO	4.26	4.31	4.29	4.23	3.91	4.04	4.19	4.14	4.05	4.11	4.01	4.11	4.04	4.42	8.31	7.38
Na_2O	0.06	0.06	0.06	0.06	0.05	0.05	0.04	0.05	0.05	0.05	0.05	0.05	0.05	0.06	0.05	0.13
K_2O	b.d.	b.d.	b.d.	b.d.	b.d.	b.d.	b.d.	b.d.	b.d.	0.01	b.d.	b.d.	b.d.	b.d.	b.d.	b.d.
Total	100.21	99.93	101.08	100.65	98.76	99.54	99.13	100.23	99.62	99.78	100.40	99.34	99.15	99.24	100.13	100.08
Mg #	82.0	82.0	82.0	82.0	79.0	79.0	81.0	81.0	81.0	81.0	76.0	81.0	81.0	80.0	43.0	57.0
n grains	*5*	*5*	*8*	*7*	*3*	*3*	*3*	*3*	*3*	*4*	*4*	*2*	*3*	*3*	avg 9	*1*
spots	*50*	*50*	*53*	*50*	*15*	*15*	*15*	*24*	*30*	*25*	*37*	*20*	*24*	*30*	xenos.	*5*

	JDE 01	**JDE 02**	**JDE 03**	**JDE 07**	**JDE 16**	**JDE 17**	**JDE 18**	**JDE 19**	**JDE 21**	**JDE 22**	**JDE 23**	**JDE 24**	**44-9**	**Group B**
	Cpx	*Cpx*	*Cpx*	*Cpx*	*Cpx*	*Cpx*	*Cpx*	*Cpx*	*Cpx*	*Cpx*	*Cpx*	*Cpx*	*Cpx*	*Cpx*
SiO_2	55.21	54.97	55.42	55.05	54.32	54.48	54.50	54.50	54.64	54.82	54.64	54.62	54.54	55.36
TiO_2	0.13	0.13	0.13	0.11	0.13	0.12	0.10	0.11	0.10	0.14	0.11	0.10	0.23	0.12
Al_2O_3	2.44	2.72	2.66	2.90	2.41	2.47	2.42	2.26	2.36	2.12	2.32	2.34	1.92	9.21
Cr_2O_3	0.33	0.33	0.33	0.34	0.22	0.24	0.35	0.39	0.39	0.13	0.40	0.35	0.71	0.08
FeO	2.11	2.09	2.09	2.07	2.41	2.44	2.11	2.10	2.09	2.81	2.10	2.10	3.30	3.41
MnO	0.07	0.07	0.08	0.08	0.08	0.08	0.08	0.08	0.08	0.08	0.08	0.08	0.10	0.03
MgO	16.71	16.36	16.42	15.75	16.67	16.68	16.74	16.99	16.79	16.59	16.86	16.86	17.20	10.63
CaO	20.70	20.43	20.50	20.17	19.99	20.10	20.91	20.60	20.58	20.53	20.56	20.44	19.89	15.78
Na_2O	1.75	1.91	1.87	1.92	1.63	1.68	1.63	1.57	1.61	1.40	1.58	1.62	1.63	5.03
K_2O	0.01	0.01	0.01	0.02	0.01	0.01	0.01	0.01	0.01	0.00	0.01	0.01	0.04	0.01
Total	99.46	99.02	99.50	98.40	97.87	98.28	98.85	98.62	98.65	98.64	98.65	98.52	99.56	99.66
Mg #	93.0	93.0	93.0	93.0	93.0	93.0	93.0	93.0	93.0	93.0	93.0	93.0	90.0	82.0
n grains	*5*	*5*	*9*	*7*	*1*	*3*	*3*	*2*	*2*	*2*	*3*	*4*	*2*	avg 9
spots	*50*	*50*	*50*	*42*	*3*	*13*	*22*	*15*	*20*	*9*	*28*	*29*	*20*	xenos.

(Continued)

	JDE 01	**JDE 02**	**JDE 03**	**JDE 07**	**JDE 16**	**JDE 17**	**JDE 18**	**JDE 19**	**JDE 21**	**JDE 22**	**JDE 23**	**JDE 24**	**44-9**	**Group B**
	WR.	*WR.*	*WR.*	*WR.*	*WR.*	*WR.*	*WR.*	*WR.*	*WR.*	*WR.*	*WR.*	*WR.*	*WR.*	*WR.*
SiO_2	48.74	48.59	49.02	48.75	47.87	48.19	48.10	48.50	48.44	48.55	48.25	48.33	48.74	47.44
TiO_2	0.14	0.15	0.15	0.12	0.14	0.15	0.13	0.13	0.12	0.17	0.13	0.13	0.14	0.10
Al_2O_3	12.73	12.84	13.19	13.34	13.03	13.07	12.97	12.93	13.07	12.91	12.83	12.94	12.73	16.31
Cr_2O_3	0.45	0.46	0.45	0.47	0.28	0.35	0.49	0.56	0.54	0.22	0.56	0.48	0.45	0.07
FeO	5.20	5.18	5.17	5.19	5.90	5.87	5.22	5.21	5.20	6.63	5.22	5.22	5.20	10.45
MnO	0.23	0.23	0.25	0.26	0.23	0.24	0.24	0.23	0.23	0.23	0.23	0.23	0.23	0.17
MgO	18.94	18.67	18.69	18.20	18.06	18.10	18.46	18.68	18.43	17.81	18.62	18.42	18.94	10.98
CaO	12.48	12.37	12.39	12.20	11.95	12.07	12.55	12.37	12.34	12.27	12.33	12.24	12.48	11.97
Na_2O	0.91	0.98	0.97	0.99	0.84	0.86	0.84	0.81	0.83	0.73	0.82	0.83	0.91	2.48
K_2O	-	-	-	-	-	-	-	-	0.01	-	-	-	-	-
Total	99.83	99.47	100.29	99.52	98.31	98.91	98.99	99.42	99.21	99.52	99.00	99.83	99.83	99.98
Mg #	87.5	87.5	87.5	87.5	86.0	86.0	87.0	87.0	87.0	84.5	87.0	87.0	85.0	62.5
mode	50/50	50/50	50/50	50/50	50/50	50/50	50/50	50/50	50/50	50/50	50/50	50/50	50/50	variable

	JDE 02		**JDE 03**		**JDE 07**	
	Phlogopite		*Phlogopite*		*Phlogopite*	
	1g 7 pts	2σ	1g 10pts	2σ	1g 10pts	2σ
SiO_2	39.84	*2.26*	41.35	*0.57*	42.06	*0.5*
TiO_2	1.21	*0.22*	0.70	*0.06*	0.84	*0.1*
Al_2O_3	14.03	*0.73*	12.32	*0.19*	12.47	*0.2*
Cr_2O_3	0.46	*0.05*	0.11	*0.01*	0.15	*0.0*
FeO	4.31	*0.22*	3.42	*0.22*	3.70	*0.1*
MnO	0.04	*0.02*	0.03	*0.01*	0.03	*0.0*
MgO	23.39	*0.46*	24.48	*0.83*	24.10	*0.5*
CaO	0.04	*0.03*	0.01	*0.02*	0.05	*0.0*
Na_2O	0.16	*0.08*	0.14	*0.05*	0.10	*0.2*
K_2O	9.85	*0.16*	10.05	*0.11*	9.84	*0.3*
F	0.00	*0.00*	0.00	*0.00*	0.00	*0.0*
Cl	0.08	*0.01*	0.41	*0.04*	0.72	*0.1*
BaO	0.41	*0.14*	0.42	*0.05*	0.43	*0.1*
Total	93.39	*3.08*	92.94	*1.56*	93.89	*0.4*

	JDE 02	**JDE 03**	**JDE 07**
	sulphide	*sulphide*	*sulphide*
	1g 10 pts	1g 10 pts	1g 8 pts
SiO_2	0.05	0.0	0.05
FeO	2.84	4.3	1.69
CuO	0.0	0.0	0.0
NiO	72.27	70.7	71.89
SO_3	25.4	25.7	25.14
Total	100.6	100.7	98.77

Major element data in wt%; Average Jericho group B eclogite data from Appendix A

Mg # calculated using Mg/(Mg+Fe)*100

Calc.W.R.: whole-rock eclogite composition calculated on the mode estimation of 50% garnet, 50% clinopyroxene. See text for explanation.

Table 3.2 Trace-element composition and Sr-Pb isotopic data of garnet and clinopyroxene from the Jericho eclogites

Trace element composition and Sr, Pb isotopic data of garnet and clinopyroxene from the Jericho eclogites

	JDE 01		JDE 02		JDE 03		JDE 07		JDE 17		JDE 19		JDE 20		JDE 22		JDE 23		44-9		Group B	
	Grt	2σ	*Grt*	2σ	*Grt*	2σ	*Grt*	2σ	*Grt*	2σ	*Grt*	2σ	*Grt*	2σ	*Grt*	2σ	*Grt*	2σ	*Grt*	2σ	*Grt*	2σ
V	255	18	283	33	270	25	250	32	234	12	232	14	241	15	236	18	229	16	211	17	52.5	39
Ni	24.6	3	25.6	2	19.8	1	20.4	2	23.9	4	23.1	1	22.7	3	20.7	5	23.9	6	27.9	3	16.9	11
Sc	107	8	113	6	92.0	4	87.5	6	99.7	3	110	6	109	6	94.7	8	106	6	102	13	48.4	18
Rb	0.02		b.d		0.06	0.05	0.16	0.05	0.14	0.03	0.29		0.20		0.16	0.1	b.d.		b.d.		0.13	0.2
Ba	b.d.		0.05	0.03	b.d.		b.d.		b.d.		0.04		b.d.		b.d.		0.19	0.3	b.d.		0.22	0.3
U	0.03	0.01	0.03	0.01	0.02	0.01	0.03	0.01	0.02	0.01	0.04	0.03	0.03	0.008	0.04	0.01	b.d.		b.d.		0.03	0.9
Nb	0.38	0.04	0.38	0.1	0.46	0.12	0.51	0.1	0.24	0.07	0.75	0.6	0.50	0.2	0.58	0.5	0.59	0.2	0.17	0.1	0.06	0.0
Ta	0.04	0.01	0.08	0.03	0.03	0.01	0.04	0.02	0.04	0.01	0.07	0.03	0.06	0.02	0.08	0.03	0.07	0.01	0.04	0.02		
La	0.03	0.02	0.03	0.01	b.d.		0.08	0.06	b.d.		b.d.		0.05	0.03	0.07	0.01	b.d.		0.04	0.02	0.05	0.1
Ce	0.30	0.09	0.30	0.03	0.76	0.6	0.66	0.2	0.23	0.09	0.35	0.1	0.33	0.07	0.55	0.3	0.41	0.2	0.12	0.03	0.16	0.1
Pr	0.13	0.02	0.11	0.05	0.16	0.07	0.16	0.01	0.11	0.05	0.14	0.07	0.13	0.05	0.17	0.1	0.14	0.09	0.05	0.01	0.08	0.05
Pb	b.d.		b.d		0.07	0.04	0.10	0.1	b.d.		b.d.		b.d.		b.d.		0.07	0.06	b.d.		0.12	0.2
Sr	0.28	0.2	0.28	0.06	b.d.		1.22	0.8	0.27	0.09	0.38	0.5	0.29	0.1	0.33	0.3	0.28	0.1	0.17	0.09	0.52	0.3
Nd	1.41	0.3	1.46	0.5	1.44	0.09	1.41	0.3	1.43	0.2	1.59	0.3	1.58	0.3	1.3	0.6	1.37	0.6	0.57	0.4	1.15	1
Sm	1.10	0.1	1.30	0.5	0.93	0.3	0.87	0.3	0.85	0.4	1.20	0.1	0.83	0.2	0.77	0.3	0.88	0.3	0.60	0.1	1.53	1
Zr	32.4	1	35.0	1	32.9	4	33.9	3	29.6	1	33.1	1	32.7	0.7	31.3	5	31.4	2	34.4	2	6.44	6
Hf	0.75	0.2	0.74	0.3	0.55	0.2	0.63	0.1	0.57	0.1	0.71	0.2	0.70	0.2	0.62	0.2	0.62	0.2	1.17	0.4	0.15	0.1
Eu	0.42	0.07	0.45	0.06	0.34	0.1	0.34	0.03	0.35	0.1	0.48	0.1	0.37	0.06	0.39	0.08	0.45	0.1	0.28	0.1	1.08	0.7
Gd	1.82	0.7	1.65	0.6	1.04	0.2	0.89	0.2	1.61	0.2	1.53	0.9	1.26	0.4	1.75	0.6	1.42	0.4	1.56	0.4	3.54	3
Ti	1171	51	1233	91	506	26	782	42	1216	84	1038	76	987	46	1406	115	1022	93	3360	189	476	462
Tb	0.38	0.07	0.38	0.1	0.26	0.02	0.23	0.03	0.39	0.07	0.30	0.07	0.28	0.08	0.37	0.07	0.31	0.09	0.40	0.2	0.69	3
Dy	3.59	0.5	3.29	0.8	2.39	0.3	2.04	0.4	3.87	0.3	3.29	0.8	3.11	0.3	3.38	0.6	3.04	0.7	3.48	1	5.1	0.7
Y	23.7	1	24.7	2	22.4	1	21.8	2	29.4	2	25.1	2	24.8	1	26.7	3	24.2	2	15.7	2.1	25.4	6
Ho	1.13	0.2	1.06	0.1	0.75	0.03	0.68	0.1	1.11	0.1	0.95	0.15	0.96	0.08	0.92	0.2	0.94	0.1	0.76	0.1	1.10	31
Er	4.59	0.5	4.22	0.7	3.07	0.2	2.69	0.4	3.84	0.2	3.73	0.8	3.87	0.4	3.52	0.3	3.66	0.5	2.11	0.4	3.09	1
Tm	0.83	0.09	0.81	0.06	0.55	0.05	0.50	0.05	0.68	0.09	0.74	0.03	0.71	0.1	0.63	0.2	0.63	0.09	0.30	0.08	0.47	4
Yb	6.77	0.6	6.15	0.9	4.34	0.5	3.78	0.3	5.48	0.8	5.64	0.8	5.75	0.7	5.37	0.5	4.99	0.7	1.81	0.6	3.21	0.7
Lu	1.17	0.1	1.17	0.1	0.78	0.08	0.73	0.08	0.88	0.07	1.02	0.1	1.00	0.1	0.86	0.1	0.86	0.1	0.26	0.1	0.51	5.0
$^{1}Eu/Eu_N$*	0.84		0.80		1.05		1.16		0.91		1.09		1.09		0.67		1.21		0.74		1.23	
Lu_N	47.7		47.4		31.9		29.6		35.7		41.6		40.6		35.1		35.2		10.6		20.7	
Lu/Gd_N	5.21		5.72		6.11		6.62		4.42		5.41		6.43		3.99		4.93		1.35		1.15	
n (grains)	7		6		5		6		4				4		4		6		7		avg 9 xenos	

Trace element data in ppm. Average and ranges of Jericho group B eclogite data from Appendix A.

Eu* calculated using 2*Eu/(Sm+Gd), where all values are chondrite-normalized (subscript 'N') using McDonough and Sun, 1995.

(Continued)

	JDE 01		JDE 02		JDE 03		JDE 07		JDE 17		JDE 19		JDE 22		JDE 23		44-9		Group B	
	Cpx	2σ	*Cpx*	2σ	*Cpx*	2σ	*Cpx*	2σ	*Cpx*	2σ	*Cpx*	2σ	*Cpx*	2σ	*Cpx*	2σ	*Cpx*	2σ	*Cpx*	2σ
V	536	47	585	85	693	234	629	116	479	5	471	19	470	13	465	8	258	43	201	132
Ni	250	7	267	14	247	102	184	45	240	0.6	234	8	228	24	231	7	193	11	242	99
Sc	27.0	2	27.0	2	25.2	2	24.6	4	25.0	2	25.8	2	24.7	0.1	25.6	1	102	4	16.6	14
Rb	b.d.		0.20	0.04	0.21	0.5	0.12	0.05	b.d.		0.29	0.1	0.18	0.1	b.d.		0.12	0.08	0.08	0.3
Ba	1.09	0.4	1.35	0.7	3.00	0.8	1.95	1.0	5.79	0.7	4.68	4	1.04	0.9	4.19	8	0.39	0.3	0.23	1
U	0.04	0.02	0.04	0.01	b.d.		0.07	0.03	0.03	0.01	0.08	0.02	0.06	0.01	0.07	0.03	b.d.		0.021	0.02
Nb	1.04	0.1	1.12	0.08	1.14	0.2	1.32	0.3	0.84	0.3	1.42	0.4	1.45	0.3	1.61	0.6	0.22	0.09	0.07	0.2
Ta	0.14	0.02	0.12	0.02	0.10	0.02	0.12	0.02	0.07	0.02	0.14	0.02	0.12	0.02	0.12	0.02	0.04	0.02		
La	18.5	1	18.8	0.5	21.5	1	24.6	4	14.8	0.3	24.7	7	14.9	7	22.8	3	3.04	0.3	1.23	2
Ce	55.7	3	56.3	1	71.8	12	79.9	11	44.1	0.8	59.7	9	43.5	9	56.1	6	9.39	0.9	4.70	8
Pr	8.59	0.4	8.37	0.4	8.93	0.6	9.15	0.9	6.92	0.4	8.42	1	6.88	0.7	8.03	0.3	1.58	0.1	1.00	2
Pb	1.18	0.1	1.17	0.3	1.52	0.6	1.85	0.9	0.91	0.4	1.55	0.6	0.84	0.2	1.31	0.2	0.27	0.08	0.57	1
Sr	464	33	499	23	498	33	498	155	425	35	495	88	409	50	469	25	131	10	331	347
Nd	38.6	1.0	36.7	2	36.1	4	35.2	4	30.9	1	36.2	5	32.2	2	33.9	1	7.93	0.8	6.08	9
Sm	5.70	0.3	5.20	0.7	4.80	0.5	4.41	0.6	4.53	0.3	4.66	1	4.31	0.2	4.52	0.3	1.67	0.4	1.60	2
Zr	23.3	2.3	23.7	3	24.7	2.3	25.7	12	17.8	0.7	18.9	4	17.8	4	18.8	2	8.35	3	9.14	5
Hf	1.56	0.2	1.49	0.2	1.29	0.3	1.30	0.5	0.95	0.03	1.08	0.5	1.06	0.1	1.10	0.05	0.77	0.3	0.61	0
Eu	1.13	0.1	1.11	0.1	1.00	0.10	0.91	0.1	0.94	0.03	0.90	0.03	0.92	0.1	0.89	0.01	0.48	0.09	0.60	1
Ti	882	44	894	73	335	45	381	38	889	81	728	45	991	52	723	63	1411	80	736	415
Gd	2.82	0.4	2.75	0.4	1.86	0.3	1.46	0.2	2.03	0.1	2.08	0.07	2.43	0.6	1.91	0.5	1.41	0.3	1.08	1
Tb	0.22	0.02	0.21	0.08	0.18	0.05	0.16	0.04	0.20	0.07	0.17	0.03	0.25	0.01	0.17	0.03	0.15	0.06	0.10	0
Dy	1.19	0.2	1.14	0.4	0.84	0.1	0.77	0.2	1.17	0.1	0.89	0.2	1.19	0.1	0.89	0.07	0.68	0.2	0.39	1
Y	3.67	0.1	3.80	0.4	3.82	0.3	3.40	0.3	4.57	0.1	3.77	0.1	4.38	0.1	3.78	0.2	1.99	0.4	0.99	2
Ho	0.19	0.03	0.17	0.05	0.16	0.04	0.12	0.03	0.20	0.03	0.16	0.05	0.18	0.02	0.14	0.01	0.10	0.03	0.04	0.1
Er	0.44	0.05	0.41	0.07	0.36	0.07	0.31	0.06	0.37	0.06	0.38	0.05	0.47	0.05	0.36	0.2	0.20	0.1	0.10	0
Tm	0.05	0.02	0.05	0.04	0.04	0.02	0.03	0.02	0.04	0.01	0.05	0.01	0.04	0.01	0.04	0.02	b.d.		0.01	0.03
Yb	0.24	0.06	0.24	0.1	0.22	0.06	0.20	0.08	0.20	0.1	0.28	0.2	0.36	0.1	0.21	0.09	0.10	0.05	0.05	0.08
Lu	0.04	0.01	0.04	0.01	0.03	0.01	0.02	0.01	0.05	0.01	b.d.		b.d.		0.03	0.01	0.02	0.01	0.02	0.01
n (grains)	5		5		6		6		2		2		2		3		7		avg 9 xenos	
$^{2}Eu/Eu_N$*	0.76		0.86		0.85		0.87		0.82		0.76		0.79		0.79		0.92		1.33	
La_N	78.1		79.3		90.9		104		62.3		104		62.9		96.4		12.8		1.02	
La/Sm_N	2.03		2.26		2.80		3.48		2.04		3.31		2.16		3.16		1.14		0.22	
$^{87}Sr/^{86}Sr$	0.7057		0.7059		0.7047		0.7061		-		-		-		-		0.7032		0.7042	
$^{206}Pb/^{204}Pb$	18.68±0.05		-		18.54±0.12		18.68±.05		-		-		-		-		18.75±0.13		14.67 - 18.033	
$^{207}Pb/^{204}Pb$	15.50±0.05		-		15.73±0.03		15.50±0.05		-		-		-		-		15.55±0.10		15.08 - 15.553	

Table 3.3 Comparison of JDE garnet and clinopyroxene to experimental results and minerals from Jericho peridotite xenoliths

Geochemical comparison of JDE garnet and clinopyroxene to experimental results and minerals from Jericho peridotite xenoliths

	Yaxley and Green 1998 Eclogite-peridotite experiments				Average Jericho Coarse Grt Peridotite				Average Jericho Diamond Eclogite			
Run	*9117 Garnet*	*9117 Cpx*	*520 Garnet*	*520 Cpx*	*Garnet*		*Cpx*		*Garnet*		*Cpx*	
T (°C)	1300	1300	1500	1500								
Assemblage	ga+cpx layer	ga+cpx layer	mixed	mixed	n=6	2σ	n=6	2σ	n=12	2σ	n=11	2σ
SiO_2	42.3	53.4	42.7	54.3	41.33	0.5	54.47	0.6	42.15	0.7	54.74	0.8
TiO_2	0.7	0.4	0.5	0.2	0.16	0.2	0.15	0.1	0.16	0.0	0.12	0.0
Al_2O_3	23.2	5.7	23.0	6.2	21.59	1.2	2.19	0.5	23.50	0.5	2.51	0.5
Cr_2O_3	0.4	0.3	0.5	0.3	3.13	1.7	1.51	0.7	0.57	0.3	0.31	0.2
FeO	8.5	5.2	7.7	6.6	8.81	0.5	2.45	0.5	8.62	1.3	2.21	0.5
MnO	0.2	0.1	0.1	0.1	0.40	0.1	0.06	0.0	0.39	0.0	0.08	0.0
MgO	19.9	19.1	21.4	24.5	19.48	1.1	16.27	0.7	20.27	1.3	16.60	0.6
CaO	5.3	14.5	4.2	6.8	4.60	0.6	20.11	1.8	4.14	0.2	20.44	0.6
Na_2O	0.0	1.3	0.0	1.0	0.05	0.0	1.96	0.3	0.05	0.0	1.70	0.3
K_2O	0.0	0.0	0.1	0.0			0.06	0.0	0.00	0.0	0.01	0.0
Total	100.5	100.0	100.2	100.0	99.49	1.0	99.33	1.1	99.86	1.3	91.14	0.9

Data from Yaxley and Green, 1998. All experiments at 3.5 Gpa. Data from Kopylova et al., 1999b.
Run 9117: equal amounts of basalt and pyrolite layered together.
Run 520: equal amounts of basalt and pyrolite homogeneously mixed.

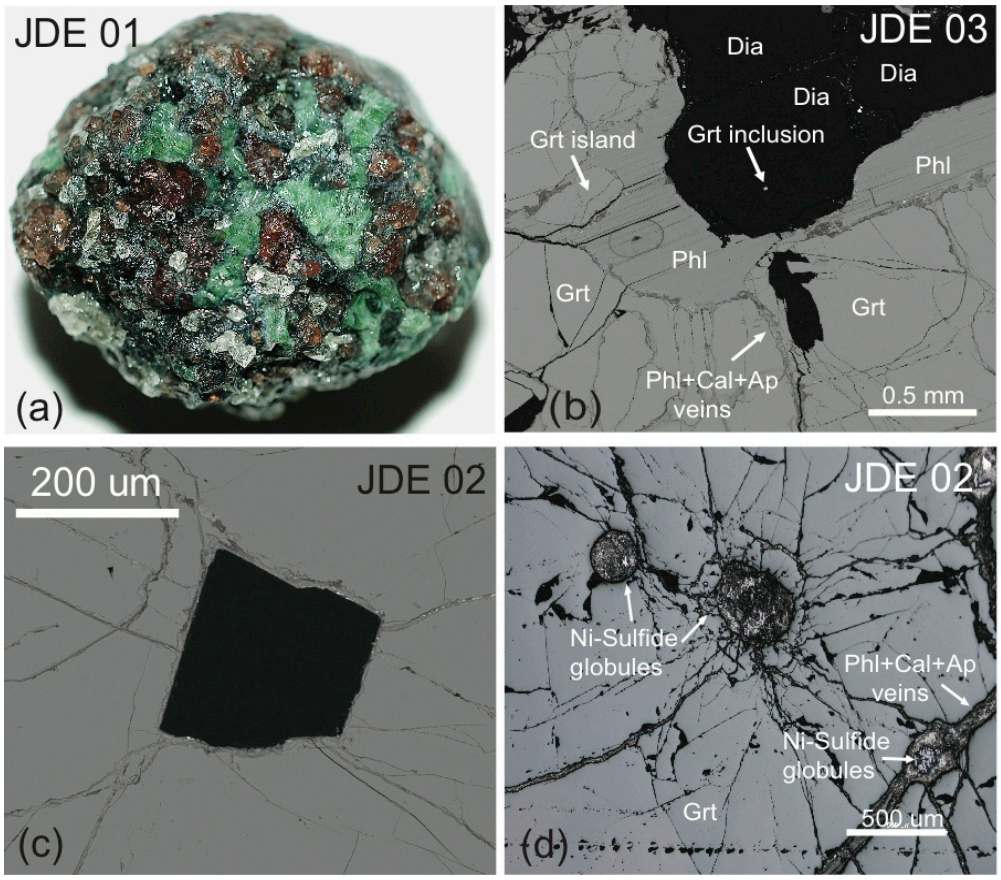

Figure 3.1 Photograph and photomicrographs of a representative high-MgO Jericho Diamond Eclogite

(a) Photograph of Jericho diamond eclogite (JDE) 01. Xenolith is four cm wide (b) Backscattered electron microprobe image of JDE 03 showing the textural relationship of diamond, pholgopite and garnet. The small light dot included in the central diamond is actually a garnet inclusion that was exposed during polishing of these sections, and is approximately 20μm across. (c) Backscattered electron microprobe image of a diamond inclusion in garnet in JDE 02. (d) Reflected light photomicrograph showing pholgopite+apatite+calcite veins and associated Ni-sulfides. Grt=garnet, Phl=phlogopite, Cal=calcite, Ap=apatite, Di=diamond.

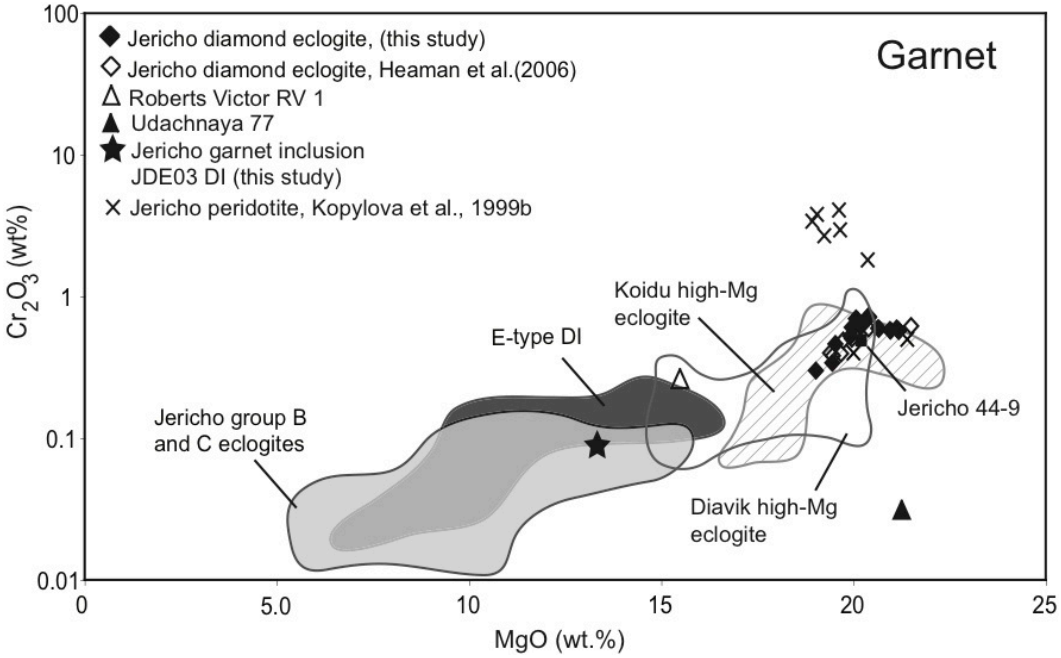

Figure 3.2 MgO and Cr_2O_3 contents in weight percent of garnets from high-MgO diamond eclogites

MgO and Cr_2O_3 contents of garnets. The JDE garnets have similar MgO contents to garnets from Jericho peridotite and pyroxenite (Kopylova et al., 1999b) and are clearly distinct from Jericho Group B and C garnets and also diamond inclusion garnets (Stachel et al., 2004, Donnelly et al., 2007). JDE garnets also compositionally overlap with high-MgO garnets from Koidu (Hills and Haggerty, 1989) and Diavik (Aulbach et al., 2007; Schmidberger et al., 2007). Garnets from two other high-MgO diamond eclogites from Udachnaya (77, Jacob and Foley, 1999) and Roberts Victor (RV 1 Jacob et al., 2005) are shown for comparison.

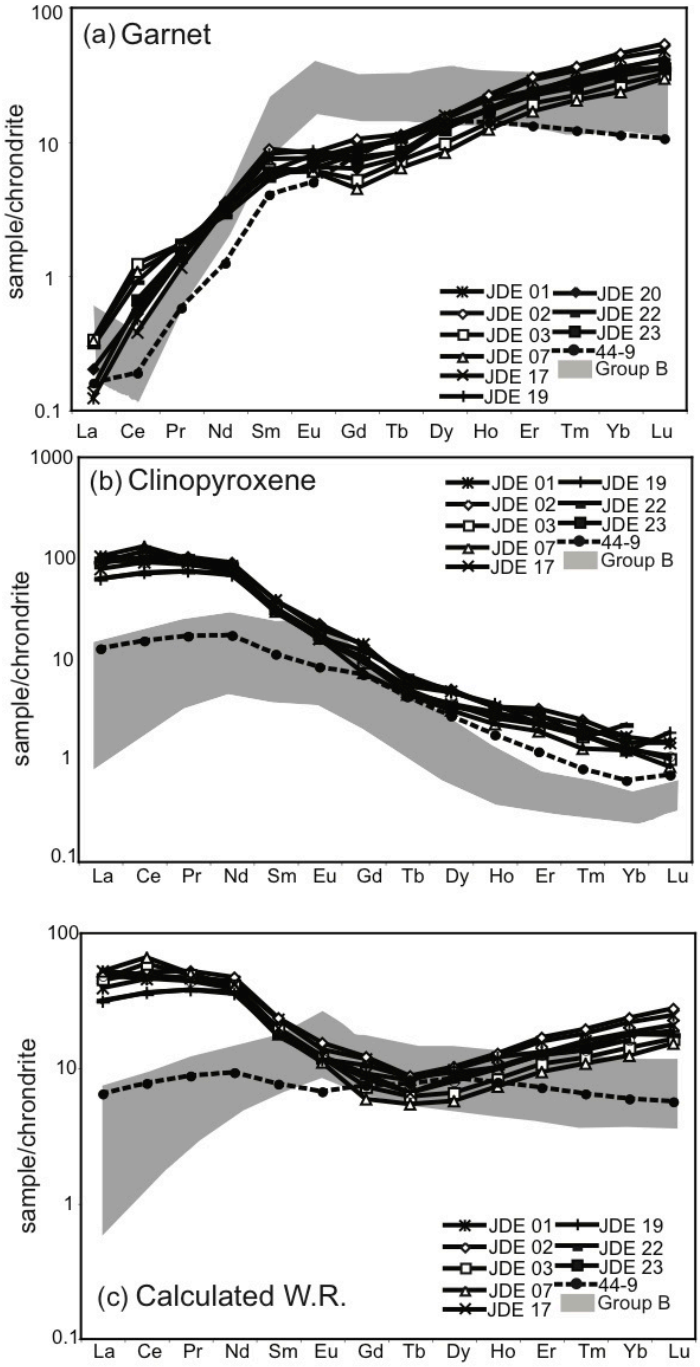

Figure 3.3 Chondrite-normalized REE diagram for garnet, clinopyroxene and calculated whole-rock Jericho eclogites

Chondrite-normalized rare-earth element diagram for (a) garnet, (b) clinopyroxene, and (c) calculated whole rock comparing all group A Jericho eclogites, including the JDE, to the Jericho group B eclogites. Chondrite normalizing values are from McDonough and Sun, 1995.

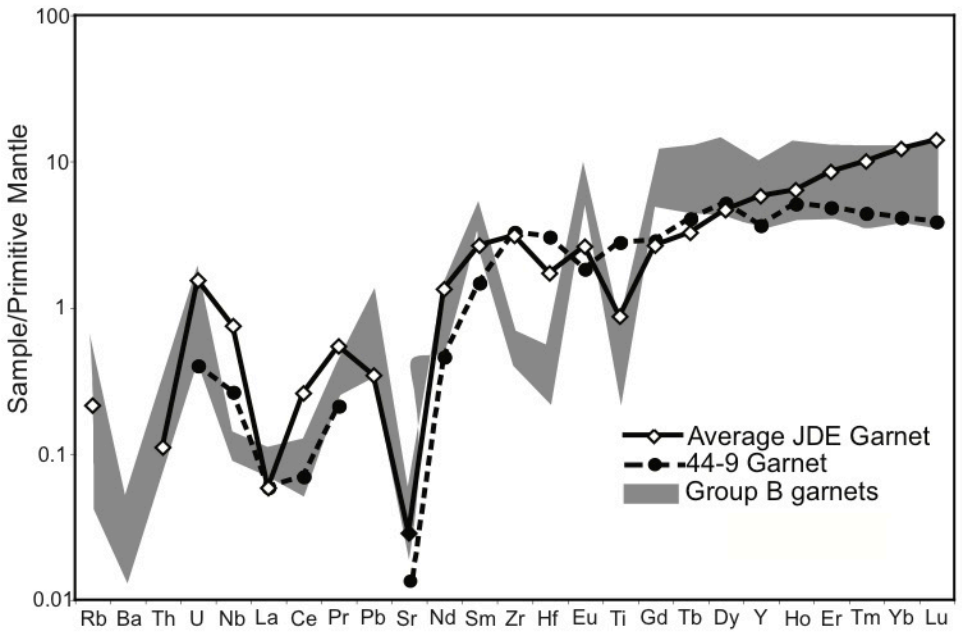

Figure 3.4 Primitive mantle-normalized multi-element plot of garnet from Jericho eclogites

Primitive-mantle normalized multi-element plot of garnet from the Jericho group A and B eclogites. Normalizing values are from McDonough and Sun (1995).

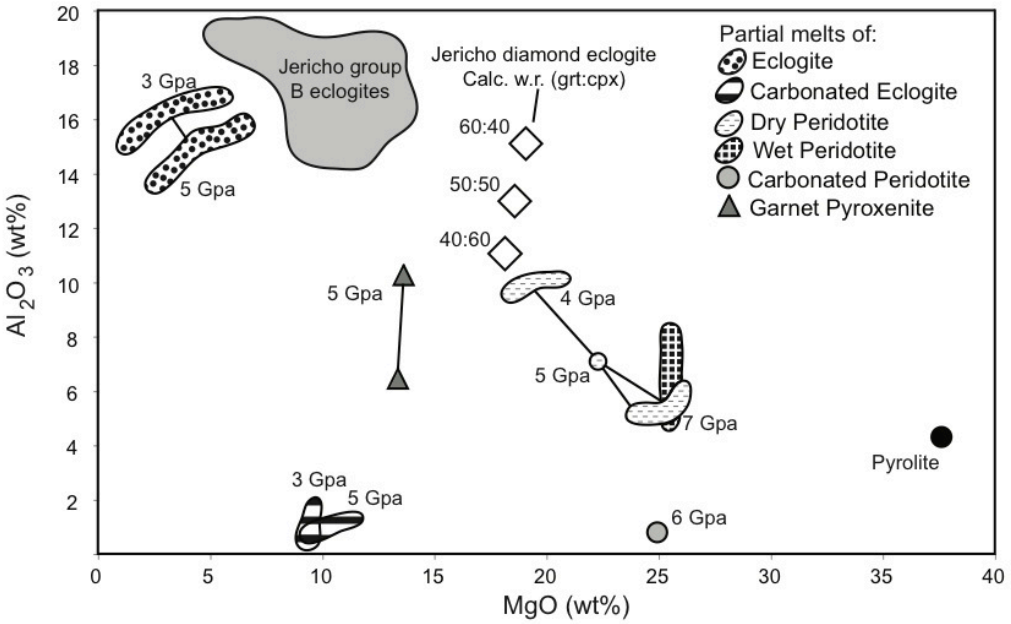

Figure 3.5 Comparison of whole-rock calculated Jericho high-MgO diamond eclogites with various mantle lithologies and mantle-derived melts

Comparison of whole rock calculated JDE and melts generated from various mantle lithologies. The variable whole-rock JDE composition is calculated by the mode percentage of garnet:clinopyroxene denoted in brackets beside each symbol. Melts generated from peridotite (Walter, 1998), wet peridotite (Kawamoto and Holloway, 1997) and carbonated peridotite (Brey et al., 2008) are too Al-poor and often Mg-rich to coincide with JDE compositions. The JDE are too Mg-rich to coincide with melts derived from garnet pyroxenites (Tuff and Gibson, 2007), eclogites (Spandler et al., 2008) or carbonated eclogites (Yaxley and Brey, 2004) and therefore did not crystalize from melts of common mantle lithologies. Pyrolite composition from McDonough and Sun (1995).

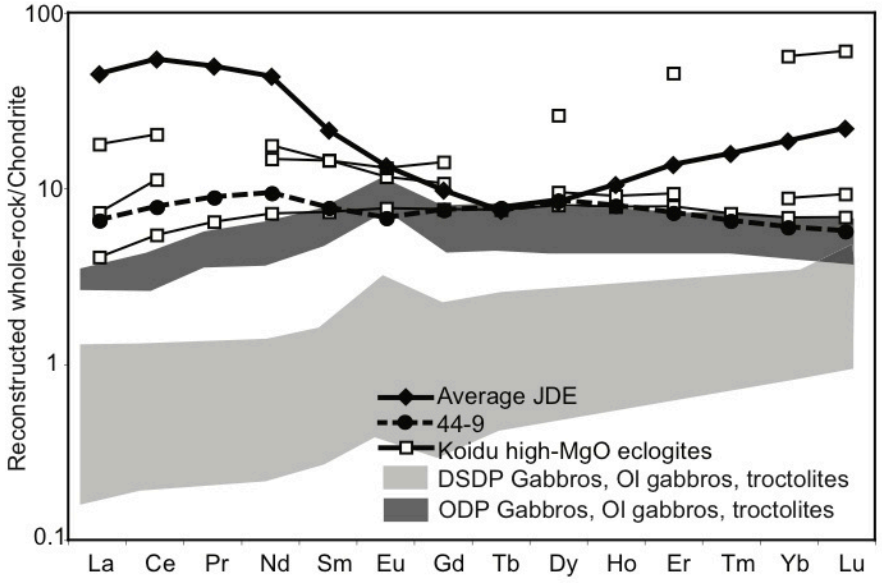

Figure 3.6 Chondrite-normalized REE plot comparing JDE with other high-MgO eclogites and lower oceanic crust

Chondrite-normalized REE diagram of calculated whole-rocks for Jericho eclogite 44-9, average JDE, and three Koidu high-Mg eclogites (Barth et al., 2002a). Also shown are fields for lower crust olivine gabbros and troctolites recovered from oceanic drilling expeditions. Ocean Drilling Program data from Hart et al. (1999) and Bach et al. (2001); Deep Sea Drilling Program data from Aumento et al. (1977).

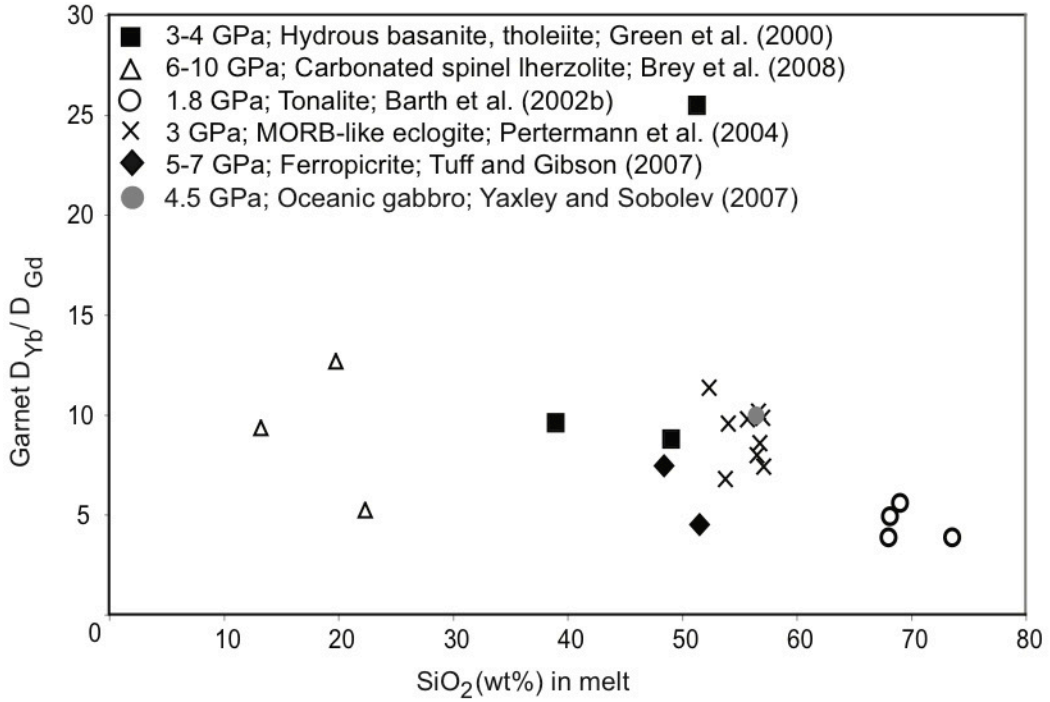

Figure 3.7 Melt polymerization and Yb/Gd partition coefficient for residual garnets during partial melt extraction from various mafic and ultramafic lithologies

The effect of melt polymerization on Gd/Yb partition coefficient ratios for garnets coexisting with partial melts produced from various lithologies. Garnets coexisting with silica-poor melts (e.g., Brey et al., 2008) have higher D_{Yb}/D_{Gd} and thus have more fractionated (steeply sloping) chondrite-normalized HREE than garnets in equilibrium with more silicic melts (e.g., Barth et al., 2002b). The experimental pressure and starting lithology are listed with the appropriate reference.

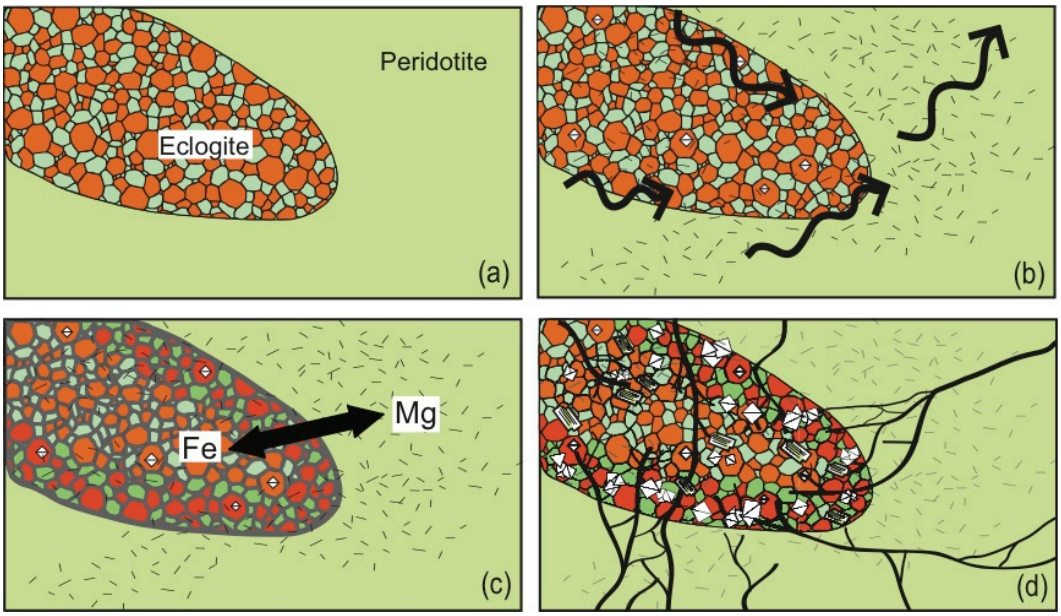

Figure 3.8 Petrogenesis of the Jericho high-MgO diamond eclogites

Schematic diagram depicting the petrogenesis of the high-MgO Jericho Diamond Eclogites. (a) Emplacement of basaltic, Group B eclogites into peridotite (light green) in the northern Slave CLM. This event may be related to the Paleoproterozoic eclogite formation described by Schmidberger et al. (2005). (b) Metasomatism of Group B eclogites and peridotite (indicated by black arrows and dashes), which facilitated diamond growth, some of which occur as inclusions in garnets. Excluding diamond growth, this metasomatic event is largely cryptic, and is responsible for LREE-enrichment and the radiogenic Sr and Pb isotopic signatures observed in JDE clinopyroxene. The metasomatism must have occurred during garnet growth due to the diamond inclusions in garnet, and most likely occurred early in eclogite formation, perhaps during emplacement and eclogitization of a basaltic protolith. (c) Partial melting of Group B eclogites, represented by thick grey lines on eclogite mineral boundaries. A dacitic or carbonatitic melt, depending on the extent of eclogite metasomatism described in (b), is extracted from eclogite and facilitates Fe-Mg exchange between Group B eclogite and peridotite. The Fe-Mg elemental diffusion produces Mg-rich garnet and clinopyroxene (indicated by darker colors), where the degree of chemical exchange is more extensive closer to the peridotite-eclogite contact. The exact timing of partial melting and Fe-Mg exchange is uncertain, but encapsulation of a Group B garnet in diamond suggests this event may have been triggered by, or coeval with, diamond formation associated with the cryptic metasomatic event. (d) Modal metasomatism of the eclogite-peridotite assemblage by a potential carbonatitic-kimberlitic agent. This metasomatism produced coarse-grained phlogopite, potentially more diamond, and veins of fine-grained phlogopite, apatite, carbonate and sulfide in the JDE.

4 Chapter 4: Eclogitic diamond growth from oxidized crustal sources: a δ^{13}C-N study of diamond-bearing eclogites from the Jericho kimberlite[2]

4.1 Introduction

Diamonds are robust, unique probes of Earth's interior that dominantly sample the cratonic lithospheric mantle. Although studies of inclusions in diamond show that peridotite is the main diamond host rock (e.g., Stachel and Harris 2008), diamondiferous eclogite xenoliths are far more abundant than diamondiferous peridotite xenoliths. Mantle-derived eclogite xenoliths are taken by many to represent slivers of subducted oceanic crust (Helmstaedt and Doig, 1975), however this view is not universally accepted (Griffin and O'Reilly, 2007). A crustal origin for eclogite xenoliths is contended based on their compositional similarity to oceanic basalts, Eu anomalies in constituent minerals that indicate the presence of plagioclase in the protolith, and oxygen isotope compositions that fall outside the range of the isotopic composition of the unaltered mantle (e.g., Helmstaedt and Doig, 1975; MacGregor and Manton, 1986; Jacob, 2004). The source of carbon in eclogitic diamonds is also controversial and debate continues around derivation from subducted sediments or from primary mantle carbon introduced metasomatically into the eclogites (e.g., Cartigny, 2005; Stachel et al., 2009).

The majority of eclogitic and peridotitic diamonds have δ^{13}C values from -8‰ to -2‰, with a major mode at -5±1‰ that overlaps the inferred carbon isotope composition of the mantle (Deines, 2002; Cartigny, 2005). This similarity is interpreted to represent diamond formation from mantle-sourced carbon (Deines, 1980). In contrast to peridotitic diamonds, eclogitic diamonds also have a wide range of δ^{13}C values from -41‰ to +2.9‰ with primary and secondary

[2]This chapter is published as: Smart K.A., Chacko T., Stachel T., Muehlenbachs K., Stern R. and Heaman L.M. Diamond growth from oxidized carbon sources beneath the Northern Slave Craton, Canada: A δ^{13}C-N study of eclogite-hosted diamonds from the Jericho kimberlite. Geochimica et Cosmochimica Acta 75: 6027-6047.

modes at -5 and -14‰, respectively (Stachel et al., 2009). However, most eclogitic diamonds have $\delta^{13}C$ values > -25‰, as diamonds with $\delta^{13}C$ values of -40‰ values only occur from the Jericho kimberlite in the Slave craton (De Stefano et al., 2009). The low $\delta^{13}C$ values of some eclogitic diamonds have been proposed to represent subducted organic matter, as both organic sediments and eclogitic diamonds have overlapping distributions of ^{13}C-depleted carbon isotope compositions (Sobolev and Sobolev, 1980; Milledge et al., 1983). Parallel to the debate surrounding the host eclogite xenoliths, a crustal origin for the carbon in eclogitic diamonds has been challenged by alternative models involving isotopic fractionation of mantle-derived carbon-bearing fluids/melts or preferential tapping of a preserved low $\delta^{13}C$ primordial reservoir (e.g., Cartigny et al., 2001a; Deines et al., 2001).

Significant advances have been made concerning the origin and formation of diamond in the mantle based on information extracted from diamond samples. From carbon, nitrogen and silicate inclusion data, it is clear that diamond concentrates from kimberlites generally reflect mixed populations, and may contain diamonds of different sources and ages (e.g., Richardson et al., 1993). In contrast, diamondiferous xenoliths represent 'in situ' examples of diamond source regions and are more likely to contain single populations of diamonds, or at least represent similar growth conditions during diamond formation (Thomassot et al., 2007; Palot et al., 2009). Thus, study of such samples enables evaluation of diamond formation models. Recent studies demonstrated the power of coupled cathodoluminescence (CL) imaging and secondary-ion mass spectrometry (SIMS) analyses of carbon isotope composition and nitrogen abundance in diamond, in order to determine both the growth history and nature of the fluids/melts involved in diamond formation (e.g., Harte et al., 1999; Bulanova et al., 2002; Schulze et al., 2004; Zedgenizov et al., 2006). Application of these micro-scale techniques to diamonds liberated from mantle xenoliths can provide powerful constraints on the formation of diamond in accessible 'natural laboratories'.

Smart et al. (2009a) described the petrology of the high-MgO Jericho diamond eclogites and concluded that these eclogites formed by melt-facilitated

peridotite and low-MgO eclogite hybridization, coupled with diamond formation associated with carbon-bearing (carbonatite-like) metasomatism. In this study, we apply FTIR, conventional combustion and SIMS C-isotope analysis techniques to evaluate the origin of diamonds from two distinct groups of diamond eclogites from the Jericho kimberlite. Using SIMS, we also examine intra-stone variations in the carbon isotope composition and nitrogen content of a subset of these diamonds. In total, we present results from 42 diamonds from five eclogite xenoliths, with SIMS analyses on 12 diamonds representing three xenoliths. The aim of this study is to determine the origin and mode of formation of eclogitic diamonds in the cratonic lithospheric mantle beneath the northern Slave craton.

4.2 Background

The Jericho kimberlite (173 Ma; Heaman et al., 2006) is located in Nunavut, Canada, about 150 kilometers north of the Lac de Gras kimberlites in the northern Slave craton. Eclogite xenoliths are abundant at Jericho and previous studies revealed a wide range of compositions (Kopylova et al., 1999; Smart et al., 2009a). Based on the geochemical classification of garnet compositions from Coleman et al. (1965), Jericho eclogites have been subdivided into three groups: A) high-MgO (19.6–21.3 wt.% MgO), B) high-FeO (up to 27.5 wt.% FeO), and C) high-CaO (up to 17.7 wt.% CaO). Both Paleo- and Mesoproterozoic ages have been obtained for the Jericho zircon-bearing eclogites; the former ages are proposed to represent eclogite formation associated with subduction of oceanic crust during the ca. 1.9 Ga Wopmay Orogeny (Schmidberger et al., 2005) and the latter coincide with metasomatic overprinting concomitant with the 1.27 Ga Mackenzie Igneous Event (Heaman et al., 2006).

Of the 15 diamond eclogites investigated in the present study, most belong to Group A and contain pyrope-rich garnets with elevated Cr_2O_3 (up to 0.7 wt.%) and jadeite-poor clinopyroxene (1.4-1.9 Na_2O wt.%). We refer to these diamond eclogites as 'JDE A' (Jericho Diamond Eclogite Group A). The JDE A are extraordinarily fresh and have up to 20 vol.% diamond. In some cases, diamonds occur in veins surrounded by thin veneers of a dark, fine-grained assemblage of

phlogopite + apatite + carbonate + glass (Section 3.1.2; Smart et al. 2009a). Unlike other eclogites where diamonds occur in zones of intense metasomatism (Schulze et al., 1996; Taylor et al., 2000), the JDE A contain randomly distributed diamonds in direct contact with silicate minerals and as inclusions in garnet indicating eclogite recrystallization after diamond formation (see Section 3.1.2; Smart et al., 2009a for detailed eclogite petrogenesis). Using the Krogh-Ravna (2000) calibration of the Fe-Mg geothermometer, temperatures and pressures were calculated iteratively for the JDE A eclogites to be compatible with the Jericho peridotite geotherm from Kopylova et al. (1999b). This approach yields temperatures of 860-930ºC (P = 4.2-4.4 GPa).

A second group of diamond eclogites from Jericho has lower MgO contents than the JDE A. De Stefano et al. (2009) reported one diamond eclogite from Jericho containing garnet with 13.6 wt.% MgO. In the present study, we discovered two additional diamond eclogites with similar compositions, containing garnet with ~15 wt. % MgO, low Cr_2O_3 (<0.1 wt.%), elevated Na_2O (>0.1 wt.%) and moderate-Na_2O clinopyroxene (4.9-6.4 wt.%). The pressure-temperature calculation methodology described above indicates that the JDE B eclogite equilibrated at higher temperatures and pressures (1070-1110ºC; 4.8-5.0 GPa) than the JDE A. These lower-MgO eclogites classify as 'Group B' (termed 'JDE B') and fall within the compositional field of most diamond eclogites worldwide (e.g., Jacob, 2004). Compared to JDE A, the JDE B eclogites are quite altered and only remnants of alteration-free clinopyroxene remain. Diamonds in the JDE B invariably occur in areas of intense metasomatism and are generally distributed in a vein-like fashion, similar to other diamond eclogites (e.g., Schulze et al., 1996). Compositional data for the JDE A and B eclogites can be found in Smart et al. (2009a) and in Table 4.1.

De Stefano et al. (2009) reported carbon isotope compositions, nitrogen contents and nitrogen aggregation states for a random sample of Jericho diamonds. $\delta^{13}C$ values ranged from -3 to -41‰, and included the most ^{13}C depleted diamonds yet discovered (De Stefano et al., 2009). Nitrogen contents varied from <20ppm to 1524 ppm in mostly Type IaA diamonds. $\delta^{13}C$ values and

silicate inclusion data were interpreted to indicate that ^{13}C-depleted diamonds are associated with both eclogitic and websteritic parageneses. The latter paragenesis was largely inferred on the basis of pyrope-rich garnets which are virtually identical to garnets from the JDE A eclogites of Smart et al. (2009a) and the present study. Thus, the putative websteritic inclusion suite of De Stefano et al. may partially or wholly derive from Mg-rich eclogites.

4.3 Methods

Of fifteen Jericho diamond eclogite xenoliths, five (three JDE A and two JDE B) were selected for diamond extraction on the basis of xenolith size, freshness and diamond content. Forty-two diamonds selected for nitrogen analysis were cleaned first in dilute ~5N HF for 24 hours to remove residual silicate material, followed by a petroleum ether ultrasonic bath. Cleaned diamonds were analyzed for nitrogen content and nitrogen aggregation state using a Thermo-Nicolet Fourier Transform Infrared (FTIR) spectrometer coupled with a Continuum microscope and a KBr beam splitter. The system was continuously purged with a dry nitrogen-oxygen mix, allowing for background measurements to be taken only every 3-4 hours. Analysis time was 200s during which spectra were taken from 600-4000 cm^{-1} with a resolution of 4 cm^{-1}. Spectral data were reduced by a baseline correction, subtraction of a pure Type II diamond spectrum, conversion into adsorption coefficients and were then deconvoluted into the A, B and D components using software provided by David Fisher (Diamond Trading Center). Nitrogen concentrations (in atomic ppm) were then determined from the absorption strength at 1282 cm^{-1} for both the A- and B-centers (Boyd et al., 1994; Boyd et al., 1995). Sources of uncertainty in FTIR measurements include the quality of the diamond surface analysed (e.g., prepared diamond plates vs. rough diamonds), the nitrogen content of the diamond, and the potential sampling of separate growth layers (in zoned diamonds) with different nitrogen characteristics. Sample quality strongly affects the detection limits and analytical uncertainties, but in general the detection limit is 5-20 atomic ppm, and the associated relative

error for nitrogen concentrations and aggregation states is ~10% (e.g., Stachel et al., 2003).

Following nitrogen quantification, the diamonds were cleaned again in petroleum ether for carbon isotope analysis. The analyzed diamonds weighed between 0.2-2.2 mg and were loaded into quartz tubes to which ~1-2g of CuO was added. Evacuated and sealed tubes were placed in an oven at 980°C for a minimum of 12 hours to achieve diamond combustion. $^{13}C/^{12}C$ ratios were measured on a Finnigan MAT 252 gas source mass spectrometer with an analytical precision of 0.1‰ at the 1σ level. $\delta^{13}C$ values are reported relative to the V-PDB standard.

Twelve diamonds displaying both well-developed octahedral and irregular forms were chosen for SIMS carbon isotope composition analyses. Diamonds were cut and polished parallel to the {100} plane, mounted into indium with a synthetic reference material (S0011, derived from the larger source diamond 1808/16L-2i) and coated with gold for imaging and subsequent analysis. The isotopic composition of S0011, as determined by combustion methods in two laboratories (University of Alberta and Institut de Physique du Globe de Paris), is between -22.58‰ and -22.54‰. High-resolution backscattered electron and CL images were taken using a Zeiss EVO 15 SEM equipped with a Gatan ChromaCL™ detector. This detector utilizes a parabolic mirror for light collection, and a diffraction grating coupled to a 16-channel linear array photomultiplier (PMT) collecting light of wavelengths spanning 300 nm to 800 nm. The signals are then recombined into RGB components, with gains adjusted to compensate for PMT bias so that colors are rendered accurately. $^{13}C/^{12}C$ ratios in diamond were measured using a Cameca IMS 1280 ion microprobe in the Canadian Centre for Isotopic Microanalysis at the University of Alberta. Details of the analysis are given in Table 4.2 and are similar to the methods given by Hauri et al. (2002). $^{133}Cs^+$ primary ion beam of ~3 nA and a spot size of ~15μm was used for analysis. Collection of 10 keV C^- secondary ions was carried out with dual Faraday cups at a mass resolution sufficient to resolve $^{13}C^-$ from $^{12}C^1H^-$. Analyses of S0011 diamond were interspersed regularly throughout several

separate analytical sessions for error analysis and correction for instrumental mass fractionation. Individual analyses comprise a 100s counting period (>1x10^9 cps for $^{12}C^-$), following pre-analysis sputtering (30s) to remove surface contaminants and automated secondary ion tuning. Repeated analysis of the diamond standard (Table 4.3) yields within-spot uncertainties of 0.03‰ and standard deviations of 0.06‰ (the latter of which was calculated from the diamond standard analyses for a particular session). Propagated uncertainties to unknowns include within-spot and between-spot uncertainties, as well as those associated with IMF correction, and are 0.10-0.15 ‰ (95% confidence).

SIMS (IMS 1280) nitrogen abundances were determined in diamond by measuring the ratio $^{12}C^{14}N^-/ {}^{24}C_2^-$. The axial (mono) detector (either Faraday cup or electron multiplier) was utilized at high mass resolution (R ~ 7000 at 10% peak height) in order to completely resolve the isobaric interferences $^{13}C_2^-$ and $^{12}C^{13}C^1H^-$ from $^{12}C^{14}N^-$. The reference material for SIMS calibration was a synthetic diamond fragment, S0011G, for which the N abundances were determined by FTIR. The SIMS analyses were taken from the same pit locations as the previous C-isotope analysis, following a 60s pre-analysis rastering to remove surface contamination. The within-spot measurement uncertainties are generally much less than ± 1% (1 SE), and the uncertainty relating to abundance calibration is estimated at ± 5% (1 SE).

4.4 Results

4.4.1 Diamond Characteristics

Almost all JDE A diamonds were clear and colorless, however rare light yellow stones (n=2) and grey coated stones (n=3) were also observed. Small, 1-2 mm-size diamonds from JDE B eclogites were clear and colorless but several larger diamonds (up to 1cm) had grey coats, cloudy interiors and abundant graphite inclusions. Many of the JDE A and B diamonds exhibited irregular shapes and in some cases occurred as aggregates, where two or more diamonds appeared to have grown together (not polycrystalline diamond). About 30% of the diamonds were well-formed octahedra that lacked any sign of resorption.

Diamonds commonly showed surface features such as striations, trigons and terracing and regardless of shape, commonly contained thin graphite inclusions.

4.4.2 Nitrogen Content and Aggregation State

Nitrogen content and aggregation for the Jericho diamonds are presented in Table 4.4 and Figure 4.1. Diamonds are classified in terms of their nitrogen content and aggregation following Evans et al. (1981). Excluding three Type II diamonds, all JDE A diamonds are Type IaA and have nitrogen contents ranging from 5-82 at. ppm. Diamonds from JDE-2 and JDE-3 have the lowest nitrogen contents (5-28 at. ppm) while those from JDE-7 have systematically higher nitrogen contents (58-82 at. ppm, excluding one diamond with 16 at. ppm). JDE B diamonds have much higher nitrogen contents and are dominantly Type IaAB. The exceptions are two aggregate diamonds from JDE-15, which are Type IaA with nitrogen contents of 2350 and 1130 at.ppm. Most diamonds from JDE-25 have similar nitrogen contents (1080-1400 at. ppm) and relative proportions of nitrogen present in the B-center (%B) of 21-35%, but diamond JDE-25 D5 has higher nitrogen (1784 at. ppm) and %B (56%).

4.4.3 Nitrogen Thermometry

Nitrogen aggregation in diamonds is controlled by temperature, nitrogen content and mantle residence time (Evans and Harris, 1989). Nitrogen aggregation temperatures were calculated for the JDE B diamonds according to Taylor et al. (1990) and Leahy and Taylor (1997) for mantle residence times of 1.8 and 2.5 Ga, which represent the proposed subduction and possible eclogite formation events in the Slave craton at ca. 2.0 (Schmidberger et al., 2005) and 2.7 Ga (Smart et al., 2009b). For the Type IaA JDE A diamonds maximum nitrogen aggregation temperatures can be calculated following the method of Leahy and Taylor (1997), where a 0.5 % B-defect is assumed diamonds. Calculated temperatures for JDE A diamonds range from 1040-1110ºC and, for the JDE B diamonds from 1030-1100˚C; temperatures calculated for 1.8 and 2.5 Ga mantle residence times differ by less than 10°C (Figure 4.1).

4.4.4 Carbon Isotope Analyses by Conventional Methods

$\delta^{13}C$ values for diamonds obtained using the conventional sealed tube combustion technique are reported in Table 4.4 and displayed in Figure 4.2a. As with nitrogen content and aggregation, JDE A and B diamonds also have distinct carbon isotope compositions (Figure 4.2a). Diamonds from three JDE A xenoliths have $\delta^{13}C$ values that range from -37.1 to -40.1‰, with an average of -39.0‰ (n=22) and the individual averages for JDE-2, -3 and -7 are -39.0, -39.3 and -38.5‰, respectively. In contrast, diamonds from JDE B sample JDE-25 have $\delta^{13}C$ values ranging from -3.5 to -5.3‰ and an average of –4.7‰ (n=10). There is no difference in carbon isotope composition between the small, mm-size diamonds and a clear chip from one of the large JDE B diamonds (-4.8‰). All diamonds from JDE B sample JDE-15 were too small for conventional carbon isotope analysis. The overall distribution of the carbon isotope data from JDE A and B diamonds is more tightly constrained with discrete modes at ~-39‰ and -4.5‰ respectively, compared to the wider range in $\delta^{13}C$ values for eclogitic diamonds (-25 to -41‰; see Figure 4.2a) given by De Stefano et al. (2009). The De Stefano et al. data show a wider range of values for the very ^{13}C-depleted diamond population (down to -41‰), likely reflecting the larger number of diamonds analyzed in that study.

4.4.5 Carbon Isotope and Nitrogen Content Analyses by SIMS

Twelve diamonds from two JDE A and one JDE B eclogite xenoliths were studied by SIMS with a total of 107 and 71 spot carbon isotope analyses, respectively, in order to investigate intra-stone variations. The results are listed in Table 4.5 and displayed in Figure 4.2b. One diamond (JDE-2 S2) was cut in half and analyzed by both conventional and SIMS techniques. The relatively small difference between the conventional (-39.0‰) and SIMS (-40.3 to –39.9 ‰, n=5) data for this diamond most likely represents isotopic heterogeneity on the scale of a single diamond grain (see below). Following SIMS carbon isotope analyses, four diamonds were selected for SIMS nitrogen abundance analyses. Eighty-two spots were placed at previous carbon isotope analysis spots such that the

covariation of nitrogen and $\delta^{13}C$ could be investigated. SIMS nitrogen abundances can be found in Table 4.5 and graphically on Figure 4.5 for diamond JDE-25 S1. In the sections below, we assess the intra-diamond variations in the carbon isotope composition and nitrogen abundance of JDE A and B diamonds by reference to CL images.

4.4.5.1 JDE A diamonds

Cathodoluminescence images of eleven JDE A diamonds reveal that the diamonds fall into two groups: well-formed octahedral diamonds that have a uniformly deep blue color in CL (Figure 4.3a), and fragmented, irregularly-shaped diamonds that have narrow (~50μm-thick) light blue rims and light blue areas in the interior of the stones (Figure 4.3b,c; Figure 4.4). Blue CL colors for diamond are due to the naturally occurring N3 color center and typical for diamonds that have not experienced significant metamorphism (Bruce et al., 2011). Diamonds commonly display resorbed edges and plastic deformation. $\delta^{13}C$ values from the interiors of most JDE A diamonds are remarkably uniform, with only small differences in average composition between diamonds from JDE-2 (-40.21 ± 0.15‰, 1 SD) and JDE-7 (-39.42 ± 0.21‰). Nitrogen analyses from the homogeneous stones also show little variability. Even for diamonds that show some growth zonation in the interior (Figure 4.3b), there is little difference in $\delta^{13}C$ values between the irregular light-colored areas and the dark diamond interior. However some isotopic and nitrogen abundance differences between the interior and narrow light-colored rim can be observed on diamond JDE-2 S7 (Figure 4.3b). The irregular contact between diamond rim and interior is suggestive of partial resorption followed by re-growth of the rim. The rims have $\delta^{13}C$ values 0.5 to 1.8‰ higher than the cores (Figure 4.3b) and have significantly lower nitrogen abundances (from 20 to <1 at.ppm on JDE-2 S7). In addition, there are several JDE A diamonds with complex CL images that show much more pronounced variations in $\delta^{13}C$ values and nitrogen abundances. One large, irregularly shaped diamond, JDE-7 S1 (Fig. 3c), has distinctive light and dark CL concentric zoning at the rim and displays variation from -38.9‰ and ~90 at.ppm

N (core) to -34.1‰ and 5 at.ppm N (rim). JDE-2 S4 has a dark interior with a center cross structure only partially visible due to fragmentation of this diamond and has sharp demarcated boundaries to a large (~400 x 800 μm) inhomogeneous light-colored structure near the corner of the grain that exhibits both a ~10‰ increase in $\delta^{13}C$ values relative to the adjacent isotopically homogeneous core and an internal variation from -13.3‰ to -30.9‰.

4.4.5.2 JDE B diamonds

One 0.5 cm diameter, clear octahedral JDE B diamond (JDE-25 S1) was selected for CL imaging and SIMS analyses. CL images (Figure 4.5) reveal a dark inner core surrounded by a broad area with a uniform lighter-blue color. We refer to these two areas as the *inner* and *outer core zones*, respectively, and collectively as the *core zone*. The core zone is surrounded concentrically by alternating light and dark layers that become progressively darker blue in CL towards the outermost rim of the diamond. We refer to this area as the *oscillatory zone*. The boundary between the core zone and the oscillatory zone is generally sharp and straight except along the right side of the diamond in Fig 4.5. The ragged nature of this contact is preserved throughout the subsequent oscillatory growth layers. The outermost part of the diamond, which we refer to as the *rim zone*, ranges from non-luminescent to dark blue CL color.

The results of core-to-rim carbon isotope and nitrogen abundance analyses are shown in Figure 4.5. $\delta^{13}C$ values increase slightly (–4.2 to –3.9‰) in the inner core zone but then increase more markedly in the outer core zone to a maximum value of –2.6‰ at the boundary between outer core and oscillatory zones. The inner core zone is characterized near its center by nitrogen abundances that oscillate between ~5200 and 4300 ppm, which then drop sharply to ~3500 ppm near the boundary with the outer core zone (Figure 4.5). The outer core zone exhibits a nearly continuous rimward decrease in nitrogen contents from ~3400 to 1100 ppm at the boundary with the oscillatory zone. The transition from the outer core zone to the oscillatory zone is characterized by a sharp decrease in $\delta^{13}C$ values from ~ -2.7 to -5.5‰ and sharp fluctuations in nitrogen abundances (1900

and 115 at. ppm on the right and left sides, respectively) which is followed by somewhat erratic variations in both $\delta^{13}C$ values and nitrogen abundances between –5.9 and –4.3‰ and 5 to ~1500 ppm over most of the oscillatory zone. The rim zone is characterized by an outward increase in $\delta^{13}C$ values from ~ -5.8 to –3.0‰, accompanied by erratic, yet generally decreasing nitrogen abundances. The intra-stone carbon isotope and nitrogen abundance variations noted above appear to be symmetrical, as shown by the nearly identical results of core-rim transects running to opposite rims of the diamond.

4.5 Discussion

It is evident from the nitrogen and carbon isotope data presented here that the eclogitic Jericho diamonds comprise two distinct populations, corresponding to their occurrence in two distinct eclogite groups (Smart et al., 2009a and Table 4.3). Furthermore, the JDE A and JDE B eclogites have distinct calculated temperatures of 860-930 and 1070-1110°C, respectively, which suggests that these two eclogite groups last equilibrated at different depths in the lithospheric mantle. The combined eclogite and diamond datasets suggest the two eclogite groups and their extracted diamonds do not have shared origins and we thus evaluate their genesis separately.

4.5.1 Origin of JDE A diamonds

Diamonds extracted from the high-MgO, Group A Jericho eclogites have very low nitrogen contents of <70 at. ppm and low $\delta^{13}C$ values of ca. -40‰ (Figure 4.1, 4.2). These are amoung the most ^{13}C-depleted carbon isotope compositions known for diamonds to date (cf., De Stefano et al., 2009). The extreme $\delta^{13}C$ values of these diamonds have consequently led to difficulties in interpreting their origin, which is not surprising as considerable debate still surrounds the origin of diamonds with less extreme $\delta^{13}C$ values of ca. -20‰ (e.g., Kirkley et al., 1991; Cartigny, 2005). The majority of eclogitic diamonds worldwide have mantle-like $\delta^{13}C$ values (~-5‰) and are thought to form from

mantle-derived carbon, however there are diamond populations that have partially or exclusively low $\delta^{13}C$ values (e.g., Cartigny, 2005; Stachel et al., 2009). Several models have been proposed to account for isotopically light carbon in diamonds ($\delta^{13}C$<-10‰). These include primordial heterogeneities preserved in the Earth's interior (Haggerty 1999; Deines et al., 2001), ^{13}C-depleted "neutral" carbon dissolved at trace levels in major mantle minerals such as olivine (Deines, 2002), Rayleigh fractionation of mantle-derived carbon (Cartigny et al., 2001a) and organic matter subducted to great depths (Sobolev and Sobolev, 1980; Milledge et al., 1983). In order to better understand the origin of the low $\delta^{13}C$ values in the JDE A diamonds, we present a detailed assessment of each of these explanations.

4.5.1.1 Origin of extreme negative $\delta^{13}C$ values

Remnant primordial heterogeneities from planetary accretion have been proposed as a possible source of ^{13}C-depleted carbon in the mantle, on the basis of low $\delta^{13}C$ values of carbon dissolved in metal phases in iron meteorites (Deines and Wickman, 1975), some organic carbon in carbonaceous chondrites (Pearson et al., 2006) and nano-scale, pre-solar diamonds from primitive chondritic meteorites (Russell et al., 1991). Deines et al. (2001) argued that these isotopic heterogeneities could remain unmixed in the mantle on a small scale, and could be the source of carbon in ^{13}C-depleted diamonds. However, it is difficult envision how primordial, ^{13}C-depleted reservoirs would be exclusively associated with the eclogite paragenesis. Moreover, the $\delta^{13}C$ values of carbon in most of the purported reservoirs are > -30‰ (Pearson et al., 2006), distinctly too ^{13}C-enriched to explain the –40‰ JDE A diamonds. Only the nano-diamonds present in chondrites have $\delta^{13}C$ values (–32 to –38‰) approaching ca. -40‰,, but because the diamonds constitute just a small percentage of the total carbon in their host meteorites (Zinner, 1998), the bulk $\delta^{13}C$ values of these meteorites are too high.

Deines (2002) suggested that another potential source for strongly ^{13}C-depleted carbon is unbonded, "neutral" C dissolved in lattice defects in mantle minerals such as olivine, pyroxene and garnet. Fractionation factors between dissolved C and CO_2, carbonate and CH_4 inferred from theoretical calculations

range from ~ -10 to -20‰ at mantle temperatures. Although these large fractionation factors could potentially account for diamonds with strongly negative $\delta^{13}C$ values, the process by which trace quantities of dissolved C is extracted from mantle silicate phases and then concentrated sufficiently to form diamond is unknown. Moreover, experiments by Keppler et al. (2003) indicate that the solubility of C in olivine (0.1-1ppm) and other mantle minerals is one to two orders of magnitude lower than suggested by previous studies. If correct, this greatly limits the viability of ^{13}C-depleted diamond formation through exsolution of silicate-hosted C.

Rayleigh fractionation processes have also been invoked to explain eclogitic diamond populations with low $\delta^{13}C$ values (e.g., Deines 1980; Kirkley et al. 1991). There are two scenarios within a Rayleigh fractionation model: (1) fractionation of carbon isotopes during diamond precipitation directly from source fluids/melts (e.g., Deines, 1980), and (2) fractionation of carbon isotopes related to evolution of the source fluid or melt (e.g., CO_2 separation model of Cartigny et al., 2001a). In (1), continuous removal of newly formed diamond from chemical communication with its growth medium causes progressive shifts in the isotopic composition of that medium. In principle, such a process can produce extreme isotopic compositions in the final stages of fractionation when there is only a small amount of fluid/melt remaining (e.g., Valley, 1986). In the specific case of diamond growth, the oxidation state of the source fluid/melt controls the carbon speciation in the fluid/melt, which in turn controls both the direction and magnitude of carbon isotope fractionation between the diamond and the fluid/melt. The nature of the source fluid/melt is critical when modeling diamond growth, as diamond crystallization from oxidized fluids/melts (e.g., containing CO_2 or CO_3^{-2}) will produce diamonds with successively ^{13}C-enriched carbon isotope compositions, whereas growth from reduced fluids/melts (e.g., containing CH_4) has the opposite effect on carbon isotope compositions (e.g., Deines, 1980). Therefore, to form diamonds with very low $\delta^{13}C$ values from mantle-derived carbon with $\delta^{13}C$= -5‰, only reduced fluids/melts need to be considered. It has been shown from Rayleigh fractionation models that only trace volumes of

diamond with $\delta^{13}C$<-10‰ can be produced from reduced fluids/melts with an initial mantle-like carbon isotope composition (Deines 1980; Kirkley et al. 1991 and Figure 4.6a). As shown by our own modeling (see Figure 4.6 caption), in order to form the JDE A diamonds with a mode of $\delta^{13}C$ values at -39 to -40‰, the source fluid/melt must have an initial $\delta^{13}C$ value no higher than -35 to -34‰, under reducing conditions.

In model (2) Cartigny et al. (2001a) argued that low $\delta^{13}C$ values coupled with low nitrogen contents observed in some eclogitic (and rare websteritic) diamonds reflect carbon isotope fractionation and nitrogen depletion during evolution of the diamond growth medium (e.g., a CO_2 fluid or carbonate-bearing melt) prior to diamond crystallization. In this model, isotopic fractionation is driven by the separation of CO_2 from the growth medium, which progressively depletes the residual fluid/melt in ^{13}C. As can be seen from Figure 4.6b, although the CO_2 escape model produces a carbon reservoir with considerably lower $\delta^{13}C$ values than the model described previously, only a minute amount (<1%) of the initial fluid/melt reaches a $\delta^{13}C$ value less than –14‰ by this process and virtually none reaches values less than -20‰. Additionally, if the JDE A diamonds formed by an extensive Rayleigh fractionation process, we would expect to see a distribution of diamond $\delta^{13}C$ values similar to the curve in Figure 4.6b (assuming a single fractionation process), reflecting diamond formation from a range of fluid/melt isotopic compositions. The data distribution in Figure 4.2 shows tightly constrained peaks, and does not support diamond formation by extensive fractionation. We conclude, therefore, that JDE A diamonds did not attain their strongly ^{13}C-depleted compositions by Raleigh fractionation of a fluid/melt with initial mantle-like carbon isotope composition, which is in agreement with the interpretations of De Stefano et al. (2009) for the Jericho diamonds.

Recycled sediments are commonly invoked as a carbon source for eclogitic diamonds with low $\delta^{13}C$ values (Sobolev and Sobolev, 1980; Milledge et al, 1983). Whereas marine carbonates have $\delta^{13}C$ values of ~ 0‰ and clearly cannot be the source for diamonds with strongly ^{13}C-depleted compositions,

organic, carbon-rich sediments have much lower $\delta^{13}C$ values, averaging about -25‰ (Schidlowski, 2001; Eigenbrode and Freeman, 2006). Based on the similar distribution of $\delta^{13}C$ values in marine organic sediments and eclogitic diamonds (excluding the dominant mode at -5‰), the carbon in these ^{13}C-depleted eclogitic diamonds may be sourced from subducted organic matter (Sobolev and Sobolev, 1980; Milledge et al., 1983). However, most organic matter is isotopically too heavy (ca. -25‰) to be a viable carbon source for the JDE A diamonds, as even extreme Rayleigh fractionation of a reduced carbon source with $\delta^{13}C$ value of ~ -25‰ cannot produce diamond with $\delta^{13}C$ of ~ -40‰.

Organic matter with extremely ^{13}C-depleted isotope compositions, ranging to -60‰, is known from some Neoarchean and Paleoproterozoic sedimentary rocks (Figure 4.7; Hayes et al., 1983; Schidlowski, 2001; Eigenbrode and Freeman, 2006). Of particular interest are two negative excursions observed in the carbon isotope composition of organic sediments at ca. 2.7 and 2.0 Ga, where there is an abundance of sediments with $\delta^{13}C$ values from -40 to -60‰ (Figure 4.7). This anomaly is found, for example, in rocks of the ca. 2.0 Ga Zaonezhskaya Formation located on the Kola Peninsula, NW Russia (Melezhik et al, 1999), the 2.7 Ga Abitibi and Wabigoon Belts of the Superior craton, Canada (Strauss, 1986), and from Late Archean sediments of the Hamersley Basin in Australia (Kakegawa et al., 2000; Eigenbrode and Freeman, 2006; Thomazo et al., 2009). These extreme carbon isotope compositions are thought to be the product of methane-fixation by methanogenic bacteria (Eigenbrode and Freeman, 2006).

Some of these very ^{13}C-depleted organic sediments are hosted within low-grade limestone in which the organic matter co-exists with abundant carbonate with $\delta^{13}C$ values of ~0‰ (e.g., the Tumbiana Fm., Thomazo et al., 2009). With increasing metamorphic grade (e.g., during subduction), carbon isotope exchange between the organic matter and host carbonates would erase the strongly ^{13}C-depleted isotopic signature of the organic matter. Thus, such carbonate-rich rocks could not be viable carbon sources for the JDE A diamonds. However, there are also examples in the Archean to Proterozoic sedimentary record where ^{13}C-depleted organic matter is hosted within thick black shales with little

carbonate content. For example, the carbonate-poor Neoarchean shales of the Jeerinah Formation of the Hamersley Basin contain abundant organic matter (TOC 2-4 wt.%) with $\delta^{13}C$ values from -35 to -39‰ and (Kakegawa et al., 2000). Similarly, in the ca. 2.7 Ga Abitibi and 2.8 Ga Wabigoon metasedimentary belts of the Superior craton, Strauss (1986) reported graphite from black shales that have $\delta^{13}C$ values from -15 to -47‰ and high TOC (up to 15 wt.%) with negligible carbonate. A striking Paleoproterozoic example is the thick successions of ^{13}C-depleted organic matter from the ca. 2.0 Ga Zaonezhskaya Formation in the Kola Peninsula (Melezhik et al., 1999). This formation comprises dominantly 'shungites': thick, massive deposits of carbonaceous material that are interbedded with siliciclastic and rare dolomitic sediments. The shungites are extremely carbon-rich (up to 98 wt. % TOC) and have $\delta^{13}C$ values ranging from -17 to -47‰. Additional support for the preservation of extreme ^{13}C-depleted sediments is found in the ultra-high pressure (UHP) Maksyutov complex, located in the Ural Mountains of Russia. ^{13}C-depleted graphite with a range of $\delta^{13}C$ values from -21 to -42‰ is found in graphite-mica schists, eclogite boudins and quartzites and is thought to be biogenic in origin (Leech and Ernst, 1998). This UHP-complex records pressure-temperature conditions of 640ºC and 3 GPa (Leech and Ernst, 1998), and thus the extreme carbon isotope composition of graphite within the Matsyutov complex has been preserved to UHP conditions.

Interestingly, the ca. 2.7 and 2.0 Ga negative carbon isotope excursions in the sedimentary rock record correspond to putative subduction events that affected the Slave craton and its underlying lithospheric mantle. From 2.7 to 2.6 Ga, voluminous arc-like volcanism and tonalite intrusion occurred in the Slave craton, and this event is proposed to represent amalgamation of the eastern and western halves of the craton (Davis et al., 2003). The amalgamation process has been attributed to subduction of oceanic lithosphere and therefore it is possible that oceanic crust was imbricated into the Slave lithospheric mantle at this time. Although ca. 2.7 Ga ages are rare for eclogite xenoliths in the Slave craton, some incompatible-element depleted eclogites from Jericho have Pb-Pb model ages of ~2.7 Ga and could represent remnants from this Late Archean subduction event

(Smart et al., 2009b). The 1.9-1.8 Ga Wopmay orogenesis involved eastward-directed subduction on the western margin of the craton (Hildebrand et al., 1987) and is much better represented by eclogite xenoliths from the Slave cratonic lithospheric mantle. Seismic reflection images of the Slave lithospheric mantle display prominent east-dipping reflectors, interpreted to represent remnants of subducted oceanic crust emplaced into the Slave lithospheric mantle during the Wopmay orogenesis (Cook et al., 1999). Furthermore, eclogite xenoliths with Paleoproterozoic ages have been found in the Jericho and Diavik kimberlites, and are proposed to be the remnants of oceanic crust subducted underneath the craton at this time (Schmidberger et al., 2005, 2007; Heaman et al., 2006; Aulbach et al., 2009a). If these aforementioned subduction events brought ^{13}C-depleted, graphitized organic matter into the Slave cratonic lithospheric mantle, then this carbon could have been remobilized to form diamond in the JDE A. Smart et al. (2009a) noted that the high-MgO composition of the JDE A eclogites is hard to reconcile with a purely crustal origin, and therefore diamond formation from sediment-derived carbon indicates decoupling between eclogite and diamond formation as is generally assumed in models of metasomatic eclogitic diamond formation (e.g., Taylor et al., 2000; Cartigny et al., 2004). However, JDE A diamond inclusions indicate that the eclogites previously resembled typical "basaltic" eclogites before hybdridization with peridotite (Smart et al., 2009a) and as such, potentially the carbon source and JDE A eclogites have a common oceanic lithosphere history.

4.5.1.2 Origin of low nitrogen contents

The incorporation of nitrogen into diamond has been ascribed to both kinetic processes (Cartigny et al., 2001a) and equilibrium processes (e.g., Stachel et al., 2009) during diamond growth. In the former model nitrogen is believed to be incompatible in diamond, such that nitrogen content is related to diamond growth rate, where only disequilibrium, rapid growth conditions can appreciably concentrate nitrogen in diamond. In the latter model, the nitrogen content of diamond is directly dependent on the nitrogen concentration in the source fluid/melt. We favor the latter model based on the co-variation of $\delta^{13}C$-N found in

peridotitic diamonds worldwide from Stachel et al. (2009) and the SIMS analyses of nitrogen in diamond from Bulanova et al. (2002) and the JDE-B diamond of the present study, which show core-to-rim decreases in nitrogen content, implying that nitrogen was steadily depleted from the growth medium during diamond formation. Bulanova et al. (2002) further demonstrated micro-scale co-variations of δ^{13}C-N, implying fractional crystallization processes during diamond growth rather than nitrogen incorporation during disequilibrium growth. SIMS nitrogen abundance and carbon isotope analyses from our study show similar relationships (discussed below). From these micro-scale examples, we believe the nitrogen content of diamond is generally controlled by equilibrium processes and therefore the JDE A diamonds formed from a nitrogen-poor fluid/melt.

The nitrogen contents of Archean to Phanerozoic carbonaceous sediments vary widely, from <100 to >1000ppm (Jia and Kerrich, 2004). Nitrogen may also be partially or largely stripped by devolatilization during subduction (Bebout, 1995; Fischer et al., 2002). However, exhumed UHP sediments and metamorphic diamonds are known to contain appreciable amounts of nitrogen (Cartigny et al., 2001b; Busigny et al., 2003), demonstrating that significant quantities of nitrogen can be retained in slabs carried to at least 3 GPa. In addition, recent experiments show that nitrogen can be stable as NH_4^+ in K-bearing silicates to great depths (Watenphul et al., 2009). A complicating factor in this discussion is the possibility of differences in geothermal gradients between Archean and post-Archean subduction zones. Archean subduction-zone geotherms were on average higher than their post-Archean counterparts (e.g., Martin, 1986); consequently, sheet silicates such as micas, the main hosts of nitrogen in metasedimentary rocks (Honma and Itihara, 1981), would have broken down at shallower depths than in lower-temperature modern subduction zones. Hence, such ancient, hot subduction zones would be more effective in stripping nitrogen through dehydration and/or dehydration melting reactions. We suggest, therefore, that the low nitrogen content of the JDE A diamonds could be due to a combination of several factors: a nitrogen-poor protolith and or as well as nitrogen loss by devolatilization or melting reactions during subduction.

4.5.1.3 Growth mechanism of the JDE A diamonds

The CL images and SIMS analyses of a subset of JDE A diamonds indicate that two diamond growth events occurred in the JDE A eclogites. The main mode in $\delta^{13}C$ values at -40‰ (Figure 4.2a) likely represents the primary diamond growth event in the JDE A eclogites and is represented by diamonds with interiors that are largely homogenous in CL with constant nitrogen contents (e.g., Figure 4.3a). The -40‰ $\delta^{13}C$ distribution in Figure 4.2b also contains a small tail to higher $\delta^{13}C$ values and is represented by growth zones on some diamond rims (Figure 4.3b,c), which also contain lower nitrogen contents. Often there is an irregular contact between the interior and rim, indicating that some resorption occurred before the rim growth (e.g., Figure 4.3b). This skewness to higher $\delta^{13}C$ values indicates diamond growth occurred from an oxidized fluid/melt (see Section 4.5.1.1), which could be related to the carbonatite-like metasomatism observed in the host eclogites (Section 3.4.2.2.). Models of the $\delta^{13}C$ distribution of diamond precipitation from carbonate melt or CO_2 fluids ($\delta^{13}C_{initial}$ ~-38.9 to -37.2‰; T = 1100°C) match well with that observed in the JDE A diamonds (Figure 4.8). The isotopic effect of diamond precipitation is observed on one larger aggregate diamond (JDE-7 S1; Figure 4.3c) where growth zones are marked by a rimward progression in $\delta^{13}C$ values from -38.9 to -34.1‰. In contrast, the overall carbon isotope and nitrogen content homogeneity of most JDE A diamonds indicates that diamond growth must have occurred from a fluid/melt-rich system such that precipitation of diamond did not greatly change the isotopic composition of the residual fluid. Further support for a relatively fluid/melt-rich system is provided by the restriction of isotopic fractionation to the rims

In addition to the main population of JDE A diamonds, there are a few JDE A diamonds with clear secondary growth areas in CL containing higher $\delta^{13}C$ values (see section 4.5.1.). This is exemplified by an area of secondary complex growth on the edge of one pre-existing, irregularly shaped JDE A diamond (JDE-2 S4, Figure 4.4). Based on textural observations from similar irregular diamonds (e.g., JDE-2 S7 rim, Figure 4.3a), we infer that the later growth event involved

minor dissolution of JDE A diamonds and mixture of this dissolved carbon with carbon in the infiltrating fluid, which was then followed by precipitation of new diamond rims with progressively higher $\delta^{13}C$ values (e.g., Figure 4.4b). The exact nature of the secondary fluid or melt is speculative, but it clearly had a more ^{13}C-enriched composition ($\delta^{13}C > -13.3‰$) than the strongly ^{13}C-depleted fluid/melt that gave rise to the bulk of the JDE A diamonds.

4.5.2 Origin of JDE B diamonds

4.5.2.1 Behavior of $\delta^{13}C$ and nitrogen during diamond growth

Our high-precision SIMS analyses of the JDE 25 S1 diamond have allowed for a detailed examination of diamond formation, in particular, the behavior of C-isotope compositions and nitrogen contents during diamond growth. Major questions raised in previous diamond SIMS studies concerned (1) the partitioning behavior of nitrogen in diamond relative to the diamond-forming fluid/melt and (2) the degree of coupling, if any, between C-isotope compositions and nitrogen contents during diamond crystallization (cf. Harte et al., 1999; Bulanova et al., 2002). In order to address these questions, we first focus our attention on the *outer core zone* of JDE 25 S1, which, based on the CL image and the smooth anti-correlation of nitrogen contents and $\delta^{13}C$ values (Figure 4.5) most likely represents a coherent growth zone formed from a single pulse of fluid/melt. If this interpretation is correct, we can use the combined N-$\delta^{13}C$ dataset for this zone to model quantitatively the distribution coefficient of nitrogen in diamond relative to the growth medium. In contrast to the outer core zone, the *inner core*, *oscillatory* and *rim zones* exhibit variable nitrogen contents, complex growth layering and no apparent correlation $\delta^{13}C$-N and will be discussed separately in section 4.5.2.2.

The rimward decrease in nitrogen concentration in the outer core zone of JDE 25 S1 (Figure 4.5) dictates that the source fluid/melt is depleted in nitrogen during diamond growth and therefore nitrogen must be compatible in diamond relative to the source fluid/melt. The compatibility of nitrogen in diamond has previously been inferred from single xenolith-derived diamond populations

(Thomassot et al., 2007) and by modeling of worldwide inclusion-bearing diamonds (Stachel et al., 2009). Both these studies found nitrogen to be compatible; the former study found nitrogen to be moderately compatible in diamond precipitating from a reduced fluid ($K_N = 2$, where $K_N = C_{diamond}/C_{fluid}$) and the latter concluded that nitrogen was strongly compatible when diamond formed from an oxidized fluid ($K_N = 4$). Our SIMS results for JDE 25 S1 are ideal for further evaluating the compatibility of nitrogen in that, unlike the two studies noted above, the high precision isotopic and elemental data of the present study were not acquired from multiple diamonds but from a single growth zone in an individual diamond.

Following the approach of Cartigny et al. (2001a) and Thomassot et al. (2007), we have used the co-variation in $\delta^{13}C$ values and nitrogen contents observed in the outer core zone of JDE 25 S1 to quantitatively determine K_N. This is accomplished by combining equations defining equilibrium partitioning of carbon isotopes and nitrogen between diamond and source fluid/melt during diamond formation. Written in logarithmic form, the partitioning of nitrogen during fractional crystallization of diamond is (Rollinson, 1993):

$$\ln(N_f)=\ln(N_o)+(K_N-1)*\ln(f) \quad (1)$$

where f is the fraction of fluid/melt remaining, N_o and N_f are the nitrogen contents of diamond at f=1 and at any other value of f, respectively, and K_N is the diamond-fluid/melt distribution coefficient. Written in delta notation, the equation describing the effects of Rayleigh fractionation on the carbon isotope composition of the diamond is (Javoy et al., 1986):

$$\delta^{13}C - \delta^{13}C_o \approx \Delta_C*\ln(f) \quad (2)$$

where Δ_c is the diamond-fluid/melt fractionation factor, f is the fraction of fluid/melt remaining and $\delta^{13}C_o$ and $\delta^{13}C$ are the carbon isotope compositions of diamond at f=1 and any other value of f, respectively. Solving equation (1) for ln(f) and substituting that expression into equation (2) and rearranging yields:

$$\delta^{13}C = [\Delta_C/(K_N-1)]*\ln(N) - [\Delta_C/(K_N-1)]*\ln(N_o) + \delta^{13}C_o \qquad (3)$$

which indicates that carbon isotope and nitrogen abundance data should form linear arrays in $\delta^{13}C$ vs. ln(N) space and the slope of such a linear array is given by $\Delta_C/(K_N-1)$.

We determined K_N using equation (3), assuming that Δ_C = -1.7‰ (Chacko et al., 1991 and Polyakov and Kharlashina, 1995) and that, similar to measured values in the core zone of JDE 25 S1, the nitrogen content and $\delta^{13}C$ value of the first crystallized diamond (f =1) were 5000 ppm and –4.0‰, respectively. First, ln(N) is calculated from equation (1) by using the appropriate input parameters at f values from 0 to 1, and the resulting ln(N) values were then used in equation (3) to calculate a corresponding set of $\delta^{13}C$ values for variable K_N values from 1.5 to 10. Figure 4.9a shows how varying the K_N in equation (3) produces $\delta^{13}C$-N arrays with different slopes and that the SIMS $\delta^{13}C$-N data for two core-zone transects of JDE 25 S1 scatter along the K_N = 5 line. Nitrogen partition coefficients can be also be directly calculated from the slope of the SIMS data array, independent of assumed values for $\delta^{13}C_o$ and $\ln(N_o)$. Least squares regression of the SIMS data arrays obtained from the right and left transects across the outer core zone yield slopes of -0.39 and -0.49, respectively, which correspond to K_N values of 5.4 and 4.6. A regression of all the data from both transects yields a slope of –0.42 and a corresponding K_N of 5.1.

The above calculations of K_N are based on diamond-carbonate melt fractionation factors of –1.7‰. If diamond formation occurred from CO_2-bearing fluids, then the fractionation factor used would be -3.7‰ at 1100^{O}C, and the K_N value would nearly double (7.1-9.5) to account for the slope of the data array. Therefore, irrespective of whether the JDE B diamond formed from a carbonate melt or a CO_2 fluid, nitrogen was strongly compatible in diamond compared to its source fluid/melt. We would note, however, that our conclusion applies only to the type of oxidized fluid/melt involved in JDE B diamond growth. It remains

possible that nitrogen would behave differently in a different type of fluid/melt and as such, additional studies similar to the type described here would have to be carried out to fully evaluate this possibility.

The nitrogen compatibility modeling provides some insight into the expected co-variation patterns in $\delta^{13}C$ values and nitrogen contents, if these parameters are indeed controlled by equilibrium fractionation processes. Figure 4.9b shows the calculated zoning patterns in $\delta^{13}C$-N that would be produced by 0 to 50% Rayleigh fractional crystallization of diamond from a carbonate melt. The input parameters for the calculations were set such that the nitrogen content and $\delta^{13}C$ value of the initially crystallized diamond would approximate the inner core of the JDE 25 S1 (N≈5000 ppm, $\delta^{13}C$ = -4.0‰, Δ_C = -1.7‰ and K_N = 5, from above). The key feature illustrated by these calculations is that small degrees of diamond fractionation (e.g., 10%) cause little change in $\delta^{13}C$ values (<0.2‰) but large changes (>1500 ppm) in the nitrogen content of the crystallizing diamond. In general, while diamond fractionation will invariably produce readily observable changes in nitrogen content, the degree of fractionation must be large (>30-50%) and the precision of the C-isotope measurements must be high in order produce observable changes in the carbon isotope composition of diamond, as was the case in the present study. In cases where degree of fractionation is lower or the C-isotope analyses less precise, correlations between $\delta^{13}C$ and nitrogen may remain undetected. This may in part explain the conclusions of the SIMS diamond study of Harte et al. (1999), which found no apparent correlation between $\delta^{13}C$ and nitrogen in any of their diamond growth zones, in contrast to those of Bulanova et al. (2002) and our study, which found some correlation in the core of the studied diamonds. Additionally, it should be noted that smooth co-variations in $\delta^{13}C$ values and nitrogen contents, such as are present in the outer core zone of the JDE B diamond, will only be observed in cases where growth occurs from a single pulse of fluid/melt. Diamond formed by small degrees of fractionation from multiple fluid/melt pulses will exhibit more complex relationships between $\delta^{13}C$ and nitrogen because of the different nitrogen and C-

isotope partition coefficients. In the next section, we evaluate the role of these parameters in generating the δ^{13}C-N variations noted in other zones of the JDE B diamond.

4.5.2.2 Growth mechanism of JDE B diamonds

From the multiple growth layers, changing C-isotope compositions and nitrogen contents observed in Figure 4.5, we infer that diamond growth in the JDE B diamond was episodic and involved at least two major growth events and a resorption event. Specifically, we interpret the *inner core zone*, which is characterized by very high but variable nitrogen contents at nearly constant δ^{13}C values, to reflect continuous diamond growth by small degrees (<5%) of diamond fractionation from multiple nitrogen-rich fluid/melt pulses. Diamond formation by such a mechanism would cause major fluctuations in nitrogen content at essentially undetectable C-isotope variations. The large drop in nitrogen content from the edge of the inner core zone (~5000 ppm) to beginning of the outer (~3500 ppm) core zone and accompanying small change in carbon isotope composition (from -4.1 to -3.9‰) can be explained by slightly larger degrees of diamond fractionation (~10%) from a separate pulse of the melt/fluid.

In contrast to the nitrogen variability of the inner core, the *outer core zone* displays nitrogen contents and carbon isotope compositions that correlate smoothly, indicating this zone represents a singular growth event and likely involved only one fluid. The growth event documented here records a positive isotopic shift of 1.3‰ and therefore occurred from oxidized fluids/melts. This isotopic shift required the oxidizing growth medium to have fractionated between 30 to 55% of its carbon, depending on whether that medium was a CO_2 fluid or a carbonate-bearing melt, respectively.

Irregular contacts found on the lower right outer edge of the core zone indicate a period of diamond dissolution that followed initial diamond growth (indicated in Figure 4.5). Compared to the core zone, δ^{13}C values and nitrogen abundances in the *oscillatory zone* vary erratically, likely resulting from numerous discrete fluid pulses that reflect mixing between new, infiltrating fluid and

remobilized pre-existing diamond, coupled with fractional crystallization processes. The lack of correlation between δ^{13}C-N may also be due our inability to adequately analyze the very fine growth layers that occur in the oscillatory zone (<10μm), as the our spot size is ~15μm, and therefore, an individual analytical spot may sample multiple growth layers. As the oscillatory zone has overall lower δ^{13}C values and nitrogen than the core zone, the isotopic composition of the 'new' fluid/melt must have been more ^{13}C- and nitrogen-depleted than the remobilized diamond. Towards the outer edge of the oscillatory zone the carbon isotope composition stabilizes at -5.6‰ (observed on both sides of the diamond), indicating that the 'new' diamond forming fluid/melt eventually became dominant and controlled the composition of the precipitating diamond. Oscillatory growth layers in the *rim zone* have similar, albeit less coherent trends of δ^{13}C-N as compared to the core zone, again reflecting diamond precipitation from oxidized fluids.

4.5.2.3 Source of carbon in the JDE B diamonds

If the core of the JDE B diamond (δ^{13}C ~-4.0‰) formed in isotopic equilibrium with the diamond-forming fluid/melt, then that fluid would have had an initial δ^{13}C value of -2.3 to -0.3‰, based on diamond-carbonate melt (-1.7‰) or diamond- CO_2 fluid (-3.7‰) fractionation factors at 1100°C. The final pulse of fluid/melt that formed the rim zone diamond would have had a lower δ^{13}C value, between -3.9 to -1.9‰, reflected in the more ^{13}C-depleted (~-5.6‰) layers. Thus, the SIMS data indicates that the fluids/melts involved in JDE B diamond formation have δ^{13}C values >-5‰ and could be sourced from either a fractionated mantle carbon reservoir or subducted carbonate sediments. An oxidized C-bearing fluid/melt with an initial δ^{13}C value of -5‰ will shift to higher values of ~-2.3 to -0.3‰ after 70-80% carbon fractionation. This fractionation could be envisaged as diamond formation that accompanies upward percolation of a mantle-derived fluid (Stachel and Harris, 2008). Similar carbon isotope fractionation processes in the same direction and magnitude are observed in the formation of cratonic carbonatite magmas, which separate from primitive mantle-

derived carbonated silicate magmas such as aillikites or kimberlites (Tappe et al., 2008). Measured oxygen fugacities for the deep lithospheric mantle and calculated depth-fO_2 relationships for the underlying asthenosphere (Frost and McCammon, 2008, and references therein) appear to be too reducing to allow for the formation of mantle-derived oxidizing fluids/melts. Alternatively, carbon in the JDE B diamonds could be derived from subducted carbonate sediments which have a $\delta^{13}C$ value of ~0‰ (Schidlowski, 2001). During subduction, devolatilization of the carbonate sediments would drive remaining carbonates to lower $\delta^{13}C$ values (<0‰) and approach carbon isotope compositions similar to that of the JDE B diamond-forming fluids.

4.5.3 General Observations Regarding Diamond Growth

The general rimwards increase in $\delta^{13}C$ values observed in JDE A and JDE B diamonds indicate that both groups of diamonds formed from an oxidizing fluid/melt, but the markedly different carbon isotope compositions of JDE A and B diamonds require two separate fluid/melts. Other SIMS studies of intra-diamond variations in C-isotope composition locally show similar results (e.g., Bulanova et al., 2002; Hauri et al., 2002; Zedgenizov et al., 2006; Janson et al., 2008; Spetsius et al., 2009), suggesting that an oxidized growth medium may be common for diamond formation. Diamond growth from either carbonate melts or CO_2-fluids is compatible with the multitude of fluid and micro-inclusion studies in diamond that invariably contain a carbonatite-like end-member (e.g., Klein-BenDavid et al., 2007; Tomlinson et al., 2009). Additionally, results from this study provide quantitative evidence for the compatible behavior of nitrogen in diamond during growth from oxidized fluids, corroborating the model for worldwide diamond populations of Stachel et al. (2009).

4.6 Conclusions

Diamonds from two groups of diamondiferous eclogites from the Jericho kimberlite have grossly different nitrogen contents, nitrogen aggregation states and carbon isotope compositions. The host eclogite xenoliths also have markedly

different compositions and equilibration temperatures, such that the eclogites may also have different origins. While conventional C-isotope analyses yield a relatively narrow range of $\delta^{13}C$ values for the JDE A (~-40‰) and JDE B (-3.5 to -5.1‰) diamonds, SIMS C-isotope analyses indicate much internal complexity and wider ranges, particularly for the JDE A diamonds (-40.6 to –13.3‰). Diamonds in both suites show core to rim increases in $\delta^{13}C$ values, indicative of diamond growth from an oxidized growth medium (CO_2 fluid or carbonate-bearing melt). The outer core zone of one JDE B diamond displays increases in $\delta^{13}C$ values coupled to steady decreases in nitrogen content, indicating the growth medium was depleted in nitrogen during diamond growth. Diamond/fluid nitrogen distribution coefficients calculated from the variation in nitrogen across a single JDE B diamond growth zone are ~5, indicating that nitrogen is strongly compatible in diamond relative to oxidized fluids/melts.

The extreme -40‰ carbon isotope composition of the JDE A diamonds excludes diamond formation from fractionated mantle-derived carbon or typical organic matter with $\delta^{13}C$ values of -20‰. Instead, we propose the JDE A diamonds formed from methanogenically-mediated, organic matter with very low $\delta^{13}C$ values that only existed in significant abundances in the sedimentary rock record at 2.0 and 2.7 Ga. These ages generally coincide with proposed subduction events affecting the Slave craton. $\delta^{13}C$ values from JDE B diamond core zone require the fluid/melt involved in diamond growth to have $\delta^{13}C$ values from -2 to 0‰, and, to accommodate the rimward increase in $\delta^{13}C$, the fluid/melt must also have been oxidizing. While the overall reducing nature of the lithospheric mantle may rule out derivation from oxidized mantle fluids/melts, diamond formation in the JDE B eclogites may be related to migrating kimberlitic or carbonatitic melts/fluids which had fractionated some carbon prior to JDE B diamond precipitation. Alternatively, it is also possible that the JDE B diamonds formed from subducted carbonate sediments.

References

Aulbach S., Creaser R.A., Pearson N.J., Simonetti S.S., Heaman L.M., Griffin W.L. and Stachel T. (2009) Sulfide and whole-rock Re-Os systematics of eclogite and pyroxenite xenoliths from the Slave craton, Canada. Earth and Planetary Science Letters **283**, 48-58.

Bebout G.E. (1995) The impact of subduction-zone metamorphism on mantle-ocean chemical cycling. Chemical Geology **126**, 11-218.

Boyd S.R., Kifawi, I. and Woods G.S. (1994) The relationship between infrared absorption and the A defect concentration in diamond. Philosophical Magazine B **69**, 1149–1153.

Boyd S.R., Kifawi, I., Woods, G.S. (1995) Infrared absorption by the B nitrogen aggregate in diamond. Philosophical Magazine B **72**, 351–361.

Bruce L.F., Kopylova M.G., Longo M., Ryder M. and Dobrzhinetskaya L.F. (2011) Luminescence of diamonds from metamorphic rocks. *Amer. Mineral*. **96**, 14-22

Bulanova G.P., Pearson D.G., Hauri E.H., Griffin B.J. (2002) Carbon and nitrogen isotopes systematics within a sector-growth diamond from the Mir kimberlite, Yakutia Chemical Geology **188**, 105–123

Busigny V., Cartigny P., Philippot P., Ader M. and Javoy M. (2003) Massive recycling of nitrogen and other fluid-mobile elements (K, Rb, Cs, H) in a cold slab environment: evidence from HP to UHP oceanic metasediments of the Schistes Lustres nappe (western Alps, France). Earth and Planetary Science Letters **215**, 27-42.

Cartigny P. (2005) Stable Isotopes and the Origin of Diamond. Elements **1**, 70-84.

Cartigny P., Harris J.W. and Javoy M. (2001a) Diamond genesis, mantle fractionations and mantle nitrogen content: a study of $\delta^{13}C$-N concentrations in diamonds. Earth and Planetary Science Letters **185**, 85-98.

Cartigny P., De Corte K., Shatsky V.S., Ader M., De Paepe P., Sobolev N.V. and Javoy M. (2001b) The origin and formation of metamorphic microdiamonds from the Kokchetav massif, Kazakhstan: a nitrogen and carbon isotopic study. Chemical Geology **176**, 265-281.

Cartigny P., Stachel T., Harris J.W. and Javoy M. (2004) Constraining diamond metasomatic growth using C- and N-stable isotopes: examples from Namibia. Lithos **77**, 359-373.

Chacko T., Mayeda T.K., Clayton R.N. and Goldsmith J.R. (1991) Oxygen and carbon isotope fractionations between CO_2 and calcite. Geochimica et Cosmochimica Acta **55**, 2867-2882.

Coleman R.G., Lee E.D., Beatty L.B. and Brannock W.W. (1965) Eclogites and eclogites: their differences and similarities. Geologic Society of America Bulletin **76**, 483-508.

Cook F.A., van der Velden A.J., Hall K.W. and Roberts B.J. (1999) Frozen subduction in Canada's Northwest Territories: Lithoprobe deep lithospheric reflection profiling of the western Canadian Shield. Tectonics **18**, 1-24.

Davis W. J., Jones A.G., Bleeker W. and Grütter H. (2003) Lithosphere development in the Slave craton: a linked crustal and mantle perspective: Lithos, **71,** 575-589.

Deines P. (1980) The carbon isotopic composition of diamonds: relationship to diamond shape, color, occurrence, and vapor composition. Geochimica et Cosmochimica Acta **44**, 943–961.

Deines P. (2002) The carbon isotope geochemistry of mantle xenoliths. Earth Science Reviews **58**, 247–278.

Deines, P. and Wickman, F.E. (1975) A contribution to the stable isotope geochemistry of iron meteorites. Geochimica et Cosmochimica Acta **39**, 547-557.

Deines P., Viljoen F. and Harris, J.W. (2001) Implications of the carbon isotope and mineral inclusion record for the formation of diamonds in the mantle underlying a mobile belt: Venetia, South Africa. Geochimica et Cosmochimica Acta **65**, 813–838.

De Stefano A., Kopylova M.G., Cartigny P. and Afanasiev V. (2009) Diamonds and eclogites of the Jericho kimberlite (Northern Canada). Contributions to Mineralogy and Petrology **158**, 295-315.

Eigenbrode J.L. and Freeman K.H. (2006) Late Archean rise of aerobic microbial ecosystems. Proceedings of the National Academy of Science **103** (43), 15759-15764.

Evans T., Qi Z. and Maguire J. (1981) The stages of nitrogen aggregation in diamond. Journal of Physics C **14**. L379-L384.

Evans T. and Harris J.W. (1989) Nitrogen aggregation, inclusion equilibration temperatures and the age of diamonds. In: *Ross, J. (Ed.), Kimberlites and*

Related Rocks. GSA Special Publication, vol. 14. Blackwell, Carlton, pp. 1001–1006.

Fischer T.P., Hilton D.R., Zimmer M.M., Shaw A.S., Sharp Z.D. and Walker J.A. (2002) Subduction and Recycling of Nitrogen Along the Central American Margin. Science **297**, 1154-1157.

Frost D.J. and McCammon C.A. (2008) The Redox State of Earth's Mantle. Annual Reviews in Earth and Planetary Sciences **36**, 389-420.

Griffin W.L. and O'Reilly, S.Y. (2007). Cratonic lithospheric mantle: Is anything subducted? Episodes **30**, 43-53.

Haggerty, S.E. (1999) A diamond trilogy: Superplumes, supercontinents and supernovae. Science **285**, 851-860.

Harte B., Fitzsimons W., Harris J.W. and Otter M.L. (1999) Carbon isotope ratios and nitrogen abundances in relation to cathodoluminescence characteristics for some diamonds from the Kaapvaal Province, S. Africa. Mineralogical Magazine **63**, 829-856.

Hauri E.H., Wang J., Pearson D.G. and Bulanova G.P. (2002) Microanalysis of $\delta^{13}C$, $\delta^{15}N$, and N abundances in diamonds by secondary ion mass spectrometry. Chemical Geology **185**, 149-163.

Hayes J.M., Kaplan I.R. and Wedeking K.W. (1983) Precambrian organic geochemistry: Preservation of the record. In: Schopf, J.W., (Ed.), *Earth's Earliest Biosphere: Its Origin and Evolution*. Princeton University Press, Princeton, NJ, p. 93-134.

Heaman L.M., Creaser R.A., Cookenboo H.O., Chacko T., (2006) Multi-stage modification of the Northern Slave mantle lithosphere: evidence from zircon-and diamond-bearing eclogite xenoliths entrained in Jericho kimberlite, Canada. Journal of Petrology **47**, 821-858.

Helmstaedt H. and Doig R. (1975) Eclogite nodules from kimberlite pipes in the Colorado Plateau-samples of subducted Franciscan type oceanic lithosphere. Physics and Chemistry of the Earth **9**, 95-111.

Hildebrand R. S. Hoffman P. F. and Bowring, S. (1987) Tectono-magmatic evolution of the 1.9 Ga Great Bear magmatic zone, Wopmay orogen, northwestern Canada. Journal of Volcanology and Geothermal Research **32**, 99–118.

Honma H. and Itihara Y. (1981) Distribution of ammonium in minerals of metamorphic and granitic rocks. Geochimica et Cosmochimica Acta **45**,

983-988.

Jacob D.E. (2004) Nature and origin of eclogite xenoliths from kimberlites. Lithos. **77**, 295–316.

Janson G., Muehlenbachs, K., Stachel, T. and Eichenberg, D. (2008) Carbon isotope variations across diamonds with clear and opaque growth zones measured by secondary ion mass spectrometry. 9th International Kimberlite Conference, Frankfurt (Germany). 3p. (CD)

Javoy M., Pineau F. and Delorme H. (1986) Carbon and Nitrogen Isotopes in the Mantle. Chemical Geology **57**, 41-62.

Jia Y. and Kerrich R. (2004) Nitrogen 15-enriched Precambrian kerogen and hydrothermal systems. Geochemistry Geophysics Geosystems. **5**, Q07005, doi: 10.1029/2004GC00716.

Kakegawa T., Kasahara Y., Hayashi K.I. and Ohmoto H. (2000) Sulfur and carbon isotope analyses of the 2.7 Ga Jeerinah Formation, Fortescue Group, Australia. Geochemical Journal **34**, 121-133.

Keppler H., Wiedenbeck M. and Shcheka S.S. (2003) Carbon solubility in olivine and the mode of carbon storage in the Earth's mantle. Nature **424**, 414-416.

Kirkley M.B., Gurney J.J., Otter M.L., Hill S.J. and Daniels, L.R. (1991) The application of C isotope measurements to the identification of the sources of C in diamonds — a review. Applied Geochemistry 6 **5**, 477–494.

Klein-BenDavid O., Izraeli E.S., Hauri E. and Navon O. (2007) Fluid inclusions in diamonds from the Diavik mine, Canada and the evolution of diamond-forming fluids. Geochimica et Cosmochimica Acta **71**, 723-744.

Kopylova M.G., Russell J.K. and Cookenboo H. (1999). Mapping the lithosphere beneath the north central Slave Craton. In: Gurney, J. J., Gurney, J. L., Pascoe, M. D. & Richardson, S. H. (eds) *Proceedings of the 7th International Kimberlite Conference*. Cape Town: Red Roof Design pp. 468-479.

Krogh Ravna, E. (2000) The garnet-clinopyroxene Fe^{2+}-Mg geothermometer: an updated calibration. Journal of Metamorphic Geology **18**, 211-219.

Leahy K. and Taylor W.R. (1997) The influence of the Glennie domain deep structure on the diamonds in Saskatchewan kimberlites. Russian Geology and Geophysics **38**, 481–491.

Leech M.L. and Ernst W.G. (1998) Graphite pseudomorphs after diamond? A carbon isotope and spectroscopic study of graphite cuboids from the Maksyutov Complex, south Ural Mountains, Russia. Geochimica et Cosmochimica Acta **62**, 2143-2154.

MacGregor I.D. and Manton W.I. (1986) Roberts Victor eclogites: ancient oceanic crust. Journal of Geophysical Research **91 (B14)**, 14063-14079.

Martin H. (1986) Effect of steeper Archean geothermal gradient on geochemistry of subduction-zone magmas. Geology **14**, 753-756.

Mattey D.P. (1991) Carbon dioxide solubility and carbon isotope fractionation in basaltic melt. Geochimica et Cosmochimica Acta **55**, 3467-3473.

Melezhik V.A., Fallick A.E., Filippov M.M. and Larsen O. (1999) Karelian shungite – an indication of 2.0-Ga-old metamorphosed oil-shale and generation of petroleum: geology, lithology and geochemistry. Earth Science Reviews **47**, 1-40.

Milledge H.J., Mendelssohn M.J., Seal M., Rouse J.E., Swart P.K. and Pillinger C.T. (1983) Carbon isotopic variation in spectral type II diamonds. Nature **303**, 791-792.

Palot M., Cartigny P. and Viljoen F. (2009) Diamond origin and genesis: A C and N stable isotope study on diamonds from a single eclogitic xenolith (Kaalvallei, South Africa). Lithos **112S**, 758-766.

Pearson, V.K., Sephton, M.A., Franchi, I.A., Gibson, J.M. and Gilmour, I. (2006) Carbon and nitrogen in carbonaceous chondrites: Elemental abundances and stable isotopic compositions. Meteoritics and Planetary Science **41**, 1899-1918.

Polyakov V.B. and Kharlashina N.N. (1995) The use of heat capacity data to calculate carbon isotope fractionation between graphite, diamond and carbon dioxide: A new approach. Geochimica et Cosmochimica Acta **59**, 2561-2572.

Rayleigh J.W.S. (1902) On the distillation of binary mixtures. Philosophical Magazine **S.6, 4**: 521-537.

Richardson S.H., Harris, J.W. and Gurney J.J. (1993) Three generations of diamonds from old continental mantle. Nature **366**, 256-258.

Richet P., Bottinga Y. and Javoy, M. (1977) A review of hydrogen, carbon, nitrogen, oxygen, sulphur and chlorine stable isotope fractionation among

gaseous molecules. Annual Reviews in Earth and Planetary Sciences **5**, 65-110.

Rollinson H.R. (1993) *Using Geochemical Data: Evaluation, Presentation, Interpretation*. John Wiley & Sons, Inc. New York.

Russell S.S., Arden J.W. and Pillinger C.T. (1991) Evidence for Multiple Sources of Diamond from Primitive Chondrites. Science **254**, 1188-1191.

Schidlowski M. (2001) Carbon isotopes as biogeochemical recorders of life over 3.8 Ga of Earth history: evolution of a concept. Precambrian *Res*earch **106**, 117-134.

Schmidberger S.S., Heaman L.M., Simonetti A., Creaser R.A. and Cookenboo, H.O. (2005) Formation of Paleoproterozoic eclogitic mantle, Slave Province (Canada): Insights from in-situ Hf and U-Pb isotopic analyses of mantle zircons. Earth and Planetary Science Letters **240**, 621-633.

Schmidberger S.S., Simonetti A., Heaman L.M., Creaser R.A. and Whiteford S. (2007) Lu-Hf, in-situ Sr and Pb isotope and trace element systematics for mantle eclogites from the Diavik diamond mine: Evidence for Paleoproterozoic subduction beneath the Slave craton, Canada. Earth and Planetary Science Letters **254**, 55-68.

Schulze D.J., Weise D. and Steude J. (1996) Abundance and Distribution of Diamonds in Eclogite Revealed by Volume Visualization of CT X-Ray Scans. Journal of Geology **104**, 109-113.

Schulze D.J., Harte B., Valley J.W. and De R. Channer D.M. (2004) Evidence of subduction and crust-mantle mixing from a single diamond. Lithos **77**, 349-358.

Smart K.A., Heaman L.M., Chacko T., Simonetti A., Kopylova M., Mah D., Daniels D. (2009a) The origin of high-MgO diamond eclogites from the Jericho kimberlite, Canada. Earth and Planetary Science Letters **284**, 527-537.

Smart K.A., Heaman LM. and Chacko T. (2009b) Jericho eclogites of the Slave craton record multiple subduction-related crust formation events. Geochimica et Cosmochimica Acta **73(S1)**, A1238.

Sobolev, V.S., Sobolev, N.V., 1980. New proof on very deep subsidence of eclogitized crustal rocks. Doklady Akademii Nauk SSSR 250 (3), 683–685.

Spetsius Z.V., Wiggers de Vries D.F. and Davies G.R. (2009) Combined C isotope and geochemical evidence for a recycled origin for diamondiferous eclogite xenoliths from kimberlites of Yakutia. Lithos **112S**, 1032-1042.

Stachel T. and Harris J.W. (2008) The origin of cratonic diamonds – Constraints from mineral inclusions. Ore Geology Reviews **34**, 5-32.

Stachel T., Harris J.W., Tappert R. and Brey G.P. (2003) Peridotitic diamonds from the Slave and the Kaapvaal cratons – similarities and differences based on a preliminary data set. Lithos **71**, 489-503.

Stachel T., Harris, J.W., and Muehlenbachs, K. (2009) Sources of carbon in inclusion bearing diamonds. Lithos **112S**, 625-637.

Strauss H. (1986) Carbon and sulfur isotopes in Precambrian sediments from the Canadian Shield. Geochimica et Cosmochimica Acta **50**, 2653-2662.

Tappe S., Foley S.F., Kjarsgaard B., Romer R.L., Heaman L.M., Stracke A. and Jenner G.A. (2008) Between carbonatite and lamproite-Diamondiferous Torngat ultramafic lamprophyres formed by carbonate-fluxed melting of cratonic MARID-type metasomes. Geochimica et Cosmochimica Acta **72**, 3258-3286

Taylor W.R., Jaques A.L. and Ridd M. (1990) Nitrogen-defect aggregation characteristics of some Australasian diamonds; time–temperature constraints on the source regions of pipe and alluvial diamonds. American Mineralogist **75**, 1290–1310.

Taylor L., Keller R., Snyder G., Wang W., Carlson W., Hauri E., McCandless T., Kim K-R., Sobolev N. and Bezborodov S. (2000) Diamonds and Their Mineral Inclusions, and What They Tell Us: A Detailed "Pull-Apart" of a Diamondiferous Eclogite. International Geology Reviews **42**, 959-983.

Thomassot E., Cartigny P., Harris J.W. and Viljoen K.L. (2007) Methane-related diamond crystallization in the Earth's mantle: Stable isotope evidence from a single diamond-bearing xenolith. Earth and Planetary Science Letters **257**, 362-371.

Thomazo C., Ader M., Farquhar J. and Philippot P. (2009) Methanotrophs regulated atmospheric sulfur isotope anomalies during the Mesoarchean (Tumbiana Formation, Western Australia). Earth and Planetary Science Letters **279**, 65-75.

Tomlinson, E.L., Müller, W. and EIMF. (2009) A snapshot of mantle metasomatism: Trace element analysis of coexisting fluid (LA-ICP-MS)

and silicate (SIMS) inclusions in fibrous diamonds. Earth and Planetary Science Letters **279**, 362-372.

Valley J.W. (1986) Stable isotope geochemistry of metamorphic rocks. In: *Stable Isotopes in High Temperature Geological Processes* (eds. J.W. Valley et al.) Reviews in Mineralogy **16**, pp 445-489.

Watenphul A., Wunder B. and Heinrich W. (2009) High-pressure ammonium-bearing silicates: Implications for nitrogen and hydrogen storage in the Earth's mantle. American Mineralogist **94**, 283-292.

Zedgenizov D.A., Harte B., EIMF, Shatsky V.S., Politov A.A., Rylov G.M. and Sobolev N.V. (2006). Contributions to Mineralogy and Petrology. **151**, 45-57.

Zinner, E. (1998) Trends in the study of presolar dust grains from primitive meteorites. Meteoritics and Planetary Science **33**, 549–564.

Table 4.1 Host eclogite mineral geochemistry

Host eclogite mineral geochemistry

Garnet	Average JDE A n=13	JDE 15 Group B	JDE 25 Group B
SiO_2	42.1	41.0	40.4
TiO_2	0.16	0.28	0.37
Al_2O_3	23.5	23.4	22.5
Cr_2O_3	0.56	0.08	0.07
FeO	8.65	13.7	13.7
MnO	0.39	0.25	0.22
MgO	20.2	14.7	13.4
CaO	4.13	6.80	8.26
Na_2O	0.05	0.11	0.14
K_2O	0.01	0.00	0.00
Total	99.8	100.2	99.0
Mg #	81	66	64
Clinopyroxene			
SiO_2	54.8	55.0	55.7
TiO_2	0.12	0.34	0.39
Al_2O_3	2.45	8.70	10.65
Cr_2O_3	0.32	0.09	0.08
FeO	2.21	3.46	3.23
MnO	0.08	0.04	0.03
MgO	16.6	11.6	9.63
CaO	20.5	14.6	13.3
Na_2O	1.68	4.88	6.44
K_2O	0.01	0.10	0.05
Total	98.7	98.7	99.5
Mg #	93	86	84
$T_{KR\ 5\ GPA}$ (^oC)	860-930	1070	1110

Table 4.2 SIMS operating conditions for collection of $\delta^{13}C$ and N in diamond

Parameter	Carbon Isotopes	[Nitrogen]
Primary beam species	$133Cs^+$	$133Cs^+$
Primary beam impact energy (keV)	20	20
Primary beam diameter (μm)	15	15
Primary beam current (nA)	3-4	1
Electron charge neutralization	yes	no
Field aperature (μm)	5000	2000
Entrance slit (μm)	120	45
Exit slit (s) width (μm)	500	500, 140
Energy slit width (μm)	40	40
Contrast aperture (μm)	400	400
Image magnification at FA (X)	100	100
Seconday ions	$13C^-$, $^{12}C^-$	$^{12}C^{12}C^-$, $^{12}C^{14}N^-$
Secondary extraction potential (keV)	10	10
Counting Mode	multi-collection	multi-collection
Detectors (Faraday Cup, electron multiplier)	FC-FC	FC-FC or FC-EM
FC Baseline frequency per session	1	1
Baseline count time (s)	60	60
Pre-analysis raster time (s)	30	60
Mass Resolution (dM/M @ 10%)	$12C^-$ = 2000, $^{13}C^-$ = 2300	$^{12}C^{12}C^-$= 1850, $^{12}C^{14}N^-$= 7000
Count time per cycle (s)	5	5
Number of cyles	20	10
ion count rate for least abundant species (c/s)	~$2x10^7$	$2x10^2$ - $6x10^6$
Total analysis time (min)	4.5	3
Frequency of standardization per session	after every 4 unknowns	session start and session end
Reference materials	S0013D diamond	S0013G diamond
Instrumental mass fractionation (‰)	20	

Table 4.3 SIMS analyses of diamond standard S1100B from March-May 2010

SIMS analyses of diamond standard S0011B

	$\delta^{13}C$ (‰)		$\delta^{13}C$ (‰)		$\delta^{13}C$ (‰)
Day 1	-45.03	*Day 2a*	-45.54		-45.50
	-45.05		-45.56		-45.40
	-45.13		-45.59		
	-45.18		-45.56	*avg.*	*-45.46*
	-45.03		-45.60	*st dev.*	*0.042*
	-45.10		-45.71		
	-45.14		-45.65	*Day 3*	-45.85
	-45.10		-45.69		-45.85
	-45.17		-45.68		-45.84
	-45.07		-45.60		-45.73
	-45.12		-45.59		-45.87
	-45.04		-45.59		-45.83
	-45.08		-45.57		-45.84
	-45.12				-45.84
	-45.04	*avg.*	*-45.61*		-45.87
	-45.16	*st dev.*	*0.055*		
	-45.02			*avg.*	*-45.8*
	-45.00	*Day 2b*	-45.43	*st dev.*	*0.043*
	-45.03		-45.43		
	-45.06		-45.53		
			-45.46		
avg.	*-45.08*		-45.49		
st dev.	*0.06*		-45.45		

Table 4.4 Nitrogen and carbon characteristics of Jericho diamonds

Nitrogen and carbon characteristics of Jericho diamonds

Sample		N				$\delta^{13}C$
Eclogite	Diamond	(at. ppm)	(%B)	Type	T_{NA} (°C)	(‰)
JDE A 2	D1	19	0	IaA	1080	
	D2	14	0	IaA	1068	-39.3
	D5	16	0	IaA	1084	-39.0
	D4	20	0	IaA	1079	-39.6
	D8	12	0	IaA	1091	-39.2
	D8	12	0	IaA	1090	
	D9	21	0	IaA	1091	
	D10	11	0	IaA	1091	
	D10(a)	12	0	IaA	1090	
	D11	18	0	IaA	1081	
	D12	11	0	IaA	1093	
	D13	13	0	IaA	1088	
	D15	21	0	IaA	1078	
	D16	15	0	IaA	1086	-38.5
	DI 1	28	0	IaA	1071	-39.1
	DI 2	10	0	IaA	1096	
	DI 3	5	0	IaA	1110	-40.1
	DI 3	7	0	IaA	1101	
	DI 5	0	0	II		-37.5
	DI 6	0	0	II		-38.7
	DI 7	21	0	IaA	1079	-39.7
	DI 8	8	0	IaA	1099	-38.8
JDE A 3	D1	14	0	IaA	1088	-39.6
	D2	11	0	IaA	1093	-39.8
	D2(a)	10	0	IaA	1094	
	D3	10	0	IaA	1094	-39.5
	D5	14	0	IaA	1086	-37.9
	D7	14	0	IaA	1087	-39.7
JDE A 7	D1	82	0	IaA	1048	-38.1
	D2	61	0	IaA	1054	-39.5
	D3	0	0	II		-39.7
	D4	58	0	IaA	1055	-38.3
	D5	16	0	IaA	1084	-37.1
	D6	66	0	IaA	1053	
	D7	67	0	IaA	1052	
	D8	71	0	IaA	1051	
	D9	77	0	IaA	1049	
	D10	75	0	IaA	1050	-38.3
JDE B 25	D1	1405	25	IaAB	1077	-5.0
	D1 (a)	1293	26.03	IaAB	1081	-4.6
	D2	1214	21	IaAB	1076	-4.7
	D3	1317	22	IaAB	1042	-5.3
	D4					-5.0
	D5	1784	55.96	IaAB	1103	-4.4
	D6	1990	35	IaAB	1080	-4.8
	D7	1165	12	IaAB	1061	-4.7
	D8	1136	35	IaAB	1093	-3.5
	D9	1362	31.97	IaAB	1086	
	D10	1205	25.99	IaAB	1082	-4.8
	D11	1081	22	IaAB	1080	-5.1
	D-Big					-4.4
JDE B 15	D1	2353	10	IaA		
	D1 - agg	1129	6.4	IaA		

Table 4.5 SIMS $\delta^{13}C$ and N abundance values for JDE A and JDE B diamonds

SIMS $\delta^{13}C$ values and N abundances for JDE A and B diamonds

Sample	$\delta^{13}C$ (‰)	N (at. ppm)	Sample	$\delta^{13}C$ (‰)	N (at. ppm)	Sample	$\delta^{13}C$ (‰)	N (at. ppm)	Sample	$\delta^{13}C$ (‰)	N (at. ppm)
JDE A 2 S1	-40.56		JDE A 2 S4	-17.56		JDE A 7 S1	-39.56	48	JDE B 25 S1	-3.96	
	-40.40		*(continued)*	-17.05		*(continued)*	-35.61	83	*(W rim-core)*	-3.33	
	-40.20			-16.26			-36.58	7		-4.17	
	-40.43			-19.19			-38.79			-5.84	
	-40.27			-20.89			-36.58	94		-5.78	
	-39.24			-26.21			-34.05	6		-5.98	
	-38.62			-24.63			-38.88	55		-5.59	
	-38.86			-24.58			-35.17	85		-5.62	
	-39.54			-20.82			-38.68	65		-5.52	
	-39.93			-22.44			-38.87	62		-5.15	
	-39.75			-16.14			-38.66			-4.77	
	-40.28			-31.55			-34.11			-4.93	
	-40.23			-39.71						-4.22	
	-40.27			-39.58		JDE A 7 S2	-39.52				
				-39.92			-39.55		JDE B 25 S1	-2.72	
JDE A 2 S2	-39.89	23		-39.99			-39.18		*(indvl spots)*	-2.67	
	-40.04	22		-20.05						-3.26	
	-40.19	20		-24.26		JDE B 25 S1	-3.98	4360		-3.38	
	-40.27	23		-30.85		*(core-W rim)*	-4.06	4801		-3.45	
	-40.24	21		-27.03			-3.98	4480			
							-3.91	5004	JDE B 25 S1	-4.09	4672
JDE A 2 S3	-40.36		JDE A 2 S5	-40.26				3514	*(core-E rim)*	-4.16	5227
				-32.66			-3.82	3465		-4.14	3515
JDE A 2 S4	-24.31						-3.66	2522		-4.12	3333
	-40.15		JDE A 2 S7	-37.87	0.3			2209		-4.00	3221
	-40.20			-38.22	0.4		-3.66	2022		-4.03	3094
	-39.12			-40.14	20		-3.56	1057		-3.95	2872
	-24.99			-40.20	0.4		-3.24	1395		-3.78	2336
	-24.26			-40.22	21		-2.74	115		-	2090
	-22.19			-40.14	22		-2.71	469		-3.71	1991
	-19.79			-39.52	0.2		-3.74	1415		-3.67	1601
	-26.87			-38.64	0.2		-5.44	-		-3.46	1102
	-39.51			-37.83	0.3		-4.74	268		-3.38	1946
	-40.02			-40.21	21		-4.28	1426		-2.83	1916
	-17.01						-4.60	1490		-2.58	40
	-16.82		JDE A 2 S8	-40.16			-5.25	1532		-2.67	5
	-15.93			-38.34			-5.55	1265		-2.85	10
	-19.64							1185		-5.68	1406
	-17.33		JDE A 2 S9	-40.26			-5.26	1517		-4.78	1510
	-17.11						-5.93	1267		-4.88	1478
	-16.91		JDE A 2 S10	-40.27			-5.62	-		-4.43	706
	-16.44						-5.61	1040		-5.15	1566
	-24.85		JDE A 7 S1	-38.84			-4.51	310		-5.57	1311
	-13.44			-38.82			-4.03	1236		-5.56	1406
	-13.31			-38.71			-3.66	999		-5.59	1155
	-24.74			-38.77			-3.63	955		-3.03	2404
	-25.36			-38.78			-3.45	997		-3.64	1105
	-37.60			-38.91			-3.06	986		-3.67	1139
	-17.12			-39.38	84						

Figure 1

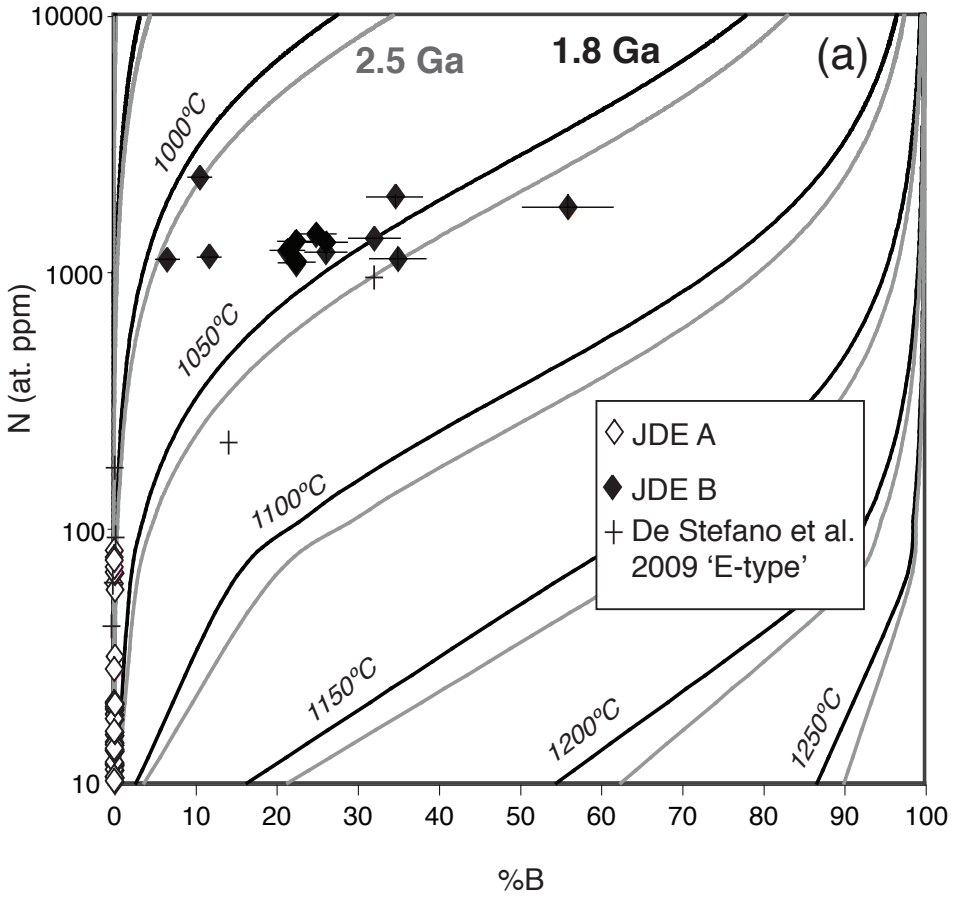

Figure 4.1. Time averaged mantle residence temperatures as calculated from nitrogen content and aggregation

Time-averaged mantle residence temperatures calculated from nitrogen content and aggregation after Taylor et al. (1990). Temperatures are indicated for isotherms calculated with residence times of 1.8 Ga (black lines) and 2.5 Ga (grey lines). Error bars indicate 10% uncertainty on both N contents and %B contents, but are only visible for %B due to the logarithmic scale on the Y-axis. The JDE B diamonds display a range of temperatures from 1000 to 1075°C, while no temperatures are available for the JDE A diamonds due to low aggregation (see text for alternate calculation). Eclogitic data from De Stefano et al. (2009) are also displayed.

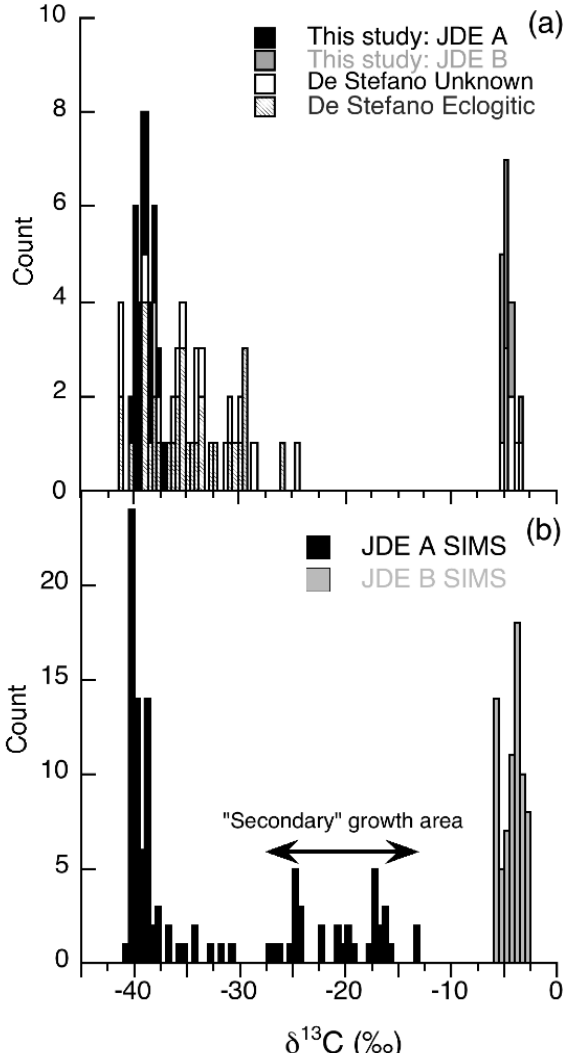

Figure 4.2 Carbon isotope composition of diamonds from Jericho eclogites from conventional combustion and SIMS analyses

Carbon isotope compositions of diamonds from Jericho eclogites from (a) conventional combustion and (b) SIMS analyses. Jericho diamond data from De Stefano et al. (2009) are shown for comparison. In (b) the peak at -40 to -35‰ represents analyses from the dark blue interiors and zoned rims of JDE A diamonds. The values from -10 to -30‰ are taken exclusively from the highlighted diamond growth area in Fig. 4(a).

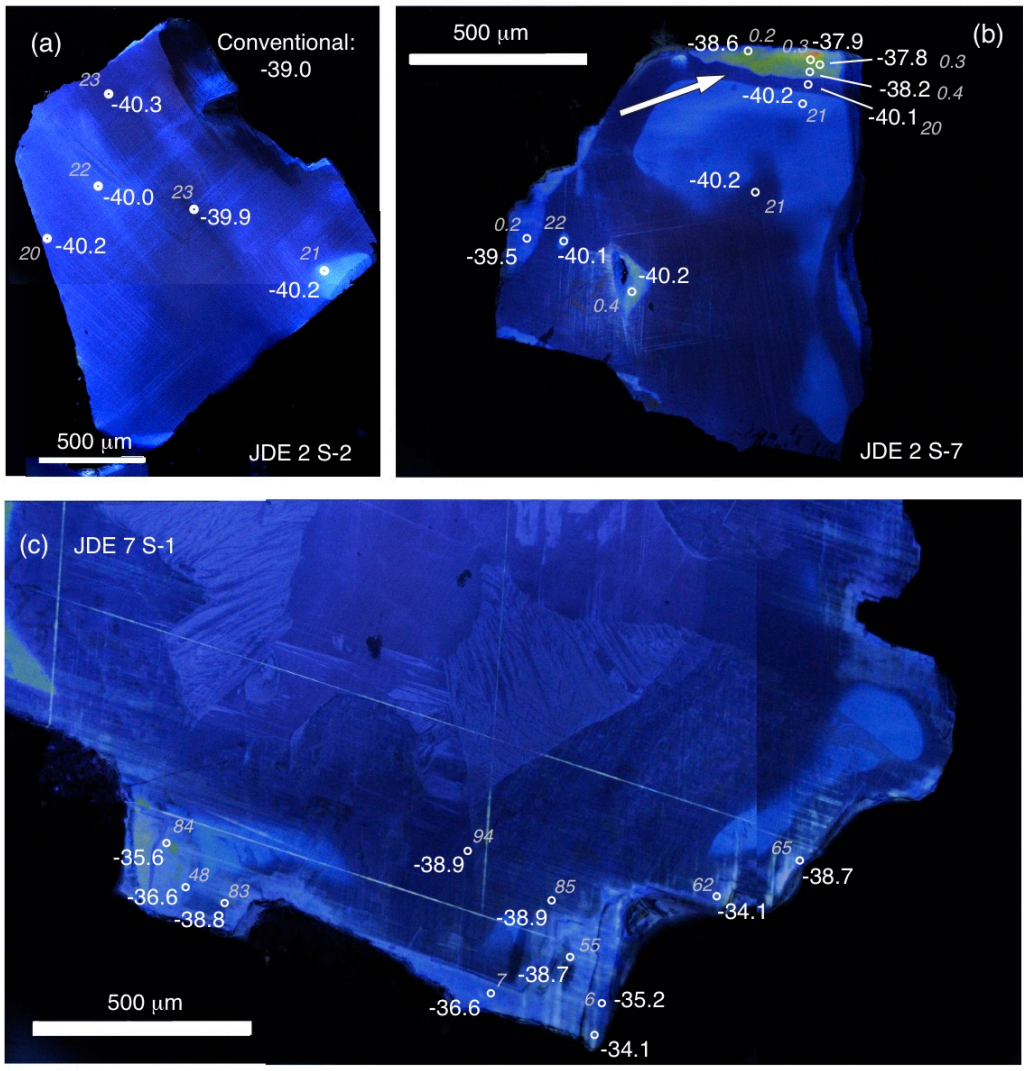

Figure 4.3 CL images of JDE A diamonds with SIMS carbon isotope compositions and nitrogen contents

CL images of JDE A diamonds with SIMS carbon isotope spot analyses in ‰ (white text) and nitrogen contents in at. ppm (in italic grey text). (a) Diamond JDE-2 S2. Broken resorbed octahedral diamond showing some plastic deformation with homogenous blue CL color and constant $\delta^{13}C$ and N values. The other half of this diamond was analyzed for carbon isotopes by conventional combustion methods. (b) Diamond JDE-2 S7. Resorbed fragment of an octahedral diamond with possible sectorial growth structure in the core followed by later octahedral zonation. Isotopic and nitrogen variations are displayed in the irregular rim (indicated with arrow). (c) Diamond JDE-7 S1 showing core-rim zonation. Smooth octahedral zonation in the center, followed by hummocky cubo/octahedron zonation and finally octahedral growth zonation that is better developed at the rims. The complexly zoned interior of this diamond (not completely shown) has homogenous $\delta^{13}C$ values. There is a change of +5‰ in

$\delta^{13}C$ values from the darker blue interior (-38.9 ‰) through the light blue growth zones at the rim (-34.1 ‰).

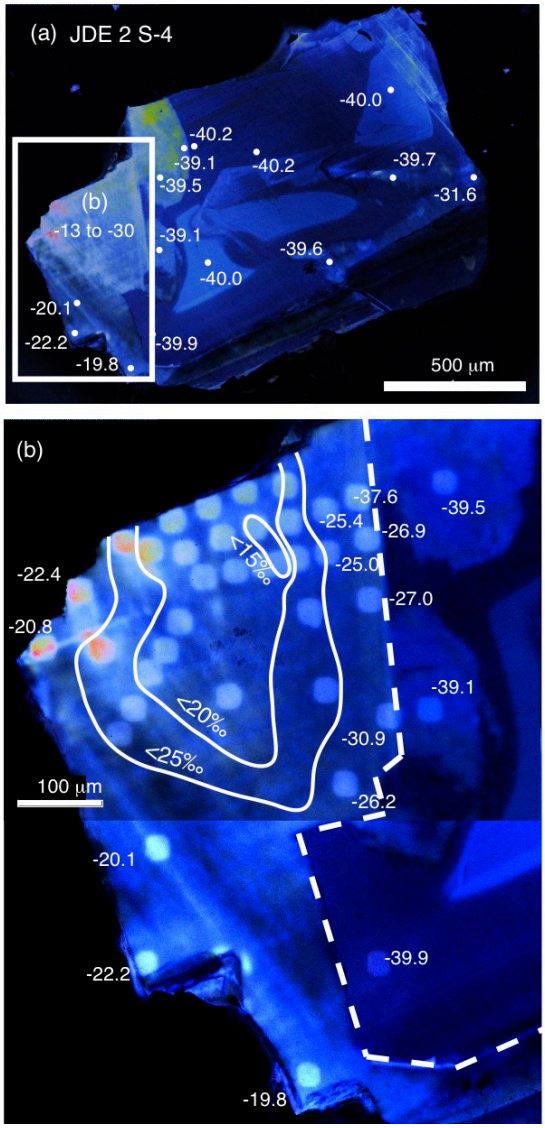

Figure 4.4 CL image of a complexly zoned JDE A diamond with SIMS carbon isotope compositions

(a) CL image of a broken and resorbed JDE A octahedral diamond with an area of complex CL structure (indicated by white box). There appears to be imperfect 'central cross structure' in the core and an area of inhomogeneous light blue and yellow CL colors in the top-right corner. The darker blue interior has constant $\delta^{13}C$ values, except for a thin rim on the lower left corner. (b) Expanded view of the complex growth area indicated in (a), which appears to represent a structure filled by later diamond growth. The dashed boundary between the dark blue 'primary' and light blue secondary diamond marks a >10‰ jump to higher $\delta^{13}C$ values. $\delta^{13}C$ values in this area range from -13.1 to -30.9‰. The isotopic composition of the secondary area is contoured with 5‰ isolines; light spots indicate locations of individual SIMS analyses.

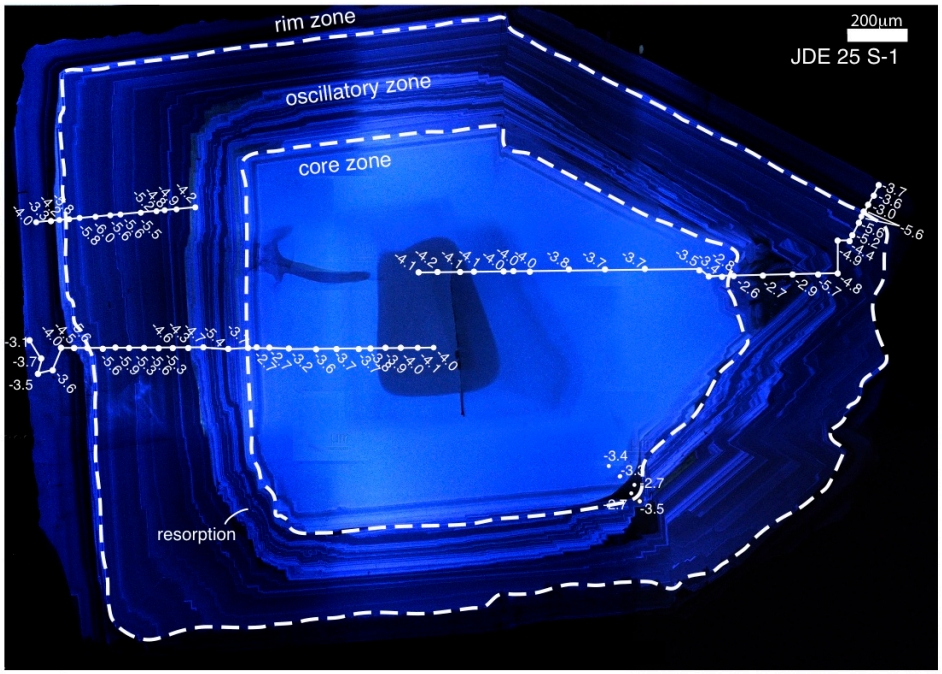

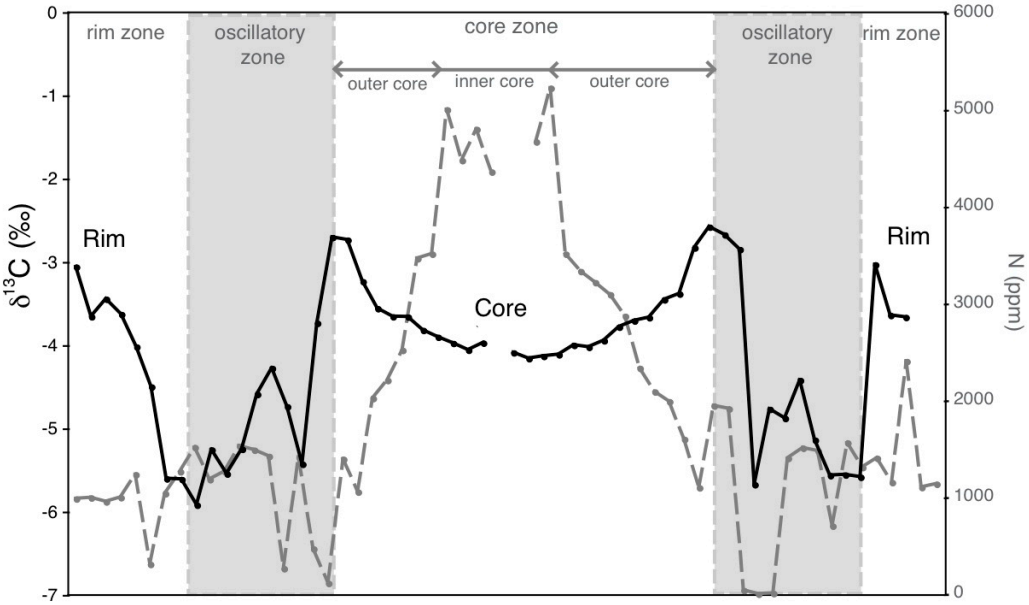

Figure 4.5 CL image of JDE B diamond exhibiting oscillatory zonation with SIMS carbon isotope compositions

(a) CL image of JDE B diamond 25-S1. Three transects (solid white lines with individual spots marked) of SIMS analyses are indicated as well as five single spot analyses. Dashed lines indicate interpreted growth stages of the diamond (see text for discussion). Note the ragged rims of the light interior core region on the right side of the core zone. (b) Carbon isotope and nitrogen abundance profiles of the core to rim transects indicated in (a). The analytical uncertainties are ± 0.10-0.15‰ (95% confidence) for $\delta^{13}C$ and <1% relative (1 SE) for the nitrogen abundance analyses.

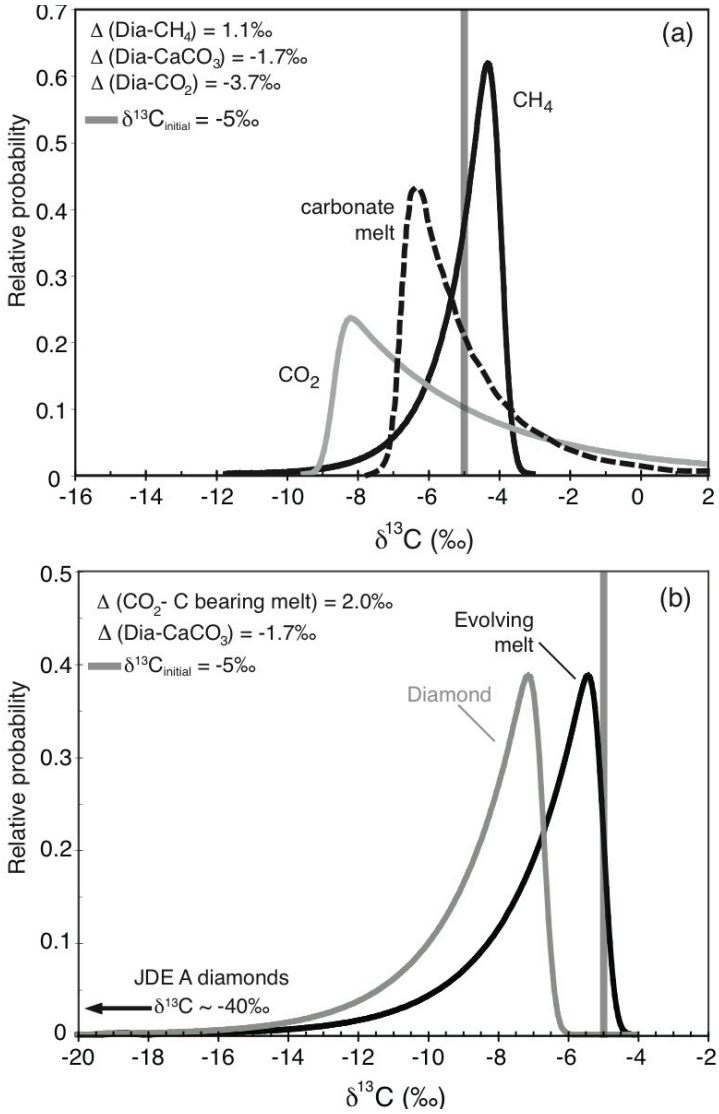

Figure 4.6 Relative probability diagram of modeled Rayleigh precipitation of diamond from oxidized and reduced diamond growth media

(a) Relative probability diagram showing modeled Rayleigh precipitation of diamond from both oxidized (CO_2-fluid and carbonate-bearing melt) and reduced (CH_4-bearing fluid) growth media. Curves represent the C-isotope composition of precipitated diamond as the amount of fluid/melt in the system decreases and were calculated using the formula from Rayleigh (1902): $R_{fluid}/R_o = f^{(\alpha-1)}$ and $R_{dia} = R_{fluid}\alpha$, where R_{fluid}, R_o, and R_{dia} are the $^{13}C/^{12}C$ ratios of the remaining fluid, initial fluid and precipitated diamond, respectively; f is the fraction of fluid or melt remaining; α is the diamond-fluid/melt fractionation factor. Choice of fractionation factors was based on theoretical calculations of C-isotope reduced partition function ratios for diamond by Polyakov and Kharlashina (1995), CH_4 by Richet et al., (1977), and CO_2 and calcite by Chacko et al., (1991) for T=1100°C (diamond growth typically occurs at 1100-1200°C from non-touching mineral inclusion and nitrogen aggregation thermometry; Stachel and Harris, 2008). Initial fluid $\delta^{13}C$ is -

5‰. (b) Relative probability diagram modeling the C-isotope effects of CO_2 escape from a carbonate bearing melt. Initial fluid has a $\delta^{13}C$ value of -5‰. We use a CO_2-carbonate melt fractionation factor of 2‰, derived from theoretical calculations of reduced partition function ratios for CO_2 and calcite noted above (at 1100°C), which is generally consistent with the experimental results of Mattey (1991) for C-isotope fractionation between CO_2 and carbonate ions dissolved in a tholeiitic melt. The companion curve shows the $\delta^{13}C$ values of diamond that would crystallize from the residual melt.

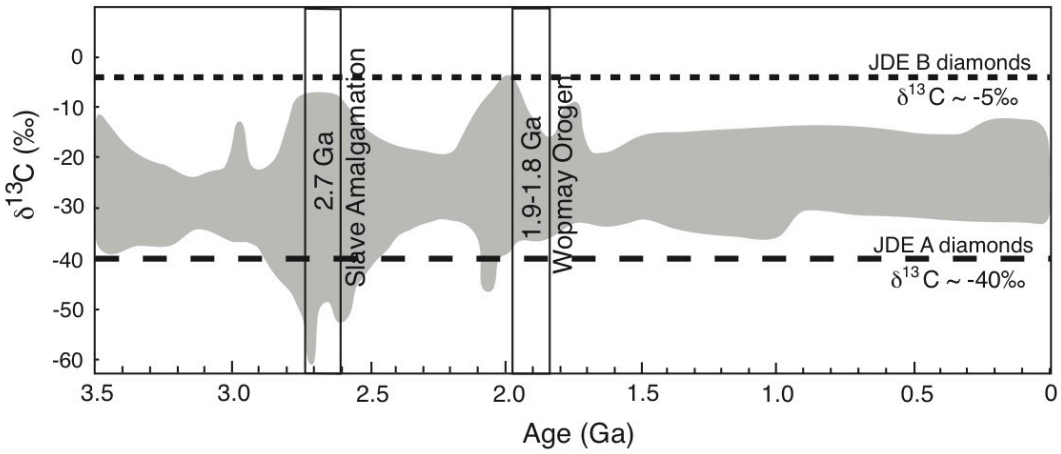

Figure 4.7 Carbon isotope composition of organic sediments from 3.5 Ga to present

The $\delta^{13}C$ values of organic sediments from 3.5 Ga to modern day, after Eigenbrode and Freeman (2006) and Schidlowski (2001). Of importance are the two negative excursions in $\delta^{13}C$ values at ca. 2.7 and 2.0 Ga, thought to be caused by methanogenic reduction of carbon in organic matter (Eigenbrode and Freeman, 2006). C-isotope composition of the JDE A and B diamonds indicated with dashed lines.

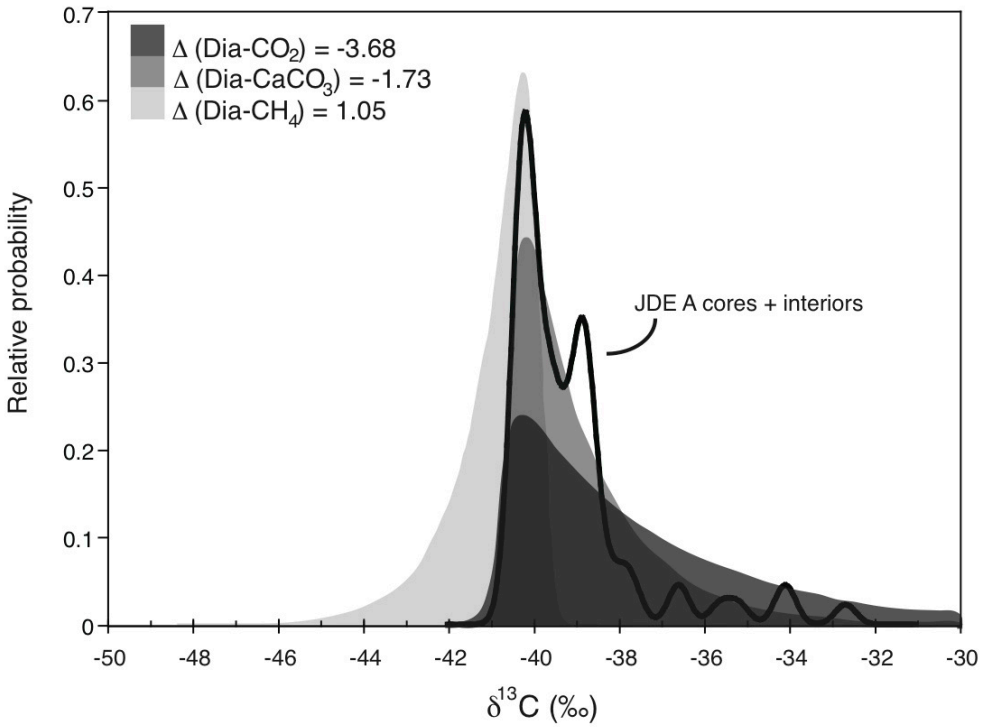

Figure 4.8 Relative probability diagram of JDE A SIMS $\delta^{13}C$ values and Rayleigh fractionation diamond growth models

Relative probability diagram of SIMS analyses of JDE A diamonds (dark curve) and Rayleigh fractionation models of diamond growth from oxidized and reduced fluids (shaded areas). The initial $\delta^{13}C$ values of the Rayleigh models were set such that the individual calculated curves have peaks overlapping with the peak at -40‰ observed for the JDE A diamonds.

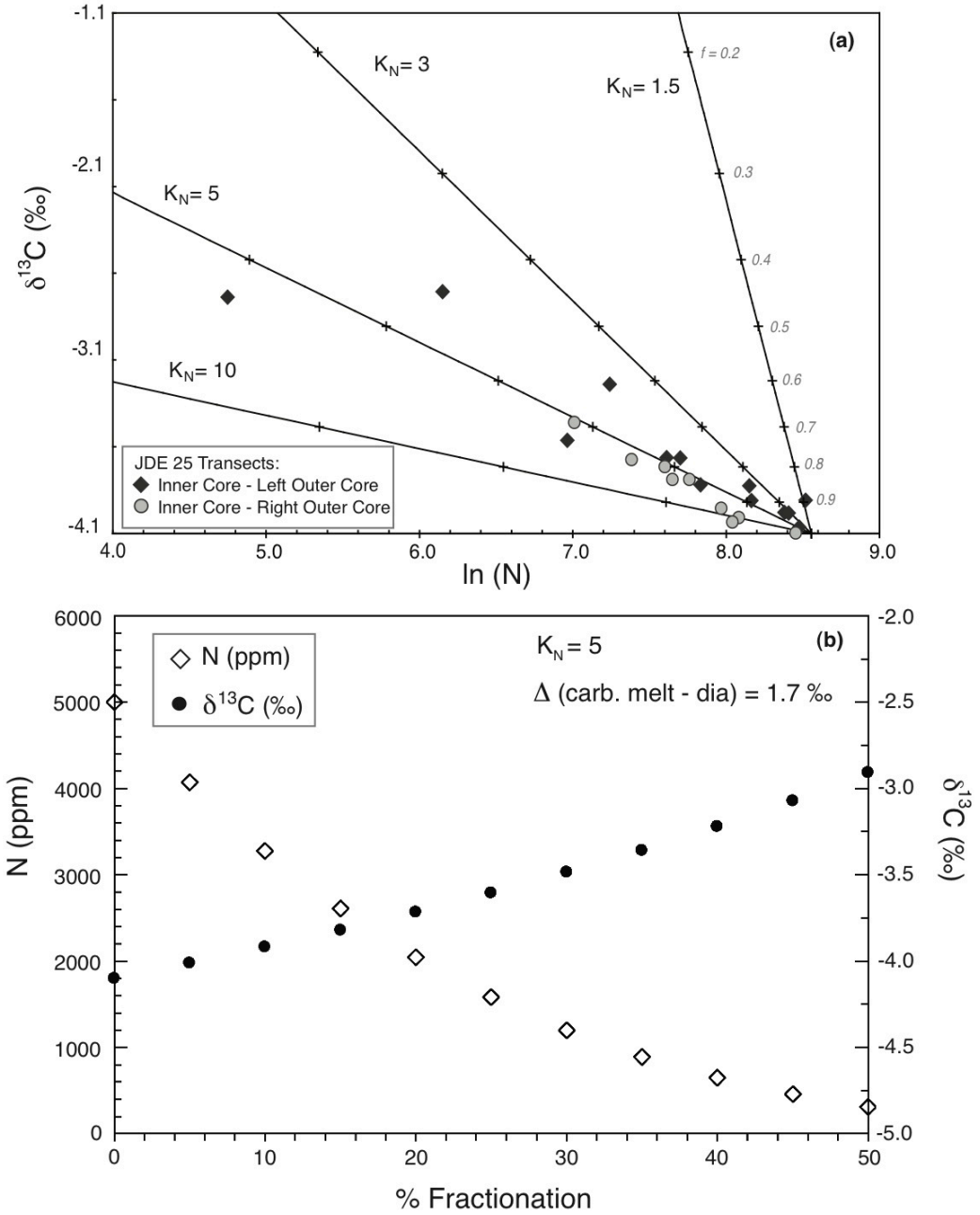

Figure 4.9 Nitrogen compatibility in diamond determined from co-variation of carbon isotope composition and nitrogen content in a JDE B diamond

(a) Plot of $\delta^{13}C$ and the natural log of nitrogen showing 1) SIMS transects across a JDE B diamond and 2) calculated distribution coefficients (K_N) of nitrogen partitioning during fractional crystallization of diamond. Equations and parameters explained in text. Crosses on K_N lines correspond to 0.1 increments of f (shown for K_N=1.5). (b) The effect of fractional crystallization of diamond from a carbonate melt. Model parameters described in text. Fractional crystallization equations for nitrogen partitioning from Rollinson (1993) and for C-isotope fractionation from Rayleigh (1902).

5 Chapter 5: Eclogite formation beneath the Slave craton revealed by diamond inclusions: shallow oceanic origin without crustal signature?[3]

5.1 Introduction

Our knowledge of the composition of cratonic lithospheric mantle (CLM) is largely based on information retrieved from mantle-derived xenoliths. However, it is recognized that the vast majority of mantle xenolith suites have been compositionally and mineralogically overprinted by melts and/or fluids during secondary processes (Harte, 1987; Simon et al., 2003). Mineral inclusions encapsulated by diamonds, on the other hand, appear to be more robust archives of the processes surrounding the early stages of CLM evolution (e.g., Ireland et al., 1994; Shirey et al., 2004). These inclusions are thought to represent the largely unmodified composition of the diamond source mantle lithologies and their study has revealed that harzburgites and eclogites represent the most important diamond source rocks within the CLM (Stachel and Harris, 2008). However, geochemical and stable isotope information indicates that some peridotitic and eclogitic portions of the CLM originally formed at low pressure and were then transported to diamond stability depths (Helmstaedt and Doig, 1975; Stachel et al., 1998; Wittig et al., 2008). Whether subduction was the mechanism that brought these lower-pressure materials to depth is a matter of debate (cf., Percival and Pysklywick, 2007).

Strong evidence for the transfer of 'shallow' oceanic lithosphere to depth via subduction comes from the geochemical and stable isotope signatures of many mantle eclogite xenolith suites and their diamonds (Jacob et al., 1994; Spetsius et al., 2009; Stachel et al., 2009). These signatures include eclogitic minerals with Eu and Sr anomalies thought to indicate involvement of the low-pressure mineral plagioclase in the petrogenesis of the eclogite protoliths (e.g., Jacob, 2004) and oxygen isotope compositions distinct from the mantle average, indicating

[3] A modified version of this chapter is submitted to Earth and Planetary Sciences as Smart K.A., Chacko T., Stachel T., Tappe S., Stern R.A., Ickert R.B. and EIMF. Eclogite formation beneath the Slave craton revealed by diamond inclusions: shallow oceanic origin without crustal signature.

hydrothermal alteration of shallow oceanic crust by seawater (Muehlenbachs et al., 1972; Jacob et al., 1994; MacGregor and Manton, 1986). Furthermore, the isotopically light carbon isotope compositions of some eclogitic diamonds (e.g., <-15‰) have been interpreted by some workers to indicate derivation from subducted organic C (e.g., Sobolev and Sobolev 1980; Tappert et al., 2005). Diamonds with isotopically light C, attributed to subducted organic matter, are reported from other Slave kimberlites (Davies et al., 2004) and the Jericho kimberlite itself (Smart et al., 2011). Interestingly, Shilobreeva et al. (2011) reported that the mean $\delta^{13}C$ value of altered oceanic crust is -4.7‰, and thus diamonds with seemingly 'mantle' $\delta^{13}C$ values of ~ -5‰ may actually be derived from oceanic crust hosted C. Although the subduction paradigm provides an elegant explanation for the existence of surface signatures at great depths, there exists eclogitic material within the CLM that does not carry clear 'crustal signatures' (Taylor and O'Neal, 1989; Barth et al., 2002; Schmickler et al, 2004) and, thus, requires different explanations. This observation indicates that there may exist alternative eclogite formation processes that do not necessarily involve subduction, and widely accepted 'crustal signatures' are not as unequivocal as previously thought (cf. Smyth et al., 1989; Griffin and O'Reilly, 2007; Williams et al., 2009).

Here we discuss new secondary ion mass spectrometry (SIMS) trace-element and oxygen isotope data for garnet and clinopyroxene inclusions from diamonds hosted in a Jericho high-MgO eclogite xenolith from the northern Slave craton, Canada. We compare and contrast the compositions of diamond inclusion minerals with those of the host eclogite xenolith reported in Smart et al. (2009). This enables us to better understand the formation and evolution of the enigmatic, exceptionally diamond-rich eclogitic components within the northern Slave CLM, which lack clear crustal signatures. On the basis of petrological modeling, we conclude that magmatic processes deep within Archean oceanic lithosphere may have led to the formation of eclogites now residing within the Slave CLM, and that even though subduction may have been the most important crust formation mechanism, its geochemical signature can be elusive.

5.2 Samples and Methods

We have examined six garnet and two clinopyroxene inclusions from diamonds extracted from a high-MgO eclogite xenolith (JDE 02) from the Jericho kimberlite (Smart et al., 2009). Inclusions were extracted using a steel breaker, then mounted in Araldite epoxy resin and polished using 0.05 mm alumina oxide. Major-element compositions were determined using a JEOL-8900 electron microprobe with a 20 nA beam current and a 20 kV accelerating voltage. Ten spots per grain were analyzed and sample data acquisition was bracketed by natural garnet and clinopyroxene standards to ensure data accuracy. Trace-element data were obtained at the Edinburgh Ion Microprobe Facility (EIMF) at the University of Edinburgh using a Cameca IMS-4f. Minerals were analyzed in Au-coated epoxy mounts using a 5nA primary beam of $^{16}O^-$ ions with a net impact energy of 15.2 kV. Molecular interferences were reduced using energy filtering techniques, including a 400 nominal mass resolution, 75 V offset and a 40 V window. Select masses were analyzed to monitor interferences, such as masses 154 and 156 on BaO and CeO, Fe+Si on Rb and YO on REE oxides. Counting times were between 2 and 8s depending on the element and ions were counted on an electron multiplier collector. Analyses were calibrated using the NIST SRM610 glass using Si as an internal standard. Garnet (KP1; Irving and Frey, 1978) and clinopyroxene (KH1; Irving and Frey, 1984) secondary standards were used to ensure data quality and yielded trace-element values that were generally well within 20% of reported values. Duplicate analyses of one garnet DI yielded results that were within 15% of each other excluding elements of ultra-low abundance (such as Rb, La, Ta, Pb, Th, and U). All data were reduced and errors calculated offline using an in-house program. The precision of the analyses are dependent on the abundance of a specific element, but in general are less than 1% for elements >100ppm, <10% for elements between 1-10ppm, but are > 15% for elements <1ppm. Uncertainties exceeding 50% are common for elements with concentrations of <0.1 ppm and as such these data are not reported.

Oxygen isotope compositions of garnet and clinopyroxene mineral separates from the host eclogite xenolith JDE 02 were completed at the University of New Mexico, following the procedure of Sharp (1990). Fractions of 1-2 mg of clean, inclusion and crack-free garnet and clinopyroxene grains were loaded into a clean Ni block and dried in an oven. Mineral samples were reacted with BrF_5 and heated with a Merchantek 25 W CO_2 laser in a sealed sample chamber. Oxygen gas samples were purified over liquid nitrogen and KCl traps, and then measured on-line using a Finnigan MAT Delta XL mass spectrometer with dual-inlet. Garnet (UWG-2, $\delta^{18}O$ = 5.74±0.15‰, 1σ; Valley et al., 1995) and quartz (Gee Whiz, $\delta^{18}O$ = 12.5±0.1‰; Larson and Sharp, 2005) standards were measured throughout the analytical sessions in order to ensure data accuracy and were within error of the accepted values (measured UWG-2: $\delta^{18}O$= 5.7±0.1‰, 1σ, n=5; measured Gee Whiz: 12.6±0.1‰ 1σ, n=18).

Oxygen isotope compositions of garnet DIs were determined by SIMS at both the EIMF at the University of Edinburgh, and the Canadian Center for Isotopic Microanalysis (CCIM) at the University of Alberta. Significant variations in instrumental mass fractionation (IMF) are known to occur in ion probe analyses of minerals such as garnet that exhibit wide ranges in major-element composition, leading to what is commonly referred to as a 'matrix effect' (Eiler et al., 1997). In particular, the studies of Vielzeuf et al. (2005) and Page et al. (2010) documented the strong effect of grossular content (X_{Ca}; where X_{Ca} = Ca/(Mg+Fe+Ca)) on IMF values. Isotopic analyses at both the EIMF and CCIM broadly followed the procedures of Vielzeuf et al. (2005) and Page et al. (2010) to determine the relationship between garnet composition and IMF. Multiple analyses of the 'master' garnet standards UWG-2 and UAG were completed to account for the overall instrumental bias before determination of garnet composition-related IMF. Secondary garnet standards with known oxygen isotope compositions and variable Ca-Mg-Fe contents were analyzed and bracketed to UWG-2 (EIMF) and UAG (CCIM). Based on the difference between the measured SIMS and known oxygen isotope compositions, an IMF value was calculated for each of the secondary garnet standards. At the EIMF, a correction scheme for IMF was

calibrated on the Ca-Mg-Fe garnet compositions from nine secondary standards and this correction was applied to the Jericho DI raw values to determine $\delta^{18}O$ values (cf. Vielzeuf et al., 2005). The Jericho garnet DIs have similar compositions to UWG-2 and as such only small corrections were necessary (-0.93±0.01, 1σ). At CCIM, matrix corrections for garnet were calculated using the molar abundance of Ca calibrated to nine well-characterized natural garnets (cf. Page et al., 2010). The Jericho garnet DIs have grossular contents similar to the master garnet standards (X_{Ca}=0.20 versus X_{Ca}=0.14) and thus the compositional correction again is small (-0.41±0.05, 95% confidence).

Oxygen isotope data ($^{18}O/^{16}O$) were collected at the EIMF in three sessions from June 28 to July 01, 2010 using a Cameca ims-1270 ion microprobe with a $^{133}Cs^+$ beam and a defocused spot size of ~30μm. O^- ions were measured by two faraday cups for ^{18}O and ^{16}O in multicollector mode. Two blocks of ten analyses were collected for each spot. Further details of the EIMF analytical techniques can be found in Eiler et al. (1997). Data collection of secondary standards and unknowns were interspersed with analyses of UWG-2, which yielded average session values of 5.8±0.12 (n= 20), 5.8±0.10 (n=15) and 5.8±0.19‰ (n=24) (1 σ). Average IMF for the three sessions derived from measurements on the UWG-2 garnet standard were -1.04±0.2, 1.35±0.1 and 0.77±0.1. Analytical uncertainties, including propagation of uncertainty in the matrix calibration correction, are ±0.5‰ (1σ). $^{18}O/^{16}O$ data were collected at the CCIM on December 21 2010 using a 15μm diameter Cs^+ primary beam and dual Faraday cups on an IMS-1280 instrument. Between two and five spot analyses were performed on four garnet inclusions. Gains and baselines were measured at the beginning of the analytical session. Analyses of the UAG standard conducted between every four unknowns yielded a repeatability of 0.21‰ (1σ; n=37) throughout the one-day session. Measurements of the UAG standard were used to determine the overall IMF for the session, which was about +3 ‰. The total analytical uncertainty on each spot is ±0.43‰ (95% confidence) and comprises of the standard deviation of UAG, the uncertainty in the matrix correction, and the uncertainty in the mean value of UAG used for the mass bias correction where the scatter in UAG dominates the

uncertainty budget. A near end-member grossular garnet, UAJM ($\delta^{18}O_{VSMOW}$ = 4.13‰) was analyzed on the same mount as the unknowns in order to assess the accuracy of the matrix correction. The high Ca content (X_{Ca}=0.97) of UAJM requires a very large matrix correction, greater than 3‰. Four spots yielded a mean $\delta^{18}O$ value of 4.25‰, suggesting that the analyses for this particular secondary standard are reproducible to 0.1‰, but does not account for the error associated with the matrix correction.

5.3 Results

Major- and trace-element compositions of garnet and clinopyroxene from the diamonds and host eclogite xenolith JDE 02 can be found in Table 5.1, together with garnet oxygen isotope data for the eclogitic diamond inclusions. All inclusions reported here are from diamonds within a single 4 cm eclogite xenolith. Eclogitic DIs from Jericho reported in De Stefano et al. (2009) overlap the DI major- and trace-element compositions described here, but generally have much larger compositional ranges. The DIs of the De Stefano study were derived from xenocrystic diamonds, i.e. diamonds not in a contact relationship with their host eclogite, and therefore the exact composition of their source rock(s) remains unknown.

5.3.1 Major-element compositions

Although extracted from separate diamonds, the six garnet DIs are compositionally indistinguishable. The garnets have approximately equal proportions of pyrope and almandine components and 20% grossular component and classify as Group B (Fig. 5.1) following the geochemical classification of Coleman et al. (1965). The two Jericho clinopyroxene DIs have diopsidic compositions with low Na_2O (2.1-2.4wt.%) and Al_2O_3 (3.6-3.9 wt.%) contents (Fig. 5.2).

5.3.2 Trace-element compositions

Chondrite normalized rare-earth element patterns for the DIs are shown in Fig. 5.3. Garnet DIs (Fig. 5.3a) have LREE-depleted (La_N/Sm_N <0.05), but enriched and fractionated HREE (Lu_N =46.6-56.6; Lu_N/Gd_N = 2.7-4.2). The REE patterns exhibit subtle negative Eu anomalies (Eu/Eu_N* 0.7-0.9). The clinopyroxene DIs are LREE-enriched (La_N/Sm_N = 1.4) and HREE-depleted, yet they show slight depletions in La relative to other LREEs such as Ce (Fig. 5.3b). Clinopyroxene DIs also have small negative Eu anomalies ranging from 0.7-0.8 (Eu/Eu*).

5.3.3 Oxygen isotope compositions

There is a small offset in the garnet DI $\delta^{18}O$ values given by the CCIM (5.2-5.7‰, median 5.4‰) and EIMF (5.6-6.0‰, median 5.8‰) laboratories, but the two sets of values are indistinguishable within the combined analytical uncertainties reported by each laboratory (0.4-0.5‰). Notably, the results obtained at both laboratories indicate that there is no significant variation in $\delta^{18}O$ values between the different garnet DIs. Garnet and clinopyroxene from the host eclogite xenolith analyzed by laser fluorination yielded a narrow range of $\delta^{18}O$ values between 5.3 and 5.5‰ ± 0.1‰ (1σ) and therefore the calculated fractionation between garnet and clinopyroxene is very small ($\Delta_{cpx\text{-}grt}$ = 0.1‰). The oxygen isotope composition of garnet and clinopyroxene from the host eclogite overlaps with that determined for the diamond inclusions.

5.3.4 Comparison to the host eclogite xenolith and worldwide eclogite DIs

Whereas the Jericho garnet DIs classify as "Group B" (Fig. 5.1) with moderate-MgO contents (11.5 wt. %), garnets from the host eclogite classify as "Group A" owing to their high MgO contents (21.0 wt. %), similar to those found in other high-MgO eclogites (e.g., Barth et al., 2002; Peltonen et al. 2002; Tappe et al., 2011). The garnet DIs also have much lower Mg-numbers (54 vs. 82) and Cr_2O_3 contents (0.10 vs. 0.59 wt. %), but higher CaO (7.6 vs. 4.3 wt. %), Na_2O

(0.11 vs. 0.06 wt. %) and TiO_2 contents (0.53 vs. 0.16 wt. %) than garnets from the host eclogite xenolith (Table 5.1). When compared to the worldwide eclogitic DI database of Stachel and Harris (2008), the Jericho garnet DIs have approximately average MgO (Jericho = 11.5 vs. worldwide median = 10.2 wt. %), FeO (17.7 vs. 16.1 wt. %) and Mg-numbers (53.7 vs. 53.9) but lower CaO contents (7.6 vs. 10.0 wt. %) (Fig.1).

In contrast to the garnet DIs, the Jericho clinopyroxene DIs are compositionally more similar to their host eclogite analogues (Fig. 5.2) but still have lower Mg-numbers (78-81 versus 93) and Cr_2O_3 contents (0.05 versus 0.33 wt%). The clinopyroxene DIs have only slightly lower CaO and higher Al_2O_3 and Na_2O contents than the host eclogite (Table 5.1 and Fig. 5.2). Unlike the Jericho garnet DIs, the clinopyroxene DIs differ significantly from most eclogitic clinopyroxene DIs compiled in the worldwide database in terms higher CaO (18.0-19.1 vs. 13.5 wt. % in the worldwide average), and lower Al_2O_3 (3.6-3.9 vs. 8.4 wt. %) and Na_2O contents (2.1-2.4 vs. 4.5 wt. %) (Fig. 5.2a-c).

In terms of trace-elements, the Jericho DIs and xenolith garnets both exhibit fractionated HREE patterns (Lu_N/Gd_N = 2.7-5.7) and enrichments in the HREE (Lu_N ~ 50). However, the garnet DIs have slightly higher total REE concentrations than garnet in the host eclogites (Fig. 5.3a). The REE patterns of Jericho garnet DIs broadly overlap the worldwide garnet DI database (cf., Stachel et al., 2004); however, flat HREE patterns and strong Eu anomalies observed in some eclogitic diamond inclusion suites from other Slave craton and southern African kimberlites (Aulbach et al., 2002; Davies et al., 2004; Stachel et al., 2004; Tappert et al., 2005; Viljoen et al., 2010) are absent or weak in the Jericho DIs. Jericho DI and host eclogite clinopyroxene have similar REE patterns, but clinopyroxene in the host is much more enriched in LREEs than the DIs (Ce_N = 92 vs 33-36). The Jericho clinopyroxene DIs have very similar REE patterns compared to worldwide eclogitic clinopyroxene DIs (cf., Stachel et al., 2004); however, both Jericho DIs and host eclogite lack strong positive Sr anomalies (Fig. 5.4), which are observed in non-diamondiferous eclogites at Jericho and in eclogitic clinopyroxenes worldwide (e.g., Viljoen et al., 2010).

5.4 Origin of Jericho eclogitic diamond inclusions

5.4.1 Significance of the presence or absence of a 'crustal signature'

Eclogite xenoliths and DIs are commonly thought to be either 1) remnants of subducted oceanic crust formed at low-pressure (Helmstaedt and Doig, 1975; Jacob 2004), or 2) cumulates of basaltic melts generated and crystallized at high pressure (O'Hara and Yoder, 1967; Smyth et al., 1989). The subduction hypothesis is widely applied to eclogitic xenoliths and DIs because of the presence of 'shallow oceanic crust signatures**':** Eu and Sr anomalies, flat MORB-like HREE patterns and anomalous, 'non-mantle' oxygen isotope signatures found in eclogitic minerals (Jacob, 2004). Eu and/or Sr anomalies found in normalized trace-element patterns of eclogitic garnet and clinopyroxene are commonly interpreted as a plagioclase signature from the basaltic/ MORB protolith (e.g., Jacob, 2004; Stachel et al., 2004), as both Eu^{2+} and Sr^{2+} substitute for Ca^{2+} in plagioclase (Schnetzler and Philpott, 1970). Eu and Sr anomalies, coupled with flat HREE patterns (a feature observed in MORB) in eclogites are taken as further evidence for low-pressure formation of the eclogite protolith, as either the volcanic or intrusive portions of oceanic crust (e.g., Barth et al., 2001). However, the most compelling evidence for an oceanic crust origin for eclogite xenoliths is provided by oxygen isotope compositions of eclogitic minerals showing $\delta^{18}O$ values significantly above or below the average mantle value of 5.5±0.4‰ (Mattey et al., 1994). The range of $\delta^{18}O$ values observed in eclogites overlaps the range observed in seawater-altered oceanic crust (Muehlenbachs et al., 1972) and ancient ophiolites (see compilation in Jacob, 2004). Given the limited fractionation of oxygen isotopes at high temperatures under mantle conditions (Clayton et al., 1975; Eiler, 2001), any deviation in the eclogite oxygen isotope signatures from the mantle average is most likely due to protolith interaction with seawater near Earth's surface. It is important to note, however, that a 'mantle-like' oxygen isotope composition of ~5.5‰ does not rule out eclogite formation from subducted oceanic crust (Schmickler et al., 2004). Oxygen isotope depth profiles

of oceanic crust show that the upper part of the sheeted dyke section is characterized by a significant proportion of seawater-altered rocks with $\delta^{18}O$ values close to 5.5‰ (Alt and Teagle, 2000). The occurrence of mantle-like $\delta^{18}O$ values in these altered rocks reflects the fact that the temperature-dependent basalt-seawater oxygen isotope fractionation factor transitions at this depth from lower-temperature values of >5.5‰ (pillowed basalts) to higher-temperature values of <5.5‰ (lower sheeted dykes and upper gabbros). Furthermore, some deeper sections of the oceanic crust may entirely escape seawater alteration (Gregory and Taylor, 1981; Muehlenbachs, 1986; Hart et al., 1999) and hence retain a mantle-like oxygen isotope composition.

Alternatively, eclogite xenoliths and DIs are also proposed to form by magmatic processes at high-pressures from primary mantle-derived melts. In this hypothesis, Eu anomalies are argued to result from redox processes (Smyth et al., 1989; Griffin and O'Reilly, 2007), thus obviating the need for a subducted oceanic crust origin involving plagioclase fractionation. This model attributes fractionated HREE patterns ($Lu_N/Gd_N>>1$) in eclogitic garnets and calculated whole-rocks, together with high Mg-numbers and Cr-contents, to garnet accumulation during eclogite crystallization at high pressures (Barth et al., 2002). Although direct eclogite formation from high-pressure magmas is preferred by some authors (see Griffin and O'Reilly, 2007), there are significant problems associated with this model. Magmas produced at high pressures (>3 GPa) from peridotite invariably have high Mg-numbers and low Al_2O_3 contents (Walter, 1998) where olivine is a ubiquitous liquidus phase (Herzberg et al., 1990) but is only rarely found in eclogites. Moreover, crystallization of garnet and clinopyroxene at high-temperature mantle conditions can generally only produce oxygen isotope fractionation effects of < 0.5‰ (Eiler, 2001) and thereby cannot explain the large range in $\delta^{18}O$ values (~ 2 to 17‰) observed in mantle eclogite DIs and xenoliths.

Several suites of eclogitic DIs have been interpreted as remnants of subducted oceanic crust based primarily on the presence of Eu anomalies and flat HREE patterns (Aulbach et al., 2002; Stachel et al., 2004; Tappert et al., 2005;

Viljoen et al., 2010). Unfortunately, there are only a small number of DI studies that include oxygen isotope analyses. This is mainly due to the small size of the inclusions precluding the application of conventional methods and laser fluorination analysis. The few oxygen isotope data available show a large range in $\delta^{18}O$ values. For example, Schulze et al. (2003, 2004) found extremely high $\delta^{18}O$ values in coesite (10.2-16.9‰) and garnet (7.9-16.9‰) DIs and argued that this large range in $\delta^{18}O$ values indicates altered oceanic crust as protoliths. In contrast, Lowry et al. (1999) found a range $\delta^{18}O$ values in eclogitic garnet DIs from 5.7-8.0 ‰ that directly overlapped $\delta^{18}O$ values found in accompanying eclogite xenoliths.

The Jericho DIs and host eclogite xenoliths lack some of the key crustal signatures discussed above. For example, the oxygen isotope compositions of the Jericho garnet DIs, and garnet and clinopyroxene from the host eclogites overlap with the stable isotopic composition of pristine mantle (although this feature does not exclude oceanic crust, see above). Furthermore, both DI and host eclogite garnets have fractionated HREE patterns that are more indicative of a high-pressure origin rather than crystallization at plagioclase-stable pressures. From these two pieces of evidence it appears the Jericho high-MgO eclogites have a 'mantle' origin. Interestingly, the mantle signatures of the DIs and host eclogites contrast with the 'crustal' signature of the diamonds. The diamonds have extremely light carbon isotope compositions of -37.5 to -40.1‰ and the carbon source, based on these very low $\delta^{13}C$ values, was likely subducted ancient organic sediments (Smart et al., 2011). Therefore, the Jericho 'mantle' eclogites (and DIs) and 'crustal' diamonds have decoupled isotopic signatures that can be reconciled with diamond formation from external (unrelated to the host eclogite) fluids/melts (e.g., Cartigny et al., 2004).

However, small negative Eu anomalies are present in both the garnet and clinopyroxene DI REE patterns. The Eu/Eu* ranges from 0.7-0.9 (garnet) and 0.7-0.8 (clinopyroxene). Given the small magnitude of the Eu anomalies, we consider the possibility that these are not significant outside of analytical uncertainty of the SIMS technique and thus do not represent real anomalies. The analytical uncertainties for the SIMS analyses of Sm, Eu and Gd concentrations ranged from

6-13% and from 5-11% relative in DI garnet and clinopyroxene, respectively. In order to assess if the Eu anomalies observed in the garnet and clinopyroxene DIs lie outside analytical uncertainty, we performed Monte Carlo simulations for the DIs. Assuming 10% (1σ) uncertainties on Sm, Eu and Gd analyses, we determined that the Eu anomalies are most likely but not unequivocally real in the garnet (Eu/Eu* = 0.80 ± 0.11, 1σ). Note that these simulations use the most conservative uncertainties for Sm, Eu and Gd, and simulations for the clinopyroxene DIs return more favorable results (Eu/Eu* = 0.73 ± 0.09, 1σ). Further evidence that the observed Eu anomalies are real is derived from the good agreement of measured and accepted Eu anomalies in the secondary garnet standard (KP1 Eu/Eu* measured = 0.75 and accepted = 0.77). Based on the consistent nature of the measured Eu anomalies in the Jericho DIs, the results of the Monte Carlo simulations and the good agreement between the measured and accepted standard values, we believe the Eu anomalies discussed here represent meaningful petrogenetic indicators of the involvement of plagioclase in the Jericho high-MgO protoliths. Thus, a relatively shallow origin for the Jericho DIs and host high-MgO eclogite xenoliths is not completely precluded, and formation of the eclogite protolith may have involved a small amount of plagioclase fractionation. The Jericho eclogite protoliths, however, show no oxygen isotope evidence of having interacted with seawater, thus making it unlikely that they were part of the upper oceanic crust. We will instead argue below that eclogite formation occurred within the deeper portions of the oceanic lithosphere, followed by transfer into the diamond stability field by subduction-stacking processes.

5.4.2 Assessment of magmatic cumulate processes

Smart et al. (2009) recognized the difficulty in determining the protolith of the Jericho high-MgO eclogites. In particular, these eclogites have calculated whole-rock compositions with high-MgO, -Cr_2O_3 and SiO_2 contents that are unlike basaltic oceanic crust or high-pressure peridotite-derived melts. Aided by the initial discovery of one garnet DI with a low Mg-number (similar to the Jericho DIs described here), Smart et al. suggested that the Jericho high-MgO eclogites

originally had a more "basaltic" composition and that diffusional Fe-Mg and Al-Cr exchange between eclogite and peridotite during or after diamond formation was responsible for the final chemical characteristics of these eclogites. Given their encapsulation in diamond, the DIs likely provide a better indication of the eclogite protolith than the minerals in the host eclogite. Therefore, in order to constrain the origin of the Jericho DIs and eclogites, we focus on the calculated whole-rock composition, major-element and newly determined trace-element and oxygen-isotope systematics of the DIs.

Using DIs to estimate whole-rock compositions is difficult as there are no constraints on the relative abundances of garnet and clinopyroxene. However a range of possible whole-rock compositions can be determined by calculating compositions for a spectrum of garnet and clinopyroxene modes. This method is commonly used in xenolith studies where there may be error in the modal estimates due to small or unrepresentative samples (e.g., Jerde et al., 1993) and has been previously used in other DI studies (Ireland et al., 1994; Viljoen et al., 2010). As variation in the garnet-clinopyroxene modes can markedly change the calculated major-element whole-rock composition, we have provided calculations for garnet-clinopyroxene modes from 70:30 to 30:70 (Table 5. 2).

Fig. 5.5 shows the range of possible whole-rock compositions of the protolith of the high-MgO Jericho eclogites derived from the compositions of the DIs. For compositions in the selected mode range, the eclogite protoliths are compositionally unlike modern oceanic gabbros and also Archean basalts and picrites (Fig. 5.5). As described above, the weak trace-element crustal signatures coupled with the 'mantle-like' oxygen isotope composition of the Jericho DIs suggest these eclogites may have an alternative origin as mafic (garnet pyroxenite) layers in the oceanic mantle lithosphere, similar to those observed in peridotite massifs (Barth et al., 2002).

5.4.2.1 Feasible melt compositions

If the Jericho DIs crystallized from mantle-derived melts, we can estimate the composition of the melt on the basis of the calculated whole-rock DI composition. Fig. 5.6 compares the composition of the Jericho protolith to melts

produced from melting of peridotite at low (1 GPa), moderate (1.2-2.5 GPa) and high (3-7 GPa) pressures. The calculated whole-rock compositions differ from the melt compositions in a number of important respects: high-pressure melts formed in the diamond stability field (P > 3 GPa) have Mg numbers that are too high and Al_2O_3 contents that are too low to be compatible with the protolith compositions, whereas low (1 GPa) melts have high SiO_2 and Al_2O_3 contents and low Mg-numbers compared to the eclogite protolith. In addition, both high and low-pressure melts have FeO and CaO contents that are too low to be consistent with the protolith compositions. However, moderate-pressure melts (1.2-2.5 GPa; Falloon and Green, 1988, Falloon et al., 1988) have Mg-numbers, SiO_2 and Al_2O_3 contents that are compatible with the Jericho DI composition, particularly at garnet:clinopyroxene ratios of 50:50 and 40:60 (Fig. 5.6).

5.4.2.2 Possible tectonic settings and depths of crystal accumulation

Melts derived from peridotite at high pressures (>4 GPa), such as komatiites, have high-Mg numbers and in general low-Al_2O_3 contents (Fig. 5.6) that rule out Jericho DI protolith crystallization at depths equivalent to their last pressure/temperatures of equilibration in the CLM (ca. 900˚C and 4.5-5 GPa, Smart et al., 2009). These compositional restrictions are also true for incipient, volatile-fluxed melts at high pressures that also are too MgO-rich (Brey et al., 2008). Therefore, if the eclogite protoliths formed from mantle-derived melts, this must have occurred at lower pressures or from different melting assemblages (e.g., Kogiso et al., 2004), where melts would be compositionally more basaltic and in equilibrium with garnet + clinopyroxene ± plagioclase assemblages. Therefore, a high-pressure cumulate origin in the diamond stability field is unlikely for the Jericho DIs.

In contrast to oceanic crust and low-pressure peridotite melts, the Jericho DI whole-rocks are compositionally similar to mafic layers found in ophiolites/ultramafic massifs (Fig. 5.5). These layers, generally occurring as cross cutting pyroxenite and olivine-gabbro veins, are commonly interpreted as cumulates from basaltic magmas either unrelated to the peridotite that comprises the massif/ophiolite, or from local melt segregations derived from the host

peridotite (Bodinier and Godard, 2003). Although the pyroxenite and gabbro veins are compositionally similar to calculated Jericho eclogite protoliths (e.g., Fig. 5.5), they have Mg-numbers that are consistently higher than the DIs (e.g., 70-90) that approach those of the surrounding peridotites. The high Mg numbers may be due to equilibration with the refractory peridotite. Some pyroxenite veins are thought to represent, or have formed from melts of, recycled oceanic crust due to the presence of distinct Eu anomalies and oxygen isotope compositions distinct from the mantle average (Pearson et al., 1991; Pearson et al., 1993; Becker, 1996), while other pyroxenites lack such features and are thought to form as cumulates of mantle-derived melts at pressures where garnet is stable (Bodinier and Godard, 2003). As indicated by model ages of other eclogite xenoliths from the Jericho kimberlite (Schmidberger et al., 2005; Smart et al., 2009b), it is possible that Jericho high-MgO eclogite protoliths formed in the Neoarchean or Paleoproterozoic when oceanic crust was likely thicker (Bickle, 1986; Herzberg et al., 2010) such that ancient pyroxenites/gabbro veins forming at the base of oceanic crust may have crystallized at greater pressures than their modern analogues. However, modeling by Herzberg et al. (2010) indicates oceanic crust was at maximum ~35 km thick and thus crystallization of basaltic magmas at its base would still produce plagioclase-rich mafic lithologies. Based on the characteristics of the JDE DIs (see above), they likely did not form as low pressure (<1 GPa) pyroxenitic or gabbroic rocks in lower oceanic crust but instead must have formed at higher pressures (~1.5 to 2 GPa) within the oceanic mantle lithosphere. Below, we explore an origin for the Jericho DIs as upper mantle cumulates from basaltic magmas, which crystallized as veins at in the oceanic mantle lithosphere (e.g., Foley et al., 2001), similar to mafic veins observed in peridotite massifs.

5.4.2.3 Cumulates from mantle-derived magmas

Experimental studies involving broadly basaltic compositions have shown that at elevated pressures (1.5-2 GPa), the crystallizing assemblage is broadly pyroxenitic to eclogitic, where clinopyroxene and garnet crystallize in variable modal abundances, depending on the composition of the starting material and P-T

conditions (O'Hara and Yoder, 1967; Green et al., 2000). In order to evaluate whether cumulates generated from basaltic magmas at upper mantle pressures have compositions comparable to the Jericho eclogite protoliths, we have compiled results from both experimental studies and thermodynamic modeling of alkaline, basalt and picro-basalt compositions at 1.5 to 2.0 GPa using the program pMELTS (Ghiorso et al., 2002). For the modeling, we have used melt compositions corresponding to 1.5-2.0 GPa picro-basaltic melts from Falloon and Green (1988) and Falloon et al. (1988) and alkali basalts from Tappe et al. (2007) and Green et al. (2000) as the starting compositions, and then generated melt and crystallizing mineral assemblages at 1.5-2 GPa, temperatures between 900-1100°C and oxygen fugacities corresponding to the QFM buffer. For comparison, we also modeled cumulates that would form from melts similar in composition to Archean basalts found in the Slave craton (Cousens, 2000; Yamashita et al., 2000). The picro- and tholeiitic basalt compositions crystallized garnet + clinopyroxene dominated assemblages with minor plagioclase (5-10 modal %) and quartz (1-10 %). Crystallization of the alkaline basalt compositions yielded assemblages dominated by clinopyroxene with variable amounts of garnet, orthopyroxene, biotite and rare alkali feldspar. Whole-rock compositions calculated for the modeled cumulates are shown on Fig 5.6.

The modeling demonstrates that cumulates generated from the picro-basalt compositions provide a reasonable match for the calculated whole-rock compositions of the Jericho DIs. The picro-basalt cumulates have slightly low CaO contents and high Al_2O_3 contents, but compositionally overlap with the eclogite protoliths at garnet-clinopyroxene modes of 55:45 to 35:65. The picro-basalt cumulates themselves have relative garnet-clinopyroxene modes ranging from 45:55 to 35:65 and thus the DIs and cumulates are in good modal agreement. The basanite cumulates have significantly lower SiO_2 contents and garnet modes than the Jericho DIs. Cumulates generated from the Archean basalt composition have higher SiO_2, Al_2O_3 and FeO contents and distinctively lower Mg-numbers and CaO contents than the protoliths (Fig. 5.6). Therefore, on the basis of both compositional and modal mineralogy constraints, it appears that the modeled

cumulates generated from the 1.5-2.0 GPa picrobasalts of Falloon and Green (1988) and Falloon et al. (1988) provide the best match to the range of calculated Jericho eclogite protoliths.

The trace-element systematics of the Jericho DIs also support a cumulate origin at 1.5-2 GPa as the fractionated HREE patterns indicate crystallization at pressures where garnet is part of the cumulate assemblage. Fig. 5.7 displays trace-element modeling of the formation of clinopyroxene-garnet cumulates from a cratonic basanite from the North Atlantic craton (Tappe et al., 2007) and an Archean basalt from the Slave craton (Yamashita et al., 2000). Partition coefficients are from Green et al. (2000) using 3 GPa experimental runs of basanite and tholeiite bulk compositions. Crystallization of a 60% clinopyroxene - 40% garnet cumulate (modes from model results) produces cumulate garnets with fractionated HREE patterns with Yb_N/Gd_N values of 3-8, similar to values observed in the Jericho garnet DIs (3.0-3.4). Therefore, from Fig. 5.7, it is clear that garnets with enriched and fractionated HREE patterns can be generated by crystallization from basaltic magmas in the upper mantle. We suggest that the Jericho eclogite protoliths originally formed as plagioclase-bearing garnet pyroxenite veins within the oceanic mantle lithosphere from picro-basalt magmas. Vein crystallization must have occurred at pressures of 1.5-2 GPa that favored both garnet and minor plagioclase crystallization, corresponding to depths of approximately 45-70 km.

5.5 Diamond growth and inclusion encapsulation

5.5.1 Eclogite emplacement into the diamond stability field

Garnet-clinopyroxene geothermometry indicates that the Jericho diamond eclogite xenoliths last equilibrated at 900°C (Smart et al., 2009), a temperature that intersects the Jericho peridotite geotherm of Kopylova et al. (1999) at approximately 4.5 GPa (Smart et al., 2011). If as argued above, the eclogites originally formed at pressures of ~1.5 -2.0 GPa as cumulates in the oceanic lithosphere, they must have been transported into the diamond stability field

following initial crystallization. One possibility is that the lithosphere containing the pyroxenitic veins delaminated (Davis et al., 2003) or sunk to deeper levels because of density contrasts (Percival and Pyskywec, 2007). However, this would require the Jericho protoliths to be part of a pyroxenite body that was large enough to trigger gravitationally instability of the lithosphere and this appears incompatible with the hypothesis that the eclogite protoliths formed as discrete veins. Alternatively, the veins could have been transported into the diamond stability field by subduction processes.

The CLM is thought by some to have formed from subduction stacking and imbrication of oceanic lithosphere slabs (Helmstaedt and Schulze 1989; Pearson and Wittig, 2008). There are multiple lines of evidence for subduction events affecting the Slave craton and CLM including: (1) geophysical reflectors detected in the CLM and interpreted as frozen subducted slabs associated with the ca. 1.9 Ga Wopmay Orogen (Cook et al., 1999); (2) ca. 2.7-2.55 Ga volcanic and granitic units exposed at surface interpreted to represent arcs and magmatism resulting from amalgamation of the craton at ca. 2.6 Ga (Davis et al., 2003) and (3) eclogite xenoliths from the Diavik and Jericho kimberlites that have been interpreted as remnants of Paleoproterozoic subducted oceanic crust (Schmidberger et al., 2005; 2007). Additionally, peridotite xenoliths from the Jericho kimberlite have chemical signatures that are compatible with melt extraction in shallow oceanic environments (Wittig et al., 2008), followed by subduction to great depth to form cratonic lithosphere. Thus, slabs of oceanic material, including the upper basaltic crust, lower crustal gabbros and peridotite mantle lithosphere with associated cumulate veins, may have been imbricated and stacked within the Slave CLM, effectively supplying a range of mafic and ultramafic lithologies beneath the Slave craton. A corollary of this process is that some eclogitic-pyroxenitic material may be recycled back into the convecting mantle (Foley et al., 2001), providing sources for other mantle-derived magmas (Sobolev et al., 2007).

5.5.2 Eclogite modification by partial melting, diamond formation and peridotite equilibration

Although the modeled picro-basalt cumulates generally satisfy the calculated whole-rock compositions of the Jericho eclogite protoliths, they have elevated Al_2O_3 and low CaO contents compared to the protolith composition (Fig. 5.6) and also fail to produce the low Al_2O_3 contents (~3.5 wt. %) found in the Jericho clinopyroxene DIs. The generation of clinopyroxene with ~7 - 8 wt% Al_2O_3 appears to be at odds with the observed composition of the Jericho eclogite DIs and xenoliths. Additionally, the modeled cumulates contain minor amounts of plagioclase and quartz. The exact reason for these discrepancies remain unknown but as described further below, they may in part be the result of processes that affected the eclogites during or after their emplacement into the diamond stability field beneath the Slave craton.

Because of their refractory major- and trace-element geochemical compositions and the lack of a free SiO_2 phase, numerous eclogite xenolith suites are interpreted to have lost a partial melt during subduction (Ireland et al., 1994; Jacob and Foley, 1999; Tappe et al., 2011). The lower solidus temperatures of most pyroxenites/eclogites compared to peridotites (Kogiso et al., 2004) dictate that the Jericho DI-cumulates would melt before the surrounding peridotite, thus altering the chemical composition of the residues. If melting occurred while the Jericho protoliths were still in the plagioclase stability field then the first mineralogical constituents to melt out would be quartz and plagioclase (Sen and Dunn, 1994; Nair, 2008), leaving behind a residue depleted in SiO_2, Na_2O and enriched in CaO relative to the original rock. Melt extraction at higher pressures from plagioclase-free, coesite-bearing eclogites has been experimentally shown to generate dacitic to andesitic melts (Yaxley and Green, 1998; Yaxley and Sobolev, 2007), some of which that are compositionally similar to the tonalite-trondjemite-granodiorite (TTG) magma suite (Rapp and Watson, 1995). Thus, extraction of these melts would again produce residues with lower SiO_2 and Na_2O contents and higher CaO contents than that of the protolith (arrows in Fig. 5.6b-d). This process would also effectively eliminate coesite from the protolith at even modest

degrees of melt extraction (Rapp and Watson, 1995; Yaxley and Sobolev 2007). The melt-depletion trajectories shown in Fig. 6 (dark arrows) are for melt-residue relationships at ~2-3 GPa, but melt extraction may have occurred at a range of depths before or during subduction, or within the diamond stability field after emplacement of the Jericho cumulates into the CLM.

The Jericho diamond eclogite xenoliths have higher Mg-numbers and Cr_2O_3 contents and are enriched in incompatible elements in comparison to the Jericho DIs investigated here. Smart et al. (2009) ascribed some of these compositional differences to melt-facilitated elemental equilibration of the eclogites with surrounding peridotite. Such a process would increase the Mg-number and Cr_2O_3 contents of minerals in the eclogites relative to those of the eclogite protolith. The timing of the peridotite-eclogite diffusional equilibration relative to that of diamond formation is not entirely clear but two lines of evidence suggest the processes may have been concurrent. The strongest evidence comes from the study of De Stefano et al. (2009), who report on the compositions of garnet inclusions found in xenocrystic diamonds from Jericho. Notably, some diamond xenocrysts of that study have the same highly ^{13}C-depleted carbon isotope compositions ($\delta^{13}C$ = -41 to -35‰) as that of the diamond-bearing xenolith investigated in the present study (Smart et al., 2011), and thus likely belong to the sample diamond population. The Mg-numbers of the garnet inclusions investigated by De Stefano et al. range from those similar to the DIs of the present study to those found in the host high-MgO Jericho eclogites (Fig. 1). This observation suggests that diamond growth occurred over the same time interval as peridotite-eclogite elemental equilibration and encapsulated inclusions at different stages of the equilibration process. The second piece of evidence is the occurrence of small diamond inclusions within high-MgO garnet in the host xenolith (see Fig. 1c in Smart et al., 2009), which indicates that some of the diamond growth in these samples must have occurred before or during formation of high-MgO garnet.

On the basis of core to rim increases in the $\delta^{13}C$ values of individual diamonds, Smart et al. (2011) argued that diamonds in the Jericho high MgO

eclogites formed from an oxidized fluid (carbonatitic melt or CO_2 fluid), which, based on the extremely low $\delta^{13}C$ values (ca. -40‰) of the diamonds, was derived from subducted organic sediments. Low-volume melts derived from pelites and/or carbonaceous eclogites at high-pressures are carbonatitic (Yaxley and Brey 2004; Grassi et al., 2011) and would likely be incompatible-element enriched (Kessel et al., 2005; Herman et al., 2006; Walter et al., 2008). Therefore, as the diamond-forming fluid/melt also served as the medium that facilitated elemental equilibration between the Jericho eclogites and surrounding peridotites, it was also likely responsible for some enrichement in incompatible elements in the Jericho eclogite – DI system (e.g., Fig. 5.3b; Smart et al., 2009).

5.5.3 Summary Model

Our multi-stage model for the petrogenesis of the Jericho high-MgO eclogites is summarized in Fig. 5.8. In stage 1, plagioclase-bearing garnet pyroxenite cumulates crystallize from basaltic melts as veins in thick, ancient oceanic mantle lithosphere at pressures ~1.5 – 2 GPa. In stage 2, subduction and stacking of the oceanic lithosphere beneath the Slave craton transports the pyroxenitic veins into the diamond stability field. Stage 3 involves extraction of a silicic, aluminous partial melt from the eclogites/pyroxenites which lowers the Si, Na and raises the Ca of the eclogite residues. Note that this melt extraction could occur between stages 1 and 2, during subduction in stage 2, or after eclogite emplacement within the diamond stability field. Stage 4 involves metasomatism of the residual eclogites by a carbonatitic melt or fluids, diamond formation and melt/fluid-assisted elemental equilibration with surrounding peridotite (c.f. Fig. 8 of Smart et al., 2009 for detail).

5.6 Implications for cratonic eclogite formation

The relationship between the Jericho high-MgO eclogites and diamond inclusions demonstrates how secondary processes in the mantle can overprint and obscure primary protolith signatures. Secondary processes affecting the host Jericho eclogites have effectively overprinted small Eu anomalies, basaltic Mg-

numbers and low LREE contents observed in the DIs. Therefore, as highlighted by the Jericho high-MgO eclogites, diamond inclusions are more likely to provide the best insight into the true nature of mantle-derived eclogite protoliths, despite metasomatic enrichment of the DIs attendant with diamond formation. The nature of the Jericho DIs raises the possibility that some deep-seated mantle eclogite xenoliths, which do not bear any hallmark 'crustal signatures', may nevertheless originate in shallow oceanic geodynamic settings. The Jericho eclogites are proposed to form as plagioclase-bearing garnet pyroxenite veins within the oceanic mantle lithosphere from basaltic melts, and thus lack oxygen isotope or strong trace-element evidence for a shallow crustal origin. "Pyroxenite" eclogites contrast sharply to typical "recycled oceanic crust" eclogites, which commonly have large Eu and/or Sr anomalies and $\delta^{18}O$ values indicating a pre-history of plagioclase involvement and seawater alteration, respectively. Multiple types of eclogites are known to occur together from the same kimberlite; for example, the low- and high-MgO suites from the Koidu kimberlite (Barth et al., 2001; 2002) where "crustal signatures" are found in the former, but are rare in the latter. Thus, subduction of a single package of oceanic crust and lithosphere potentially can bring multiple types of eclogites with distinct chemical and isotopic signatures into the mantle. This, in turn, impacts the interpretation of mantle eclogitic/pyroxenitic lithologies found as xenoliths in kimberlites and as well, supplies the material for mantle heterogeneities that are commonly thought to be involved in the formation of some mantle-derived melts (Foley et al., 2001; Sobolev et al., 2007).

References

Alt J.C. and Teagle D.A.H. (2000) Hydrothermal alteration and fluid fluxes in ophiolites and oceanic crust. In: Dilek, Y., E. Moores, and D. Elthon and A. Nicolas, eds., Geol. Soc. Am. Spec. Paper 349, Ophiolites and Oceanic Crust: New Insights from Field Studies and Ocean Drilling Program, 273-282.

Aulbach S., Stachel T., Viljoen K.S., Brey G.P., and Harris J.W. (2002) Eclogitic and websteritic diamond sources beneath the Limpopo belt – is slab-melting the link? Contributions to Mineralogy and Petrology **143**, 53-70.

Baker M.B. and Stolper E.M. (1994) Determining the composition of high-pressure mantle melts using diamond aggregates. Geochimica et Cosmochimica Acta **58**, 2811-2827.

Barth M.G., Rudnick R.L., Horn I., McDonough W.F., Spicuzza M.J., Valley J.W. and Haggerty S.E. (2001) Geochemistry of xenolithic eclogites from West Africa, Part I: A link between low MgO eclogites and Archean crust formation. Geochimica et Cosmochimica Acta, **65**: 1499-1527

Barth M.G. Rudnick R.L., Horn I., McDonough W.F., Spicuzza M.J., Valley J.W. and Haggerty S.E. (2002) Geochemistry of xenolithic eclogites from West Africa. Part 2: Origins of high MgO eclogites. Geochimica et Cosmochimica Acta **66**, 4325-4434.

Becker H. (1996) Crustal trace element and isotopic signatures in garnet pyroxenites from garnet peridotite massifs from Lower Austria. Journal of Petrology **37**, 785-810.

Bickle M.J. (1986) Implications of melting for stabilization of the lithosphere and heat loss in the Archean. Earth and Planetary Science Letters **80**, 314-324.

Bodinier J.-L. and Godard M. (2003) Orogenic, Ophiolitic, and Abyssal Peridotites, pp 103-170. In *The Mantle and Core* (ed. R.W. Carlson) Vol. 2 *Treatise on Geochemistry* (eds. H.D. Holland and K.K. Turekian), Elsevier-Pergamon, Oxford.

Brey G.P., Bulatov V.K., Girnis A.V. and Lahaye Y. (2008) Experimental melting of carbonated peridotite at 6-10 GPa. Journal of Petrology **49**, 797-821.

Canil D. (2004) Mildly incompatibly elements in peridotites and the origins of mantle lithosphere. Lithos **77**, 375-393.

Clayton R.N., Goldsmith J.R., Karel V.J., Mayeda T.K. and Newton R.C. (1975) Limits on the effect of pressure on isotopic fractionation. Geochimica et Cosmochimica Acta **39**, 1197-1201.

Coleman R.G., Lee E.D., Beatty L.B. and Brannock W.W. (1965) Eclogites and eclogites: their differences and similarities. Geologic Society of America Bulletin **76**, 483-508.

Cook F.A., van der Velden A.J., Hall K.W. and Roberts B.J. (1999) Frozen subduction in Canada's Northwest Territories: Lithoprobe deep lithospheric reflection profiling of the western Canadian Shield. *Tectonics* **18**, 1-24.

Cousens B.L. (2000) Geochemistry of the Archean Kam Group, Yellowknife Greenstone Belt, Slave Province, Canada. The Journal of Geology **108**, 181-197.

Davies R.M., Griffin W.L., O'Reilly S.Y. and Doyle B.J. (2004) Mineral inclusions and geochemical characteristics of microdiamonds from the DO27, A154, A418, DO18, DD17 and Ranch Lake kimberlites at Lac de Gras, Slave Craton, Canada. Lithos **77**, 39-55.

Davis W. J., Jones A.G., Bleeker W. and Grütter H. (2003) Lithosphere development in the Slave craton: a linked crustal and mantle perspective: *Lithos*, **71,** 575-589.

De Stefano A., Kopylova M.G., Cartigny P. and Afanasiev V. (2009) Diamonds and eclogites of the Jericho kimberlite (Northern Canada). Contributions to Mineralogy and Petrology **158**, 295-315.

Dick H.J.B., Natland J.H., Miller D.J., et al. (1999) Proc. ODP, Init. Repts., **176**: College Station, TX (Ocean Drilling Program). doi:10.2973/odp.proc.ir.176.1999

Eiler J.M. (2001) Oxygen isotope variations of basaltic lavas and upper mantle rocks. In: Reviews in Mineralogy and Geochemistry, Stable Isotope Geochemistry (Valley JW and Cole, DR Eds), pp 319-364.

Eiler J.M., Graham C. and Valley J.W. (1997) SIMS analysis of oxygen isotopes: matrix effects in complex minerals and glasses. Chemical Geology **138**, 221-244.

Falloon T.J. and Green D.H. (1988) Anhydrous partial melting of peridotite from 8 to 35 kb and the petrogenesis of MORB. Journal of Petrology Special Lithosphere Issue, 379-414.

Falloon T.J., Green D.H., Hatton C.J. and Harris K.L. (1988) Anhydrous partial melting of a fertile and depleted peridotite from 2 to 30 kb and application to basalt petrogenesis. Journal of Petrology **29,** 1257-1282.

Foley S.F., Petibon C.M., Jenner G.A. and Kjarsgaard B.A. (2001) High U/Th partitioning by clinopyroxene from alkali silicate and carbonatite metasomatism: an origin for Th/U disequilibrium in mantle melts. Terra Nova **13**,104-109.

Ghiorso M.S., Hirschmann M.M., Reiners P.W. and Kress V.C. (2002) The pMELTS: A revision of MELTS aimed at improving calculation of phase relations and major element partitioning involved in partial melting of the mantle at pressures up to 3 GPa. Geochemistry, Geophysics, Geosystems **3**, 10.1029/2001GC000217.

Green T.H., Blundy J.D., Adam J., and Yaxley G.M. (2000) SIMS determination of trace element partitioning coefficients between garnet, clinopyroxene and hydrous basaltic liquids at 2-7.5 GPa and 1080-1200ºC. Lithos **53**, 165-187.

Gregory R.T. and Taylor H.P. (1981) An oxygen isotope profile in a section of Cretaceous oceanic-crust, Samail Ophiolite, Oman – Evidence for Delta-18-O buffering of the oceans by deep (less-than 5 km) seawater-hydrothermal circulation at mid-ocean ridges. Journal of Geophysical Research **86**, 2737-2755.

Griffin W.L. and O'Reilly S.Y. (2007) Cratonic lithospheric mantle: Is anything subducted? Episodes **30**, 43-53.

Hart S.R., Blusztain J., Dick H.J.B., Meyer P.S. and Muehlenbachs K. (1999) The fingerprint of seawater circulation in a 500-meter section of ocean crust gabbros. Geochimica et Cosmochimica Acta **63**, 4059-4080.

Harte B. (1987) Metasomatic events recorded in mantle xenoliths: An overview. In: Nixon, P. H. (Ed.), Mantle Xenoliths. John Wiley and Sons, UK, pp. 625-640.

Helmstaedt H. and Doig R. (1975) Eclogite nodules from kimberlite pipes in the Colorado Plateau-samples of subducted Franciscan type oceanic lithosphere. Physics and Chemistry of the Earth **9**, 95-111.

Hermann J., Spandler C., Hack A. and Korsakov A.V. (2006) Aqueous fluids and hydrous melts in high-pressure and ultra-high pressure rocks: Implications for element transfer in subduction zones. Lithos **92**, 399-417.

Herzberg C.M., Gasparik T. and Sawamoto H. (1990) Origin of mantle peridotite: constraints from melting experiments to 16.5 GPa. Journal of Geophysical Research **95**, 15779-15803.

Herzberg C., Condie K. and Korenaga J. (2010) Thermal history of the Earth and its petrological expression. Earth and Planetary Science Letters **292**, 79-88.

Ireland T.R., Rudnick R.L. and Spetsius Z. (1994) Trace elements in diamond inclusions from eclogites reveal link to Archean granites. Earth and Planetary Science Letters **128**, 199-213.

Irving A.J. and Frey F.A. (1978) Distribution of trace elements between garnet megacrysts and host volcanic liquids of kimberlitic to rhyolitic composition. Geochimica et Cosmochimica Acta **48**, 771-787.

Irving A.J. and Frey F.A. (1984) Trace element abundances in megacrysts and their host basalts: Constraints on partition coefficients and megacrysts genesis. Geochimica et Cosmochimica Acta **42**, 1201-1221.

Jacob D.E. (2004) Nature and origin of eclogite xenoliths from kimberlites. Lithos **77**, 295-316.

Jacob D.E. and Foley S.F. (1999) Evidence for Archean ocean crust with low high field strength element signature from diamondiferous eclogite xenoliths. Lithos **48**, 317-336

Jacob D., Jagoutz E., Lowry D., Mattey D. and Kudrjavtseva G. (1994) Diamondiferous Eclogites from Siberia - Remnants of Archean Oceanic-Crust. Geochimica et Cosmochimica Acta **58**, 5191-5207.

Jerde E.A., Taylor L.A., Crozaz G., Sobolev N.V. and Sobolev V.N. (1993) Diamondiferous eclogites from Yakutia, Siberia: evidence for a diversity of protoliths. Contributions to Mineralogy and Petrology **114**, 189-202.

Kessel R., Schmidt M.W., Ulmer P. and Pettke T. (2008) Trace element signature of subduction-zone fluids, melts and supercritical liquids at 120-180 km depth. Nature **437**, 724-727.

Kogiso T., Hirschmann M.M. and Pertermann M. (2004) High-pressure partial melting of mafic lithologies in the mantle. Journal of Petrology **45**, 2407-2422.

Kopylova M.G., Russell J.K., and Cookenboo H. (1999). Petrology of peridotite and pyroxenite xenoliths from the Jericho kimberlite: Implications for the

thermal state of the mantle beneath the Slave craton, Northern Canada. Journal of Petrology **40**, 79-104.

Larson T.E. and Sharp Z.D. (2005) Interpreting prograde-growth histories of Al_2SiO_5 triple-point rocks using oxygen-isotope thermometry: an example from the Truchas Mountains, USA. Journal of Metamorphic Geology **23**, 847-863.

Lowry D., Mattey D.P. and Harris J.W. (1999) Oxygen isotope composition of syngenetic inclusions in diamond from the Finsch Mine, RSA. Geochimica et Cosmochimica Acta **63**, 1825-1836.

MacGregor I.D. and Manton W.I. (1986) Roberts Victor eclogites: ancient oceanic crust. Journal of Geophysical Research **91 (B14)**, 14063-14079.

Mattey D., Lowry D., MacPherson C. (1994) Oxygen isotope composition of mantle peridotite. Earth and Planetary Science Letters **128**, 231-241.

McDonough W.F. and Sun S.S. (1995) The composition of the Earth. Chemical Geology **120**, 223-253.

Muehlenbachs K., and Clayton R. N. (1972) Oxygen isotope geochemistry of submarine greenstones. Canadian Journal of Earth Sciences **9**, 471-478.

Muehlenbachs K. (1986) Alteration of the oceanic-crust and the O-18 history of seawater. Reviews in Mineralogy **16**, 425-444.

Nair R.K.S. (2008) Dehydration-melting of MORB-composition amphibolites at 7-22.5 kbar and 775-1050ºC: constraints on phase relations, metamorphic facies transitions and origins of Archean TTG magmas. PhD thesis, University of Alberta. 334p.

O'Hara M.J. and Yoder H.S. (1967) Formation and fractionation of basic magmas at high pressures, Scottish Journal of Geology **3**, 67–117.

Page F.Z., Kita N.T. and Valley J.W. (2010) Ion microprobe analysis of oxygen isotopes in garnets of complex chemistry. Chemical Geology **270**, 9-19.

Pearson D.G. and Wittig N. (2008) Formation of Archaean continental lithosphere and its diamonds: the root of the problem. Journal of the Geological Society of London **165**, 895-914.

Pearson D.G., Davies G.R., Nixon P.H., Greenwood P.B. and Mattey D.P. (1991) Oxygen isotope evidence for the origin of pyroxenites in the Beni Bousera peridotite massif, North Morocco: derivation from subducted oceanic lithosphere. Earth and Planetary Science Letters **102**, 289-301.

Pearson D.G., Davies G.R. and Nixon P.H. (1993) Geochemical constraints on the petrogenesis of diamond facies pyroxenites from the Beni Bousera peridotite massif, North Morocco. Journal of Petrology **34**, 125-172.

Peltonen P., Kinnunen K.A., and Huhma H. (2002) Petrology of two diamondiferous eclogite xenoliths from the Lahtojoki kimberlite pipe, eastern Finland. Lithos **63**, 151-164.

Percival J.A. and Pysklywec R.N. (2007) Are Archean lithospheric keels inverted? Earth and Planetary Science Letters **254**, 393-403.

Polat A., Appel P.W.U., Frei R., Pan Y., Dilek Y., Ordonez J.C., Fryer B., Hollis J.A. and Raith J.G. (2007) Field and geochemical characteristics of Mesoarchean (~3075 Ma) Ivisaartoq greenstone belt, southern West Greenland: Evidence for seafloor hydrothermal alteration in supra-subduction oceanic crust. Gondwana Research **11**, 69-91.

Polat A., Frei R., Appel P.W.U., Dilek Y., Fryer B., Ordonez J.C. and Yang Z. (2008) The origin and compositions of Mesoarchean oceanic crust: Evidence from the 3075 Ma Ivisaartoq grenstone belt, SW Greenland. Lithos **100**, 293-321.

Rapp R.P. and Watson B. (1995) Dehydration melting of metabasalt at 8-32 kbar: Implications for continental growth and crust-mantle recycling. Journal of Petrology **36**, 891-931.

Schmickler B., Jacob D.E. and Foley S.F. (2004) Eclogite xenoliths from the Kuruman kimberlites, South Africa: geochemical fingerprinting of deep subduction and cumulate processes. Lithos **75**, 173-207.

Schmidberger S.S., Heaman L.M., Simonetti A., Creaser R.A. and Cookenboo H.O. (2005) Formation of Paleoproterozoic eclogitic mantle, Slave Province (Canada): Insights from in-situ Hf and U-Pb isotopic analyses of mantle zircons. Earth and Planetary Science Letters **240**, 621-633.

Schmidberger S.S., Simonetti A., Heaman L.M., Creaser R.A. and Whiteford S. (2007) Lu-Hf, in-situ Sr and Pb isotope and trace element systematics for mantle eclogites from the Diavik diamond mine: Evidence for Paleoproterozoic subduction beneath the Slave craton, Canada. Earth and Planetary Science Letters **254**, 55-68.

Schnetzler C.C. and Philpotts J.A. (1970) Partition coefficients of rare-earth elements between igneous matrix material and rock-forming mineral phenocrysts – II. Geochimica et Cosmochimica Acta **34**, 331-340.

Schulze D.J., Harte B., Valley J.W., Brenan J.M. and De R. Channer D.M. (2003) Extreme crustal oxygen isotope signatures preserved in coesite in diamond. Nature **423**, 68-70.

Schulze D.J., Harte B., Valley J.W. and De R. Channer D.M. (2004) Evidence of subduction and crust-mantle mixing from a single diamond. Lithos **77**, 349-358.

Sen C. and Dunn T. (1994) Dehydration melting of a basaltic composition amphibolite at 1.5 and 2.0 GPa: implications for the origin of adakites. Contributions to Mineralogy and Petrology **117**, 394-409.

Sharp Z.D. (1990) A laser-based microanalytical method for the *in situ* determination of oxygen isotope ratios of silicates and oxides. Geochimica et Cosmochimica Acta **54**, 1353-1357.

Shilobreeva S., Martinez I., Busigny V., Agrinier P. and Laverne C. (2011) Insights into C and H storage in the altered oceanic crust: Results from ODP/IODP Hole 1256D. Geochimica et Cosmochimica Acta **75**, 2237-2255.

Shirey S.S., Richardson S.H. and Harris J.W. (2004) Integrated models of diamond formation and craton evolution. Lithos **77**, 923-944.

Simon NSC, Irvine, GJ. Davies GR, Pearson DG and Carlson RW (2003) The origin of garnet and clinopyroxene in "depleted" Kaapvaal peridotites. Lithos **71**, 289-322.

Smart K.A., Heaman L.M., Chacko T., Simonetti A., Kopylova M., Mah D. and Daniels D. (2009a) The origin of high-MgO diamond eclogites from the Jericho kimberlite, Canada. Earth and Planetary Science Letters **284**, 527-537.

Smart K.A., Heaman L.M. and Chacko T. (2009b) Jericho eclogites of the Slave craton record multiple subduction-related crust formation events. Geochimica et Cosmochimica Acta **73(S1)**, A1238.

Smart K.A., Chacko T., Stachel T., Muehlenbachs K., Stern R.A. and Heaman L.M. (2011) Diamond growth from oxidized carbon sources beneath the Northern Slave Craton, Canada: A δ^{13}C-N study of eclogite-hosted diamonds from the Jericho kimberlite. In press.

Smyth J.R., Caporuscio F.A. and McCormick T. (1989) Mantle eclogites: evidence of igneous fractionation in the mantle. Earth and Planetary Science Letters **93**, 133-141.

Sobolev V.S. and Sobolev N.V. (1980) New proof on very deep subsidence of eclogitized crustal rocks. Doklady Akademii Nauk SSSR 250 (3), 683–685.

Sobolev A.V., Hofmann A.W., Kuzmin D.V., Yaxley G.M., Arndt N.T., Chung S.L., Danyushevsky L.V., Elliott T., Frey F.A., Garcia M.O., Gurenko A.A., Kamenetsky V.S., Kerr A.C., Krivolutskaya N.A., Matvienkov V.V., Nikogosian I.K., Rocholl A., Sigurdsson I.A., Sushchevskaya N.M. and Teklay M. (2007) The amount of recycled crust in sources of mantle-derived melts. Science **316**, 412–417.

Spetsius Z.V., Wiggers de Vries D.F. and Davies G.R. (2009) Combined C isotope and geochemical evidence for a recycled origin for diamondiferous eclogite xenoliths from kimberlites of Yakutia. *Lithos* **112S**, 1032-1042.

Stachel T. and Harris J.W. (2008) The origin of cratonic diamonds - Constraints from mineral inclusions. Ore Geology Reviews **34**, 5-32.

Stachel T., Viljoen K.S., Brey G. and Harris J.W. (1998) Metasomatic processes in lherzolitic and harzburgitic domains of diamondiferous lithospheric mantle: REE in garnets from xenoliths and inclusions in diamond. Earth and Planetary Science Letters **159**, 1-12.

Stachel T., Aulbach S., Brey G.P., Harris J.W., Leost I. and Viljoen K.S. (2004) The trace element composition of silicate inclusions in diamonds: a review. Lithos **77**, 1-19.

Stachel T., Harris J.W. and Muehlenbachs K. (2009) Sources of carbon in inclusion bearing diamonds. Lithos **112S**, 625-637.

Tappe S., Foley S.F., Stracke A., Romer R.L., Kjarsgaard B.A., Heaman L.M. and Joyce N. (2007) Craton reactivation on the Labrador Sea margins: $^{40}Ar/^{39}Ar$ age and Sr-Nd-Hf-Pb isotope constraints from alkaline and carbonatite intrusives. Earth and Planetary Science Letters **256**, 433-454.

Tappe S., Smart K.A., Pearson D.G., Steenfelt A. and Simonetti A. (2011) Craton formation in Late Archean subduction zones revealed by first Greenland eclogites. Geology *In press*.

Tappert R., Stachel T., Harris J.W., Muehlenbachs K., Ludwig T., and Brey G. (2005) Subducting oceanic crust: The source of deep diamonds. Geology **33**, 565-568.

Taylor L.A. and Neal C.R. (1990) Eclogites with oceanic crustal and mantle signatures from the Bellsbank kimberlite, South Africa, Part 1:

Mineralogy, petrology, and whole-rock chemistry. Journal of Geology **97**, 551-567.

Valley J.W., Kitchen N., Kohn M.J., Niendorf C.R. and Spicuzza M.J. (1995) UWG-2, a garnet standard for oxygen isotope ratios: Strategies for high precision and accuracy with laser heating. Geochimica et Cosmochimica Acta **59**, 5223-5231.

Vielzeuf D., Champenois M., Valley J.W., Brunet F and Devidal J.L. (2005) SIMS analyses of oxygen isotopes: Matrix effects in Fe-Mg-Ca garnets. Chemical Geology **223**, 208-226.

Viljoen F., Dobbe R., Harris J.W. and Smit B. (2010) Trace element chemistry of mineral inclusions in eclogitic diamonds from the Premier (Cullinan) and Finsch kimberlites, South Africa: Implications for the evolution of their mantle source. Lithos **118**, 156-168.

Walter M.J. (1998). Melting of garnet peridotite and the origin of komatiite and depleted lithosphere. Journal of Petrology **39**, 29-60.

Walter M.J., Bulanova G.P., Armstrong L.S., Keshav S., Blundy J.D., Gudfinnsson G., Lord O.T., Lennie A.R., Clark S.M., Smith C.B. and Gobbo L. (2008) Primary carbonatite melt from deeply subducted oceanic crust. Nature **454**, 622-625.

Williams H.M., Nielsen S.G., Renac C., Griffin W.L., O'Reilly S.Y., McCammon C.A., Pearson N., Viljoen F., Alt J.C. and Halliday A.N. (2009) Fractionation of oxygen and iron isotopes by partial melting processes: Implications for the interpretation of stable isotope signatures in mafic rocks. Earth and Planetary Science Letters **283**, 156-166.

Wittig N., Pearson D.G., Webb M., Ottley C.J., Irvine G.J., Kopylova M., Jensen S.M. and Nowell G. (2008) Origin of cratonic lithospheric mantle roots: A geochemical study of peridotites from the North Atlantic Craton, West Greenland. Earth and Planetary Science Letters **274**, 24-33.

Yamashita K., Creaser R.A., Jensen J.E. and Heaman L.M. (2000) Origin and evolution of mid- to late-Archean crust in the Hanikahimajuk Lake area, Slave Province, Canada; evidence from U–Pb geochronological, geochemical and Nd-Pb isotopic data. Precambrian Research **99**, 197-224.

Yaxley G.M. and Green D.H. (1998) Reactions between eclogite and peridotite: mantle refertilization by subduction of oceanic crust. Schweiz. Mineral. Petrogr. Mitt, **78**, 243-255.

Yaxley G.M., and Sobolev A.V. (2007) High-pressure partial melting of gabbro and its role in the Hawaiian magma source. Contributions to Mineralogy and Petrology **154**, 371-383.

Table 5.1 Composition of Jericho Diamond Inclusions from JDE 02

Composition of Jericho Diamond Inclusions from eclogite xenolith *JDE 02*

	D1-I	**D1-II**	**D3-II**	**D5-II**	**D8-I**	**D8-II**	**D6-I**	**D6-II**	**JDE 02**	**JDE 02**
	grt	*grt*	*grt*	*grt*	*grt*	*grt*	*cpx*	*cpx*	*grt*	*cpx*
SiO_2	40.28	40.50	40.12	40.06	40.27	39.91	54.38	54.96	42.22	54.97
TiO_2	0.54	0.54	0.51	0.54	0.52	0.52	0.24	0.23	0.16	0.13
Al_2O_3	22.07	22.26	22.15	22.28	22.30	21.87	3.93	3.58	22.96	2.72
Cr_2O_3	0.10	0.10	0.10	0.10	0.11	0.11	0.05	0.05	0.59	0.33
FeO	17.78	17.64	17.77	17.53	17.75	17.74	6.74	5.86	8.27	2.09
MnO	0.39	0.39	0.39	0.39	0.39	0.39	0.09	0.08	0.38	0.07
MgO	11.38	11.69	11.49	11.38	11.40	11.53	13.07	14.07	20.98	16.36
CaO	7.56	7.65	7.59	7.53	7.61	7.54	18.0	19.1	4.31	20.4
Na_2O	0.11	0.11	0.11	0.10	0.10	0.11	2.39	2.13	0.06	1.91
K_2O	-	-	0.01	-	-	-	0.17	0.15	0.00	0.01
Total	100.2	100.9	100.3	99.92	100.4	99.72	99.09	100.2	99.93	99.02
Mg #	53	54	54	54	53	54	78	81	82	93
$\delta^{18}O$ (‰):										
CCIM	5.3		5.5	5.2		5.5			5.4	5.6
EIMF	5.7	6.0			5.8					
V	319	319		313	320		456	469	283	585
Sc	102	102		103	102		31.4	31.6	113	27
Rb	-	-		-	-		-	-	b.d	0.43
Ba	0.09	0.12		0.09	0.11		0.7	0.7	0.05	2.09
Th	-	-		-	-		-	-	0.01	0.23
U	-	-		-	-		-	-	0.03	0.04
Nb	0.20	0.21		0.16	0.22		0.1	0.1	0.38	1.12
Ta	0.17	0.15		0.37	0.37		-	-	0.08	0.12
La	0.11	0.06		0.02	0.05		4.9	5.7	0.03	18.8
Ce	0.93	0.79		0.21	0.80		20.5	21.9	0.30	56.3
Pr	0.26	0.34		0.11	0.41		3.0	3.5	0.11	8.37
Sr	0.86	0.77		0.40	0.62		178	185	0.28	499
Nd	2.95	3.61		2.01	3.02		14.7	14.7	1.46	36.7
Sm	1.52	1.65		1.84	1.84		2.1	2.5	1.30	5.20
Zr	41.2	41.6		40.7	42.6		22.4	21.8	35.0	23.7
Hf	1.30	1.22		0.61	1.19		1.1	1.3	0.74	1.49
Eu	0.59	0.65		0.57	0.67		0.6	0.5	0.45	1.11
Gd	2.69	3.43		3.33	2.87		1.9	1.4	1.65	2.75
Tb	0.68	0.70		0.74	0.74		0.1	0.3	0.38	0.21
Dy	5.72	6.40		5.96	6.32		1.1	b.d.	3.29	1.14
Y	55.4	54.9		54.8	54.3		4.8	4.6	24.7	3.80
Ho	1.65	1.84		1.60	1.58		0.2	0.1	1.06	0.17
Er	5.14	5.63		5.77	5.96		0.3	0.4	4.22	0.41
Tm	0.83	1.05		0.94	1.15		-	-	0.81	0.05
Yb	7.38	8.52		7.96	7.46		-	-	6.15	0.24
Lu	1.39	1.15		1.27	1.28		-	-	1.17	0.04
Eu/Eu_N*	0.88	0.81		0.70	0.88		0.83	0.73	0.9	
Yb/Gd_N	3.4	3.1		3.0	3.2				4.6	2.3
La/Sm_N							1.4	1.4		0.8

Uncertaintiy on $\delta^{18}O$ values is ±0.4‰ (CCIM) and ±0.5‰ (EIMF)
N= normalized to chondrite of McDonough and Sun (1995)
Eu/Eu* = 2*Eu/(Sm+Nd)

Table 5.2 Calculated whole-rock compositions of Jericho Diamond Inclusions

Calculated whole-rock compositions of Jericho Diamond Inclusions

	DI *30/70*	DI *40/60*	DI *50/50*	DI *60/40*	DI *70/30*	JDE 02 *50/50*
SiO_2	50.33	48.88	47.43	45.98	44.53	48.59
TiO_2	0.32	0.35	0.38	0.41	0.44	0.15
Al_2O_3	9.27	11.11	12.95	14.79	16.63	12.84
Cr_2O_3	0.07	0.07	0.08	0.08	0.09	0.46
FeO	9.72	10.86	12.00	13.14	14.28	5.18
MnO	0.18	0.21	0.24	0.27	0.30	0.23
MgO	12.94	12.73	12.52	12.31	12.10	18.67
CaO	15.26	14.17	13.07	11.97	10.87	12.37
Na_2O	1.61	1.40	1.18	0.97	0.75	0.98
K_2O	0.11	0.10	0.08	0.07	0.05	0.01
Total	99.81	99.87	99.93	99.99	100.1	99.47
Mg #	72	69	67	64	61	88
V	419	404	390	375	361	434
Sc	52.8	59.9	66.9	74.0	81.1	70
Rb	-	-	-	-	-	-
Ba	0.53	0.47	0.41	0.35	0.29	1.07
Th	-	-	-	-	-	0.12
U	-	-	-	-	-	0.04
Nb	0.16	0.16	0.17	0.18	0.18	0.75
Ta	0.08	0.11	0.13	0.16	0.19	0.10
La	3.73	3.21	2.68	2.16	1.63	9.41
Ce	15.0	13.0	10.9	8.89	6.84	28.3
Pr	2.38	2.08	1.78	1.48	1.18	4.24
Sr	127	109	91.1	73.0	54.9	249
Nd	11.2	10.0	8.80	7.62	6.44	19.1
Sm	2.14	2.07	2.01	1.95	1.89	3.25
Zr	27.9	29.9	31.8	33.8	35.7	29.3
Hf	1.17	1.16	1.14	1.13	1.12	1.11
Eu	0.55	0.56	0.57	0.58	0.59	0.78
Ti	1859	2010	2161	2312	2464	1064
Gd	2.09	2.23	2.37	2.51	2.66	2.20
Tb	0.36	0.41	0.46	0.51	0.56	0.30
Dy	2.30	2.85	3.39	3.93	4.47	2.21
Y	19.7	24.8	29.8	34.8	39.8	14.3
Ho	0.62	0.77	0.92	1.07	1.22	0.61
Er	1.96	2.48	3.01	3.53	4.05	2.31
Tm	0.31	0.41	0.51	0.60	0.70	0.43
Yb	2.37	3.15	3.93	4.71	5.49	3.20
Lu	0.40	0.52	0.65	0.77	0.90	0.60
Eu/Eu_N*	0.8	0.8	0.8	0.8	0.8	0.8
Yb/Gd_N	1.4	1.7	2.0	2.3	2.6	1.8
La/Sm_N	1.1	1.0	0.8	0.7	0.5	1.8

Modes of garnet/clinopyroxene are indicated in parantheses
N= normalized to chondrite of McDonough and Sun (1995)
Eu/Eu* =2* Eu/(Sm+Nd)

Figure 1

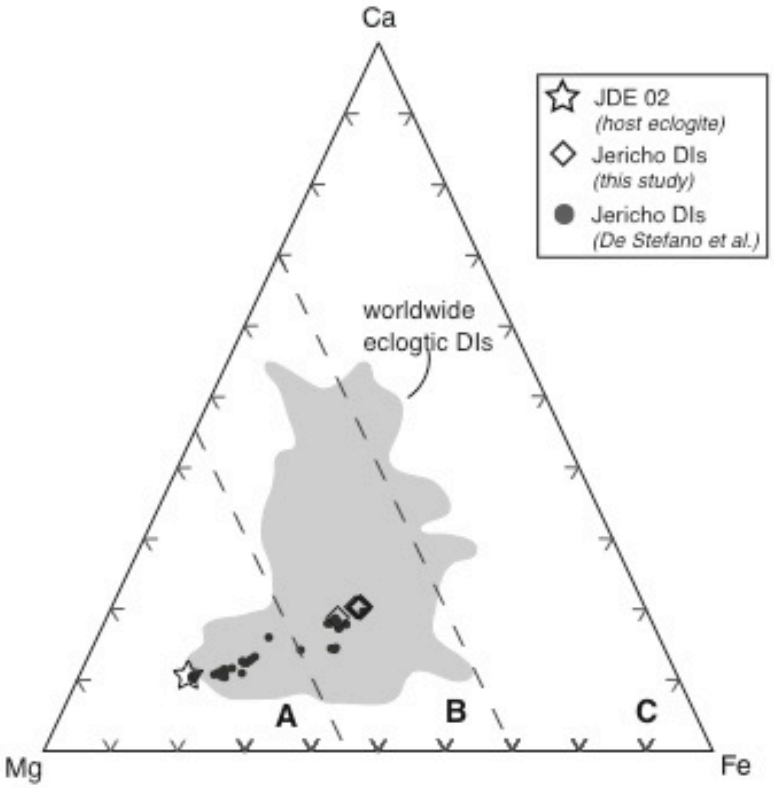

Figure 5.1 Garnet Fe-Mg-Ca compositions of Jericho diamond inclusions compared to garnet from host eclogite and worldwide eclogitic garnet DIs

Garnet Ca-Mg-Fe compositions of Jericho diamond inclusions (diamonds, this study) and from De Stefano et al. (2009; dark circles). Jericho diamond eclogite host shown for comparison (star; Smart et al., 2009). Worldwide eclogitic diamond inclusion compositional field from Stachel et al. (2008), with additions of De Stefano et al. (2009), Viljoen et al. (2010). Group A-B-C classification based on the geochemical classification of Coleman et al. (1965).

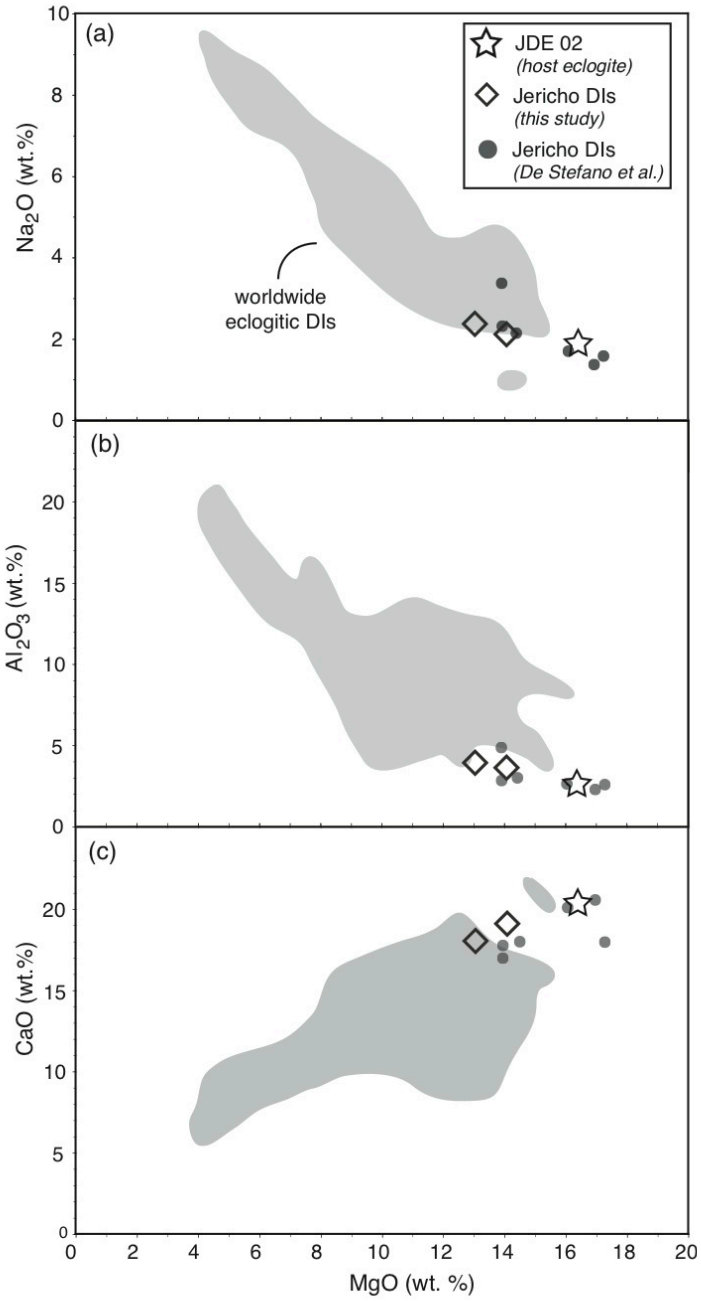

Figure 5.2 Clinopyroxene diamond inclusion compositions compared to clinopyroxene from host eclogite and worldwide DI compilation

Clinopyroxene diamond inclusion compositions. Symbols and worldwide eclogitic diamond inclusion compilation as in Fig. 5.1.

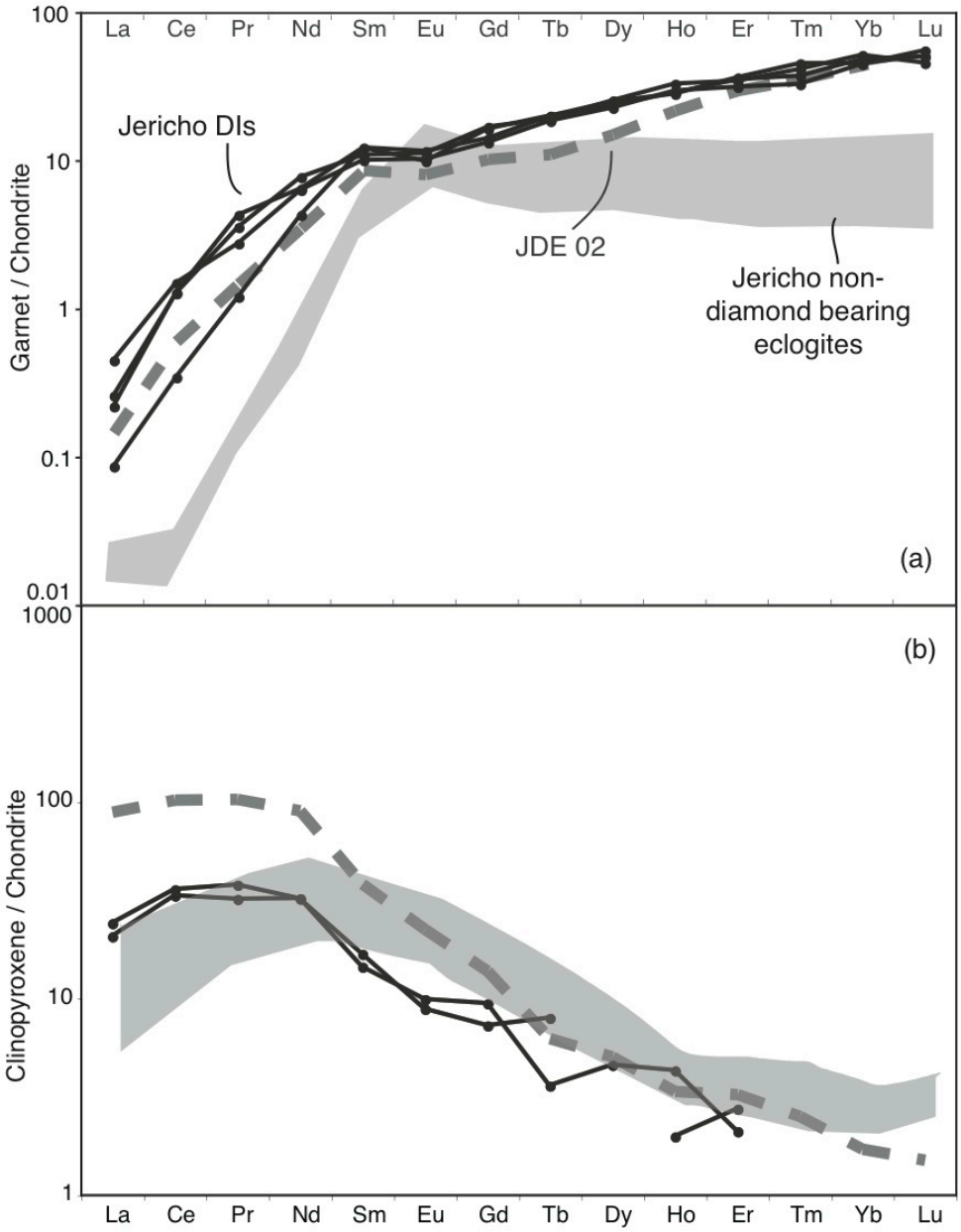

Figure 5.3 Chondrite-normalized REE diagrams of Jericho garnet and clinopyroxene diamond inclusions

Chondrite-normalized REE plots for garnet (a) and clinopyroxene (b) comparing the Jericho diamond inclusions (solid dark lines) to minerals from the host diamond eclogites (thick dashed line, Smart et al., 2009) and non-diamondiferous Jericho eclogites (grey field). Normalizing values from McDonough and Sun (1995).

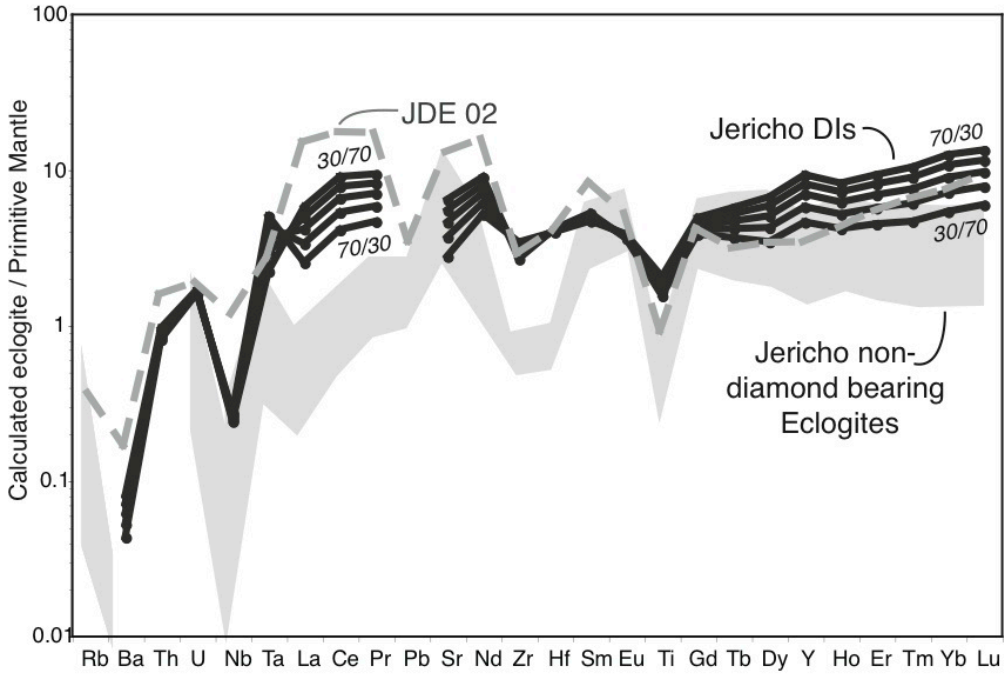

Figure 5.4 Primitive mantle-normalized multi-element diagram for calculated Jericho diamond inclusions whole rock for a range of garnet-clinopyroxene modes

Calculated whole-rock primitive mantle-normalized multi-element diagram. A range of DI whole-rock compositions with variable garnet – clinopyroxene modes are shown and the garnet/clinopyroxene modes are as indicated for the maximum and minimum modes. Jericho diamond eclogite host and non-diamond eclogites from Smart et al. (2009).

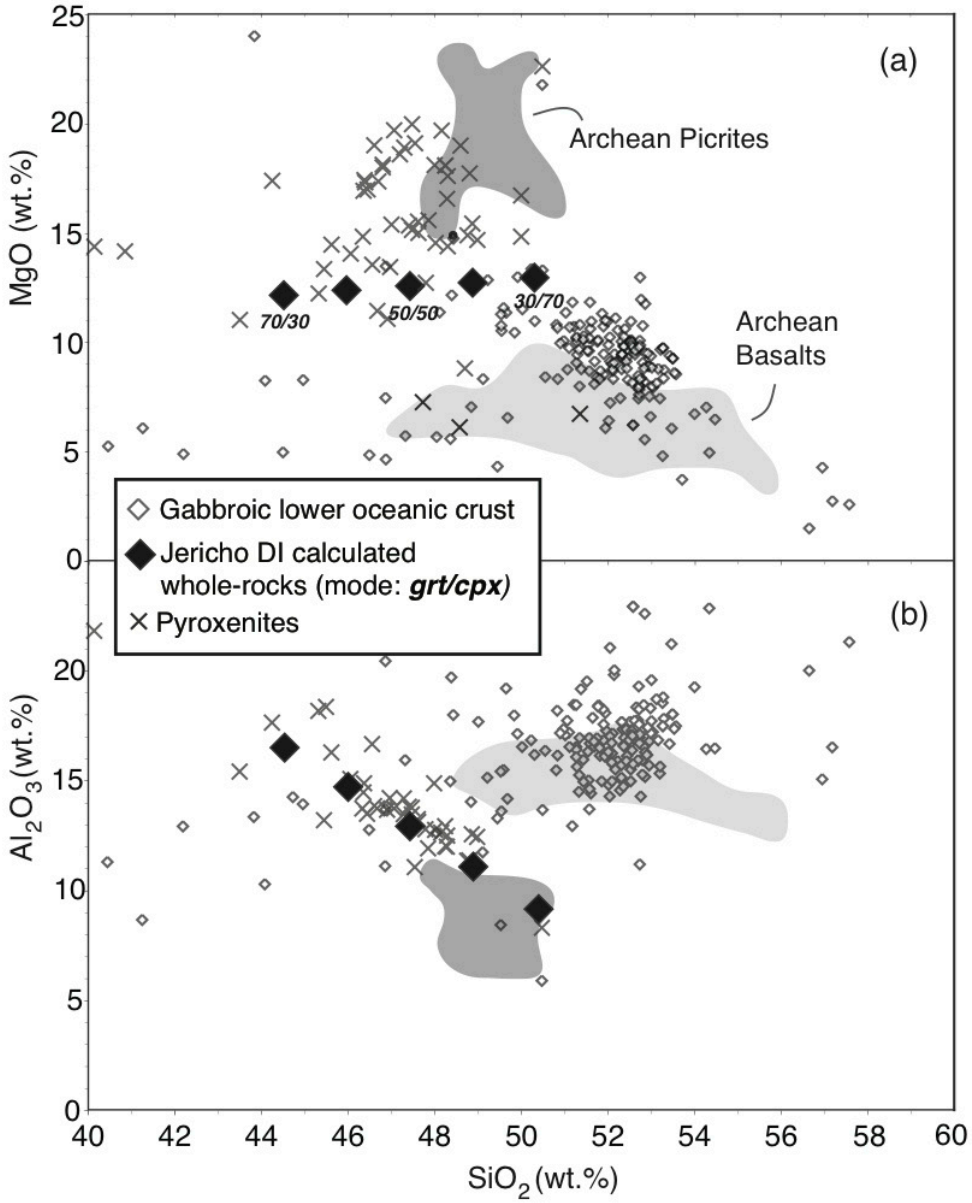

Figure 5.5 Calculated whole-rock Jericho DI compositions compared to Archean basalts and picrites and oceanic crust rocks

Calculated whole-rock composition of the DIs with variable modes as indicated. The DI whole-rocks are compositionally distinct from Archean picrites (Polat et al., 2007; 2008) and basalts (Cousens, 2000; Polat et al., 2008; Yamashita et al., 2000) and from most lower oceanic crust (Dick et al., 1999). Pyroxenite veins from ultramafic complexes (Becker, 1996; Pearson et al., 1993) have a range of compositions that overlap with the DI whole-rock compositions.

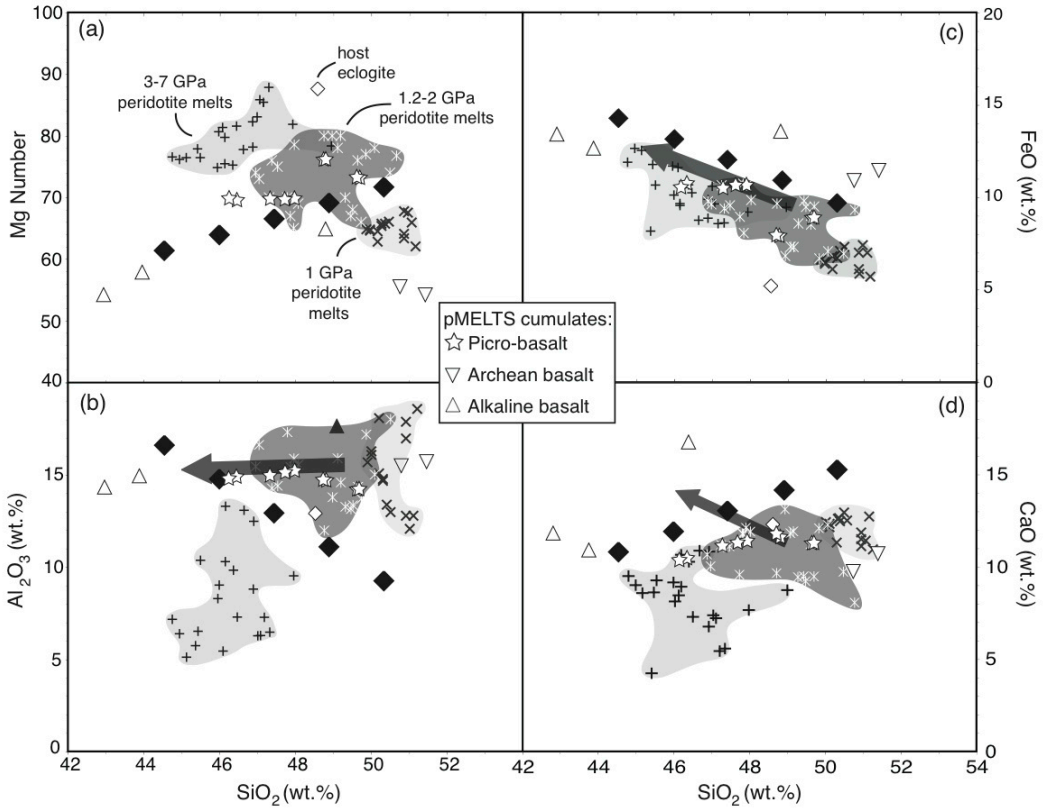

Figure 5.6 Calculated whole-rock Jericho DI compositions compared to experimentally derived peridotite melts and pMELTS-modeled pyroxenite cumulates

Calculated whole-rock compositions of the Jericho DIs and host eclogites compared to experimentally derived primary melts of the mantle and modeled pyroxenite cumulates. Low-pressure 1 GPa melts from Baker and Stolper (1994), 1.2-2 GPa melts from Falloon and Green (1988) and Falloon et al. (1988) and 3-7 GPa melts from Walter (1998). Details of the generation of the plagioclase-bearing pyroxenite cumulates from picro-basalt, basalt and basanite compositions in Section 5. Dark grey arrow in (b)-(d) represents compositional evolution of eclogitic residues after TTG-melt extraction from Rapp and Watson (1995) and Sen and Dunn (1994).

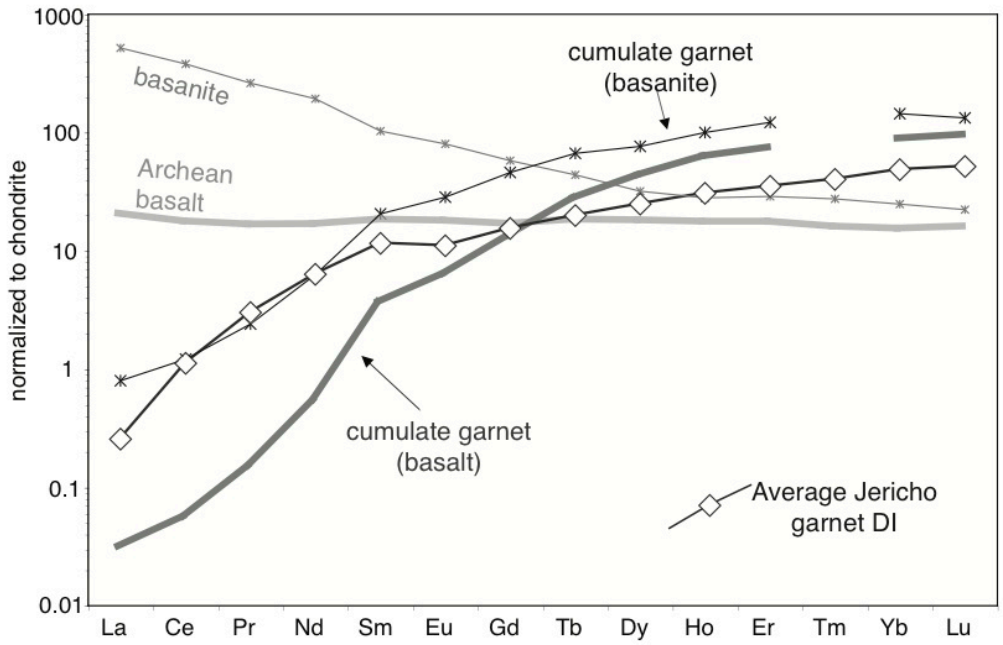

Figure 5.7 Trace-element modeling of garnet crystallized from basaltic melts

Calculated REE patterns for garnet crystallized from an Archean basalt (Yamashita et al., 2000) and a cratonic basanite (Tappe et al., 2007) using the partition coefficients of Green et al. (2000). Modeled garnets from both starting compositions have fractionated HREE patterns with Yb_N/Gd_N from 3-8, similar to the average Jericho DI garnet values of 3-4.

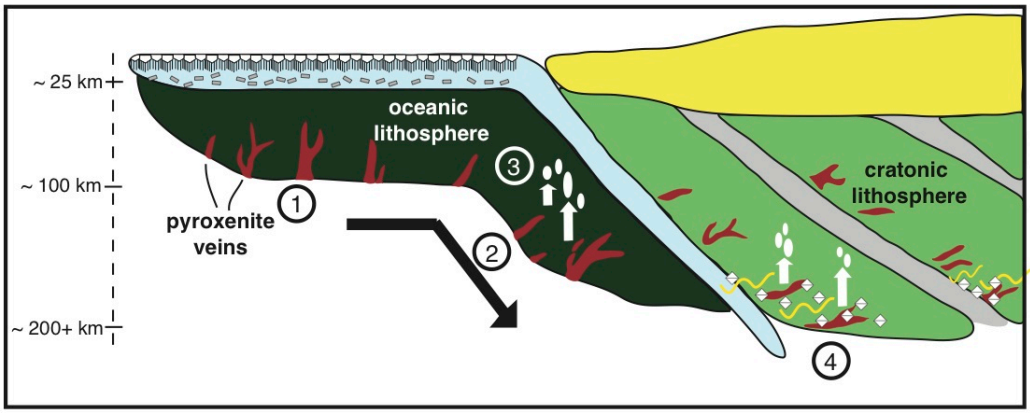

Figure 5.8 Petrogenesis of the Jericho Diamond eclogites

Schematic diagram displaying the formation and modification of the Jericho diamond eclogites. Depths indicated are approximate and diagram is not to scale. Stage 1: Crystallization of clinopyroxene-garnet-plagioclase veins in the oceanic mantle from picro-basaltic melts. Stage 2: Subduction and accretion of the oceanic lithosphere containing the pyroxenite veins to form the northern Slave cratonic lithospheric mantle, facilitating emplacement of the pyroxenite veins into the diamond stability field. Stage 3: Partial melting of the pyroxenite veins either before or during subduction, or after emplacement into the cratonic mantle. Extraction of TTG/dacitic melts from the eclogites slightly decreased Si, Al and increased Ca contents in the eclogitic residues. Stage 4: Metasomatism and associated diamond formation in the Jericho eclogites concurrent with elemental equilibration with surrounding peridotite that was responsible for the increase in Mg-number of the diamond eclogites (c.f. Smart et al., 2009). Diamond-forming fluids/melts were likely sourced from organic sediments subducted into the Jericho lithospheric mantle based on extremely depleted carbon isotope compositions of the diamonds (c.f. Smart et al., 2011).

6 Chapter 6: Conclusions

6.1 Major findings

In this thesis, I investigated the geochemical, isotopic and petrologic characteristics of diamond-bearing eclogites recovered from the Jericho kimberlite. These investigations revealed that the diamond eclogites can be divided into high- and low-MgO groups. Diamonds extracted from these groups have distinct carbon isotope compositions and nitrogen contents. Garnet-clinopyroxene Fe-Mg exchange temperatures calculated for the two groups show that the high-MgO eclogites record much lower temperatures (860-930°C calculated at 5 GPa) than the low-MgO eclogites (1070-1110°C at 5 GPa). These different equilibration temperatures for the two eclogite groups may indicate eclogite derivation from different levels the northern Slave CLM, however, this relative difference from the calculated temperatures assumes that Fe^{3+} contents are negligible in garnet and clinopyroxene and that the activity-composition models used in the Krogh-Ravna calibration adequately account for compositional differences between the two groups of eclogites. The distinct compositions, diamond characteristics and equilibration temperatures of the two groups indicate that the high- and low-MgO eclogites most likely had different formation histories.

6.2 Mantle eclogite xenolith petrogenetic models

The formation of mantle-derived eclogite xenoliths is generally attributed to subduction of oceanic crust or the deep-seated crystallization of basaltic-composition melts. However, it is also widely recognized that eclogite formation is a multi-stage process, involving episodes of melt depletion and metasomatism that ultimately produces the observed mineralogy and composition of eclogite xenoliths (e.g., Ireland et al., 1994; Jacob and Foley 1999). Eclogite xenoliths thought to represent subducted oceanic crust typically contain geochemical signatures that indicate crystallization at lower (plagioclase-stable) pressures and alteration of the eclogite protolith by seawater; the absence of such signatures has

been taken as evidence for a so-called "mantle" origin for eclogites (e.g., Snyder et al., 1997; Heaman et al., 2006; Section 5.4.1.). However, as observed from some eclogite suites, including the Jericho high-MgO diamond eclogites, the absence of these shallow oceanic crust signatures does not preclude the possibility that subduction-related processes also played an important role in the genesis of such eclogites (e.g., Jacob et al., 1998; Barth et al., 2002; Schmickler et al., 2004).

6.2.1 Origin of the Jericho Diamond Eclogites

The high-MgO diamond eclogites from Jericho do not contain any obvious crustal signatures and instead have elevated MgO and Cr_2O_3 contents, fractionated HREE patterns and oxygen isotope compositions that overlap with the mantle average (Section 3.4.3; 5.4.1). Such features are generally taken as evidence of a mantle origin (e.g., Shervais et al., 1988). However, the high-MgO diamond eclogites could not have crystallized from mantle-derived melts in the diamond stability field as partial melts generated from a peridotitic source rock at these pressures are very MgO-rich (e.g., Walter, 1998; Brey et al., 2008), and would likely crystallize olivine-rich assemblages (e.g., Herzberg et al., 1990). The petrogenesis of the Jericho high-MgO diamond eclogites is further complicated by the fact that garnet inclusions in diamonds from these eclogites have much lower MgO and Cr_2O_3 contents and higher CaO and FeO contents than garnets in the host eclogites. These observations suggest that the protolith of the high MgO eclogites originally had a more basaltic composition. Moreover, both the garnet and clinopyroxene diamond inclusions from these eclogites possess small negative Eu anomalies (Figure 5.3; Table 5.1), which suggests that some part of the protolith's history involved crystallization of plagioclase. Therefore, any petrogenetic model for the Jericho high-MgO eclogites must account for an early lower-pressure origin for the eclogites and a shift from a lower to a higher MgO bulk composition.

6.2.1.1 **Veins in the oceanic lithosphere**

The relatively low Mg-numbers of the eclogite protolith and the presence of small but consistent negative Eu anomalies in the DIs suggest the eclogites did not form in-situ in the diamond stability field, but originally crystallized at lower pressures and were then transported to deeper levels (Section 5.5.1). Eclogite protoliths in an oceanic setting are conventionally thought of as the upper extrusive to lower gabbroic portions of the oceanic crust. However, oceanic lithosphere also contains a thick peridotite mantle section that contains basaltic to pyroxenitic 'mafic' layers and veins, known from field evidence in ophiolites and exhumed peridotite massifs (e.g., Bodinier and Garrido 2003). Therefore, I propose that eclogites that do not have clear affinities with either the upper oceanic pillow basalt, sheeted dyke or gabbro sections of oceanic crust, or with deep-seated (> 3 GPa) peridotite-derived magmas, could form as basaltic melt veins at the base of the oceanic crust or within the deeper oceanic mantle lithosphere (e.g., Section 5.4.1; Foley et al., 2001; Barth et al., 2002). Many eclogite xenoliths have ages that indicate formation in the Neoarchean and Paleoproterozoic when, due to the higher mantle potential temperatures prevalent at these times, oceanic lithosphere may have been much thicker (Bickle, 1986; Herzberg, 2010) such that crystallization of melts within the deep oceanic lithosphere would have occurred at great depths and high, garnet-stable pressures. Thus the 'mantle' chemical and isotopic properties of the Jericho high-MgO eclogites and DIs can be reconciled with formation as plagioclase-bearing pyroxenite or eclogite veins in the deep oceanic mantle lithosphere.

6.2.1.2 **Secondary elemental diffusion**

The elevated Mg and Cr contents of the high MgO eclogites can be explained by diffusional Fe-Mg and Cr-Al exchange between the eclogite protolith and surrounding CLM peridotite. The Jericho eclogites presumably existed as relatively small-scale bodies in dominantly peridotitic CLM (e.g., Kopylova et al., 1999). The difference in Mg-number between the eclogites (~60-70) and the surrounding lherzolites (~90 at 150 km depth; Kopylova and Russel, 2000) would set up a chemical potential gradient, which in the presence of a melt

or fluid would enable significant amounts of elemental exchange (e.g., Fe-Mg exchange) between the two rock types on relatively short time-scales of 0.1-1 million years (Section 3.5.5). Thus, the only preserved remnant of the former chemical disposition of the Jericho high-MgO eclogites would be the entrapped DIs, which also indicates that diamond formation must have occurred relatively early during the elemental exchange process. The DIs I discuss here are compositionally homogeneous, whereas garnet and clinopyroxene DIs from Jericho diamonds with $\delta^{13}C$ values of -40‰ (presumably indicating diamond derivation from eclogites similar to the Jericho high-MgO eclogites) reported by De Stefano et al. (2009) have a wider range of compositions, in some cases with Mg-numbers equivalent to minerals in the Jericho high-MgO eclogites. Therefore, it appears that elemental exchange and diamond formation operated concurrently in the high MgO-eclogites, and inclusion entrapment occurred at various stages throughout the process, preserving a range of eclogitic compositions.

6.2.1.3 Age and tectonic constraints

Ages determined for eclogite xenoliths from the Diavik and Jericho kimberlites in the Slave craton are mostly Paleoproterozoic, which have been linked to subduction of basaltic oceanic crust accompanying ca. 1.9 Ga arc accretion to the west of the Slave Craton (e.g., Schmidberger et al., 2005; 2007; Section 2.1). It is possible that the same Paleoproterozoic subduction event emplaced other eclogitic lithologies, including the Jericho diamond eclogites, into the Slave CLM. The presence of Paleoproterozoic subducted oceanic crust in the Slave CLM is supported by the detection of flat, shallow and east-dipping, deep seismic reflectors below the Slave craton (Bostock, 1998; Cook et al., 1999). These reflectors, interpreted as potential remnants of Neoarchean and Paleoproterozoic oceanic lithosphere, respectively (e.g., Bostock, 1998; Cook et al., 1999; Section 2.2), may be the source of eclogite xenoliths sampled by Slave kimberlites. There are currently no radiometric age constraints for the Jericho diamond eclogites as Pb isotope systematics do not have age significance (Section 3.4.2.2).

6.2.2 Wider implications for eclogite petrogenesis

In general, elemental diffusion processes are likely more prevalent than previously recognized, especially if the length-scales between two compositionally or isotopically distinct bodies are relatively small and melts are present to facilitate rapid diffusion along grain boundaries. Other studies of diamond-bearing eclogites also show DIs with lower Mg-numbers than host minerals (Ireland et al., 1994; Taylor et al., 1996), such that diffusional processes may be quite common in producing Mg-enrichments in mantle-derived eclogites. However, because of the long residence times of mantle xenoliths, evidence for these processes will probably only be preserved in diamond-bearing xenoliths due to the properties of diamond. In contrast, exposed ophiolites and peridotite massifs commonly show evidence of chemical and isotopic diffusion/equilibration processes (see Loubet and Allègre 1982; Bodinier and Goddard, 2003), where mafic layers can preserve chemical and isotopic gradients between different rock types (e.g., Pearson et al., 1993). The petrogenesis of the Jericho diamond eclogites also emphasizes that a subducted package of oceanic lithosphere will introduce several compositionally different "eclogitic" assemblages at high pressure into the mantle. The location and formation conditions of the different eclogite protoliths will impart each with a distinctive geochemical and isotopic flavor (e.g., upper basaltic crust, lower gabbroic cumulates, deep pyroxenite veins), resulting in the wide variety of eclogite (and pyroxenite) mantle-derived xenoliths observed from kimberlites.

6.3 Diamond formation

On the basis of the occurrence of diamonds in veins or zones of alteration and incompatible element enrichments in diamond eclogite xenoliths (e.g., Cartigny et al., 2004; Stachel et al., 2004), diamond growth in eclogite is thought to be the product of secondary metasomatic events rather than part of the primary eclogite mineral assemblage (e.g., Schulze et al., 1996; Taylor et al., 2000). The nature of carbon in diamond-forming fluids/melts is also the subject of debate, with particular focus on both the speciation (e.g., oxidized or reduced; Stachel and

Harris, 2009) and the source(s) of carbon (e.g., subducted sediments vs. mantle-derived; Cartigny, 2005) in the fluid/ melt.

6.3.1 Origin of diamonds in the Jericho eclogites

Deciphering the diamond formation event(s) in the Jericho eclogites has shed light on the nature of metasomatic processes that affected the northern Slave CLM. As described in Chapter 4, diamond formation in both the high- and low-MgO Jericho eclogites appears to be related to multiple pulses of oxidized (CO_2 or carbonate-bearing) fluids or melts (Section 4.5.1.3, 4.5.2.2). However, diamonds in the two eclogite groups have markedly different carbon isotope compositions and nitrogen contents, clearly showing that at least two diamond-forming events, involving separate carbon sources, occurred in the eclogitic portions of the Jericho CLM.

6.3.1.1 Source and speciation of Carbon

The extremely low $\delta^{13}C$ values (-40‰) in diamonds from high-MgO eclogites may be related to a distinctive organic carbon source, whereas the higher (-5 to -2.7‰) $\delta^{13}C$ values in diamonds from low-MgO eclogites indicate derivation from either mantle carbon or carbonate sediment sources (Section 4.5.1.1; 4.5.2.3). Deep CLM peridotite is thought to be predominantly reducing in character (Frost and McCammon, 2008), and as such, derivation of an oxidized fluid from mantle carbon sources seems unlikely. It is more plausible that carbon derived from subducted sedimentary carbonate sources would have provided an oxidizing fluid. Thus, although very different in isotopic composition, I suggest that diamonds in both Jericho eclogite types may have involved crustal carbon sources. The anomalously ^{13}C-depleted carbon isotope composition of the high-MgO diamonds requires special explanation. As argued in Chapter 4, if the carbon in these diamonds is derived from organic matter, then those organics most likely formed at either 2.7 or 2.0 Ga, two periods in Earth history characterized by extreme negative excursions in the carbon isotope composition of organic matter (Eigenbrode and Freeman, 2006). Interestingly, those two time periods correspond to proposed subduction events in the Slave (see Chapter 2) and thus,

diamonds from the Jericho eclogites also stress the importance of subduction-related modification of the Slave CLM.

Detailed SIMS analyses of diamonds from both groups of Jericho eclogites revealed considerable differences in the carbon isotope compositions and nitrogen contents of the two groups. However, in both cases, there is a rimward progression to higher $\delta^{13}C$ values and lower nitrogen contents, which suggests coupled ^{13}C-N fractionation processes during diamond crystallization. The $\delta^{13}C$-N systematics also highlight two important findings: 1) diamond growth in Jericho eclogites occurred from relatively oxidized fluids or melts, and 2) nitrogen behaves compatibly in diamond relative to that growth medium.

6.3.2 Metasomatic processes in the Jericho CLM

The finding that diamond growth in eclogites from Jericho occurs from oxidized fluids/melts helps constrain metasomatic fluids operating in the northern Slave CLM. Previous studies of the oxidation state of Jericho peridotite xenoliths showed a general reduction of fO_2 with depth (McCammon and Kopylova, 2004), but Creighton et al. (2008) indicated that some high-temperature peridotite xenoliths from Jericho may have experienced oxidizing metasomatism. Evidence for a relatively oxidized, carbonatitic metasomatic event in the northern Slave CLM has also been indicated by Jericho eclogites that contain apatite, carbonate and phlogopite (e.g., Heaman et al., 2006; Section 3.4.2.2; Table B.1) and the enrichment of incompatible elements in the Jericho diamond eclogites themselves (Section 3.4.2.1). From model Nd ages, Heaman et al. (2006) further predicted that this carbonatite metasomatism event was linked to modification of the northern Slave CLM by the Mesoproterozoic Mackenzie igneous event. If this interpretation was correct, the diamond growth associated with the Mackenzie event would have occurred from infiltrating mantle-derived carbonatites. Conversely, diamond formation could have accompanied subduction and emplacement of oceanic crust into the CLM at either approximately 2.7 or 1.9 Ga during putative subduction events (e.g., Chapter 1, 2; Section 4.5.1.1). Melting of carbonaceous sediments and/or the eclogitized slab can produce carbonatitic melts

(e.g., Yaxley and Brey 2004; Grassi and Schmidt, 2011), which, upon percolation into relatively reduced (from melt depletion, McCammon and Kopylova, 2004) eclogite horizons, would cause diamond formation. In summary, although there are no firm age constraints on the timing of diamond growth in the Jericho eclogites, diamond growth likely did not occur earlier than the Neoarchean.

6.4 Summary and Future Directions

The Jericho diamond-bearing eclogite xenoliths demonstrate that not all eclogite xenoliths represent the high-pressure derivatives of upper volcanic or gabbroic oceanic crust, and some may have formed deep in the oceanic lithosphere, similar to basaltic layers and veins in ophiolites and peridotite massifs. The case for subducted oceanic crust as the protolith for Diavik eclogites and zircon-bearing Jericho eclogites was in part made by the correspondence of eclogite ages to a known subduction event. The same tie for the Jericho diamond eclogites could be made if firm age constraints were developed. Although Pb isotopes did not yield meaningful age information, application of Lu-Hf or Re-Os isotopic systems to the Jericho diamond eclogites may lead to better age constraints and thus eclogite and diamond petrogenesis. Furthermore, in addition to secondary melt depletion and metasomatism events, the process of elemental diffusion can significantly effect the final disposition of eclogite xenoliths, which has been highlighted by the diamond inclusion-host eclogite geochemical relationship in the Jericho diamond eclogites.

The carbon isotope characteristics of diamonds from Jericho eclogites show that diamond formation was accomplished by oxidized, carbonatite-like melts or fluids, which may have also changed the composition of the host eclogites and DIs (Section 3.6). The compositional evolution of the diamond-bearing eclogitic portion of the Jericho CLM has been constrained in terms of major- and trace-element composition from the Jericho DIs and host xenoliths (Section 3.4.2; 5.5.2). However, further insight into the effect of the diamond-forming process could be explored by investigating 1) the composition of the diamond-forming fluid/melt by trace-element and isotopic analysis of the

diamond itself (e.g., Klein-BenDavid et al., 2010) and 2) the ferric iron contents (an therefore an estimation fO_2) of the Jericho diamond eclogites, their DIs and other diamond-absent eclogites from Jericho (e.g., Creighton et al., 2008). As predicted by the oxidized nature of the diamond-forming fluid/melts, one would expect to also see relative increases in oxidation state from DI to host eclogite. Comparing the diamond-absent to diamond-bearing eclogite suites may also shed light on the diamond-forming process at Jericho.

The pervasiveness of carbonatite-driven metasomatism has already been observed from mantle xenoliths, from recent studies of diamond fluid inclusions (e.g., Klein-BenDavid et al., 2007) and from isotopic variations in xenocrystic diamonds (e.g., Bulanova et al., 2002) such that oxidized fluids or melts may play a large role in the formation of diamond. However, not all diamonds indicate formation from oxidized fluids/melts (cf., Thomassot et al., 2007) and it is more likely that diamond formation occurs from both reduced and oxidized fluids/melts, and both processes may have occurred at different times in different lithologies in the same piece of CLM. In order to better understand and constrain the process of diamond growth and its influence on the mantle, more investigations of diamond-bearing xenoliths from worldwide occurrences are required.

References

Barth M.G., Rudnick R.L., Horn I., McDonough W.F., Spicuzza M.J., Valley J.W. and Haggerty S.E. (2002) Geochemistry of xenolithic eclogites from West Africa. Part 2: Origins of high MgO eclogites. Geochimica et Cosmochimica Acta **66**, 4325-4434.

Bodinier J.-L. and Godard M. (2003) Orogenic, Ophiolitic, and Abyssal Peridotites, pp 103-170. In *The Mantle and Core* (ed. R.W. Carlson) Vol. 2 *Treatise on Geochemistry* (eds. H.D. Holland and K.K. Turekian), Elsevier-Pergamon, Oxford.

Brey G.P., Bulatov V.K., Girnis A.V., and Lahaye Y. (2008). Experimental melting of carbonated peridotite at 6-10 GPa. Journal of Petrology **49**, 797-821.

Bulanova G.P., Pearson D.G., Hauri E.H., Griffin B.J. (2002) Carbon and nitrogen isotopes systematics within a sector-growth diamond from the Mir kimberlite, Yakutia. Chemical Geology **188**, 105–123

Cartigny P., Stachel T., Harris J.W. and Javoy M. (2004) Constraining diamond metasomatic growth using C- and N-stable isotopes: examples from Namibia. Lithos **77**, 359-373.

Creighton S., Stachel T., McLean H., Muehlenbachs K., Simonetti A., Eichenberg D., and Luth R. (2008). Diamondiferous peridotitic microxenoliths from the Diavik Diamond Mine, NT. Contributions to Mineralogy and Petrology **155**, 541-554.

Foley S.F., Petibon C.M., Jenner G.A. and Kjarsgaard B.A. (2001) High U/Th partitioning by clinopyroxene from alkali silicate and carbonatite metasomatism: an origin for Th/U disequilibrium in mantle melts. Terra Nova **13**,104-109.

Foley S.F., Buhre S. and Jacob D. (2003) Evolution of the Archean crust by delamination and shallow subduction. Nature **421**, 249-252.

Frost D.J. and McCammon C.A. (2008) The Redox State of Earth's Mantle. *Ann. Rev. Earth Planet. Sci.* **36**, 389-420.

Grassi D. and Schmidt M.W. (2011) Melting of carbonated pelites at 8-13 GPa: generating K-rich carbonatites for mantle metasomatism. Contributions to Mineralogy and Petrology DOI 10.1007/s00410-010-0589-9

Heaman L.M., Creaser R.A., Cookenboo H.O., Chacko T. (2006) Multi-stage modification of the Northern slave mantle lithosphere: evidence from

zircon-and diamond-bearing eclogite xenoliths entrained in Jericho kimberlite, Canada. Journal of Petrology **47**, 821-858.

Helmstaedt H.H. and Schulze D.J. (1989) Southern African kimberlites and their mantle sample: implications for Archean tectonics and lithosphere evolution. In: Ross J., Jacques A.L., Ferguson J., Green D.H., O'Reilly S.Y., Danchin R.V., and Janse A.J.A. (eds), Kimberlites and related rocks. Geological Society of Australia Special Publication, vol. 14. Blackwell, Carlton, pp. 358-368.

Herzberg C., Condie K. and Korenaga J. (2010) Thermal history of the Earth and its petrological expression. Earth and Planetary Science Letters **292**, 79-88.

Ireland T.R., Rudnick R.L. and Spetsius Z. (1994) Trace elements in diamond inclusions from eclogites reveal link to Archean granites. Earth and Planetary Science Letter*s* **128**, 199-213.

Jacob D. and Foley S.F. (1999) Evidence for Archean ocean crust with low high field strength element signature from diamondiferous eclogite xenoliths. Lithos **48**, 317-336

Jacob D., Jagoutz E., Lowry D. and Zinngrebe E. (1998) Comment on 'The Origins of Yakutian Eclogite Xenoliths' by G.A. Snyder, L.A. Taylor, G. Crozaz, A.N. Halliday, B.J. Beard, V.N. Sobolev and N.V. Sobolev. Journal of Petrology **39**, 1527-1533.

Klein-BenDavid O., Izraeli E.S., Hauri E. and Navon O. (2007) Fluid inclusions in diamonds from the Diavik mine, Canada and the evolution of diamond-forming fluids. Geochimica et Cosmochimica Acta **71**, 723-744.

Klein-BenDavid O., Pearson D.G., Nowell G.M., Ottley C., McNeill J.C.R. and Cartigny P. (2010) Mixed fluid sources involved in diamond growth constrained by Sr-Nd-Pb-C-N isotopes and trace elements. Earth and Planetary Science Letters **289**, 123-133.

Kopylova M.G. and Russell J.K. (2000) Chemical stratification of the cratonic lithosphere: Constraints from the northern Slave craton, Canada. Earth and Planetary Science Letters **181**, 71-87.

Kopylova M.G., Russell J.K. and Cookenboo H. (1999). Mapping the lithosphere beneath the north central Slave Craton. In: Gurney, J. J., Gurney, J. L., Pascoe, M. D. & Richardson, S. H. (eds) Proceedings of the 7th International Kimberlite Conference. Cape Town: Red Roof Design pp. 468-479.

Loubet M. and Allègre C.J. (1982) Trace elements in orogenic lherzolites reveal the complex history of the upper mantle. Nature **298**, 809-814.

McCammon C. and Kopylova M.G. (2004) A redox profile of the Slave mantle and oxygen fugacity control in the cratonic mantle. Contributions to Mineralogy and Petrology **148**, 55-68.

Pearson D.G., Davies G.R. and Nixon P.H. (1993) Geochemical constraints on the petrogenesis of diamond facies pyroxenites from the Beni Bousera peridotite massif, North Morocco. Journal of Petrology **34**, 125-172.

Shervais J.W., Taylor L.A., Lugmair G., Clayton R.N., Mayeda T.K. and Korotev R. (1988) Archean oceanic crust and the evolution of sub-continental mantle: eclogites from southern Africa. Geological Society of America Bulletin **100**, 411-423.

Schulze D.J., Weise D. and Steude J. (1996) Abundance and Distribution of Diamonds in Eclogite Revealed by Volume Visualization of CT X-Ray Scans. Journal of Geology **104**, 109-113.

Schmickler B., Jacob D.E. and Foley S.F. (2004) Eclogite xenoliths from the Kuruman kimberlites, South Africa: geochemical fingerprinting of deep subduction and cumulate processes. Lithos **75**, 173-207.

Schmidberger S.S., Heaman L.M., Simonetti A., Creaser R.A. and Cookenboo H.O. (2005) Formation of Paleoproterozoic eclogitic mantle, Slave Province (Canada): Insights from in-situ Hf and U-Pb isotopic analyses of mantle zircons. Earth and Planetary Science Letters **240**, 621-633.

Schmidberger S.S., Simonetti A., Heaman L.M., Creaser R.A. and Whiteford S. (2007) Lu-Hf, in-situ Sr and Pb isotope and trace element systematics for mantle eclogites from the Diavik diamond mine: Evidence for Paleoproterozoic subduction beneath the Slave craton, Canada. Earth and Planetary Science Letters **254**, 55-68.

Snyder G.A., Taylor L.A., Crozaz G., Halliday A.N., Beard B.L., Sobolev V.N. and Sobolev N.V. (1997) The origins of Yakutian eclogite xenoliths. Journal of Petrology **38**, 85–113.

Stachel T., Aulbach S., Brey G.P., Harris J.W., Leost I. and Viljoen K.S. (2004) The trace element composition of silicate inclusions in diamonds: a review. Lithos **77**, 1-19.

Taylor L.A., Snyder G.A., Crozaz G., Sobolev V.N., Yefimova E.S. and Sobolev N.V. (1996) Eclogitic inclusions in diamonds: Evidence of complex

mantle processes over time. Earth and Planetary Science Letters **142**, 535-551.

Taylor L., Keller R., Snyder G., Wang W., Carlson W., Hauri E., McCandless T., Kim K-R., Sobolev N. and Bezborodov S. (2000) Diamonds and Their Mineral Inclusions, and What They Tell Us: A Detailed "Pull-Apart" of a Diamondiferous Eclogite. International Geology Reviews **42**, 959-983.

Thomassot E., Cartigny P., Harris J.W. and Viljoen K.L. (2007) Methane-related diamond crystallization in the Earth's mantle: Stable isotope evidence from a single diamond-bearing xenolith. Earth and Planetary Science Letters **257**, 362-371.

Walter M.J. (1998) Melting of garnet peridotite and the origin of komatiite and depleted lithosphere. Journal of Petrology **39**, 29-60.

Yaxley G.M., and Brey G.P. (2004) Phase relations of carbonate-bearing eclogite assemblages from 2.5 to 5.5 GPa: implications for petrogenesis of carbonatites. Contributions to Mineralogy and Petrology **146**, 606-619.

A. Appendix A: Additional Data

The following appendix contains geochemical and isotopic data for Jericho eclogite xenoliths that were not discussed in the thesis.

Table A.1 Garnet, clinopyroxene and calculated whole rock compositions of Jericho eclogites

Major element composition of garnet, clinopyroxene and calculated whole-rocks of Jericho eclogites

	8-12	**35-2**	**1-1**	**55-7**	**Jd6Fn**	**R183**	**53-11**	**54-5**	**44-9**	**10-13**	**53-6**	**51-10**	**11-17**	**7-5**	**Jer 1**	**Jer 2**	**Jer 3**	**Jer 4**	**Jer 5**	**Jer 6**	**Jer 7**	**Jer 8**	**Jde 15**	**Jde 25**
	Grt	*Grt*	*Grt*	*Grt*	*Grt*	*Grt*	*Grt*	*Grt*	*Grt*	*Grt*	*Grt*	*Grt*	*Grt*	*Grt*	*Grt*	*Grt*	*Grt*	*Grt*	*Grt*	*Grt*	*Grt*	*Grt*	*Grt*	*Grt*
Mode	50	60	40	55	50	40	25	50	50	65	50	50	60	50	50	60	60	65	10	60	50	75	50	50
SiO_2	39.0	38.6	39.6	38.6	39.6	40.5	39.2	40.0	41.5	38.7	39.5	39.3	38.8	40.1	40.4	41.1	39.8	39.7	39.6	39.2	40.2	38.5	41.0	40.4
TiO_2	0.04	0.07	0.12	0.12	0.07	0.11	0.12	0.09	0.49	0.11	0.09	0.16	0.11	0.23	0.08	0.04	0.15	0.05	0.06	0.07	0.04	0.09	0.28	0.37
Al_2O_3	22.7	22.8	23.3	22.7	22.7	23.2	22.4	22.8	22.6	22.0	22.6	22.3	22.0	22.6	23.4	23.8	22.9	22.8	22.6	22.5	23.2	22.1	23.4	22.5
Cr_2O_3	0.13	0.04	0.05	0.04	0.11	0.07	0.03	0.02	0.54	0.01	0.07	0.04	0.01	0.07	0.07	0.11	0.04	0.01	0.12	0.02	0.11	0.01	0.02	0.07
FeO	22.0	21.2	13.5	15.4	19.3	13.5	16.9	15.6	9.2	22.5	17.4	14.0	22.5	16.7	11.6	11.9	14.4	18.6	22.4	23.6	17.4	26.5	13.7	13.7
MnO	0.33	0.36	0.25	0.32	0.35	0.25	0.32	0.31	0.37	0.30	0.30	0.32	0.29	0.40	0.23	0.22	0.27	0.29	0.50	0.42	0.29	0.39	0.25	0.22
MgO	11.1	11.7	12.9	7.02	8.86	12.7	6.51	9.67	20.1	5.91	9.51	5.50	5.76	12.0	11.0	15.3	7.55	10.1	11.6	9.24	12.9	4.97	14.7	13.4
CaO	4.58	4.54	9.22	14.6	9.33	9.34	14.1	11.4	4.42	10.6	10.1	17.7	10.6	7.56	13.8	8.12	15.59	8.43	3.99	5.75	6.23	8.60	6.8	8.26
Na_2O	0.03	0.05	0.05	0.05	0.04	0.06	0.05	0.04	0.06	0.05	0.04	0.06	0.05	0.10	0.04	0.04	0.07	0.04	0.03	0.06	0.04	0.06	0.11	0.14
K_2O	0.001	0.005	0.003	0.002	0.002	0.003	0.003	0.004	0.003	0.003	0.004	0.003	0.004	0.002	0.002	0.003	0.001	0.003	0.001	0.001	0.001	0.002	0.002	0.001
Total	99.9	99.4	99.1	98.9	100.4	99.7	99.7	99.8	99.2	100.1	99.7	99.3	100.2	99.8	100.6	100.7	100.7	99.9	100.9	100.9	100.5	101.3	100.2	99.0
Mg #	47	49	63	45	45	63	41	53	80	32	49	41	31	56	63	71	52	49	48	44	59	27	66	64
Class.	B	B	B	C	B	B	C	B	A	C	B	C	C	B	B	B	C	B	B	B	B	C	B	B

(Continued)

	8-12	**35-2**	**1-1**	**55-7**	**Jd6Fn**	**R183**	**53-11**	**54-5**	**44-9**	**10-13**	**53-6**	**51-10**	**11-17**	**7-5**	**Jer 1**	**Jer 2**	**Jer 3**	**Jer 4**	**Jer 5**	**Jer 6**	**Jer 7**	**Jer 8**	**Jde 15**	**Jde 25**
	Cpx	Cpx	Cpx	Cpx	Cpx	Cpx	Cpx	Cpx	Cpx	Cpx	Cpx	Cpx	Cpx	Cpx	Cpx	Cpx	Cpx	Cpx	Cpx	Cpx	Cpx	Cpx	Cpx	Cpx
Mode	50	40	60	45	50	60	75	50	50	35	50	50	40	50	50	40	40	35	90	40	50	25	50	50
SiO_2	55.8	55.6	55.9	56.0	56.1	55.9	56.3	56.1	54.5	55.9	56.0	56.0	56.2	55.5	55.0	55.5	55.1	55.0	54.2	54.5	54.9	55.1	55.0	55.7
TiO_2	0.12	0.11	0.15	0.12	0.12	0.15	0.14	0.12	0.23	0.14	0.12	0.15	0.14	0.31	0.11	0.11	0.22	0.12	0.08	0.11	0.10	0.17	0.34	0.39
Al_2O_3	7.54	7.50	9.40	13.4	10.8	9.00	14.6	11.7	1.92	12.9	12.2	14.3	13.0	8.49	10.7	11.4	14.0	9.87	3.89	6.53	7.67	11.2	8.7	10.7
Cr_2O_3	0.16	0.08	0.06	0.04	0.09	0.06	0.04	0.02	0.71	0.01	0.07	0.01	0.01	0.08	0.08	0.15	0.04	0.02	0.09	0.02	0.14	0.01	0.09	0.08
FeO	5.53	5.47	2.36	2.58	3.71	2.33	2.81	2.55	3.30	5.12	2.71	2.44	5.06	4.24	1.83	1.67	2.28	3.59	6.44	6.22	3.54	7.54	3.46	3.23
MnO	0.04	0.04	0.03	0.02	0.02	0.03	0.02	0.03	0.10	0.03	0.02	0.03	0.02	0.05	0.02	0.02	0.02	0.03	0.08	0.05	0.03	0.03	0.04	0.03
MgO	10.9	11.0	11.5	8.13	9.28	11.7	7.20	9.46	17.2	6.88	8.67	7.70	6.66	10.7	10.3	9.86	7.76	9.61	12.9	10.9	11.5	6.36	11.6	9.63
CaO	15.7	15.9	16.7	13.1	14.4	16.5	12.0	14.6	19.9	11.4	13.7	12.8	11.2	15.0	16.2	14.6	13.5	14.8	18.1	16.3	16.6	11.0	14.6	11.3
Na_2O	4.66	4.58	4.34	6.88	5.92	4.82	7.50	6.09	1.63	7.33	6.30	7.14	7.9	5.70	4.96	5.96	6.51	5.58	3.00	4.49	4.57	7.90	4.88	6.44
K_2O	0.00	0.01	0.03	0.00	0.01	0.03	0.01	0.00	0.04	0.00	0.01	0.00	0.00	0.01	0.00	0.00	0.01	0.00	0.00	0.00	0.00	0.00	0.1	0.05
Total	100.4	100.3	100.6	100.2	100.5	100.5	100.6	100.6	99.6	99.8	99.9	100.5	100.1	100.0	99.2	99.2	99.4	98.5	98.8	99.1	99.0	99.4	98.7	99.6
Mg #	78	78	90	85	82	90	82	87	90	71	85	85	70	82	88	85	78	83	78	73	81	55	86	84

(Continued)

	8-12	35-2	1-1	55-7	Jd6Fn	R183	53-11	54-5	44-9	10-13	53-6	51-10	11-17	7-5	Jer 1	Jer 2	Jer 3	Jer 4	Jer 5	Jer 6	Jer 7	Jer 8	Jde 15	Jde 25
	WR	WR	WR	WR	WR	WR	WR	WR	WR	WR	WR	WR	WR	WR	WR	WR	WR	WR	WR	WR	WR	WR	WR	WR
SiO_2	47.4	45.4	49.4	46.4	50.3	49.7	52.0	48.0	48.0	44.7	47.8	47.6	47.5	47.8	47.7	46.8	45.9	45.0	52.8	45.3	47.6	42.7	48.0	48.1
TiO_2	0.08	0.09	0.14	0.12	0.10	0.13	0.13	0.10	0.36	0.12	0.10	0.16	0.12	0.27	0.10	0.06	0.18	0.08	0.08	0.09	0.07	0.11	0.31	0.38
Al_2O_3	15.1	16.7	15.0	18.5	15.0	14.7	16.6	17.2	12.3	18.8	17.4	18.3	17.5	15.6	17.1	18.9	19.3	18.2	5.76	16.1	15.4	19.4	16.1	16.6
Cr_2O_3	0.14	0.06	0.06	0.04	0.10	0.07	0.04	0.02	0.63	0.01	0.07	0.03	0.01	0.08	0.07	0.12	0.04	0.01	0.09	0.02	0.12	0.01	0.06	0.08
FeO	13.8	14.9	6.82	9.65	9.16	6.80	6.33	9.05	6.25	16.4	10.1	8.20	13.8	10.5	6.70	7.83	9.53	13.3	8.04	16.7	10.5	21.8	8.58	8.46
MnO	0.19	0.23	0.12	0.18	0.14	0.11	0.10	0.17	0.24	0.21	0.16	0.17	0.15	0.22	0.13	0.14	0.17	0.20	0.12	0.27	0.16	0.30	0.15	0.125
MgO	11.0	11.4	12.1	7.52	9.13	12.1	7.03	9.57	18.6	6.25	9.09	6.60	6.21	11.3	10.6	13.1	7.63	9.93	12.8	9.89	12.2	5.32	13.1	11.5
CaO	10.1	9.09	13.7	13.9	12.6	13.7	12.5	13.0	12.2	10.9	11.9	15.3	10.9	11.3	15.0	10.7	14.8	10.6	16.7	9.97	11.4	9.21	10.7	9.78
Na_2O	2.35	1.86	2.63	3.12	3.86	2.91	5.64	3.06	0.85	2.60	3.17	3.60	3.99	2.9	2.50	2.41	2.64	1.98	2.71	1.83	2.31	2.02	2.50	3.29
K_2O	0.00	0.01	0.02	0.00	0.00	0.02	0.01	0.004	0.02	0.00	0.005	0.004	0.004	0.008	0.00	0.00	0.00	0.00	0.00	0.00	0.00	0.00	0.05	0.03
Total	100.2	99.7	100.0	99.5	100.4	100.2	100.4	100.2	99.4	100.0	99.8	99.9	100.2	99.9	99.9	100.1	100.2	99.4	99.0	100.2	99.8	100.8	99.5	99.3
Mg #	63	61	79	63	63	79	72	70	85	46	67	63	45	69	75	77	62	61	74	55	70	34	76	74
$T_{KR}(^oC)$	903	932	862	920	894	843	940	883	1121	994	863	931	1000	1053	1085	1408	1414	903	885	1207	1164	1252	1065	1113

Mg # Mg/(Mg+Fe) calculated from cations

Class. Eclogite classification based on the geochemical parameters of Coleman et al. (1965)

$T_{KR}(^oC)$ Temperature calculated at 5 Gpa using Krogh-Ravna (2000)

Table A.2 Trace-element composition of garnet and clinopyroxene from Jericho eclogites

Trace element composition of garnet and clinopyroxene from Jericho eclogites

	35-2		**1-1**		**R183**		**10-13**		**53-11**		**55-7**		**44-9**		**Jd6fn**		**Jer 1**		**Jer 2**	
	Grt	*1σ*	*Grt*	*1σ*	*Grt*	*1σ*	*Grt*	*1σ*	*Grt*	*1σ*	*Grt*	*1σ*	*Grt*	*1σ*	*Grt*	*1σ*	*Grt*	*1σ*	*Grt*	*1σ*
V	590	4	794	3	851	4	664	5	1070	1	771	2	3360	8	378	2	497	6	216	2
Ni	10.30	1	23.2	2	24.80	3	2.17	0.3	7.69	0.7	7.91	0.7	27.90	2	9.46	0.8	19.50	5	19.0	5
Sc	39.7	2	51.3	2	49.9	2	61.2	2	35.7	1	56.4	2	102	4	53.5	2.0	64.5	4	39.0	3
Rb	0.03	0.01	b.d.		0.11	0.02	0.02	0.01	0.14	0.02	0.05	0.02	0.00	0.02	0.04	0.02	0.30	0.05	0.05	0.02
Ba	0.30	0.02	0.15	0.01	0.28	0.01	0.06	0.01	0.13	0.02	0.12	0.02	0.06	0.01	0.61	0.03	0.26	0.05	0.06	0.02
U	b.d.		b.d.		0.01	0.003	0.4	0.02	0.02	0.01	b.d.		b.d.		0.04	0.01	0.03	0.01	0.02	0.01
Nb	0.03	0.1	0.09	0.03	0.06	0.02	0.02	0.02	0.16	0.03	0.08	0.02	0.2	0.04	b.d.		0.05	0.03	b.d.	
Ta	0.12	0.02	0.03	0.02	0.02	0.01	b.d.		0.03	0.02	0.04	0.02	0.04	0.02	0.03	0.01	b.d.		0.05	0.02
La	0.12	0.01	0.04	0.02	0.06	0.01	0.02	0.01	0.03	0.02	0.07	0.02	0.04	0.02	0.04	0.01	0.04	0.03	0.04	0.03
Ce	0.18	0.02	0.15	0.03	0.19	0.02	0.10	0.02	0.29	0.03	0.15	0.03	0.12	0.02	0.15	0.03	0.31	0.06	0.13	0.04
Pr	0.08	0.01	0.08	0.02	0.07	0.01	0.07	0.02	0.19	0.02	0.10	0.02	0.05	0.01	0.09	0.02	0.13	0.03	0.09	0.03
Pb	0.05	0.02	0.13	0.03	0.04	0.02	0.04	0.03			0.09	0.03	0.00	0.03	0.07	0.03	0.34	0.05	0.08	0.04
Sr	0.59	0.05	0.52	0.06	0.62	0.06	0.74	0.06	2.65	0.1	1.54	0.1	0.17	0.03	0.44	0.04	0.84	0.08	0.35	0.05
Nd	1.17	0.1	0.88	0.1	0.84	0.1	0.93	0.1	2.98	0.2	1.84	0.2	0.57	0.1	1.64	0.2	2.15	0.4	1.35	0.3
Sm	1.84	0.3	1.23	0.3	1.16	0.2	0.94	0.2	2.13	0.3	2.35	0.3	0.60	0.2	2.58	0.3	1.54	0.4	1.56	0.5
Zr	4.50	0.3	9.04	0.6	9.05	0.5	3.42	0.2	24.4	0.9	14.1	0.6	34.4	1.3	3.94	0.3	11.5	0.7	5.38	0.4
Hf	0.11	0.05	0.15	0.06	0.15	0.05	0.09	0.04	0.19	0.06	0.19	0.06	1.17	0.1	0.13	0.05	0.19	0.09	0.18	0.09
Eu	1.52	0.1	0.77	0.08	0.76	0.06	0.97	0.08	1.83	0.1	1.55	0.1	0.28	0.04	1.66	0.1	0.87	0.1	1.35	0.2
Ti	590	52	794	97	851	67	664	38	1070	61	771	44	3360	189	378	22	497	150	216	65
Gd	4.12	0.4	2.45	0.3	2.48	0.3	2.29	0.3	3.25	0.3	4.93	0.4	1.56	0.2	6.31	0.5	2.31	0.4	3.50	0.6
Tb	0.78	0.06	0.47	0.05	0.44	0.04	0.35	0.04	0.56	0.05	0.94	0.06	0.40	0.04	1.24	0.08	0.36	0.07	0.52	0.09
Dy	5.59	0.4	2.99	0.3	2.96	0.2	2.09	0.2	4.33	0.3	5.99	0.3	3.48	0.2	9.35	0.5	2.72	0.5	2.97	0.5
Y	30.3	1.3	15.6	0.8	15.1	0.7	9.69	0.4	20.7	0.7	26.2	0.9	15.7	0.6	40.5	1.4	13.0	0.6	11.2	0.6
Ho	1.18	0.08	0.62	0.06	0.61	0.05	0.38	0.04	0.98	0.07	1.22	0.08	0.76	0.06	1.93	0.1	0.52	0.09	0.52	0.09
Er	3.39	0.3	1.62	0.2	1.58	0.1	0.89	0.1	2.71	0.2	3.04	0.2	2.11	0.2	5.41	0.3	1.63	0.3	1.16	0.2
Tm	0.51	0.05	0.24	0.04	0.23	0.03	0.09	0.02	0.40	0.04	0.42	0.04	0.30	0.03	0.82	0.06	0.27	0.05	0.14	0.04
Yb	3.77	0.3	1.59	0.2	1.51	0.2	0.64	0.1	2.78	0.2	2.92	0.2	1.81	0.2	5.27	0.3	1.73	0.3	0.89	0.2
Lu	0.64	0.05	0.23	0.04	0.22	0.03	0.10	0.02	0.40	0.04	0.47	0.05	0.26	0.03	0.81	0.06	0.27	0.05	0.15	0.04
Eu/Eu*	1.6		1.3		1.3		1.9		2.1		1.4		0.8		1.2		1.4		1.7	
Lu_N	26.1		9.3		9.0		4.1		16.3		19.1		10.6		32.9		11.0		6.1	
Lu/Gd_N	1.26		0.76		0.72		0.36		1.00		0.77		1.35		1.04		0.94		0.34	
n (grains)	28		20		29		6		9		6		7		6		5		5	

$Eu^* = 2*Eu_N/(Gd_N+Sm_N)$

Subscript 'N' indicates normalization to chondrite from McDonough and Sun (1995). *Chem. Geol.* **120**, 223-253.

Continued

	Jer 3		Jer 4		Jer 5		Jer 6		Jer 7		Jer 8		Jde 15		Jde 25	
	Grt	*1σ*	*Grt*	*1σ*	*Grt*	*1σ*	*Grt*	*1σ*	*Grt*	*1σ*	*Grt*	*1σ*	**Grt**	*1σ*		*1σ*
V	919	8	326	3	430	7	422	4	212	3	385	5	74.9	5	80.3	0.5
Ni	12.70	3	12.20	3	8.39	0.7	6.51	0.7	16.7	1	2.72	0.5	21.8	2	-	
Sc	51.7	3	35.0	2	96.7	4	58.6	2	52.6	2	33.0	2	46.4	2	37	0.2
Rb	0.67	8	0.07	0.03	0.12	0.03	0.35	0.1	0.18	0.1	0.07	0.04	0.15	0.04	b.d.	
Ba	0.07	0.02	0.09	0.03	0.04	0.02	0.18	0.03	0.08	0.02	0.03	0.02	0.81	0.03	0.04	0.02
U	0.07	0.01	b.d.		b.d.		0.05	0.01	0.03	0.01	b.d.		0.04	0.01	b.d.	
Nb	b.d.		0.10	0.03	b.d.		0.03	0.02	b.d.		b.d.		0.18	0.05	0.2	0.03
Ta	0.05	0.03	0.12	0.03	b.d.		0.03	0.02	b.d.		b.d.		b.d.		0.1	0.03
La	0.05	0.03	0.06	0.02	0.04	0.01	0.04	0.02	0.04	0.02	b.d.		0.19	0.02	b.d.	
Ce	0.67	0.1	0.11	0.03	0.07	0.02	0.11	0.02	0.07	0.02	0.22	0.03	0.12	0.03	0.09	0.03
Pr	0.35	0.05	0.06	0.02	0.05	0.01	0.04	0.01	0.06	0.02	0.09	0.02	0.05	0.02	0.05	0.02
Pb	0.09	0.03	0.09	0.04	0.07	0.04	0.13	0.05	0.17	0.04	0.17	0.05	0.06	0.03	b.d.	
Sr	2.06	0.1	0.56	0.06	0.22	0.03	0.43	0.05	0.31	0.04	0.62	0.06	0.51	0.1	0.52	0.05
Nd	4.58	0.6	0.88	0.2	0.78	0.1	0.53	0.1	0.90	0.10	1.53	0.2	0.38	0.2	0.45	0.1
Sm	3.66	0.6	1.75	0.4	1.24	0.3	1.02	0.3	1.12	0.30	2.54	0.4	0.43	0.2	0.93	0.1
Zr	19.4	1	6.24	0.4	8.26	0.5	4.21	0.3	4.07	0.30	7.88	0.6	7.86	0.5	18.9	0.4
Hf	0.27	0.09	0.19	0.08	0.20	0.06	0.17	0.07	0.07	0.05	0.20	0.06	0.21	0.07	0.62	0.1
Eu	1.78	0.3	1.15	0.2	0.72	0.07	0.82	0.08	0.82	0.07	2.16	0.1	0.20	0.04	0.7	0.08
Ti	919	276	326	98	430	47	423	52	212	32	385	65	2026	117	1765	7
Gd	5.17	0.8	4.92	0.7	3.72	0.3	3.32	0.4	2.44	0.3	8.61	0.7	0.99	0.2	2.44	0.2
Tb	0.90	0.1	1.04	0.2	0.96	0.07	0.97	0.07	0.39	0.04	1.86	0.1	0.23	0.03	0.49	0.06
Dy	5.99	0.9	7.49	1	8.45	0.5	8.72	0.5	2.69	0.2	13.6	0.8	1.86	0.2	3	0.2
Y	26.1	1	33.9	2	49.4	1.9	54.9	2	13.9	0.7	74.6	4	9.84	0.6	13.2	0.2
Ho	1.19	0.2	1.58	0.2	1.96	0.1	2.31	0.1	0.59	0.06	3.07	0.2	0.38	0.04	0.39	0.05
Er	3.26	0.4	3.96	0.5	6.50	0.4	7.32	0.5	1.70	0.2	7.80	0.6	1.03	0.1	1.07	0.1
Tm	0.51	0.08	0.57	0.08	0.96	0.07	1.20	0.09	0.28	0.04	0.97	0.08	0.14	0.03	0.13	0.02
Yb	3.59	0.5	3.55	0.5	7.50	0.3	8.69	0.5	1.87	0.2	5.76	0.4	0.98	0.1	0.87	0.1
Lu	0.51	0.08	0.48	0.08	1.20	0.08	1.51	0.1	0.26	0.04	0.84	0.07	0.13	0.02	0.12	0.02
Eu/Eu*	1.2		1.1		0.9		1.2		1.5		1.3		0.9		1.3	
La_N	0.22		0.23		0.18		0.18		0.16				0.81			
Lu_N	20.8		19.5		48.8		61.6		10.5		34.1		5.1		4.9	
Lu/Gd_N	0.80		0.79		2.61		3.69		0.85		0.79		1.03		0.40	
n (grains)	5		5		4		3		4		5		7		1	

Continued

	35-2		**1-1**		**R183**		**10-13**		**55-7**		**44-9**		**Jd6fn**		**Jer 1**		**Jer 2**		**Jer 3**	
	Cpx	*1σ*	*Cpx*	*1σ*	*Cpx*	*1σ*	*Cpx*	*1σ*	*Cpx*	*1σ*	*Cpx*	*1σ*	*Cpx*	*1σ*	*Cpx*	*1σ*	*Cpx*	*1σ*	*Cpx*	*1σ*
V	360	14	182	9	191	9	156	17	127	5	258	9	248	9	180	16	135	12	191	17
Ni	209	11	264	18	280	21	136	2	146	7	193	9	203	9	282	65	267	62	167	38
Sc	20.4	0.8	12.8	0.6	12.4	0.6	31.1	0.8	17.5	1	24.9	1	17.8	0.7	17.6	1	8.04	0.6	14.7	1
Rb	0.45	0.01	0.03	0.01	0.08	0.02	0.12	0.01	0.25	0.07	0.12	0.03	0.02	0.01	0.04	0.02			0.21	0.03
Ba	1.32	0.1	0.12	0.02	0.13	0.02	0.39	0.01	0.04	0.01	0.39	0.03	0.03	0.01	0.09	0.02	0.07	0.02	0.07	0.03
U	0.29	0.004	0.03	0.005	0.06	0.003	0.09	0.01	b.d.		0.22	0.005	0.04	0.01	0.07	0.01	0.03	0.01	0.02	0.01
Nb	b.d.		b.d.		b.d.		b.d.		b.d.		b.d.		0.02	0.01	b.d.		b.d.		b.d.	
Ta	0.03	0.01	0.03	0.01	0.02	0.01	0.04	0.01	b.d.		0.04	0.02	b.d.		b.d.		b.d.		b.d.	
La	4.17	0.2	1.07	0.07	1.00	0.06	1.08	0.04	0.04	0.02	3.04	0.1	0.54	0.05	0.24	0.05	1.07	0.2	0.56	0.1
Ce	14.1	0.5	3.63	0.2	3.49	0.2	3.62	0.07	0.14	0.02	9.39	0.3	2.37	0.1	1.32	0.2	4.57	0.6	2.85	0.4
Pr	2.83	0.1	0.64	0.04	0.60	0.03	0.71	0.03	0.04	0.01	1.58	0.07	0.59	0.04	0.39	0.06	0.95	0.1	0.67	0.09
Pb	1.10	0.1	0.39	0.05	0.37	0.04	0.35	0.04	0.22	0.04	0.27	0.04	0.30	0.04	0.31	0.06	0.32	0.05	0.66	0.09
Sr	678	23	209	8	201	7	182	5	169	5	131	4	211	7	201	8	231	10	240	10
Nd	16.4	0.6	3.14	0.2	3.03	0.2	4.25	0.1	0.33	0.07	7.93	0.4	3.88	0.3	2.58	0.4	6.07	0.8	3.86	0.6
Sm	4.29	0.3	0.90	0.2	0.84	0.2	1.71	0.1	0.26	0.1	1.67	0.2	1.16	0.2	0.69	0.3	1.17	0.3	0.79	0.3
Zr	12.3	0.5	11.0	0.6	10.5	0.5	9.41	0.2	6.24	0.3	8.35	0.4	7.10	0.3	6.94	0.4	6.02	0.4	24.9	1
Hf	1.00	0.1	0.62	0.09	0.57	0.07	0.44	0.04	0.41	0.07	0.77	0.1	0.59	0.08	0.37	0.1	0.31	0.08	1.00	0.2
Eu	1.68	0.1	0.31	0.04	0.31	0.03	0.89	0.03	0.08	0.02	0.48	0.04	0.41	0.04	0.20	0.05	0.54	0.09	0.18	0.05
Ti	856	60	1032	108	1013	64	856	56	836	48	1411	80	826	47	610	183	595	179	1221	367
Gd	2.54	0.2	0.62	0.1	0.55	0.1	2.13	0.07	0.24	0.07	1.41	0.2	0.95	0.1	0.47	0.2	0.96	0.2	0.48	0.2
Tb	0.21	0.02	0.06	0.02	0.05	0.01	0.33	0.01	0.03	0.01	0.15	0.02	0.10	0.02	0.05	0.02	0.06	0.02	0.05	0.02
Dy	0.75	0.07	0.22	0.07	0.19	0.05	2.12	0.04	0.15	0.05	0.68	0.09	0.29	0.06	0.22	0.07	0.20	0.07	0.25	0.08
Y	2.02	0.1	0.56	0.06	0.52	0.05	10.7	0.03	0.26	0.04	1.99	0.1	0.81	0.06	0.27	0.04	0.34	0.05	0.32	0.05
Ho	0.09	0.01	0.03	0.01	0.03	0.01	0.43	0.01	0.02	0.01	0.10	0.02	0.04	0.01	0.03	0.02	b.d.			
Er	0.15	0.03	0.08	0.03	0.07	0.02	1.15	0.02	b.d.		0.20	0.04	0.07	0.03	0.05	0.04	0.05	0.03	0.13	0.06
Tm	0.02	0.01	0.02	0.009	b.d.		0.17	0.01	0.02	0.01	0.02	0.01	0.01	0.01	b.d.		b.d.		0.01	0.01
Yb	0.10	0.03	0.07	0.04	0.05	0.03	1.18	0.03	0.05	0.03	0.10	0.04	0.06	0.03	0.02	0.95	b.d.		b.d.	
Lu	0.02	0.007	0.02	0.01	b.d.		0.19	0.01	b.d.		0.02	0.01	b.d.		b.d.		b.d.		b.d.	
Eu/Eu*	1.4		1.2		1.3		1.4		1.0		0.9		1.2		1.0		1.5		0.8	
La_N	17.6		4.5		4.2		4.5		0.2		12.8		2.3		1.0		4.5		2.3	
La/SmN	0.61		0.74		0.75		0.39		0.09		1.14		0.29		0.22		0.57		0.44	
n (grains)	40		24		27		6		8		7		7		5		5		5	

Continued

	Jer 4		**Jer 5**		**Jer 6**		**Jer 7**		**Jer 8**		**Jde 15**		**Jde 25**
	Cpx	*1σ*	*Cpx*	*1σ*	*Cpx*	*1σ*	*Cpx*	*1σ*	*Cpx*	*1σ*	*Cpx*	*1σ*	*Cpx*
V	182	16	378	20	267	15	207	14	236	18	221	15	404
Ni	231	53	201	10	144	7	298	17	79.9	5	139	12	-
Sc	10.6	0.7	52.8	2	32.3	1	17.6	0.9	15.8	0.8	11.3	0.5	1117
Rb	0.03	0.02	0.02	0.01	0.05	0.02	b.d.		0.05	0.01	0.12	0.04	28
Ba	0.05	0.02	0.17	0.02	0.16	0.02	0.08	0.02	0.08	0.02	0.09	0.02	0.24
U	b.d.		b.d.		0.02	0.01	0.10	0.01	0.03	0.007	0.01	0.005	b.d.
Nb	b.d.		0.02	0.01	0.04	0.01	0.03	0.02	b.d.		0.13	0.04	0.29
Ta	0.03	0.02	b.d.		0.03	0.01	0.06	0.01	b.d.		b.d.		0.04
La	0.38	0.07	3.51	0.2	1.00	0.07	1.58	0.1	0.64	0.06	0.35	0.03	1.23
Ce	2.19	0.3	15.3	0.6	4.42	0.2	6.25	0.3	2.56	0.2	1.27	0.09	4.07
Pr	0.53	0.07	3.23	0.1	1.01	0.06	1.44	0.08	0.54	0.04	0.23	0.02	0.66
Pb	0.51	0.07	2.11	0.2	1.18	0.1	0.63	0.08	0.27	0.05	0.11	0.03	-
Sr	310	13	732	25	537	19	400	16	205	9	79.5	4	62
Nd	3.96	0.5	17.2	0.7	6.44	0.4	9.22	0.5	3.41	0.3	1.12	0.1	3.62
Sm	1.26	0.3	4.14	0.3	2.00	0.2	2.13	0.3	0.84	0.2	0.30	0.1	0.86
Zr	8.16	0.5	9.46	0.5	12.5	0.7	7.58	0.6	15.4	1	6.97	0.4	9.66
Hf	0.61	0.1	0.79	0.1	0.88	0.1	0.50	0.09	1.08	0.1	0.53	0.06	0.63
Eu	0.44	0.08	1.37	0.08	0.84	0.06	0.66	0.06	0.40	0.05	0.12	0.002	0.25
Ti	643	193	451	51	643	83	402	65	586	104	2424	140	1781
Gd	0.91	0.2	3.43	0.3	1.70	0.2	1.05	0.2	0.90	0.2	0.35	0.09	b.d.
Tb	0.10	0.03	0.41	0.03	0.19	0.02	0.09	0.02	0.09	0.02	0.05	0.01	0.1
Dy	0.32	0.1	1.79	0.2	1.09	0.1	0.25	0.07	0.36	0.08	0.19	0.05	0.44
Y	0.74	0.07	4.97	0.2	3.08	0.2	0.57	0.06	1.21	0.1	0.68	0.06	1.34
Ho	0.05	0.02	0.20	0.03	0.12	0.02	0.02	0.01	0.05	0.02	0.04	0.01	0.06
Er	0.10	0.04	0.46	0.07	0.28	0.05	0.07	0.03	0.06	0.03	0.07	0.03	0.14
Tm	b.d.		0.04	0.01	0.05	0.01	b.d.				0.02	0.01	0.03
Yb	b.d.		0.22	0.06	0.10	0.04	0.06	0.01	0.05	0.04		0.04	b.d.
Lu	0.03	0.01	0.03	0.01	0.02	0.01	b.d.		0.02	0.009		0.01	b.d.
Eu/Eu*	1.2		1.1		1.3		1.2		1.4		1.1		
La_N	1.6		14.8		4.2		6.7		2.7		1.5		5.2
La/SmN	0.19		0.53		0.31		0.46		0.48		0.74		0.89
n (grains)	5		5		3		5		5		3		2

Table A.3 Sr and Pb isotope compositions of clinopyroxene from Jericho eclogites

Table A-3. In situ Sr and Pb isotope compositions of clinopyroxene from Jericho eclogites determine by ICPMS

	$^{87}Sr/^{86}Sr$	2σ	n	$^{206}Pb/^{204}Pb$	2σ	$^{207}Pb/^{204}Pb$	2σ	n
35-2	0.7043	0.00008	7	16.74	0.07	15.30	0.07	8
1-1	0.7054	0.0002	7	17.99	0.13	15.24	0.11	8
R183	0.7052	0.0003	7	18.03	0.15	15.23	0.12	8
10-13	0.7041	0.0003	5	17.04	0.19	15.31	0.13	4
55-7	0.7040	0.0003	7	16.25	0.15	15.27	0.09	6
44-9	0.7032	0.0003	8	18.75	0.13	15.55	0.10	4
Jd6fn	0.7044	0.0001	7	16.97	0.04	15.37	0.06	4
Jer 1	0.7042	0.0004	7	15.79	0.13	15.14	0.13	5
Jer 2	0.7042	0.0002	4	16.18	0.23	14.94	0.22	5
Jer 3	0.7037	0.0003	9	14.68	0.10	15.12	0.10	5
Jer 4	0.7041	0.0003	8	15.95	0.14	15.21	0.14	5
Jer 5	0.7032	0.0002	6	16.58	0.07	15.23	0.05	5
Jer 6	0.7036	0.0002	9					
Jer 7	0.7042	0.0002	6					
Jer 8	0.7036	0.0004	7	16.34	0.18	15.08	0.1	1
Coral Standard						**NIST SRM 614**		
measured	0.709115	0.000071	5	17.43	0.10	15.58	0.13	4
	0.709011	0.000074	7	17.62	0.07	15.59	0.06	4
accepted	0.709098	0.000019		17.833	0.013	15.53	0.007	

Notes:
Acccepted Sr standard values from Bizzaro et al. (2003) *GCA* **67**, 289-302.
Accepted Pb standard values from Woodhead & Hergt (2001) *Geostan News* ***25****, 261-266*.

Table A.4 Oxygen isotope composition of garnet and clinopyroxene from Jericho eclogites

Table A-4. Oxygen isotope compositions of ganet and clinopyroxene from Jericho eclogites

Samples		$\delta^{18}O$ (‰)			1σ
35-2	grt	5.73	5.59		±0.1
	cpx				
Mx8A	grt	5.64	5.65		±0.1
Jd6fn	grt	5.22	5.36	5.44	±0.1
	cpx				
53-11	grt	5.67	5.49		±0.1
	ky	6.3			±0.1
44-9	grt	5.64	5.75	5.67	±0.1
	cpx				
55-7	grt	5.57	5.61		±0.18
	cpx				
1-1	grt	5.62	5.54		±0.18
	cpx				
10-13	grt	6.25	6.31	6.55	±0.18
	cpx				
JDE 02	grt	5.30	5.50		±0.15
	cpx	5.45			±0.15
JDE 03	grt	5.47			±0.15
	cpx				
JDE 07	grt	5.49	5.53		±0.15
	cpx				
JDE 25	grt	6.56	6.5		±0.15
	cpx				
JDE 15	grt	6.64	6.61		±0.15
	cpx				

Standards	measured:	accepted:	
Gee Whiz Qtz	12.52 ± 0.14 (1σ) n=15	12.5 ± 0.1 (1σ)	*Larson & Sharp (2005)*
Gore - 3	5.64 ± 0.06 (1σ) n=5	5.74 ± 0.15 (1σ)	*UWG-2; Valley et al. (1995)*

Notes:

1σ calculated for each day session based on the Gee Whiz Qtz standard

Gore-3 is sampled from the same locality as UWG-2

Appendix B: Eclogite xenolith index and petrography

The following table lists and summarizes the petrography for all Jericho eclogite xenoliths.

Table B.1 Petrography of Jericho eclogite xenoliths

Sample	Class.	Mineralogy						Texture	Comments
		Gt	Cpx	Dia	Ky	Rut	Other		
8-12	B	x	x			x		m	secondary phlog+cc+ap
35-2	B	x	x			x	ap	f	phlog
1-1	B	x	x			x		m	secondary phlog+cc+ap
55-7	C	x	x					m	secondary phlog+cc+ap
Jd6Fn	B	x	x			x		f	secondary phlog+cc+ap
R183	B	x	x			x		f	secondary phlog+cc+ap
53-11	C	x	x		x		ap	f	
54-5	B	x	x					m	secondary phlog+cc+ap
44-9	A	x	x						secondary phlog+cc+ap
10-13	C	x	x			x		f	secondary phlog+cc+ap
53-6	B	x	x			x			secondary phlog+cc+ap
51-10	C	x	x		x	x	ap	m	
11-17	C	x	x		x	x		f	secondary phlog+cc+ap
7-5	B	x	x					m	secondary phlog+cc+ap
Jer 1	B	x	x		x			m	
Jer 2	B	x	x		x		ap, cor	m	
Jer 3	C	x	x		x			m	
Jer 4	B	x	x					m	
Jer 5	B	x	x			x	opx	f	
Jer 6	B	x	x			x	ap	f	
Jer 7	B	x	x			x		f	
Jer 8	C	x	x				ap	m	
JDE 01	A	x	x	x				m	phlog, cc, glass, sulf
JDE 02	A	x	x	x				m	phlog, cc, glass, sulf
JDE 03	A	x	x	x				m	phlog, cc, glass, sulf
JDE 07	A	x	x	x				m	phlog, cc, glass, sulf
JDE 15	B	x	x	x				m	
JDE 16	A	x	x	x				m	phlog, cc, glass, sulf
JDE 17	A	x	x	x				m	phlog, cc, glass, sulf
JDE 18	A	x	x	x				m	phlog, cc, glass, sulf
Jde 19	A	x	x	x				m	phlog, cc, glass, sulf
JDE 20	A	x	x	x				m	phlog, sulf
JDE 21	A	x	x	x				m	phlog, sulf
JDE 22	A	x	x	x				m	phlog, cc, glass, sulf
JDE 23	A	x	x	x				m	phlog, cc, glass, sulf
JDE 24	A	x	x	x				m	phlog, cc, glass, sulf
JDE 25	B	x	x	x				m	

Class: Classification based on garnet composition from Coleman et al. (1965) See 3.1.1.
Mineral Abbreviations: Gt - garnet, cpx - clinopyroxene, dia - diamond, ky - kyanite, rut - rutile, ap - apatite, phlog- phlogopite, cc - calcite, opx - orthopyroxene, sulf - sulfide, cor - corundum
Texture following Kopylova et al. (1999a) - m, massive and a, anisotropic. See 2.3.1.